

Haldis Døvre Kalland

# Snow forces, avalanches, and avalanche mitigation methods

Master's thesis in Mechanical Engineering

Supervisor: Arne Aalberg

Co-supervisor: Tore Børvik

June 2022



Haldis Døvre Kalland



Haldis Døvle Kalland

# **Snow forces, avalanches, and avalanche mitigation methods**



Master's thesis in Mechanical Engineering  
Supervisor: Arne Aalberg  
Co-supervisor: Tore Børvik  
June 2022

Norwegian University of Science and Technology  
Faculty of Engineering  
Department of Structural Engineering



Norwegian University of  
Science and Technology





## MASTER THESIS 2022

SUBJECT AREA: Structural Engineering	DATE: June 11 <sup>th</sup> 2022	NO. OF PAGES: 10+124+5
---	-------------------------------------	---------------------------

TITLE:

**Snow forces, avalanches, and avalanche mitigation methods**

Snøkrefter, skred og skredsikring

BY:

Haldis Døvle Kalland



Snow avalanches are gravity driven mass flows that constitute a considerable threat to human lives and infrastructure in mountainous regions. Structural avalanche mitigation methods, such as rigid fences, flexible nets, deflecting or catching dams, snow sheds or tunnels, may be used to protect against the avalanche threat. A sufficiently in-depth understanding of the load actions on structures from deformations in the snowpack and from avalanches is fundamental for adequate design of mitigation measures. This thesis perform a literature review of snow, avalanches, and avalanche mitigation methods, study the design of an ongoing slush flow mitigation project using flexible net barriers, and reports elements from a research trip studying avalanche related structures near Longyearbyen, Svalbard, for the purpose of mapping problem fields where future research projects can contribute most to the field of structural avalanche protection.

Snow formation and properties of the snowpack are discussed to understand why avalanches form. In addition, an overview is given of avalanche classification and terminology, together with the characteristics of several avalanche types. Existing models used to describe snow pressure, calculate avalanche speeds, runout distance, and dynamic impact forces are discussed, and a presentation is given of both structural and non-structural avalanche mitigation measures.

The planned design of 14 slush flow barriers in Vannledningsdalen, Svalbard, has been studied in detail with the aim of reproducing and understanding the applied concepts of the design and to search for research gaps within the field of slush flows. The study found that, in the project, static load actions on the barriers from snow and slush flow deposits depend on snow density, snow height, and creep and glide in the snowpack. The dynamic loads actions depend on the square of the slush flow velocity, the flow density, the flow height, and a drag coefficient.

During field tests in Longyearbyen, the average snowpack density and temperature was measured next to a Snow Load Testing System (SLTS), and manual snow height measurements were performed in the back-pressure zone of the SLTS. The SLTS measured variations in snow pressure that coincided well with snow creep theory and observed weather conditions in March 2022. Snow deposits around already constructed snow supporting structures at Sukkertoppen had been greatly affected by wind transport.

It is suggested that further work should slush flow experiments investigating the fluid-structure interaction of slush flows and flexible net barriers, and the stabilising effect of snow supporting structures against the release of slush flows. In addition, effort should be made to create reliable numerical models of slush flows interacting with barriers, and to develop calculation procedures specifically designed for slush flow dynamics. Further work should also investigate to what extent flexible net barriers influence the deposition of wind drifted snow, and how this is affected by net mesh size. The snow drift effects around rigid support structures built near Longyearbyen is of interest for further work, in addition to the snow pressures acting on these structures. Tests should be performed to investigate the influence of different support surface inclinations on the statics of snow supporting systems.

RESPONSIBLE TEACHER: Professor Arne Aalberg

SUPERVISOR(S): Professor Arne Aalberg, Professor Tore Børvik

CARRIED OUT AT: The Departement of Structural Engineering, NTNU





## MASTEROPPGAVE 2022

FAGOMRÅDE: Konstruksjonsteknikk	DATO: 11. juni 2022	ANTALL SIDER: 10+124+5
------------------------------------	------------------------	---------------------------

TITTEL:

### **Snøkrefter, skred og skredsikring**

Snow forces, avalanches, and avalanche mitigation methods

UTFØRT AV:

Haldis Døvle Kalland



SAMMENDRAG:

Snøskred utgjør en betydelig trussel mot menneskeliv og infrastruktur i fjellområder. Permanente sikringstiltak, slik som stive gjerder, fleksible nett, voller, skredoverbygg eller tunneler, kan brukes for å beskytte mot skredfare. For å oppnå tilfredsstillende utforming og dimensjonering av sikringstiltak er det viktig med tilstrekkelig forståelse av lastene som virker på konstruksjoner fra bevegelse i snødekket og fra snøskred er viktig. Denne oppgaven gjennomgår litteratur relatert til snø, snøskred og skredsikring, studerer utformingen og dimensjoneringen av et pågående sikringsprosjekt der fleksible nettkonstruksjoner brukes som tiltak mot sørpeskred, og rapporterer elementer fra en studietur som så på sikringstiltak nær Longyearbyen, Svalbard. Formålet med oppgaven er å kartlegge hvilke fremtidige forskningsprosjekter som kan bidra mest til å øke kunnskapen rundt permanent skredsikring.

Dannelsen av snø og egenskapene til snødekket undersøkes for å forstå hvorfor snøskred dannes. I tillegg presenteres ulike skredtyper og hva som kjennetegner dem. Eksisterende modeller for å beregne snøtrykk, skredhastigheter, utløpsdistanse og dynamiske støtkrefter diskuteres, etterfulgt av etablerte sikringstiltak mot skred. Prosjekteringen av 14 planlagte nettkonstruksjoner i Vannledningsdalen, Svalbard, er studert i detalj. Målet var forstå hele dimensjoneringen av nettkonstruksjonene og undersøke hvilke utførelser ingeniørene møtte på i prosjekteringsfasen. Feltforsøk i Longyearbyen målte gjennomsnittlig densitet og temperatur ved siden av et målesystem for snøtrykk (SLTS). I tillegg ble snødybdeprofiler målt på oversiden av målesystemet. En økning i snøtrykk ble målt av systemet (SLTS) i mars 2022 som stemte overens med økt snøsig fra observert varmere vær og regn. Det ble observert at snødekket rundt støtteforbygningene på Sukkertoppen var sterkt påvirket av vind.

I videre arbeid foreslås det å utføre forsøk med sørpeskred som undersøker interaksjonen mellom nettbarrierer og sørpeskred, og hvilken effekt støtteforbygninger har på utløsning av sørpeskred. I tillegg foreslås det å lage pålitelige numeriske modeller av interaksjonen mellom sørpeskred og barrierer, og modeller som beskriver den dynamiske bevegelsen til sørpeskred. Videre arbeid kan også undersøke i hvilken grad fleksible nettkonstruksjoner påvirker drivsnø, og hvordan dette igjen påvirkes av maskestørrelsen. Effekten vind har på snødekket rundt støtteforbygningene i Longyearbyen er av interesse for videre arbeid, i tillegg til snøtrykket som virker på disse konstruksjonene. Det kan også utføres tester som undersøker effekten av hellingen til støtteflaten i stive støtteforbygninger.

FAGLÆRER: Professor Arne Aalberg

VEILEDER(E): Professor Arne Aalberg, Professor Tore Børvik

UTFØRT VED: Institutt for konstruksjonsteknikk, NTNU





## **MASTER'S THESIS 2022**

for

*Haldis Døvle Kalland*

### **Snow forces, avalanches, and avalanche mitigation methods**

Snøkrefter, skred og skredsikring

#### **Background**

In Norway we have no available design standards for determining forces and designing structures for actions from snow and avalanches. Statens Vegvesen has some manuals, and Norges Geotekniske Institutt and Norges Vassdrags og Elektrisitetsvesen have some experience on the topic. The topic is not covered in depth in teaching either and the Norwegian engineering companies has limited competence. Design and construction projects for structures and mitigation works are therefore often done by companies from other countries, e.g., from Switzerland and Austria. However, Norwegian conditions are likely not identical to the alpine conditions. With the environmental changes we experience, with increased temperature and more precipitation at many locations, and the increasing demand from the public for safer roads and structures, it is time we focus on this also in the teaching and research.

#### **Problem Description**

The main topics in the research project can be as follows:

- Perform a literature review to obtain a theoretical foundation on avalanches and avalanche mitigation methods. Present the theory.
- Present the most common formulations of static load actions from snow and loads from avalanches on avalanche protection structures.
- Study the design and dimensioning of a chosen avalanche mitigation project in detail.
- Identify relevant topics for future research projects on structural avalanche protection.
- Plan and carry out relevant field measurements around the experimental Snow Load Testing System near Longyearbyen, Svalbard.
- Examine on-site the constructed avalanche mitigation measures near Longyearbyen and consider possible research projects related to these measures.
- Examine the research gaps related to structural avalanche protection, and especially slush flows and flexible nets and wire systems.

The candidate can, after conferring with his or her supervisor, choose to concentrate on some of the topics listed, adjust some, and add topics.

#### **The Report**

The thesis shall be written as a technical report and have good figures, tables, and photos. The report shall contain a title page, problem description, abstract, preface, contents list, a reasonable number of chapters (with subsections), conclusion as the last chapter, reference list, and appendix. Information about the submission process has been issued by the department. Submit the thesis in InSpera.

The thesis must be submitted no later than June 11th, 2022.



Trondheim, June 2022  
Arne Aalberg, Professor



---

# Preface

This thesis was written for the Department of Structural Engineering at the Norwegian University of Science and Technology (NTNU) during 20 weeks in the spring of 2022. The thesis is a requirement for the degree of Master of Science at NTNU, and finalised my study in the programme Mechanical Engineering with specialisation in Applied Mechanics. The master thesis was carried out under supervision of Professor Arne Aalberg and Professor Tore Børvik at the Department of Structural Engineering at NTNU.

## Acknowledgements

First of all, I would like to thank three specialists within the field of avalanche and debris flow mitigation for sharing their valuable experience and ideas. Kalle Kronholm ([Skred AS](#)) contributed with numerous suggestions on field tests and research gaps. These gave the project a flying start when deciding which areas to focus on, and have been greatly appreciated. Arni Jonsson ([HNIT](#)) advised on research gaps, and gave very helpful insights on avalanche mitigation literature and which guidelines are being used today in practical engineering. This made me confident that what I read was correct and in practical use which was a strong reassurance. Jonsson also provided access to internal reports on the Vannledningsdalen-project. Without these the detailed study of flexible net barriers as a mitigation measure against slush flows would not have been possible. Nadine Feiger ([Geobrugg AG](#)) helped me in understanding all details of the barrier dimensioning planned in Vannledningsdalen, and recommended interesting projects for further work.

Big thanks is also given to professor emeritus Kolbein Bell ([NTNU](#)) for introducing me to the frame analysis program [Fap2D](#) and for advising on its possibilities. Lastly, I would like to thank my supervisor Professor Arne Aalberg ([NTNU](#)) for helpful guidance and discussions during the work with this thesis.

(H.D.K.)



---

# Abstract

Snow avalanches are gravity driven mass flows that constitute a considerable threat to human lives and infrastructure in mountainous regions. Structural avalanche mitigation methods, such as rigid fences, flexible nets, deflecting or catching dams, snow sheds or tunnels, may be used to protect against the avalanche threat. A sufficiently in-depth understanding of the load actions on structures from deformations in the snowpack and from avalanches is fundamental for adequate design of mitigation measures. This thesis perform a literature review of snow, avalanches, and avalanche mitigation methods, study the design of an ongoing slush flow mitigation project using flexible net barriers, and reports elements from a research trip studying avalanche related structures near Longyearbyen, Svalbard, for the purpose of mapping problem fields where future research projects can contribute most to the field of structural avalanche protection.

Snow formation and properties of the snowpack are discussed to understand why avalanches form. In addition, an overview is given of avalanche classification and terminology, together with the characteristics of several avalanche types. Existing models used to describe snow pressure, calculate avalanche speeds, runout distance, and dynamic impact forces are discussed, and a presentation is given of both structural and non-structural avalanche mitigation measures.

The planned design of 14 slush flow barriers in Vannledningsdalen, Svalbard, has been studied in detail with the aim of reproducing and understanding the applied concepts of the design and to search for research gaps within the field of slush flows. The study found that in the project, static load actions on the barriers from snow and slush flow deposits are calculated according to Swiss technical guidelines (SLF) and depend on snow density, snow height, and creep and glide in the snowpack. The dynamic loads actions are calculated according to Austrian normative documents for permanent technical avalanche protection (ONR), and depend on the square of the slush flow velocity, the flow density, the flow height, and a drag coefficient.

From field test in Longyearbyen, the average snowpack density in a snow pit was measured to  $\rho \approx 360 \text{ kg/m}^3$ , and snowpack temperature measurements showed a linear temperature increase from the snow surface to the ground. Manual snow height measurements were performed in the back-pressure zone of the [Snow Load Testing System \(SLTS\)](#) showing a relatively stable snow height over a 10m distance from the wall. The slope inclination was measured to be between 25° and 30°. The variations in snow pressure measured by the [SLTS](#) coincided well with snow creep theory and observed weather conditions in March 2022. Snow deposits around already constructed snow supporting structures at Sukkertoppen had been greatly affected by wind transport.

It is suggested that further work conduct (medium or large scale) slush flow experiments investigating the fluid-structure interaction of slush flows and flexible net barriers and the stabilising effect of snow supporting structures against the release of slush flows. In addition, effort should be made to create reliable numerical models of slush flows interacting with barriers, and to develop calculation procedures specifically designed for slush flow dynamics. Further work should also investigate to what extent flexible net barriers influence the deposition of wind drifted snow, and how this is affected by net mesh size. The snow drift effects around rigid supporting structures built near Longyearbyen are of interest for further work, in addition to the snow pressures acting on these structures. Tests should be performed to investigate the influence of different support surface inclinations on the statics of snow supporting systems.



# Table of Contents

<b>Preface</b>	<b>i</b>
<b>Acknowledgements</b>	<b>i</b>
<b>Abstract</b>	<b>iii</b>
<b>Contents</b>	<b>vii</b>
<b>Abbreviations</b>	<b>ix</b>
<b>1 Introduction</b>	<b>1</b>
<b>2 Snow formation and properties of the snowpack</b>	<b>3</b>
2.1 General . . . . .	3
2.2 Formation and evolution of the snowpack . . . . .	3
2.2.1 Snow formation in the atmosphere . . . . .	3
2.2.2 Snow crystal shapes . . . . .	4
2.2.3 The layering of the snowpack . . . . .	7
2.2.4 Wind transport of snow . . . . .	7
2.2.5 Heat exchange at the snow surface . . . . .	8
2.2.6 Crystal conversion in the snowpack - metamorphism . . . . .	9
2.3 Physical and mechanical properties of the snowpack . . . . .	11
2.3.1 Density . . . . .	11
2.3.2 Snow strength . . . . .	12
2.4 Deformation of the snowpack in sloped terrain . . . . .	14
2.4.1 Creep . . . . .	14
2.4.2 Glide . . . . .	14
2.4.3 Stress distribution in the snowpack . . . . .	15
<b>3 Static snow pressure and modelling</b>	<b>17</b>
3.1 General . . . . .	17
3.2 Normative basis of design . . . . .	18
3.3 Models for calculating snow pressure . . . . .	19
3.3.1 Snow as a rigid material . . . . .	19
3.3.2 Haefeli's (1948) model . . . . .	20
3.3.3 McClung's (1982) model . . . . .	20
3.3.4 Swiss technical guidelines . . . . .	21
3.3.5 Norwegian and Icelandic adaptations to the Swiss Guideline . . . . .	27
3.3.6 Norwegian guidelines - Statens Vegvesen, Håndbook V138 . . . . .	28
<b>4 Classification of avalanches</b>	<b>31</b>
4.1 General . . . . .	31
4.2 Avalanche catchment area . . . . .	32
4.2.1 Avalanche starting zone . . . . .	33
4.2.2 Avalanche track . . . . .	34
4.2.3 Avalanche runout zone . . . . .	34
4.3 Avalanche types . . . . .	35
4.3.1 Classification based on: Manner of starting . . . . .	35
4.3.2 Classification based on: Form of movement . . . . .	36

---

4.3.3	Classification based on: Position of sliding surface . . . . .	37
4.3.4	Classification based on: Liquid water in snow . . . . .	38
<b>5</b>	<b>Avalanche dynamics and modelling</b>	<b>41</b>
5.1	General . . . . .	41
5.2	Calculating avalanche velocity . . . . .	42
5.3	Calculating runout distance . . . . .	44
5.4	Calculating impact pressure . . . . .	46
<b>6</b>	<b>Avalanche mitigation measures</b>	<b>49</b>
6.1	General . . . . .	49
6.2	Non-structural mitigation methods . . . . .	50
6.2.1	Avalanche monitoring, forecasting and warning . . . . .	50
6.2.2	Avoidance . . . . .	52
6.2.3	Artificial avalanche release . . . . .	52
6.3	Structural mitigation measures . . . . .	54
6.3.1	Snow supporting structures in the starting zone . . . . .	54
6.3.2	Deflecting and channelling structures . . . . .	55
6.3.3	Retarding- and storing structures . . . . .	56
6.3.4	Direct protection of buildings, roads, and valuable objects . . . . .	58
6.3.5	Snowdrift measures . . . . .	59
6.4	Mitigation measures against slush flows . . . . .	61
<b>7</b>	<b>A research trip studying avalanche-related structures near Longyearbyen, Svalbard</b>	<b>65</b>
7.1	Highly relevant for Longyearbyen . . . . .	65
7.2	Aim of the research trip . . . . .	66
7.3	The Snow Load Testing System (SLTS) . . . . .	67
7.3.1	About the Snow Load Testing System . . . . .	67
7.3.2	Snow density measurements . . . . .	68
7.3.3	Snowpack temperature measurements . . . . .	69
7.3.4	Air temperature measurements . . . . .	69
7.3.5	Snow height measurements . . . . .	70
7.3.6	Slope inclination measurements . . . . .	73
7.3.7	Results from the Snow Load Testing System . . . . .	74
7.4	Snow supporting structures at Sukkertoppen . . . . .	76
7.5	Snowdrift fences - snow accumulation measurements . . . . .	78
<b>8</b>	<b>A study of the design of slush flow barriers in Vannledningsdalen</b>	<b>79</b>
8.1	General . . . . .	79
8.1.1	Introduction to the Vannledningsdalen project . . . . .	79
8.1.2	Aim, scope and relevant documents . . . . .	81
8.2	The barriers . . . . .	82
8.2.1	Barrier components . . . . .	82
8.2.2	Barrier placement . . . . .	84
8.2.3	Retention volume of barriers . . . . .	85
8.3	Load cases and barrier design values . . . . .	87
8.3.1	Load case 1: Static load from the snowpack . . . . .	88
8.3.2	Load case 2: Static pressure from slush flow debris . . . . .	89
8.3.3	Load case 3: Dynamic slush flow pressure over flow height . . . . .	91
8.3.4	Load case 4: Total load from static and dynamic slush flow pressure . . . . .	91
8.3.5	Load case: Support ropes . . . . .	92

---



---

8.3.6	Load case: Support posts . . . . .	92
8.3.7	Load case: Snow avalanche . . . . .	93
8.3.8	Design values and barrier geometry . . . . .	94
8.4	Analytical proof of component strength . . . . .	94
8.4.1	General . . . . .	94
8.4.2	Multiple field rope equation . . . . .	95
8.4.3	ROCCO ring net . . . . .	97
8.4.4	Support ropes . . . . .	98
8.4.5	Brake element . . . . .	98
8.4.6	Lateral rope . . . . .	99
8.4.7	Retaining rope . . . . .	99
8.4.8	Support posts . . . . .	101
8.4.9	Post foundation . . . . .	103
<b>9</b>	<b>Research gaps</b>	<b>105</b>
9.1	General . . . . .	105
9.2	Flexible net barriers and slush flows . . . . .	105
9.2.1	Fluid-structure interaction . . . . .	106
9.2.2	Slush flow dynamics . . . . .	109
9.2.3	Stabilising effect of the net barriers against slush flow release . . . . .	110
9.2.4	Snow accumulation around the barriers . . . . .	110
9.2.5	Avalanche protection dams hit by slush flows . . . . .	111
9.3	Snow supporting structures and snow pressure forces . . . . .	111
9.3.1	Snow creep and glide . . . . .	111
9.3.2	Downslope inclination of supporting surface . . . . .	112
9.3.3	Snow drift around support structures on Sukkertoppen . . . . .	113
9.4	Discussion . . . . .	113
<b>10</b>	<b>Conclusion and further work</b>	<b>115</b>
	<b>References</b>	<b>117</b>
	<b>Appendix</b>	<b>127</b>
A	System drawing of Flexible Net Barrier Nr. 10 - Geobruigg AS . . . . .	127



# Abbreviations

**CASN** Circum - Arctic Slushflow Network.

**EAWS** European Avalanche Warning Services.

**Eurocode 0** EN 1990, Eurocode: Basis of structural design.

**Eurocode 1** EN 1991, Eurocode 1: Actions on structures.

**Eurocode 2** En 1992, Eurocode 2: Design of concrete structures.

**Eurocode 3** EN 1993, Eurocode 3: Design of steel structures.

**Eurocode 5** EN 1995, Eurocode 5: Design of timber structures.

**Eurocode 7** EN 1997, Eurocode 7: Geotechnical design.

**Eurocode 9** EN 1999, Design of aluminium structures.

**Fap2D** Frame analysis program - 2D.

**Geobrugg** Geobrugg AG.

**HNIT** HNIT verkfræðistofa (consulting engineers).

**IACS** International Association of Cryospheric Sciences.

**ICSI** International Commission on Snow and Ice.

**LL** Longyearbyen Lokalstyre (en. Longyearbyen Community Council).

**NGI** Norges Geotekniske Institutt (en. Norwegian Geotechnical Institute).

**NPRA** Statens vegvesen (en. the Norwegian Public Roads Administration).

**NTNU** Norges teknisk-naturvitenskapelige universitet (en. Norwegian University of Science and Technology).

**NVE** Norges vassdrags- og energidirektorat (en. The Norwegian Water Resources and Energy Directorate).

**ONR 24805 - 24807** *Permanent technical avalanche protection standards* [1].

**OPM** Oppmålsteknisk prosjektering (en. Terrain survey).

**Rambøll** Rambøll Norge A/S.

**RAMMS** Rapid Mass Movement Simulation.

**RIB** Rådgivende Ingeniør Byggeteknikk.

**RISK** Rådgivende innen skred og kartlegging (en. Hazard assessment and premises).

**SIA** Swiss Engineering and Architecture Association.

**Skred** Skred AS.

**SLF** WSL Institute for Snow and Avalanche Research.

**SLTS** Snow Load Testing System.

**Swiss Guideline** SLF guideline, *Defense structures in avalanche starting zones* [2].

**TEK17** Byggteknisk forskrift (en. Regulations on technical requirements for construction works).

**this author** Haldis Døvle Kalland, [NTNU](#).

**UNESCO** United Nations Educational, Scientific and Cultural Organization.

**UNIS** The University Centre in Svalbard.

**WSL** Swiss Federal Research Institute.



# Chapter 1

## Introduction

Gravitational natural hazards such as avalanches and debris flows constitute a considerable threat to human lives and infrastructure in mountainous regions. Due to its topography, geology, and climate, Norway has numerous such regions that are frequently afflicted by avalanches and debris flows, and with climate change these hazards have become more frequent. Therefore, many people live in areas that are exposed to risk. In 2021, the Norwegian Government suggested that 720 million NOK should be appropriated to the The Norwegian Water Resources and Energy Directorate (NVE) for flood and avalanche mitigation [3]. The government stated that there is a great need for protection against floods and avalanches across the country, and that they will increase the pace of the mitigation work.

Motivated by the extensive mitigation construction works at several sites in Norway, the Department of Structural Engineering at the Norwegian University of Science and Technology (NTNU) have decided to expand their research within the field of structural mitigation measures to include avalanches, debris flows and rock falls. The department is experienced within the field of structural design, calculating load actions, and modelling fluid-structure interaction, and structural mitigation against avalanches and debris flows is therefore a natural expansion of the research field.

To initiate this work, the Department of Structural Engineering advertised a vacancy for a PhD Candidate to focus protection structures, and that vacancy will be filled by [this author](#) starting August 2022. The present master thesis is a small introduction to the field. Its purpose was to gather literature and get an overview of the field, and to map where future research projects can contribute most to the field of structural avalanche protection. In additions, an objective of the thesis has been to collect material and obtain a theoretical foundation on avalanches, avalanche protective structures, snow pressures, and load actions from avalanches.



*Figure 1.1: Picture of a slush avalanche (special type of wet-snow avalanche) that released on March 17<sup>th</sup> 2011 in the valley Todalen, close to Svalbard's main settlement Longyearbyen. Source: Eckerstorfer [4]. Photo: Markus Eckerstorfer.*

In this thesis, a literature review of snow, avalanches, and avalanche mitigation methods has been performed. [Chapter 2](#) studies the formation of snow crystals, wind transport of snow, the evolution of the snowpack, deformation of the snowpack in sloped terrain, and the mechanical and physical properties of the snowpack. If a structure hinders deformations in the snowpack, it can experience great snow pressure loads. [Chapter 3](#) examines different models used to describe these loads when they act against snow supporting structures. [Chapter 4](#) presents definitions of different avalanche types and how they are commonly classified. The purpose of categorising avalanches is to create a condensed system for describing avalanche characteristics. The dynamic modelling of avalanches is discussed in [Chapter 5](#), and common models used to estimate avalanche speed, runout distance, and impact pressures are presented. [Chapter 6](#) gives a general overview of common mitigation measures used to protect against avalanches.

In Longyearbyen, Svalbard, higher temperatures, more rain and periods of mild weather in midwinter increase the risk of debris flows, avalanches and a special type of wet-snow avalanche called slush flows [5, p. 5]. A picture of a slush flow that released near Longyearbyen in 2011 is shown in [Figure 1.1](#). During the work with this thesis, a research trip was conducted studying avalanche related structures near Longyearbyen. The conducted field work and results are presented in [Chapter 7](#). The field work included examining the constructed avalanche mitigation measures near Longyearbyen and considering possible research projects related to those measures, such as where to place instruments and test structures. Measurements were also conducted around an experimental [Snow Load Testing System](#). In [Chapter 8](#), the design and dimensioning of a slush flow mitigation project near Longyearbyen, using flexible debris flow barriers, is presented in detail. The goal is to reproduce and understand the applied concepts of the design, not to propose alternative or better solutions. Finally, [Chapter 9](#) assembles all research gaps that have been found during the work with this thesis, and suggests future research projects related to structural avalanche protection.

# Chapter 2

## Snow formation and properties of the snowpack

### 2.1 General

This chapter studies snow formation and the snowpacks properties for the purpose of understanding why and how avalanches form. When studying avalanche protective structures and the loads acting on them, an important factor in finding the correct load is to have proper knowledge about snow as a material and the properties of the snowpack. To obtain this knowledge, a literature study has been carried out studying the formation of snow, the evolution of the snowpack, the physical and mechanical properties of snow, and the deformation of the snowpack in sloped terrain. In addition, the goal is to have a more thorough knowledge about the physical processes in the snowpack to better understand why avalanches happens and thereby how we can protect against them.

There are several sources in the literature that discuss the physical properties of snow in relation to avalanches. D. McClung and Schaerer [6] give information on avalanches to anyone who may be involved with snow safety on a personal or professional level. Lied and Kristensen [7] is an equivalent book in Norwegian, though somewhat less comprehensive, written in correspondence with the NGI. Rudolf-Miklau et al. [8] is a comprehensive technical handbook covering the engineering of technical avalanche protection, and includes the fundamentals of avalanche formation. In addition, Vegdirektoratet [9] includes the properties of the snowpack in their handbook covering roads and avalanches, and Arenson et al. [10] is a full chapter in the book *Snow and Ice-Related Hazards, Risks, and Disasters* covering *Physical, Thermal, and Mechanical Properties of Snow, Ice, and Permafrost*.

This chapter will first review the formation of snow in the atmosphere, the snow crystal shapes, and the effects on the snow cover caused by wind and solar radiation. After that, the process where deposited snow changes its grain structure (called metamorphism) will be outlined, followed by a discussion of some physical and mechanical properties of the snowpack. Finally, the components of snowpack deformation and how they influence the stress distribution in the snowpack will be studied.

### 2.2 Formation and evolution of the snowpack

An important term that will be used a lot throughout this thesis is the *snowpack*. The term is often used interchangeably with *snow cover*, but have a slightly different meaning. USACE Hydrologic Engineering Center [11] explains this nuance well: "*The term snowpack is used when referring to the physical and mechanical properties of the snow on the ground. The term snow cover is used when referring to the snow accumulation on ground, and in particular, the areal extent of the snow-covered ground.*" As an engineer designing structural avalanche protection it is the *snowpack* that is of main interest, but knowing where the snow accumulates and the extent of the snow cover must also be considered.

#### 2.2.1 Snow formation in the atmosphere

Knowledge about the formation and growth of snow crystals in the atmosphere is important when studying avalanches. By observing the falling crystals, such as their shape and how they sparkle, one can gain valuable insight about the forming snowpack. For example, both graupel particles (created from riming) and stellar crystals can form weak layers in the snowpack when covered [6, p. 46]. However, this knowledge should always be combined with other factors, such as wind transport

of snow, when evaluating the stability of the snowpack. D. McClung and Schaerer [6], Lied and Kristensen [7] and Vegdirektoratet [9] all give thorough explanations on the formation and growth of snow crystals in the atmosphere, and a short summary of these will be presented here.

Snow crystals are formed in air that is supersaturated with water vapour. The amount of water required to reach saturation is dependent on the temperature, and warm air can contain more water than cold air. Therefore, the most common cause of precipitation is that warm air is forced to higher altitudes where it cools and the water vapour condenses [7, p. 39].

In supersaturated air, water droplets form by condensation on condensation nuclei while snow crystals form on freezing nuclei. Condensation and freezing nuclei are both small particle types that float in the air, but freezing nuclei have a different chemical composition that allow ice crystals to form from water vapour directly (sublimation). Without these nuclei, ice crystals would not have formed unless the temperature fell as low as  $-41^{\circ}\text{C}$ .

After an ice crystal has formed, it grows by direct transfer of water-vapour molecules from the supercooled water droplets in the sky. This phenomenon is driven by a difference in vapour pressure between the water droplets and the ice crystals, meaning that the vapour pressure over the droplet is higher than over the ice crystal [6, p. 44]. The water droplets will therefore release water-vapour molecules to the atmosphere, which will freeze on an ice crystal so that the crystal grows.

Ice crystals can also grow by having two or more crystals collide with each other, or through a process called riming. Riming occurs when the ice crystals fall through the atmosphere and collide with larger, supercooled water droplets. The droplets freeze onto the crystals and thereby add to the crystals weight.

### 2.2.2 Snow crystal shapes

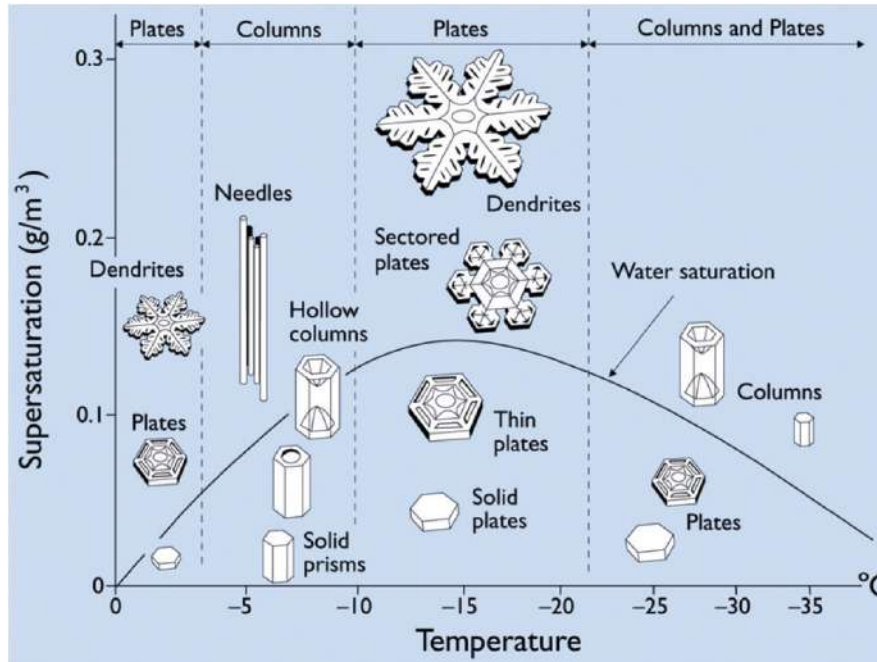
Air temperature is the most important variable influencing the ultimate form of a snow crystal, but the process of an ice crystal forming is complicated and also influenced by the amount of water vapour in the air [7, p. 40]. The crystal shapes dependence on air temperature and saturation is often summarised in a Nakaya morphology diagram, as seen in [Figure 2.1](#) [12].

The growth of a snow crystal mainly occur in two directions: in the basal plane (along three axes named a-axes) or perpendicular to the basal plane (along the c-axis) [6, p. 45]. An illustration of these axes are shown in [Figure 2.2](#). Growth in the direction along the a-axis result in plates and dendrites while growth along the c-axis result in needles and columns. The basal plane give the crystals their characteristic hexagonal symmetry.

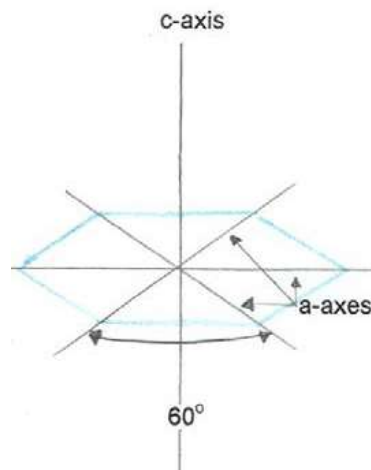
According to D. McClung and Schaerer [6] and Lied and Kristensen [7], the size of the snow crystals are mainly influenced by air temperature. At low temperatures, the rate at which crystals gain mass occur slower than at higher temperatures. This leads to smaller crystals at cold temperature and bigger crystals at temperatures around  $0^{\circ}\text{C}$ . However, Libbrecht [12] illustrates the complexity of the crystal growth rate, and suggest that the biggest dendrites occur at high saturation and temperatures around  $-15^{\circ}$ .

The [International Commission on Snow and Ice \(ICSI\)](#) classification system is an internationally used system for categorising crystals [14] (see [Figure 2.3](#)). Its first level of classification is the grain forms, where new snow is denoted with a + symbol. This is the simplest way of categorising the snow, and is often used by avalanche workers. The second level of the ICSI system classifies each grain form into categories, including new snow crystals into eight categories where five are crystals and three are particles. The first and second level of classification is presented in [Figure 2.3](#) [14, 15].





**Figure 2.1:** The Nakaya snow crystal morphology diagram, showing different types of snow crystals that grow in air at atmospheric pressure, as a function of temperature and water vapour supersaturation relative to ice. The water saturation line gives the supersaturation of supercooled water, as might be found within a dense cloud. Note that the morphology switches from plates ( $T \approx -2^\circ\text{C}$ ) to columns ( $T \approx -5^\circ\text{C}$ ) to plates ( $T \approx -15^\circ\text{C}$ ) to predominantly columns ( $T < -30^\circ\text{C}$ ) as temperature is decreased. Temperature mainly determines whether snow crystals will grow into plates or columns, while higher supersaturations generally produce more complex structures. Source: Libbrecht [12].



**Figure 2.2:** The two directions along which snow crystal growth mainly occur: In the basal plane (along the three a-axes) or perpendicular to the basal plane (along the c-axis). Source: International Ski and Snowboard Federation (FIS) [13].

### KORNFORMER (GRAIN FORMS)



a)

Basic classification	Subclass	Shape	Code	Place of formation	Physical process
<b>Precipitation Particles</b> +	Columns	Prismatic crystal, solid or hollow	<b>PP</b> PPco	Cloud; temperature inversion layer (clear sky)	Growth from water vapour at -3 to -8°C and below -30°C
	Needles	Needle-like, approximately cylindrical	PPnd	Cloud	Growth from water vapour at high super-saturation at -3 to -5°C and below -60°C
	Plates	Plate-like, mostly hexagonal	PPpl	Cloud; temperature inversion layer (clear sky)	Growth from water vapour at 0 to -3°C and -8 to -70°C
	Stellars, Dendrites	Six-fold star-like, planar or spatial	PPsd	Cloud; temperature inversion layer (clear sky)	Growth from water vapour at high supersaturation at 0 to -3°C and at -12 to -16°C
	Irregular crystals	Clusters of very small crystals	PPir	Cloud	Polycrystals growing in varying environmental conditions
	Graupel	Heavily rimed particles, spherical, conical, hexagonal or irregular in shape	PPgp	Cloud	Heavy riming of particles by accretion of supercooled water droplet Size: ≤5 mm
	Hail	Laminar internal structure, translucent or milky glazed surface	PPhl	Cloud	Growth by accretion of supercooled water Size: >5 mm
	Ice pellets	Transparent, mostly small spheroids	PPip	Cloud	Freezing of raindrops or refreezing of largely melted snow crystals or snowflakes (sleet) Graupel or snow pellets encased in thin ice layer (small hail) Size: both ≤5 mm
	Rime	Irregular deposits or longer cones and needles pointing into the wind	PPrm	Onto surface as well as on freely exposed objects	Accretion of small, supercooled fog droplets frozen in place. Thin breakable crust forms on snow surface if process continues long enough

b)

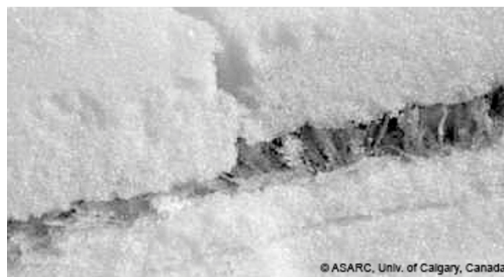
**Figure 2.3:** International Commission on Snow and Ice classification system for categorising crystals. a) First level of classification, according to grain forms. Source: Müller and H. T. Larsen [15]. b) Second level of classification, where new snow crystals are subdivided into eight shapes. Source: Fierz et al. [14].

### 2.2.3 The layering of the snowpack

To be able to evaluate avalanche danger it is necessary to have knowledge about the layering of the snowpack as the properties of the layers can be of great importance for the snowpacks stability. The snowpack is built gradually in layers, and it changes continuously. One layer of snow is a section of the snowpack that inhabit approximately the same grain structure and strength [15]. The properties of each layer depends on the weather conditions during which it was created. A period of low wind and snowfall can create one layer, while a denser and more cohesive layer can be formed from wind transported snow. Crystal conversion in the snowpack can change or create new types of layers.

A *weak layer* is a snow layer with loose structure and low shear strength. One such layer is shown in Figure 2.4. Weak layers often consist of old snow that has developed into rounded grains, faceted crystals, or depth hoar, or they can consist of surface hoar that have been buried by new snow [9, p. 24]. The development of the layers is discussed later in this chapter (Section 2.2.6). The weak layers are especially interesting because slab avalanches release after fractures in these layers [9, p. 24], and slab avalanches (see Section 4.3.1) are the most dangerous and destructive avalanches [16]. Weak layers typically fracture when the snowpack is stressed by rapid changes such as a skier, new snowfall, or wind drifted snow.

The following sections will discuss the effect of wind (2.2.4) and radiation (2.2.5) on the layering of the snowpack, while Section 2.2.6 discuss crystal conversion in the snowpack.

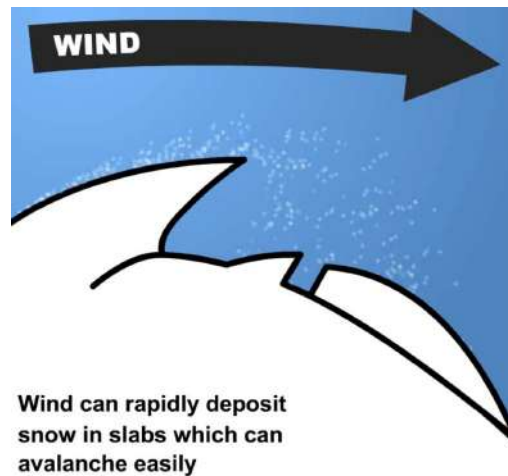


**Figure 2.4:** A weak layer of buried surface hoar that has partly collapsed (left part). Source: Solberg et al. [17]. Picture: ASARC (Applied Snow and Avalanche Research), Canada, Prof. B. Jamieson.

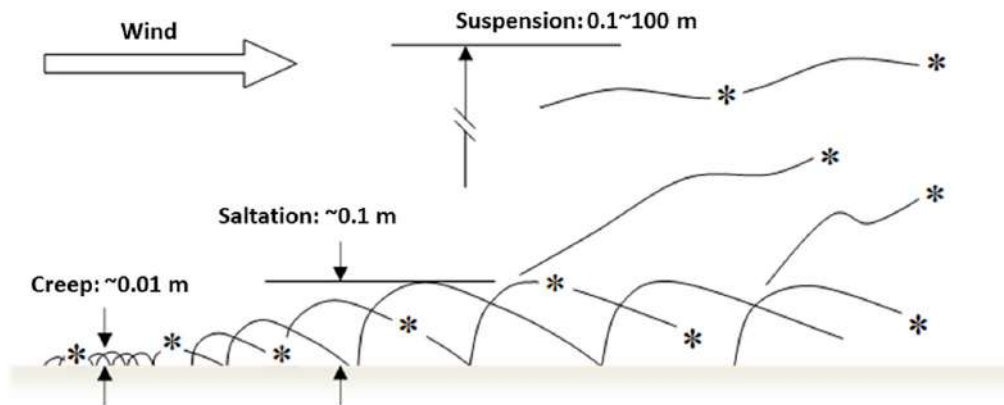
### 2.2.4 Wind transport of snow

Wind transport has a big influence on the snow cover, both with respect to the snow distribution over an area and to the structure and layering of the snowpack. In general, the wind picks up snow where wind accelerates and deposits snow where it decelerates [6, p. 30]. This acceleration and deceleration is greatly affected by local terrain features, and often lead to big deposits of snow on leeward terrain. These deposits (called wind slabs, see Figure 2.5) can lay on top of weak layers of new snow or faceted crystals, and constitutes a significant risk of slab avalanches in steep terrain [18]. If the wind drifts snow over a ridge crest where the change in slope angle is "right", a cornice can form along the crest. Cornices are formed due to the formation of vertical eddies - a reversion of air flow direction caused by a sharp break in the slope [6, pp. 31–35]. Both wind slabs and cornices consists of a tightly packed, cohesive layer of snow.

As the wind transports the snow particles, the particles are mechanically degraded as they impact the snow surface. This results in small fragments that stick together when they are deposited to form a slab. Cold, new snow can start drifting along the ground at wind speeds around  $5m/s$ , while a bounded snow cover can require wind speeds up to  $25m/s$ . This is called the threshold wind speed. Depending on how the snow is transported by the wind, its mode of transport is either called rolling, saltation or turbulent suspension. These three modes of snow particle transport are shown in Figure 2.6.



**Figure 2.5:** Illustration of a wind slab in leeward terrain right after it released as a slab avalanche. The illustration also shows a cornice above the wind slab. Source: avalanche.org [18]

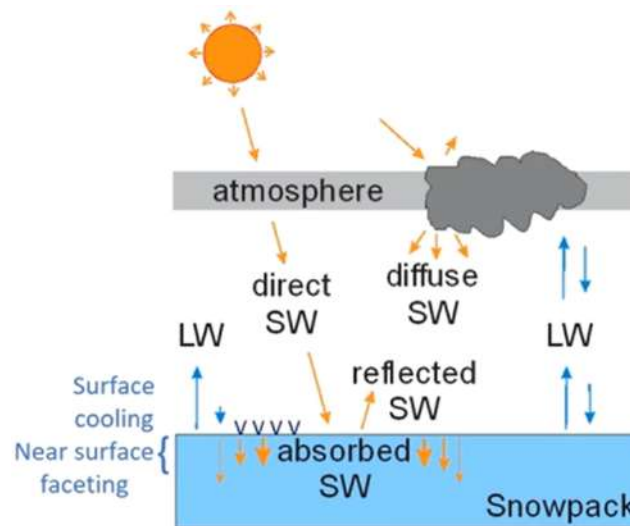


**Figure 2.6:** Three modes of snow particle transport. Source: Tominaga [19].

### 2.2.5 Heat exchange at the snow surface

Another important phenomenon that can greatly affect the structure of the snowpack is the heat transfer that occurs between the snowpack and the atmosphere. This is because heat transfer creates temperature gradients within the snowpack, which is an important factor for crystal conversions (see Section 2.2.6). In addition, heat transfer between the snow surface and the air above it can influence the snow surface and create snow crystal layers for future avalanches to glide on [7, p. 46]. An important type of heat transfer to or from the snowpack is radiation [6, 7]. Radiation influences the temperature gradient in the snowpack, and can be either short waved radiation from the sun or long waved radiation emitted from the snow surface. The energy exchange through radiation is illustrated in Figure 2.7.

Short waved radiation from the sun contains a lot of energy, and part of this radiation will be absorbed by the snowpack. How much that is absorbed is described by the snows albedo – the ratio between reflected and absorbed solar radiation (a measure of the snows "whiteness"). The short waved radiation penetrates 5 – 10cm in new snow and 20 – 25cm in old snow [7, p. 47], and the intensity of the radiation decreases exponentially with depth into the snowpack [6, p. 39]. The absorbed short waved radiation will heat the snow. This heating can lead to an increased settlement of the snowpack resulting in increased shear stresses if the terrain is sloped, and it can give and increased melt-water production. Too much melt-water can in time lead to the release of wet snow avalanches.



**Figure 2.7:** Energy exchange (heat transfer) at the snow surface through short waved (SW) and long waved (LW) radiation. Source: Jamieson [20].

The long waved radiation is a type of infrared radiation, and is emitted from the snow towards the sky. If the sky is clear then most of this radiation continues into space, which results in a cold snow surface compared to the air. However, on an overcast day most of the radiation is reflected back to earth leading to little or no temperature difference between the air and snow surface.

### 2.2.6 Crystal conversion in the snowpack - metamorphism

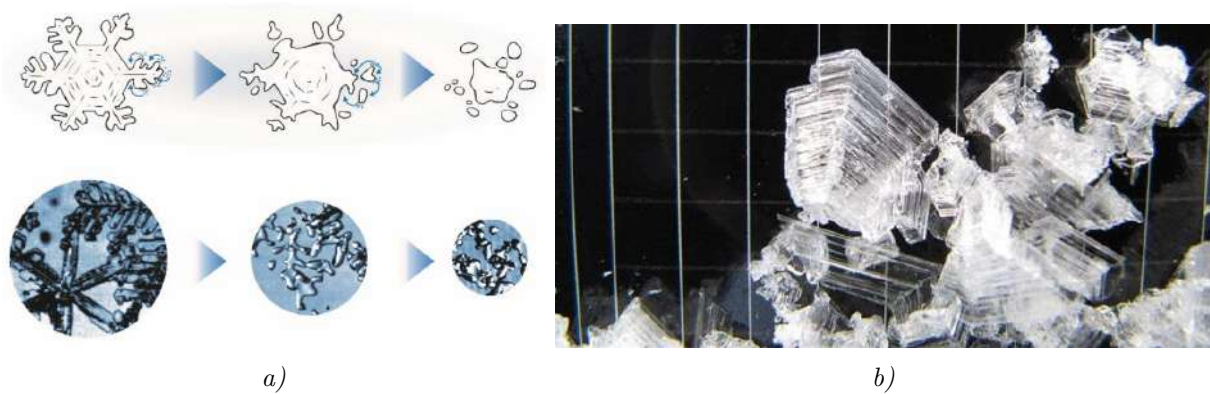
In Section 2.2.5 we mentioned that radiation can lead to temperature gradients in the snowpack, which again could lead to the formation of faceted crystals. This is an example of a crystal conversion in the snowpack, also called metamorphism. Metamorphism is defined as the process where deposited snow changes its grain structure due to varying pressure or temperature conditions [21]. It is very important when analysing the avalanche danger as it often creates weak layers. However, in this thesis it will only be discussed on a general basis. This is because the processes occurring during metamorphism are many and complicated. For a structural engineer studying avalanche mitigation it is important to be aware of metamorphism, but it is most important for experts creating avalanche forecasting and warnings.

Metamorphism causes changes in the density, structure, texture, and strength of the snowpack [22, p. 27]. Overburden pressure densifies the snowpack by rearranging the grains. However, the changes in snow crystal forms in seasonal snow are due almost entirely to heat flow within the snowpack [6, p. 55]. In non-permafrost conditions, the temperature of the snowpack near the ground is close to  $0^{\circ}\text{C}$ . When the air is cold, this sets up a temperature gradient through the snowpack, and since warm air can contain more water than cold air, water vapour moves up through the snowpack causing a net heat flux upwards [6]. This is a diffusion process that leads to growth and shrinkage of the snow crystals, and how fast the process happens is mainly dependent on the temperature gradient within the snowpack [6, 7, 22]. Steeper temperature gradients result in faster diffusion of vapour through the snowpack and thereby faster metamorphism.

Different literature categorises metamorphism into many different types of processes. Here, four different types will be presented, following Nairz et al. [22]. *Initial metamorphism* is a term used for the mechanical destruction of snow crystals and is often caused by wind and gravitation. This is the same degradation as was described under *wind transport of snow* in Section 2.2.4. *Equilibrium growth metamorphism* is a destructive vapour diffusion process where snow crystals transform from thin branched shapes into more stable and rounded ovals. The process is illustrated in Figure 2.8a.



This will first make the snowpack less stable, because the branches "hooked" the crystals together, before it makes the snow cover more dense and stable [7, 22].



**Figure 2.8:** Metamorphism. a) Equilibrium metamorphism showing how the crystals change shape from branched to rounded (Müller and H. T. Larsen [15]). b) Picture of depth hoar crystals created during faceting metamorphism (Norges Geotekniske Institutt [23]).

*Faceting* is a metamorphism process where crystals grow and create angular *faceted crystals* or cup-shaped crystals called *depth hoar*. These shapes are illustrated in Figure 2.3a and depth hoar is pictured in Figure 2.8b. Faceting is caused by the diffusion process of vapour molecules discussed in the previous paragraph. Initiated by a steep temperature gradient, vapour molecules move from the warmer snow and embed themselves on colder crystals further up. Depth hoar is stronger in compression (surface to bottom of snowpack) than in shear (parallel with the snow layers) [7]. This means that they can carry layers of new snow on top of them, but if the load is too big (for example a skier) they can collapse and lose almost all shear strength. This can release big slab avalanches. The last metamorphism process is called *melt-freeze metamorphism* and occurs when the air temperature heats to  $0^{\circ}\text{C}$ . Then the snow crystals start to melt and the free water content in the snow increases. At low water contents (under 4%), the capillary strength increases and the snowpack becomes more stable [7]. However, as the water content increases the snow becomes grainy and the cohesion between the crystals diminishes. This reduces the snow strength. Another effect during melt-freeze metamorphism is the cooling at night which can freeze the surface of the snowpack forming a hard crust [7, 22]. This crust has a load carrying capacity and therefore increases the stability of the snowpack.

The changes in the snowpack caused by metamorphism, short- and long-waved radiation is complicated, and depends on factors such as cloud cover, air humidity and temperature. Therefore, three examples of weather situations and their possible effects on the snowpack is presented below:

A thin cloud cover will allow short-waved radiation from the sun to pass through the clouds to heat the snow, while at the same time reflect the long-waved radiation from the snow back to the ground. This can lead to rapid heating of the snowpack, and the wet-snow avalanche danger may become acute [7, p. 47]. The second weather situation is when the sky is clear of clouds and the sun heats the upper region of the snow. At the same time, no clouds means that the long-waved radiation from the snow surface is not reflected back, leading to a cooled surface. This sets up a temperature gradient in the upper centimetres of the snowpack, which is the main condition necessary for *near surface faceting* [20]. Near surface faceting is a result of equilibrium metamorphism and corresponds to depth hoar. If the sky is clear at night, long-wave radiation is emitted from the snow that cools the snow surface more than the air above. If there is little wind, this sets up a temperature gradient between the surface and the air which is a necessary condition for the growth of *surface hoar* [7, 20]. Surface hoar is comparable to near surface hoar and depth hoar, but the difference is that water vapour comes from the air and not further down in the snowpack [22].

## 2.3 Physical and mechanical properties of the snowpack

### 2.3.1 Density

The density of the snowpack is an input factor in almost all calculations of snow pressure loads. It is therefore a very important snow property to have enough knowledge about when designing avalanche mitigation measures. However, the density varies greatly because it is dependent on factors such as temperature, humidity, wind conditions, and the time that have passes since deposition. There are also small discrepancies between different sources in the literature, but generally the density values given have deviated no more than  $\pm 50\text{kg}/\text{m}^3$ .

Table 2.1 compare snowpack density values for dry and wet seasonal snow as given by four different sources. The dry snow has been divided into a lower limit, corresponding to newly fallen powder snow, and an upper limit, corresponding to the tightly packed snow in wind slabs or cornices. The lower density of new, dry snow range from approximately  $10\text{kg}/\text{m}^3$  to  $100\text{kg}/\text{m}^3$  for all four sources (in Table 2.1). For older or mechanically degraded dry snow, the upper snow density range between  $550\text{kg}/\text{m}^3$  and  $600\text{kg}/\text{m}^3$ , while the wet snow density is given as  $600\text{kg}/\text{m}^3$  by D. McClung and Schaerer [6] and up to  $650\text{kg}/\text{m}^3$  by Arenson et al. [10]. D. McClung and Schaerer [6] highlights that a dry snow density of  $550\text{kg}/\text{m}^3$  is close to the density expected for a collection of ice spheres packed as close together as possible in a random fashion.

The most detailed description of snowpack density was found in Chapter 2 of the book *Snow and Ice-Related Hazards, Risks, and Disasters*, Arenson et al. [10]. They separate between snow accumulating in a continental environment (such as the Alps) and a maritime environment (more common in Norway). Continental climate generally have a lower snow density than maritime climates. Both these values given by Arenson et al. [10] are presented in Table 2.1.

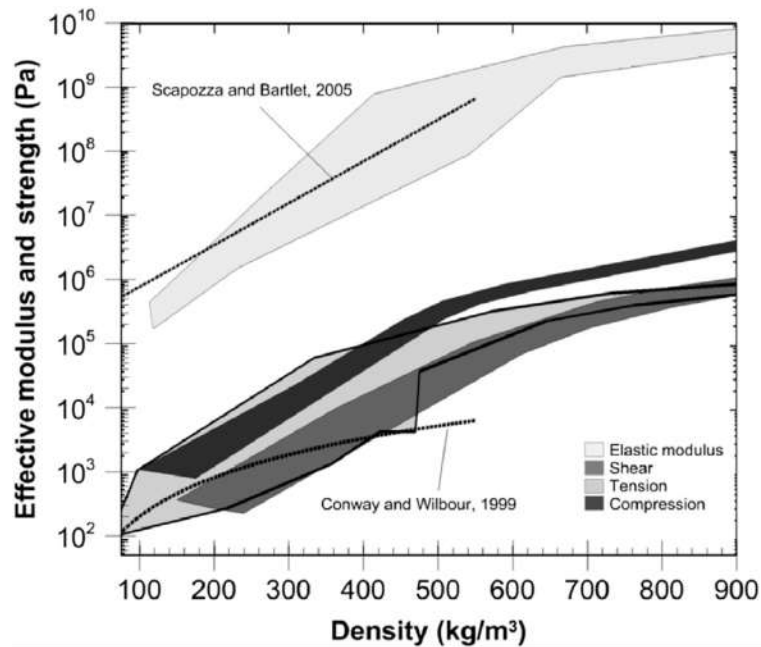
Margreth [2] (Swiss Guideline) is a Swiss guideline for calculating snow pressures against snow supporting structures, and it will be described in detail in Section 3.3.4. The guidelines have been developed based on Alpine conditions, and use a snow density dependent on elevation above sea level. The snow density  $270\text{kg}/\text{m}^3$  is used for an elevation up to  $1500\text{m}$ , and after that the density is increased by 2% every  $100\text{m}$  until a  $3000\text{m}$  elevation is reached. The guideline also gives procedures for calculating snow pressure where the snowpack density is not dependent on the elevation. No recommended snow density was found for these procedures, but they do give approximate values of a creep factor  $K$  that is dependent on snow density. The maximum snow density used in calculating this creep factor is  $600\text{kg}/\text{m}^3$ .

**Table 2.1:** Comparison of snowpack density as given by four different sources. Text in parenthesis are noted from the given source. Densities are given with unit  $[\text{kg}/\text{m}^3]$ .

Snow type / Source	Snow density of dry seasonal snow		Snow density of wet seasonal snow
	Lower limit	Upper limit	
McClung and Schaerer [6]	30 (very low value for newly fallen snow)	550	600 (bottom of spring snowpack)
Lied and Kristensen [7]	10 – 100 (300 after snow has settled)	500 (wind slab maritime climate) 300-400 (old snow) 500-600 (old snow, big snow height)	- -
Arenson et al. [10]	10 – 100 (continental climate) 100 – 300 (maritime climate)	200 – 550	400 – 650
Margreth [2] (Swiss Guideline)	Not relevant for design load calculations	270 (alpine climate up to 1500m elevation, altitude factor) 600 (from creep factor as a function of density)	

### 2.3.2 Snow strength

The mechanical properties of snow is greatly dependent on it's grain structure, temperature, and density. Since both the grain structure and density can change rapidly during metamorphism, so can the strength of snow [10]. This is illustrated in Figure 2.9, where the elastic modulus, shear strength, tensile strength, and compressive strength of snow is given as a function of density. For each density, several values of each property can be found, mainly because of varying grain structures.



**Figure 2.9:** Elastic modulus, shear strength, tensile strength, and compressive strength of snow given as a function of density. The shaded regions indicate the range of measurements in the literature. Source: Arenson et al. [10].

A snow strength property that determines what *type* of avalanche that will occur (at failure) is the *cohesion* [6, p. 84]. Cohesion describes how well the snow grains are bonded together. It depends on the bond strength between the snow grains and crystals, on the shape of the grains, and on the snow density. Snow in a cornice or snow slab consist of very cohesive snow, and will likely cause slab avalanches. Loose snow avalanches are formed from snow with low cohesion [6]. Different avalanche types will be further discussed in Chapter 4.



**Figure 2.10:** Viscous movement of spring snow gliding down a roof and folding in the roof gutter. Cohesive properties are also shown by the fold hanging over the edge. Photo: Haldis Døvlø Kalland.



Snow can be described as a viscous material [6, 10] that becomes brittle under high deformation velocities (strain rates) [22]. If the snowpack is stressed slowly, it will float as a viscous material. However, if the loading is quick it will react linear-elastically until its strength is exceeded and brittle failure occur. The strain rate where the response change from viscous to linear-elastic depends on density, microstructure, and temperature [10]. An example of viscous movement of snow is shown in Figure 2.10, where spring snow glide down a smooth roof and folds in the roof gutter. It also illustrate the cohesive properties of snow by one fold hanging over the roof gutter.

Snow shear strength is important for slope stability, and is often modelled by Mohr-Coulombs failure criterion given by Equation 2.1 [7, 9]. An illustration is given in Figure 2.11 ("skjærfasthet"=resisting shear stress).

$$\tau_f = c + \mu\sigma = c + \mu\rho gz \cdot \cos \alpha \quad (2.1)$$

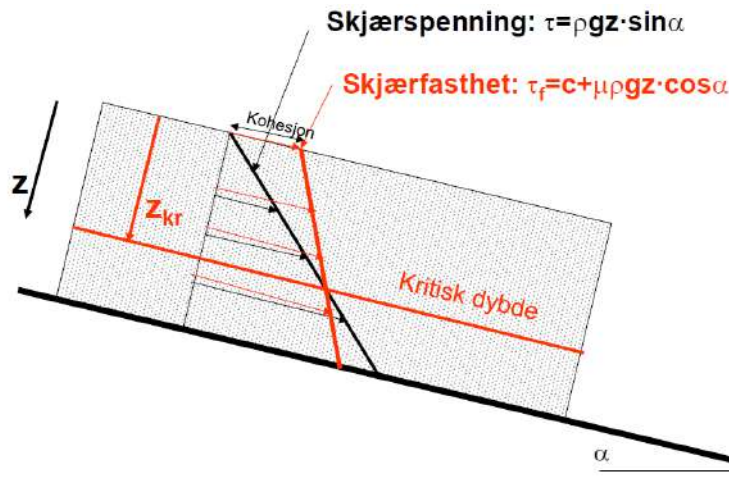
The criterion describes the shear strength in a snow layer,  $\tau_f$ , as a combination of the cohesion  $c$  and friction  $\mu\sigma$ , where  $\mu$  is the static friction coefficient and  $\sigma = \rho gz \cos \alpha$  is the normal stress at depth  $z$ . The angle  $\alpha$  is the slope inclination.

The *acting* shear stress  $\tau$  at a given depth  $z$  in a snow volume is determined from the weight force ( $W$ ) component acting in the direction down the slope ( $W \cdot \sin \alpha$ ). This stress is shown in Figure 2.11 as "skjærspenning", and will increase linearly with depth  $z$  according to Equation 2.2.

$$\tau = \frac{W \cdot \sin \alpha}{A} = \frac{\rho V g}{A} \cdot \sin \alpha = \rho g z \cdot \sin \alpha \quad (2.2)$$

Here  $V$  is the volume of the studied snow, and  $A$  is the snow cover area over which this snow volume spreads. Failure occurs and the snow slides when the acting shear stress in the snowpack equals the resisting shear stress (shear strength). This will occur at depth  $z_{kr}$  given by Equation 2.3 [9].

$$z_{kr} = \frac{c}{\rho g \cdot (\sin \alpha - \mu \cdot \cos \alpha)} \quad (2.3)$$



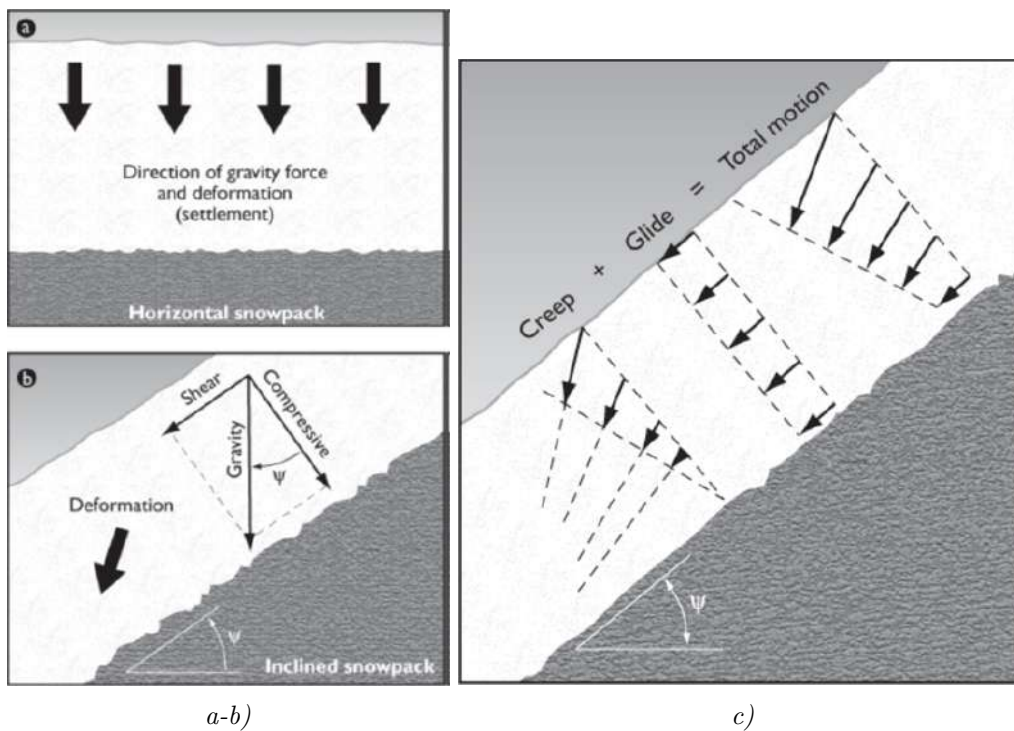
**Figure 2.11:** Acting shear stress ("skjærspenning") and resisting shear stress ("skjærfasthet") of a homogeneous snow cover. Failure occur at a critical depth ("kritisk dybde") where Source: Vegdirektoratet [9].

## 2.4 Deformation of the snowpack in sloped terrain

Creep and glide in the snowpack are the main reasons why structures built in steep slopes experience quasi-static load actions from the snow (i.e., *snow pressures* which will be described in detail in the following chapter). To fully understand these load actions it is therefore important to understand what creep and glide is, and why they occur.

### 2.4.1 Creep

The snowpack will continuously *settle* due to gravitational forces, metamorphism, and porosity. This causes a densification of the snowpack, and is illustrated in Figure 2.12a. The snow settles fastest in new snow where the porosity is high and the snow crystals can move around each other more easily [7]. Since the porosity is higher close to the surface of the snowpack, this is where the settling happens fastest. If the snow lays in an inclined slope, a component of the gravitational force will act in a direction parallel to the slope (down the slope). This is also illustrated in Figure 2.12. The settling snowpack will therefore move down the slope. This motion is called *creep*, and its intensity will increase with steeper slopes, thicker snowpack, and closer to the surface [22, p. 31].



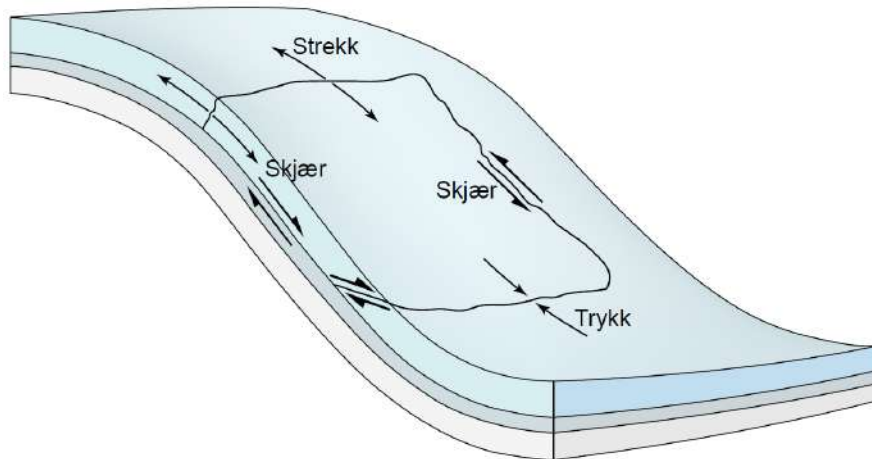
**Figure 2.12:** Deformation components of the snowpack. a) Settlement on horizontal ground and b) gravitational forces pulling the snow down the slope on inclined ground. c) Creep and glide deformation in the snowpack. Source: D. McClung and Schaerer [6].

### 2.4.2 Glide

Creep is defined to be zero by the ground and increasing up to the surface. However, if the entire snowpack moves parallel to the ground this is called *glide*. An illustration of glide is shown (together with creep) in Figure 2.12. In Norway, the snow cover generally sticks well to the ground surface and glide is mainly only observed along smooth surfaces such as bare rock-face and grass-covered hills [7, 9]. Glide is low in dry snow (high interface friction), and generally increase as the amount of water at and near the ground increase [6].

### 2.4.3 Stress distribution in the snowpack

Creep and glide movements may result in increasing or decreasing stresses in the snowpack [22]. However, the snowpack will only experience stress-differences in the plane parallel to the ground if it either lays on sloped ground with varying steepness, if the thickness of the snow cover varies, or if the terrain hinders part the snow from creeping [9]. Figure 2.13 shows how shear, tension and compression stresses may be distributed in a snow slab laying in sloped terrain [7, p. 59]. In the top-part, where the terrain changes from gentle till steeper slope, the snow will experience tension stresses because of increased creep and glide (with increasing slope inclination). Shear forces will be dominating in the steeper area, while pressure forces occur at the bottom of the hill because of decreasing creep and glide velocity.



**Figure 2.13:** Stress distribution in a snow slab laying in inclined terrain. English translation: "Strekk"=tension, "skjær"=shear, "trykk"=compression. Source: Lied and Kristensen [7]



# Chapter 3

## Static snow pressure and modelling

### 3.1 General

Structures on hills or mountain slopes with deep snow cover can experience great pressure loads if they interrupt the snowpack's deformation of creep or glide. This pressure load is called a *static snow pressure* and acts in the direction normal to the slopes contour lines. In an area up-slope of the structure, the support from the structure will reduce shear stresses in the snowpack and build up compressive stresses [24, p. 185] causing a so called *back-pressure zone* (also acting in the direction normal to the slope contour lines). This creation of a back-pressure zone is the physical phenomenon that is exploited by snow supporting structures.

Snow supporting structures are avalanche mitigation measures built in avalanche starting zones. An avalanche starting zone is an area in which it is expected that an avalanche can release. The task of snow supporting structures is to limit the snowpacks movements so much that it is harmless [24, p. 179]. By limiting the snowpacks movements, they hinder or limit shear- and tension fractures and thereby prevent big avalanches from releasing. The snow supporting structures will be discussed further in Section 6.3.1, but the modelling of the static snow pressure against them will be discussed here.

In order to design snow supporting structures it is necessary to estimate the magnitude of the snow pressure load acting on them. An example of a snow supporting structure that experienced a higher snow pressure than it was designed for is shown in Figure 3.1. Today there are several sources that give guidelines on how snow pressure can be calculated, but the most widely used is the SLF guideline, *Defense structures in avalanche starting zones* [2] (Swiss Guideline). Some countries have made adaptations to this guideline, and among them are Norway and Iceland. Most snow pressure models today are empirically based and have derived their analytical background for modelling snow pressure from analysing the actions on snow supporting structures [24, p. 185].

This chapter presents the normative basis used in designing technical avalanche protection systems, studies how various sources model snow pressure (with extra focus on the Swiss Guideline), and describes what models are being used in Norway and Iceland today.



**Figure 3.1:** Snow supporting structure with buckled supports at the end of the structure line, Valais, Switzerland. Source: Margreth [25]. Photo: Nivalp SA (2018).

## 3.2 Normative basis of design

The Eurocode construction engineering standards are the normative basis of design for technical avalanche control systems in Europe [24, p. 177]. The most important Eurocodes for the design and construction of avalanche mitigation structures are listed below [24, p. 178]. Eurocode 0 regulates the framework of the structural planning and is intended used in combination with the other Eurocodes, while Eurocode 1 provides information on the actions that should be considered in the design of civil engineering works [26]. Eurocode 2 to Eurocode 9 are standards covering individual construction types.

- EN 1990, Eurocode: Basis of structural design (Eurocode 0)
- EN 1991, Eurocode 1: Actions on structures (Eurocode 1)
- EN 1992, Eurocode 2: Design of concrete structures (Eurocode 2)
  - EN 1992-1-1: General rules and rules for buildings
  - EN 1992-3: Liquid retaining and containment structures
- EN 1993, Eurocode 3: Design of steel structures (Eurocode 3)
  - EN 1993-1-1: General rules and rules for buildings
  - EN 1993-1-8: Design of joints
  - EN 1993-1-11: Design of structures with tension components
- EN 1995, Eurocode 5: Design of timber structures (Eurocode 5)
  - EN 1995-1-1: General - Common rules and rules for buildings
- EN 1997, Eurocode 7: Geotechnical design (Eurocode 7)
  - EN 1997-1: General rules

The standards state that when designing special buildings, such as landslide protection measures, other measures than those covered by the standards may be required [27, p. 9]. In addition, the use of other standards, regulations or guidelines is allowed. One such guideline is the previously mentioned SLF guideline, *Defense structures in avalanche starting zones* [2], which is the most commonly used guideline for assessing snow supporting structures. Austria has their own series of standards for assessing and constructing snow supporting structures called the *Permanent technical avalanche protection standards* [1] (ONR 24805 - 24807), which are published by the Austrian Standards Institute. In Switzerland the SIA structural standards (Swiss Engineering and Architecture Association) are used [28].

When assessing technical avalanche control systems in Norway, no specific national standards are available [8, p. VI]. However, the Eurocodes with their national appendices (NA) are followed, in addition to (but not limited to) the documents listed below.

- SLF guideline, *Defense structures in avalanche starting zones* [2]
- Byggteknisk forskrift (en. Regulations on technical requirements for construction works) [29]
  - §7. Protection against acts of nature
  - §10. Structural safety
- NVE Guidelines for assessing safety against avalanches in steep terrain [30]
- *Permanent technical avalanche protection standards* [1] (ONR 24805 - 24807)
- Swiss Engineering and Architecture Association (SIA) structural standards [28]
- Statens vegvesen (en. the Norwegian Public Roads Administration) handbooks
  - Håndbok V137 - Veger og drivsnø (roads and drifting snow) [31]
  - Håndbok V138 - Veger og snøskred (roads and avalanches) [9]
  - Håndbok V139 - Flom- og sørpeskred (flood- and slush flows) [32]
- Avalanche protection and anchorage in permafrost. Case: Arctic regions - Longyearbyen, Svalbard [33]

### 3.3 Models for calculating snow pressure

#### 3.3.1 Snow as a rigid material

A very simplified model for calculating snow pressure is modelling the snow as a rigid material. This model is not used to calculate snow pressure against avalanche snow supporting structures, but is used in Eurocode 1 to calculate the snow load against snowguards on roofs (Figure 3.2).

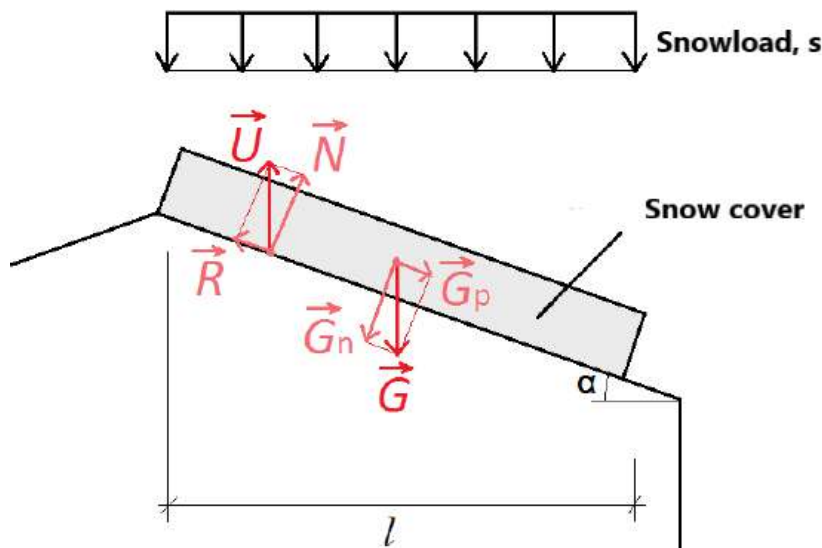
The snow cover gliding down a pitched roof is modelled as a rigid material in Eurocode 1, NS-EN 1991-1-3:2003+A1:2015+NA:2018. The coefficient of friction between the roof and snow is assumed to be zero, and therefore the only external forces acting on the snow in the direction of slope is the parallel component of the gravitational force  $G = mg$  and the supporting force from the snow guard. The load  $G_p$  exerted by the snow on a snowguard at the roof edge is then calculated according to Equation 3.1.

$$G_p = m \cdot g \cdot \sin\alpha \quad [\text{kN}] \quad (3.1)$$

Here  $m$  is the mass of the snow on the roof,  $g$  is the gravitational acceleration, and  $\alpha$  is the slope gradient of the roof. An illustration of the model is given in Figure 3.2. Snow load is usually given as a pressure over area, and therefore Equation 3.1 can be written as

$$G_p = s \cdot l \cdot \sin\alpha. \quad [\text{kN/m}] \quad (3.2)$$

Here  $G_p$  (p = parallel) is the force in the direction of slope per unit length of the building,  $s$  is the snow load in  $[\text{kN/m}^2]$ , length  $l$  is the horizontal length of the snowpack on the roof in the direction of slide.



**Figure 3.2:** Snow cover modelled as a rigid material acting with a distributed vertical load  $s$  and snow pressure  $G_p$  against the roof snowguards. Source: Jacobsen [34].

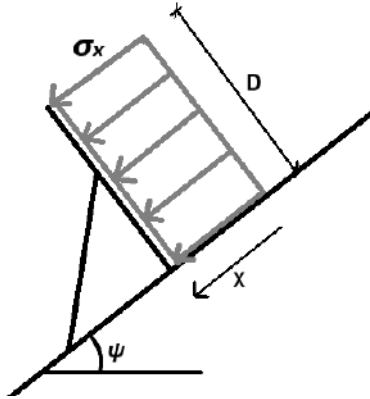


### 3.3.2 Haefeli's (1948) model

The first attempt to formulate a one-dimensional model for plane strain snow pressure was made by Haefeli [35], and his theory was developed further by Salm [36] [37]. Haefeli's model is based on the theory of the *back-pressure zone* that forms behind the snow supporting structure. It assumes that snow behaves as a linear, Newtonian viscous fluid, which is not a realistic assumption [38]. Also, his model cannot be derived using continuum mechanics, and it is not accurate in general for all slope angles and snow parameters [37, intro]. Haefeli's (1948) model describes the average creep pressure parallel to the slope  $\sigma_x$  on the supporting surface of a long rigid structure that stands perpendicular to the slope using Equation 3.3. An illustration is shown in Figure 3.3.

$$\frac{\sigma_x}{\rho g D} = \frac{2}{3} \left( \frac{1-\nu}{1-2\nu} \right)^{1/2} \tan\psi + \frac{\cos\psi}{2} \left( \frac{\nu}{1-\nu} \right) \quad (3.3)$$

Here  $\sigma_x$  is the snow pressure,  $\rho$  is the average density of the snow cover,  $g$  is the gravitational acceleration,  $D$  is the snow thickness,  $\nu$  is the viscous analog of Poisson's ratio for the Newtonian fluid, and  $\psi$  is the slope angle [38].



**Figure 3.3:** Illustration of the average creep pressure  $\sigma_x$  against a supporting surface that stands perpendicular to the slope. Figure: Haldis Kalland.

### 3.3.3 McClung's (1982) model

A continuum-mechanical model has been developed by D. M. McClung [37], where McClung reduced the plane strain problem of snow creep to a one-dimensional deformation problem by averaging quantities through the depth of the snowpack [37]. The model assumes a Newtonian viscous fluid with neglect of the static fluid pressure term, and unlike Haefeli's (1948) model it also accounts for glide [37]. D. M. McClung [37] describes the average creep pressure parallel to the slope  $\sigma_x$  on the supporting surface of a long rigid structure that stands perpendicular to the slope using Equation 3.4. This also agrees with the illustration in Figure 3.3.

$$\frac{\sigma_x}{\rho g D} = \sin\psi \left[ \left( \frac{2}{1-\nu} \right) \left( \frac{L}{D} \right) \right]^{1/2} + \frac{\cos\psi}{2} \left( \frac{\nu}{1-\nu} \right) \quad (3.4)$$

Here,  $L$  is the stagnation depth [37], and  $D$ ,  $\rho$ ,  $g$ ,  $\nu$ , and  $\psi$  are given as in Equation 3.3 [38]. The fraction  $L/D$  is given by the empirical Equation 3.5, where the cotangent  $\cot\psi = 1/(\tan\psi)$ .

$$\frac{L}{D} = 0.3 [2 \cot\psi]^{1/2} \left( \frac{1-\nu}{1-2\nu} \right)^{1/4} \quad (3.5)$$

McClung's (1982) model gives an average creep pressure that corresponds better to measured values of pressure than the model given by Haefeli (1977), but it has not been applied practically [24, p. 185]. Instead, the more conservative [Swiss Guideline](#) [2] is used in most cases.



### 3.3.4 Swiss technical guidelines

The most comprehensive and widely used literature covering the planning and dimensioning of snow supporting structures in avalanche starting zones is the Swiss technical guideline *Defense structures in avalanche starting zones* (Swiss Guideline, Margreth [2]). Margreth [2] defines the snow pressure components in line with the slope and normal to the slope, as well as end-load effects and the adaptations necessary when the support surface does not stand normal to the slope.

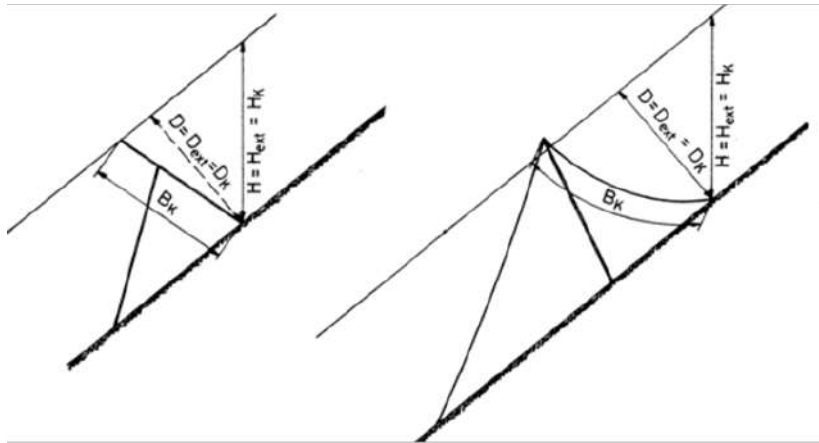
This section will first define the site factors used in the snow pressure formulas (in the *Swiss Guideline*), then presents the snow pressure formulas used to calculate snow pressure components in line with the slope, normal to the slope, and the end-effects. In the end, the resultant snow pressure force is defined.

#### Site factors

Snow pressure on a supporting structure is expressed as a function of the terms listed below [2, p. 42]. The current section will summarise the definitions of these site factors as given in Margreth [2], and the definitions will also be used in the following chapters unless otherwise stated.

- $\rho$  : average density of snow
- $H$  : vertical snow height at site of structure
- $K$  : creep factor, dependent on snow density and inclination of slope
- $N$  : glide factor, dependent on vegetation, roughness and solar exposure of the ground
- $f_c$  : altitude factor, characterising the dependency of the snow density on altitude
- $f_R$  : end-effect factor, dependent on the lateral distance between structures and on the glide factor

In the *Swiss Guideline*, the average snow density  $\rho$  is set to a uniform value of  $\rho = 0.270t/m^3$ , and then varied with altitude and slope exposure by the altitude factor  $f_c$  and the glide factor  $N$  [2, p. 42]. An increased snow density of  $\rho = 0.400t/m^3$  is used when the snow has settled. Adaptions to the density factor have been proposed by Jóhannesson and Margreth [39] for Icelandic conditions and by Nordic conditions (see Section 3.3.5).



**Figure 3.4:** Illustration of snow height, snow thickness, and structure height for grates (rigid support surface) and net. Source: Margreth [2, p. 32].

Figure 3.4 illustrates how to measure the snow height  $H$ , snow thickness  $D$ , and structure height  $B_K$  of snow supporting structures. The snow height  $H$  is measured in the vertical direction and is independent of the slope inclination when the snow fall is vertical and uniform [2, p. 28]. The snow thickness  $D$  is measured normal to the slope and is simply  $D = H \cos \psi$ , where  $\psi$  is the slope inclination. In a normal design situation, the snow height at the site of the structure  $H$  is set equal

to the structure height  $H_K$  which must be at least as great as the extreme snow height anticipated  $H_{ext}$  [2, p. 32]. The extreme snow height is the anticipated maximum snow height over a long period at the site of the structure [2, p. 28]. Note that to calculate the snow height it is recommended to observe the snow distribution in the area for several years before constructing the snow support structures [24, p. 180]. Also, because the structures change the wind field and thereby the snow distribution it is only after construction that it becomes clear whether the chosen structure height was correct [24, p. 180].

The creep factor  $K$  is a function of the snow density and the inclination of the slope. The Swiss Guideline presents common values in its Table 6, Section 4.2 (Table 3.1). To compare, Margreth et al. [24, p. 187] states that the creep factor to an extent can be calculated according to Equation 3.6.

$$K = (2.05\rho^3 - 1.86\rho^2 + 1.06\rho + 0.54) \cdot \sin(2\psi) \quad (3.6)$$

**Table 3.1:** Creep factor  $K$  as a function of average snow density ( $\rho$ ) and slope inclination ( $\psi$ ). Source: Margreth [2, p. 45].

$\rho$ [ $kg/m^3$ ]	200	300	400	500	600
$K/\sin(2\psi)$	0.7	0.76	0.83	0.92	1.05

The glide factor  $N$  is dependent on ground roughness and slope exposure, and account for the observed increase in snow pressure for easier snow glide along the ground. Margreth [2, p. 43] presents ground classes 1 to 4 in its Table 5, Section 3.10.5, and the glide factor  $N$  is given as a function of these soil classes and the slope exposure (Figure 3.5).

The altitude factor  $f_c$  accounts for the increased average snow density with increased altitude above sea level. It is not an independent factor in the snow pressure formula (Equation 3.9), but accounts for the snow density and creep factor when determining the snow pressure load in alpine climate using simplified equations (Equation 3.10). The snow pressure is set to increase with 2% per 100m at an altitude between 1500 and 3000m above sea level,

$$f_c = 1 + 0.02\left(\frac{Z}{100} - 15\right) \quad (3.7)$$

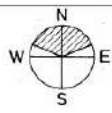
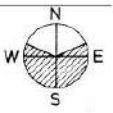
where  $Z$  is the altitude.

The end-effect factor  $f_R$  is used to calculate a supplementary load that is added at the unprotected end of the structure (see the following Subsection "End-effect forces").

### Snow pressure load case 1 and 2

Figure 3.6 illustrates a snow supporting structure experiencing load actions from the snow. These load actions will be defined in the following sections. It might be confusing that the snow load actions are drawn as forces on the figure, while the literature talks of *snow pressures*. This is because snow loads from creep and glide act as pressures over the whole supporting surface. However, when calculating the loads they are simplified as uniformly distributed over the height of the structure, and then multiplied by height. The result is a load per meter of supporting surface along the length of the structure (i.e. normal to the plane shown in Figure 3.6).

Tab. 5 > Ground classes and glide factors.

Ground classes	Glide factor	
	 Exposure WNW-N-E	 Exposure ENE-S-WNW
<b>Class 1</b>		
<ul style="list-style-type: none"> <li>• Coarse scree (<math>d^* \geq 30</math> cm)</li> <li>• Terrain heavily populated with smaller and larger boulders</li> </ul>	1.2	1.3
<b>Class 2</b>		
<ul style="list-style-type: none"> <li>• Areas covered with larger alder bushes or dwarf pine at least 1 m in height</li> <li>• Prominent mounds covered with grass and low bushes (height of mounds over 50 cm)</li> <li>• Prominent cow trails</li> <li>• Coarse scree (<math>d^*</math> ca. 10–30 cm)</li> </ul>	1.6	1.8
<b>Class 3</b>		
<ul style="list-style-type: none"> <li>• Short grass interspersed with low bushes (heather, rhododendron, bilberry, alder bushes and dwarf pine below approx. 1 m in height)</li> <li>• Fine scree (<math>d^* \leq 10</math> cm) alternating with grass and low bushes</li> <li>• Smallish mounds of up to 50 cm in height covered with grass and low bushes, and also those alternating with smooth grass and low bushes</li> <li>• Grass with shallow cow trails</li> </ul>	2.0	2.4
<b>Class 4</b>		
<ul style="list-style-type: none"> <li>• Smooth, long-bladed, compact grass cover</li> <li>• Smooth outcropping rock plates with stratification planes parallel to the slope</li> <li>• Smooth scree mixed with earth</li> <li>• Swampy depressions</li> </ul>	2.6	3.2

$d^*$  is the boulder diameter characteristic of the roughness of the ground surface.

Figure 3.5: Ground classes and glide factors as given in Margreth [2, p. 44].

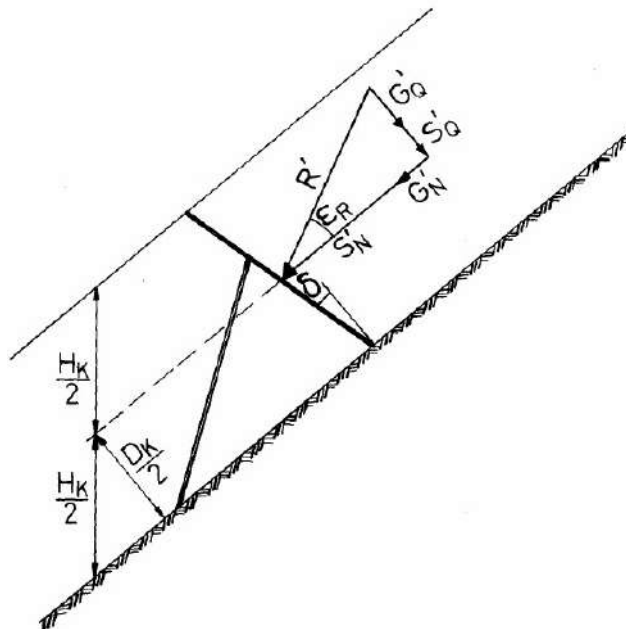


Figure 3.6: Illustration of a rigid snow supporting structure, the resultant snow load acting on it, and the resultants components. When calculating snow pressure using Equation 3.9 or Equation 3.11, the snow height  $H = H_K$ , where  $H_K$  is the structure height. Source: Margreth [2, p. 63].

The **Swiss Guideline** differentiate between a Load case 1 and a Load case 2 when dimensioning a structural system. Load case 1 assumes that the snow height is equal to the structure height ( $H = H_K$ ), which means that the whole support surface is covered in snow. Load case 2 assumes that the snow pack from Load case 1 has settled to a height  $h$  according to [Equation 3.8](#).

$$h = 0.77 \cdot H_K \quad [\text{m}] \quad (3.8)$$

This means that the resultant snow pressure force  $R'$  has the same magnitude and direction in Load case 2 as in Load case 1, but that the point of application is lower ( $h/2 = 0.385 \cdot H_K$ ) and that the snow pressure is higher (same force distributed over a lower height). Both load cases should be considered when dimensioning the structural system.

### Pressure component in line of slope

The snow pressure component in line of slope against a supporting surface  $S'_N$  can be calculated according to [Equation 3.9](#) [2]. As discussed in the previous section, the load  $S'_N$  is given per meter of supporting structure run along the contour line (line load), and is simplified as uniformly distributed across the height of the structure. The snow supporting structure is assumed to be of infinite length, and the support surface is assumed to stand perpendicular to the slope.

$$S'_N = \rho \cdot g \cdot K \cdot N \cdot \frac{H^2}{2} \quad [\text{kN/m}] \quad (3.9)$$

Density  $\rho$  is the average density of the snow cover [ $t/m^3$ ],  $g$  is the gravitational acceleration,  $K$  is the creep factor,  $N$  is the glide factor, and  $H$  is the vertical snow height. The load  $S'_N$  results from the slope parallel component of a triangularly shaped creep profile and gliding (as was illustrated in [Figure 2.12](#)).

When calculating loads on a snow supporting structure in alpine climate, [Equation 3.9](#) can be simplified to [Equation 3.10](#) [2, p. 60].

$$S'_N = H_K^2 \cdot N \cdot f_c \quad [\text{kN/m}] \quad (3.10)$$

Here  $H_K$  is the vertical structure height,  $N$  is the glide factor, and  $f_c$  is the altitude factor. [Equation 3.10](#) is derived from [Equation 3.9](#), and assumes an average snow density  $\rho = 0.270t/m^3$ , a creep factor  $K = 0.74$ , and that  $\sin(2\psi) = 1.00$  (corresponding to a slope inclination of  $45^\circ$ ).

### Pressure component normal to the slope

When the settling movement of the snowpack in front of a supporting surface is prevented by adhesion and surface roughness, an induced shear contact stress will act down along the support surface. In the literature, this load action is called a *snow pressure component normal to the slope*  $S'_Q$ . This might be a bit misleading since it is not a pressure but a shear stress, but it is a component of the resultant load acting on a support structure due to snow pressure. The direction of  $S'_Q$  is illustrated in [Figure 3.6](#).

The normal component of the snow pressure  $S'_Q$  can be calculated according to [Equation 3.11](#). As for the snow pressure component in line of slope ( $S'_N$ ), the load  $S'_Q$  is given per meter of supporting structure run along the contour line (line load), and is simplified as uniformly distributed across the height of the structure. The snow supporting structure is assumed to be of infinite length, and the support surface is assumed to stand perpendicular to the slope.

$$S'_Q = S'_N \cdot \frac{a}{N \cdot \tan(\psi)} \quad [\text{kN/m}] \quad (3.11)$$

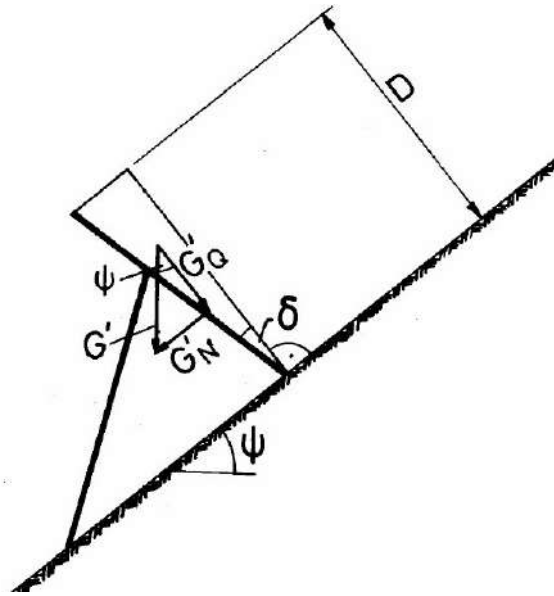
Here,  $a$  is a coefficient that depends on the compressibility of the snow type, and can vary between  $a = 0.2$  (old snow) and  $a = 0.5$  (new snow). Angle  $\psi$  is the slope gradient and  $N$  is the glide factor.

### Weight of snow prism acting on non-normal supporting surface

The [Swiss Guideline](#) recommends that rigid support structures are built with a  $\delta = 15^\circ$  inclination of the supporting surface in the down-slope direction [2, p. 58]. This angle is shown in [Figure 3.7](#). However, the snow pressure theory used to calculate  $S'_N$  and  $S'_Q$  assumes a support surface normal to the slope. This means that the horizontal and vertical components of the weight  $G'$  of a snow prism formed between the supporting surface and the plane normal to the slope must be added to the components  $S'_N$  and  $S'_Q$  ([Figure 3.7](#)). The weight of this snow prism  $G'$  per meter run along the contour line (line load) can be calculated according to [Equation 3.12](#).

$$G' = \rho \cdot g \cdot \frac{D^2}{2} \cdot \tan(\delta), \quad [\text{kN/m}] \quad (3.12)$$

Here,  $D$  is the snow thickness (normal to the slope), and  $\delta$  is the angle between the supporting surface and the normal to the slope. The components of  $G'$  in the directions parallel and normal to the slope are respectively  $G'_N = G' \cdot \sin(\psi)$  and  $G'_Q = G' \cdot \cos(\psi)$ .



**Figure 3.7:** Illustration of a rigid snow supporting structure with a non-normal supporting surface. The force resulting from the weight of the snow prism  $G'$  and its components are shown. Source: Margreth [2, p. 47].

When calculating loads on a snow supporting structure in alpine climate, the vertically acting weight of the snow prism can be calculated according to [Equation 3.13](#) [2, p. 60]. [Equation 3.13](#) is derived from [Equation 3.12](#), and assumes a somewhat higher density at the supporting surface.

$$G' = 1.50 \cdot D_K^2 \cdot \tan(\delta), \quad [\text{kN/m}] \quad (3.13)$$

Here  $D_K = H_K \cdot \cos(\psi)$  is the effective structure height (normal to the slope), and  $\delta$  is the angle between the supporting surface and the normal to the slope.

### End-effect load

As explained earlier, the snow pressure formulas until now have assumed that the support surfaces are of infinite length. However, an additional end-effect load must be taken into account when the supporting surface has a finite length. This is because the snow can flow sideways around the structure, and the sideways flow causes a restraining effect that makes the back-pressure zone extend sideways.

The end-effect load acts in the slope-parallel direction (no component calculated normal to the slope). The actual distribution of the end-effect loads on a supporting surface is a maximum load at the edges with a continuous decrease towards the middle. However in practical calculations, Margreth [2] assumes a constant end-effect pressure  $S'_R$  that acts over a length  $\Delta l$ , as illustrated in Figure 3.8. The end-effect pressure  $S'_R$  is calculated according to Equation 3.14.

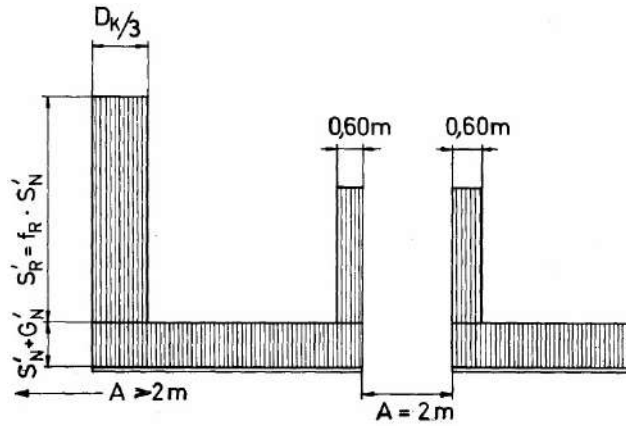
$$S'_R = f_R \cdot S'_N \quad [\text{kN/m}] \quad (3.14)$$

Here, the end-effect factor  $f_R$  is found according to Equation 3.15, and the length of applied load  $\Delta l$  according to Equation 3.16.

$$f_R = (0.92 + 0.65 \cdot N) \cdot \frac{A}{2} \leq (1.00 + 1,25 \cdot N) \quad [-] \quad (3.15)$$

$$\Delta l = 0.6 \cdot \frac{A}{2} \leq \frac{D_K}{3}. \quad [\text{m}] \quad (3.16)$$

Length  $A$  is the distance between two neighbouring support structures,  $N$  is the glide factor, and  $D_K$  is the effective support surface height. Equation 3.14 to 3.16 show that the end-effect load  $S'_R$  greatly depend on the glide factor  $N$ , in addition to the structures dimensions and placement, and the snow pressure on an infinitely long surface ( $S'_N$ ). The upper limit of Equation 3.15 and 3.16 must not be exceeded, meaning that the distance between the structures can be greater than  $2m$ , but that  $S'_R$  will never exceed  $5 \cdot S'_N$  and  $\Delta l$  will never exceed  $D_K/3$ .



**Figure 3.8:** End-effect load at the unprotected ends of a structure; a free end ( $A < 2m$ ) and a distance between structures of  $A = 2m$ . Source: Margreth [2, p. 62].

### Resulting snow pressure forces

To obtain the magnitude of the resultant snow pressure  $R'$  against an infinitely long snow supporting structure, vector addition is used of the slope-parallel and slope-vertical components (Equation 3.9, 3.11, 3.12, and 3.14).

Figure 3.6 has been repeated for better readability in Figure 3.9, and shows the resultant load for an infinitely long support surface. The resultant snow pressure  $R'$  can be calculated according to Equation 3.19.

$$R'_N = S'_N + G'_N \quad (3.17)$$

$$R'_Q = S'_Q + G'_Q \quad (3.18)$$

$$R' = \sqrt{R'^2_N + R'^2_Q} \quad [\text{kN/m}] \quad (3.19)$$



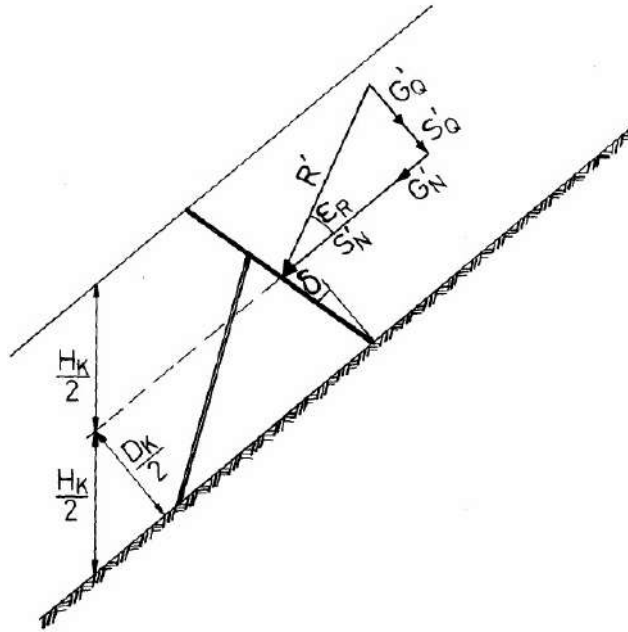
The direction of the resultant is calculated using Equation 3.20, where  $\epsilon_R$  is the angle between the resultant and the line of slope (Figure 3.9).

$$\tan(\epsilon_R) = \frac{R'_Q}{R'_N} \quad [-] \quad (3.20)$$

Where applicable, the end-effect load  $S'_R$  must be added to the slope-parallel component  $R'_N$  according to Equation 3.21.

$$R'_N = S'_N + S'_R + G'_N \quad [\text{kN/m}] \quad (3.21)$$

As previously mentioned, the snow pressure is simplified as uniformly distributed across the height. Therefore, the resultant is assumed to act at the centre height of the structure ( $H_K/2$ ).



**Figure 3.9:** Figure 3.6 repeated for better readability. Illustration of a rigid snow supporting structure, the resultant snow load acting on it, and the resultants components. Source: Margreth [2, p. 63].

### 3.3.5 Norwegian and Icelandic adaptations to the Swiss Guideline

The [Swiss Guideline](#) is based on the continental climate of the Alps, whereas Norway and Iceland have a more maritime climate. Because of this, efforts have been made to adapt the [Swiss Guideline](#) to better reflect the maritime conditions [33, p. 25].

There are three main parameters that differ when calculating snow pressure in the Alps and the Nordic countries. The first is that the snowpack is generally measured to be warmer and denser in Norway and Iceland than in the Alps [24, 33, 39, 40]. The second is that snow glide appears to be minimal in Norway and Iceland. The third is that the variation in snow density with elevation above sea level (and thereby variation in loading of snow supporting structures) appear to be minimal [39, 40].

However, the implementation of these factors differ. The comprehensive technical avalanche protective handbook, Rudolf-Miklau et al. [8], recommend using the calculation formulas from the [Swiss Guideline](#) and account for the higher snow density on Iceland by increasing the glide factor by a factor of 2. This almost corresponds to the Icelandic recommendations, Jóhannesson and Margreth

[39], which recommend adopting a gliding factor  $N = 2.5$  ( $N$  would have been set to 1.2 according to the Swiss Guideline). Jóhannesson and Margreth [39] also adopt a constant altitude factor  $f_c = 1.1$ , independent of the elevation above sea level.

J. O. Larsen [40] presents adaptations to the Swiss Guideline for the Nordic regions. The warmer and denser snow is accounted for by using an average snow density  $\rho = 500 \text{ kN/m}$  (instead of  $\rho = 270 \text{ kN/m}$  and including an altitude factor  $f_c$  as in the Swiss Guideline), and the snow pressure is set independent of the elevation above sea level (i.e., excluding the altitude factor  $f_c$ ). In addition, J. O. Larsen [40] do not account for the effect of snow gliding since there had been no observations of glide.

It should be mentioned that in the ongoing mitigating project against slush flow avalanches in Vannledningsdalen, Svalbard (see Section 7.1), the engineers chose to neither follow the Icelandic adaptations of enlarging the glide factor  $N$  [39], nor the recommendation from J. O. Larsen [40] to assume no gliding [27, p. 38]. Their argument was that they have a lot more data on the snow density than glide factor in Longyearbyen, and therefore could adapt the snow density more accurately than the glide factor. Because of this, the glide factor was set according to the Swiss Guideline and the snow density was increased.

### 3.3.6 Norwegian guidelines - Statens Vegvesen, Håndbok V138

#### Introduction to the guidelines

Statens vegvesen (en. the Norwegian Public Roads Administration) (NPRA) is a subordinate to the Norwegian Ministry of Transport and Communications, and is responsible for planning and building, operating and maintaining Norway's national and European roads [41]. The NPRA have developed several technical documents meant to guide in the building and maintenance of roads, amongst which is *Veger og snøskred, Håndbok V138* (en. *Roads and avalanches, handbook V138*) (Vegdirektoratet [9]).

Vegdirektoratet [9] gives guidelines for calculating the snow pressure in line of slope  $\sigma_x$  and normal to the slope  $\tau$ , as well as end-load effects. These load actions are illustrated in Figure 3.10. The calculations of the slope-parallel and slope-normal pressures are based on calculations made by J. O. Larsen [40]. However, the model used by Larsen is based on McClung's (1982) model [37] (presented in Section 3.3.3), with the assumption of no glide and values for the snow density  $\rho$  and Poisson's ratio  $\nu$  calibrated from measurements performed on maritime snow conditions in Norway [40, 42]. Therefore, Vegdirektoratet [9] ultimately base its calculations of snow pressure loads on McClung's (1982) model.

#### Calculating snow pressure

When calculating snow pressure, Vegdirektoratet [9] argues that snow glide in Norway is minimal. Therefore, a "no glide situation" is assumed where the effect of glide is ignored. The snow pressure in line of slope is simplified as a uniformly distributed average pressure over the height,  $\sigma_x$ , and is calculated according to Equation 3.22. The pressure is illustrated in Figure 3.10.

$$\frac{\sigma_x}{\rho g H} = 3,125 [0.25 (\sin\psi)^{1/2} + 0.05]^{1/2} \sin\psi + 0.28 \cos\psi \quad [-] \quad (3.22)$$

Here  $\rho$  is the average density of the snow cover,  $g$  is the gravitational acceleration,  $H$  is the height of the structure, and  $\psi$  is the slope gradient. The snow height is assumed to equal the structure height.

The actual pressure distribution in line of slope is proposed to have a parabolic dependence with height, see Figure 3.10. This means that the pressure is zero at the snow surface and along the ground,

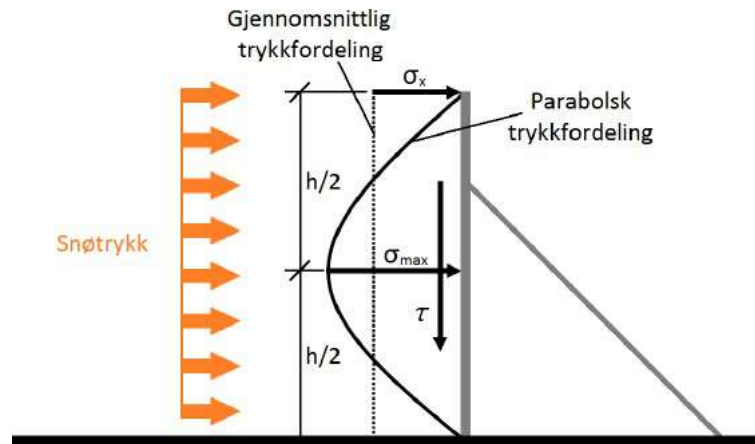


and that the maximum pressure occur against the centre of the construction. This maximum pressure is 1.5 times the average pressure ( $\sigma_{max} = 1.5\sigma_x$ ). Note that the assumption of a symmetrical and parabolic pressure distribution does not coincide with the current measured forces in Longyearbyen where much higher loads are measured at the upper load cells than by those closest to the ground (see Section 7.3). It could therefore be discussed whether it is reasonable to describe the pressure distribution with such precision.

The pressure component normal to the slope  $\tau$  is calculated according to Equation 3.23. The same applies here as for the Swiss Guideline, in that the pressure component normal to the slope is actually an induced shear contact stress.

$$\frac{\tau}{\rho g H} = 0.25 (\cos\psi)^{1/2} [1 - 0.84 (\sin\psi)^{1/2}] \quad [-] \quad (3.23)$$

Both Equation 3.22 and 3.23 applies for infinitely long supports structures. To account for the end-load effects, Vegdirektoratet [9] refers to the Swiss guidelines of 2001 [43]. There, the slope-parallel component  $\sigma_x$  is appended with an additional load that is 2 – 5 times the slope-parallel component and distributed over a length  $\Delta l = 4m$ .



**Figure 3.10:** Snow pressure load actions against a support structure according to Vegdirektoratet [9].

English translation: "Snøtrykk" = "snow pressure", "gjennomsnittlig trykkfordeling" = "average pressure distribution", "parabolsk trykkfordeling" = "parabolic pressure distribution". Source: Jacobsen [34, p. 33] after Vegdirektoratet [9, p. 61].

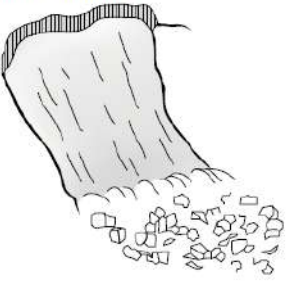
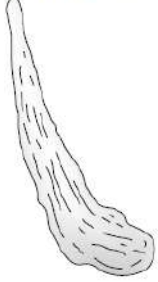

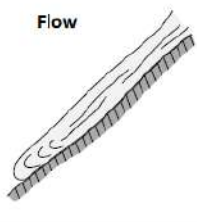

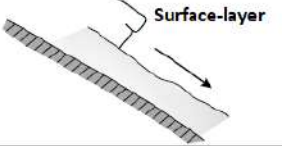
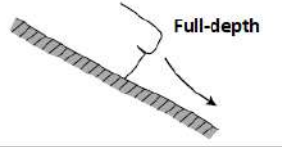




# Chapter 4

## Classification of avalanches

### 4.1 General

Avalanches are gravity driven mass flows of snow, ice, rock or mud that run rapidly down mountainsides with lengths more than 50m and volumes greater than 100m<sup>3</sup> [44, p. 17]. The focus of this thesis is snow avalanches, which refer to rapid movements of snow masses. They can be assigned to categories depending on many characteristics, for example on their material content, manner of starting, form of movement, and liquid water content. Snow avalanches are also categorised as natural catastrophes if they cause loss of human lives and severe environmental and property damage [44, p. 1].

<b>Manner of starting</b>	<b>Slab avalanche</b>		<b>Loose snow avalanche</b>	
				
<b>Form of movement</b>	<b>Powder</b>	<b>Flow</b>	<b>Mixed</b>	
				
<b>Position of sliding surface</b>	<b>Surface-layer</b>		<b>Full-depth</b>	
				
<b>Water content</b>	<b>Dry snow</b>		<b>Slush flow</b>	
				

**Figure 4.1:** Classification of some avalanche types with illustrations. Source: Vegdirektoratet [9].

The purpose of categorising avalanches is to create a condensed system for describing avalanche characteristics. There are several systems for categorising snow avalanches, and some systems are more detailed than others. However, the international standard is to follow the *Avalanche Atlas* published by UNESCO in 1981 [45]. This classification defines the morphological features of avalanches, and is presented in Table 4.1 [22, p. 18] and with illustrations in Figure 4.1 [9, p. 29]. From these presentations we observe that an important type of avalanche classification is the manner of starting, where the avalanche is characterised as either a loose snow avalanche or a slab avalanche. It is also noted that a snow avalanche can move as a flowing mass along the ground or as a snow dust cloud.

This chapter will define the different zones in an avalanche path (catchment area), give an overview of some distinct types of avalanches, and study the process of avalanche formation. It is meant as a general overview, and for more details the reader is referred to D. McClung and Schaerer [6] and Nairz et al. [22].

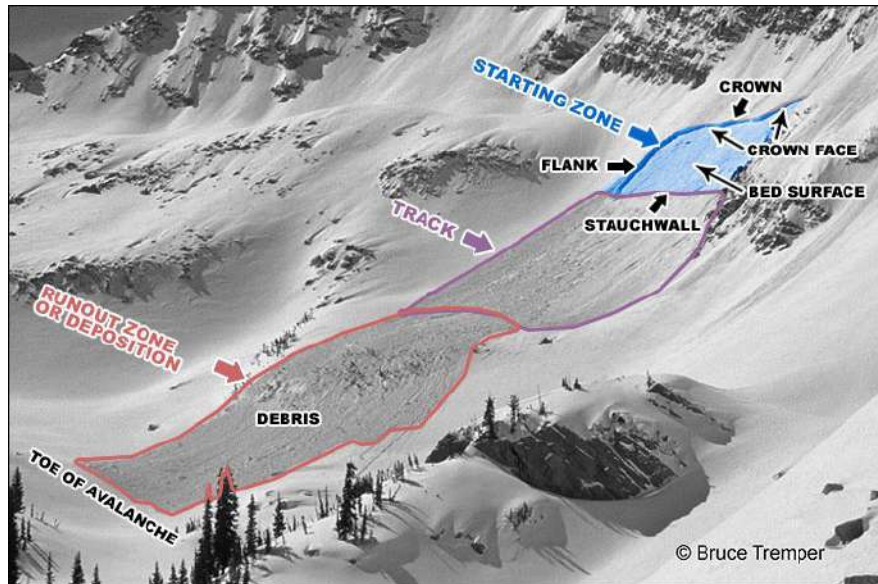
**Table 4.1:** Copy of Table 2.1 in Nairz et al. [22, p. 18]: Morphological avalanche classification, where avalanches are classified based on the manner of starting, form of movement, form of the path, and manner and form of deposition.

Zone	Criterion	Alternative characteristics	
Starting zone	Manner of starting	Starting from a point (loose-snow avalanche)	Starting from a line (slab avalanche)
	Position of sliding surface	Within snow cover (surface-layer avalanche)	On the ground (full-depth avalanche)
	Liquid water in snow	Absent (dry-snow avalanche)	Present (wet-snow avalanche)
Avalanche path	Form of path	Open slope (unconfined avalanche)	Gully or channel (channelled avalanche)
	Form of movement	Snow dust cloud (powder snow avalanche)	Flowing on ground (flow avalanche)
		Mixed (mixed avalanche)	
Runout zone	Surface roughness of deposit	Coarse (>0.3 m) (coarse deposit)	Fine (<0.3 m) (fine deposit)
	Liquid water in snow debris at time of deposition	Absent (dry avalanche deposit)	Present (wet avalanche deposit)
	Contamination of deposit	None apparent (clean avalanche)	Present (contaminated avalanche)

## 4.2 Avalanche catchment area

The avalanche catchment area is a fixed locality or terrain feature within which an avalanche move (i.e., the total area affected by an avalanche) [6, 22]. An example of one such area is shown in Figure 4.2. Within the catchment area, the release and deposition of smaller avalanches may happen at various places [6]. Each individual avalanche has its own *starting zone*, *track*, and *runout zone*. These terms can also be used for a more general definition of the locations on a slope where the release, flow, and deposition of avalanches can happen. The following section will give a broad overview of these terms.

It should be noted that the use of some terms is not the same in all literature. This can sometimes be confusing. For example, Rudolf-Miklau et al. [8] define the total area affected by an avalanche as the *avalanche catchment area*. The same area is defined by D. McClung and Schaerer [6] as the *avalanche path*. To make it worse, Rudolf-Miklau et al. [8] use the term *avalanche path* for the slope between the starting zone and runout zone, while D. McClung and Schaerer [6] name this slope the *track* (or transport zone). It does help that the terms for the *starting zone* (also termed *initiation zone* or *release zone*) and for the *runout zone* (also termed *deposit zone*) are only used for these specific areas. To avoid confusion, the term *avalanche path* will be avoided in this thesis.



**Figure 4.2:** Avalanche catchment area with the starting zone, track, and runout zone of a specific slab avalanche. Photo: Bruce Temper. Source: Avalanche.org [46].

#### 4.2.1 Avalanche starting zone

The *starting zone* is the area where unstable snow fail and an avalanche is released. As mentioned, this can either be the area in which it is expected that an avalanche can release, or it can be the area where one specific avalanche was released. Following the first definition, the starting zone is the area where *snow supporting structures* are built. For a specific avalanche the upper limit of the starting zone is the fracture line (crown) of a slab avalanche or the point of release for a loose snow avalanche. The lower limit is often harder to define.

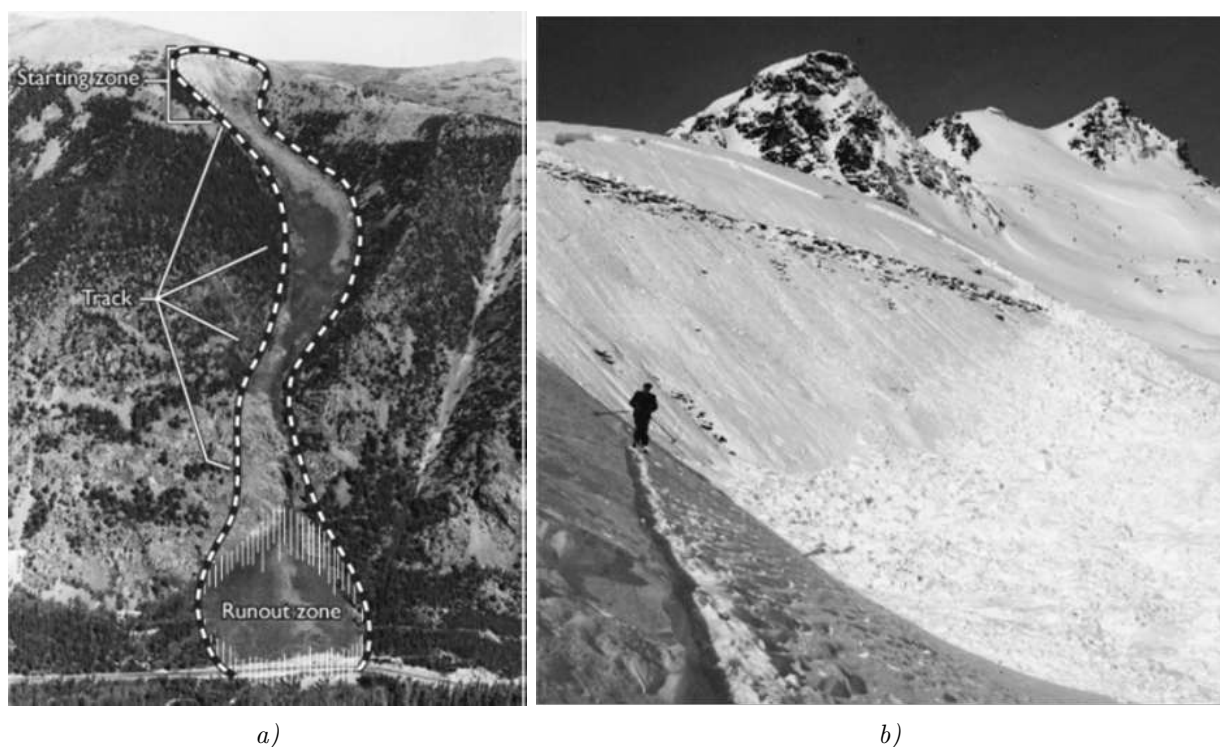
The variables highlighted by D. McClung and Schaerer [6] to affect the characteristics of a starting zone is the slope incline, orientation to the wind and sun, forest cover, ground surface, slope dimensions, altitude, and crown and flank locations. However, the main characteristic is the slope gradient. This is because avalanches are gravity driven mass flows (as mentioned), and will only initiate and gain dangerous velocities if the slope gradient is steep enough. How steep the slope have to be depends on the avalanche type (the different types are presented later in this chapter). The necessary slope for the initiation of some avalanche types are presented in Table 4.2. From the table it is noted that slab avalanches are rare below 25°, but that slush flows can release at much lower slope inclinations. Other sources defines 25° (UNESCO’s Avalanche Atlas [45]) and 28° (Austrian standards ONR 24805 - 24807 [1]) as the lower inclination for slab avalanches. The *Swiss Guideline* [2] states that supporting structures are generally required for slope inclinations between 30° and 50°, but that flatter or steeper terrain may need to be controlled in exceptional cases.

**Table 4.2:** Avalanche types by different starting zone inclines, according to D. McClung and Schaerer [6].

Slope gradient	Avalanche type
60° – 90°	Avalanches are rare; small loose snow avalanches frequent
30° – 60°	Dry loose-snow avalanches
45° – 55°	Frequent small slab avalanches
35° – 45°	Slab avalanches of all sizes
25° – 35°	Infrequent (often large) slab avalanches; wet loose snow avalanches
10° – 25°	Infrequent wet-snow avalanches and slush flows

### 4.2.2 Avalanche track

The *track* (also termed *avalanche path*, *transport zone* or *zone of transition*) is the section of the avalanche catchment area between the starting zone and runout zone (Figure 4.2). The track is the area where the avalanche reaches its maximum velocity, with accelerating flow at the start and decelerating flow at the end of the track [6]. The track can be classified as either *planar* (also termed unconfined) or *channelled* (also termed confined) [22, 45]. These two different tracks are shown in Figure 4.3. A planar track has approximately the same width as the starting zone [22], while a channelled track confines the avalanche to follow a terrain feature such as a gully. Avalanche tracks are often characterised by tree-free zones. The inclination of the slope is not required to be as steep in the track as in the starting zone, but are normally over  $15^\circ$  and often  $20^\circ - 25^\circ$  [47].



**Figure 4.3:** *Avalanche track. a) Picture of a long avalanche catchment area with a long and well defined channelled track. b) Picture of a short avalanche catchment area where the three zones are not well defined. This is a planar avalanche track. Photo: A. Roch. Source: D. McClung and Schaerer [6].*

### 4.2.3 Avalanche runout zone

The *runout zone* is the part of the catchment area where the avalanche decelerates rapidly, debris is deposited, and the avalanche stops. The runout zone is marked on two different avalanche catchment areas in Figure 4.2 and Figure 4.3a. A slope area is defined as a potential runout zone if the slope inclination is approximately  $10^\circ$  or less [22, p. 47]. This is because the area where large dry-flowing avalanches decelerate is marked by the slope inclination of  $10^\circ$  [22]. However, the transition between track and runout zone may vary for different avalanches within the same catchment area, for example can small avalanches stop (run out) in a bigger avalanche's track [6]. Slush flows can continue flowing at much lower inclinations than dry-snow avalanches (discussed further later in this chapter).



## 4.3 Avalanche types

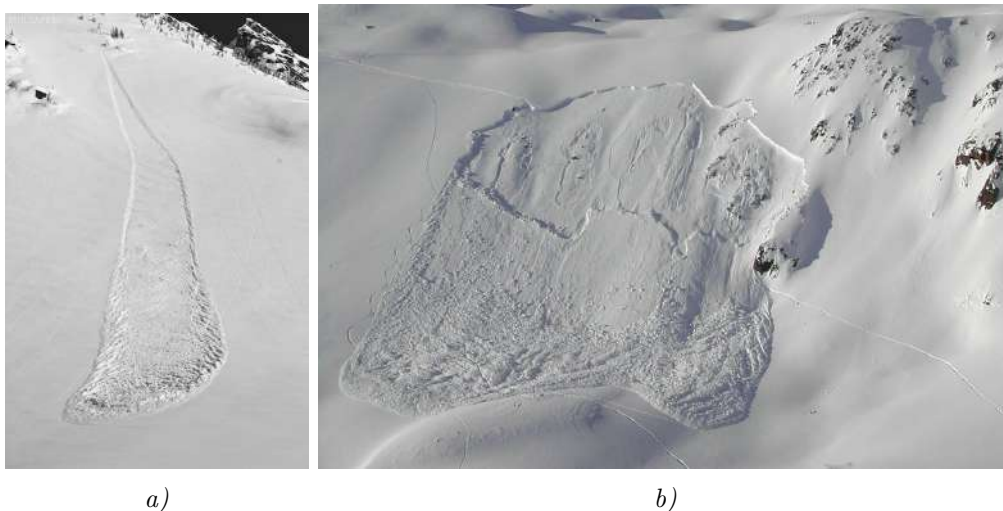
### 4.3.1 Classification based on: Manner of starting

#### Loose snow avalanches

A loose-snow avalanche release at a single area or point and spreads downhill in a triangular pattern collecting more snow [6, 48]. A picture of a loose snow avalanche is presented in Figure 4.4, and shows the typical single point release and triangular pattern. Loose-snow avalanches most often occur after a new snowfall or significant temperature increase, and are often released naturally [16]. If a loose-snow avalanche is released by a skier, the avalanche tend to fracture below the skier (as opposed to above which is often the case for slab avalanches, see the following section) [48]. Therefore, less than 10% of avalanche fatalities are attributed to the loose-snow type [16]. Loose-snow avalanches are often small in volume, but can reach considerable size in continuous steep slopes and especially if the snow is wet [16]. The slope angle required for the formation of loose-snow avalanches is normally  $35^\circ$  or more [45].

#### Slab avalanches

A picture of a slab avalanche is presented in Figure 4.4, which clearly shows a typical fracture line and release area where a shear fracture has propagated. A slab avalanche can occur when a cohesive layer of snow (slab) lays on top of a thin weak layer deeper down in the snow cover [6, 16]. The avalanche initiates when a small shear fracture occur in the weak layer and then rapidly propagates across the layer [6]. This is called the *primary fracture*. When the snowpack can no longer bear the tension trapped by the collapse of the weak layer, a *secondary fracture* occur [49, p. 60]. The slab is cut of from the surrounding snowpack along a distinct fracture line, before it is accelerated by gravitational forces and slides down the slope. The triggering of the initial fracture requires and additional load [16]. This load can for example be a new snowfall, heavy rainfall, a falling cornice, or a skier. The triggering can happen remotely (from outside the perimeter of the slab), resulting in a shear fracture propagation along the weak layer until the avalanche release in a location where the tensile stress exceed the tensile strength of the slab [10]. Slab avalanches account for more than 90% of all avalanche fatalities, an a person releasing an avalanche is often caught by it [16]. The minimum slope angle required for the formation of slab avalanches is normally  $25^\circ - 30^\circ$  [22, 45].

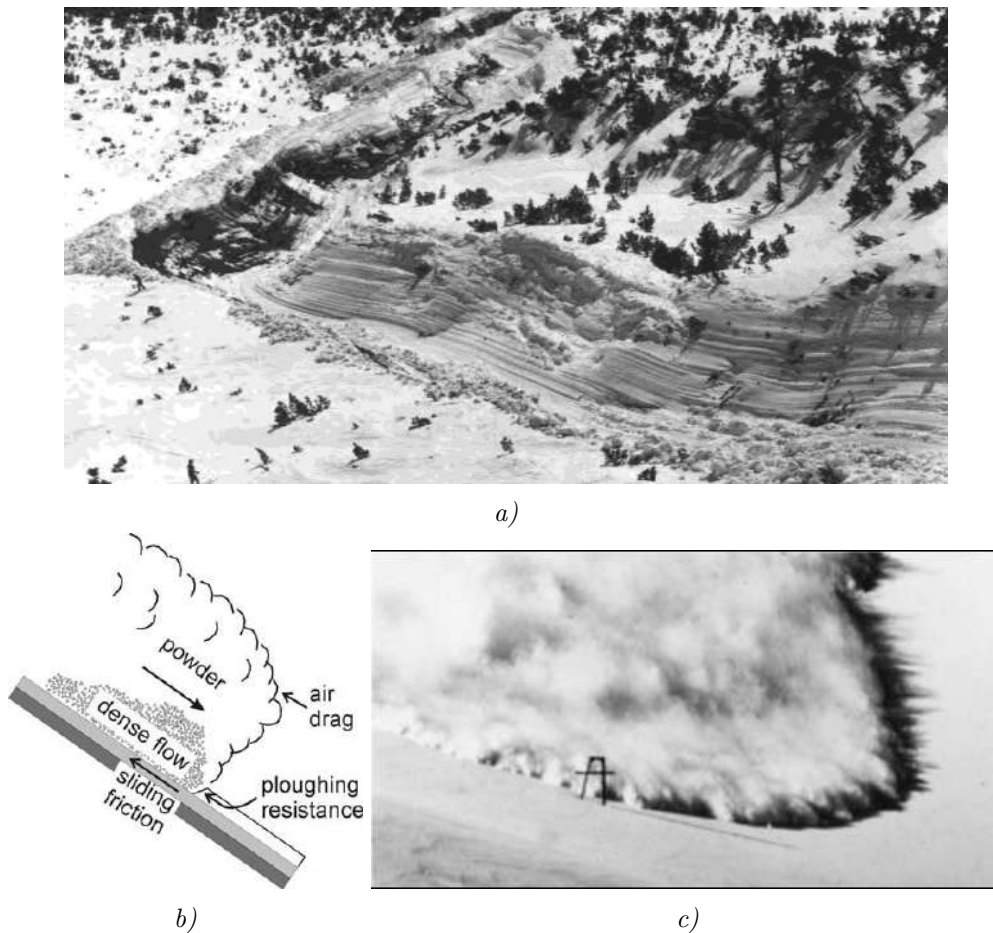


**Figure 4.4:** Loose snow and slab avalanche. a) A loose snow avalanche showing the typical single point release and triangular patten (Streater [50]). b) A slab avalanche showing the typical fracture line and release area where a shear fracture has propagated (Safeback [51]).

### 4.3.2 Classification based on: Form of movement

#### Flow avalanche

Flowing avalanches are avalanches with a high density core at the bottom [6]. An example of a wet pure flow avalanche seen in the direction of flow is shown in Figure 4.5a. A flow avalanche can release as either loose snow or a slab, but because of surface roughness (sliding friction) the slab will break up into smaller blocks and particles [49]. The flow avalanche move down the slope with continuous shearing and deformation within the snow mass and constant contact between the individual particles. Dry flowing avalanches are also termed *mixed-motion avalanches* because all high-speed dry avalanches have a powder snow cloud (suspension layer) with lower density snow around its exterior [6]. A picture and an illustration of a mixed-motion avalanche is shown in Figure 4.5b-c. The avalanche pictured has a very small powder-component and clearly show the flowing character. The powder-component is caused by a velocity gradient, and thereby a shear force, between the flowing avalanche and surrounding air [49]. At high enough speeds, this shear force will pull snow particles into the air as a result of transverse acceleration [49, p. 60]. Flow avalanches can consist of both wet and dry snow, and they can reach speeds up to 10 – 20m/s and 20 – 40m/s respectively [49]. Mixed-motion avalanches are a commonly observed avalanche type.



**Figure 4.5:** Flow avalanche and mixed-motion avalanche. a) Picture of a wet pure flow avalanche seen in the direction of flow, with sharp turns indicating low velocity (photo: E. Wengi, SLF, UNESCO [45]). b) Illustration of a mixed-motion avalanche featuring dense and powder flow (Jamieson et al. [52]). c) Picture of a dry flowing avalanche with a very small powder component (D. McClung and Schaerer [6]).



## Powder avalanche

Powder avalanches are rapidly moving avalanches consisting of a powder snow cloud where the dense core at the bottom is absent [6, 49]. This means that almost all the material in the avalanche is suspended in eddies, and gives a snow density around 10% of that of flowing avalanches [6, p. 237]. A picture of a powder avalanche flowing down a steep slope is presented in Figure 4.6, where a powder cloud of snow with apparent low density can be seen. The formation of powder avalanches is often caused by falling ice in steep terrain, and they generally require a large altitude difference [6, 45]. Powder avalanches can reach speeds up to  $30 - 70\text{m/s}$  [45], but because of their low density their destructive power is considered less than flowing avalanches [6]. However, the power component of avalanches can run farther than the main deposit, and its impact force will extend over a greater height on a structure than the flowing component [6].



**Figure 4.6:** Powder avalanche flowing down a steep slope. Source: D. McClung and Schaerer [6, p. 238]. Photo: G. Buscaini.

### 4.3.3 Classification based on: Position of sliding surface

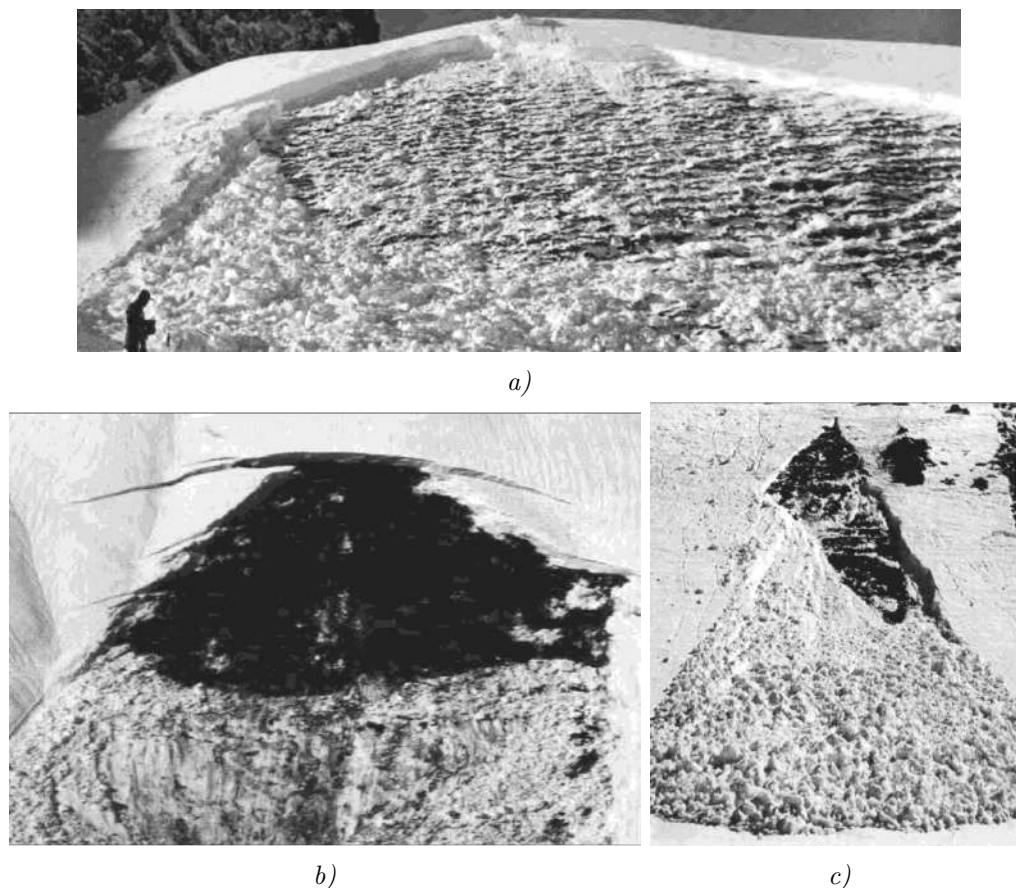
#### Surface-layer avalanche

A surface-layer avalanche refers to a loose snow avalanche or a slab avalanche where the position of the sliding surface is within the snow cover. An illustration of one such sliding surface position was presented in Figure 4.1, and a picture of a surface-layer loose snow avalanche was presented in Figure 4.4a. Surface-layer avalanches can either result from a *new-snow fracture* or an *old-snow fracture* [45]. The border between new and old snow in this context refers to whether the snow in the slab was deposited within the last 5 days (new) or if it is older than 5 days (old) [45]. A surface-layer avalanche is classified by a new-snow fracture even if the fracture was favoured by the surface of the immediately underlying old snow (e.g. surface hoar, icy crust). In an old-snow fracture the fracture lies within the old snow [45].

#### Full-depth avalanche

Full-depth avalanches are avalanches where the full height of the snowpack (down to ground) has released. Three pictures of full-depth avalanches are presented in Figure 4.7 showing different man-

ners of starting and liquid water in snow. The full-depth failure can be caused by fracture in a depth-hoar layer or gliding [45]. An increasing rate of gliding has been confirmed to occur prior to full-depth avalanches that release by gliding (also called *gliding avalanche*) [6, p. 32]. Full-depth avalanches are noted even if a snow veil or some snow patches are left on the ground after passage of the avalanche [45, p. 32].



**Figure 4.7:** Pictures of full-depth avalanches. a) Full-depth dry-slab avalanche with a remaining snow veil on the ground that was likely caused by fracture in depth hoar. Photo: R. Figilister, SLF Switzerland. b) Full-depth wet-slab avalanche starting after a glide crack had opened. Photo: M. Shoda, Japan. c) Wet full-depth loose-snow avalanche. Photo: E. Wengi, SLF Switzerland. Source: UNESCO [45].

#### 4.3.4 Classification based on: Liquid water in snow

##### Dry-snow avalanches

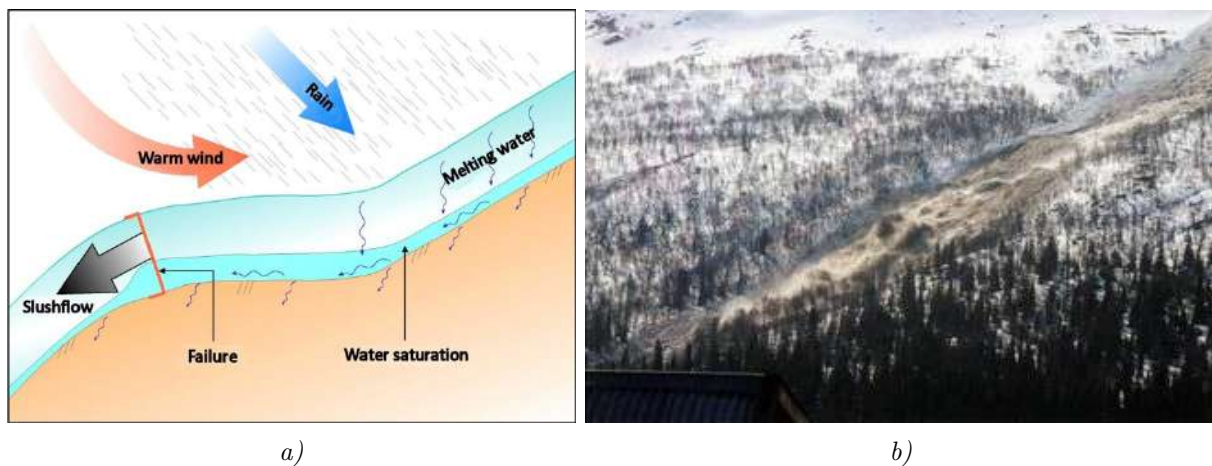
Dry-snow avalanches consist of dry snow having virtually no free water content [6, p. 123]. They can release both as loose snow and slab avalanches, and pictures of these avalanches have been shown in Figure 4.4a-b, Figure 4.5b-c, Figure 4.6, and Figure 4.7a. Usually the starting snow temperature in dry-snow avalanches is well below  $0^{\circ}$ , but the snow can be dry in temperatures up to  $0^{\circ}$  [53]. When pressed together, dry snow grains are characterised by having little tendency to adhere to each other (difficult to make a snowball) [53]. Dry-snow avalanches can start out as dry and end up as wet. The reason for this can be that the snow heats up from the frictional energy caused by the decent, or that the avalanche travel into a region of warmer snow [54].

## Wet-snow avalanches

Wet-snow avalanches are avalanches with liquid water present in the entire sliding snowpack [49, p. 63]. The IACS classification system for water content of snow [53] subdivide wet snow into four categories depending on the free water content (by volume fraction in %). These four categories are moist snow (0 – 3%), wet snow (3 – 8%), very wet snow (8 – 15%), and soaked snow (slush) (more than 15%). The bindings between the snow crystals are broken down as the water content increase leading to a reduced snow strength. Wet-snow avalanches are similar to dry-snow avalanches in the beginning, but do not develop a powder snow cloud (suspension layer) [49, p. 243]. They reach speeds up to 10 – 20m/s, and can start as both wet slab and wet loose avalanche release [49].

## Slush flows

Slush flows, also termed *slush avalanches*, is a type of wet-snow avalanche formed from slush. *Slush* consist of separated rounded snow grains completely immersed in water, and is defined to have a liquid water content of minimum 15% [55]. Because of the high water content, slush is a very unstable snow type with weak bindings [9, p. 19]. They can therefore occur at very gentle terrain inclinations [45]. Slush flows release from areas where the entry of water is bigger than the drainage, and with a slope angle of 5° – 25° [32, p. 23]. The addition of this much water to the snowpack usually occurs in periods with heavy rainfall or fast snow melt. An illustration of the release conditions for slush flows is presented in Figure 4.8. The slope angle where slush flows decelerate and run out (runout zone) is also much lower for slush flows than dry-snow avalanches, and often as low as 5° [7]. Slush flows can erode significant amounts of sediments and rocks on their way, and are for this reason often wrongly classified as debris flows or torrents [56]. In steep terrain, slush flows can reach velocities up to 30m/s, but in genteler slopes than 20° they seldom reach velocities higher than 10m/s [32]. Chute experiments on slush flows indicate that shear and normal stresses in slush flows are higher than in comparable dry-snow avalanches (similar velocities), and also indicate that the drag force against obstacles in the flow is considerably higher [57].



**Figure 4.8:** Slush flow. a) Illustration of common release conditions for slush flows. Source: Norwegian Geotechnical Institute [56]. b) Slush flow in motion at Skarmodalen, North-Norway, 16.05.2010. Release due to intense snowmelt in late season. Photo: T. Prytz, Hestnes and Kristensen [58].



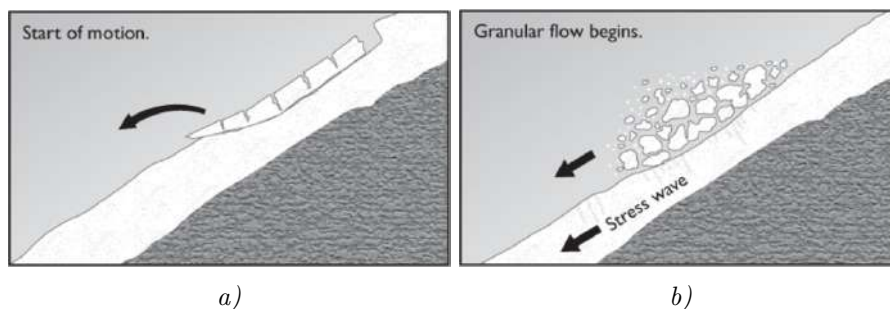
# Chapter 5

## Avalanche dynamics and modelling

### 5.1 General

Knowledge about avalanche motion (avalanche dynamics) is crucial when planning avalanche mitigation measures. This is because avalanche impact pressures in the design of structures are dependent on how far an avalanche can reach (runout distance), the avalanche velocity at the location of the structure, and how the avalanche interact with the structure. However, the physical and mechanical properties of the material snow varies greatly (Section 2.3), and the movement of avalanches is very complex. Therefore, the process of creating physically accurate and mathematically complete descriptions of the avalanche movement is very complicated and has not yet been completed [49, p. 55]. The modelling of avalanche dynamics is a very big field, and the in-depth study of avalanche dynamics will be left for further works. This chapter will only give a brief overview of the modelling of avalanche velocities, runout distance, and impact pressures in the design of structures.

Figure 5.1 illustrates the initial stages of motion of an avalanche [6]. In the beginning, all avalanches move as a laminar flow or sliding block [7, 49]. In small avalanches and low fall heights, this sliding movement is dominating [7]. The masses will then pick up speed and the blocks start breaking into smaller pieces due to surface roughness. From a velocity of approximately  $10m/s$ , a transition into a turbulent movement form is to be expected [49]. Big dry-snow avalanches are then thought to consist of three layers [7, 59]: Flowing closest to the ground is a dense core (floating section) where the snow particles are in continuous contact with neighbouring particles (as for flow avalanche discussed in Section 4.3.2). The flow height of the dense core is typically  $h = 1 - 3m$  and the density  $\rho \approx 300kg/m^3$ , though the flow height can be much higher for channelised flow [59, p. 13]. In wet-snow avalanches the density is commonly  $500 - 700kg/m^3$  [7, p. 79]. A saltation layer flows on top of the dense layer, where snow particles jump around with longer free paths and interact in pairwise collisions. This layer typically has a flow height  $h = 2 - 5m$  and density  $\rho \approx 10 - 100kg/m^3$  [59]. Surrounding the dense core and saltation layer is a powder snow cloud (suspension layer) where snow particles are suspended by turbulent eddies of air caused by friction between the air and the flowing snow (as for powder avalanche discussed in Section 4.3.2) [6, p. 123]. Not all flow avalanches become powder avalanches, and wet-snow avalanches normally keep the flowing movement form longer [7, 49]. The flow height of the powder component varies greatly, typically between a few tens of meters to  $100m$  or more, and the density is on the order of  $\rho \approx 3kg/m^3$  [59]. This compound movement makes the avalanche behave partly as a solid, partly as a fluid, and partly as a gas in motion [7].



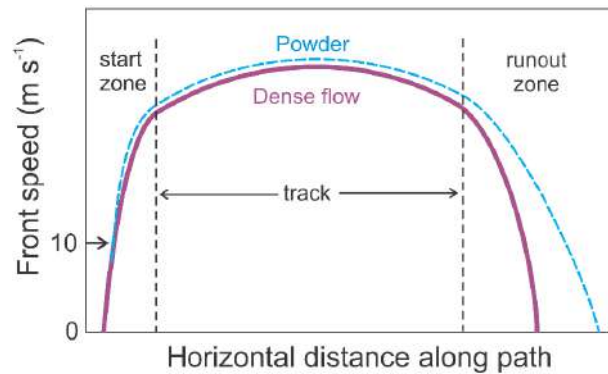
**Figure 5.1:** Initial stages of motion. a) The avalanche starts as a sliding block. b) Interaction with the ground surface causes slabs to break into smaller pieces. Source: D. McClung and Schaerer [6].



## 5.2 Calculating avalanche velocity

The intensity of avalanche impact is dependent on the avalanche velocity squared  $v^2$  (as will be discussed in Section 5.4) [7, 9, 22, 60]. The avalanche speed thus has a big influence on the choice of mitigation measure. The velocity in the runout zone is especially interesting as this is where the structures in need of protection are most often located and also where structural mitigation is most often built [9].

The highest velocities of flow-avalanches are observed at the front of the avalanche, while the avalanche body typically has a shear velocity profile (increased velocity with increased height above ground) [49]. Field measurements have shown that characteristic avalanche motion include a very rapid acceleration at the beginning of motion and very rapid deceleration at the end of motion [6, p. 124]. Figure 5.2 illustrate the velocity of a mixed-motion avalanche along an avalanche catchment area where these accelerations are evident [60]. It also illustrates that the powder snow component of the avalanche travels slightly faster than the dense core. The rapid acceleration and deceleration is likely caused by large gravitational pull in steep terrain at the beginning, and large friction forces in the runout zone [6].



**Figure 5.2:** Velocity of a mixed-motion avalanche along an avalanche catchment area, with rapid acceleration and deceleration at the beginning and end of motion. Source: Jamieson [60].

Avalanche models, used to describe avalanche motion, are often classified as either *statistical-topographical* models or *physical-dynamic* models [49]. The statistical-topographical models are one-dimensional empirical models based only on the topographical layout of the avalanche catchment area, and are developed from statistical analysis of observed avalanches [61]. One such model is the *alpha-beta* ( $\alpha - \beta$ ) model [62] used to calculate runout distances. The physical-dynamical models are mainly numerical and based on the laws of hydraulics that describe viscous fluid motion in an open channel [49, 61].

The complexity of the dynamic models varies, and one often distinguish between one-dimensional (1D), two-dimensional (2D), and three-dimensional (3D) models. The simplest (1D) models calculate the depth-averaged speed of the mass centre along the centre-line of the flow [60, p. 112]. Two examples of 1D models are the *Voellmy model* (1955) [63] and the *PCM-model* (1980) [64]. Two-dimensional models calculate the velocity along and across the flow, as well as the flow height and deposit height [60]. The velocity is depth-averaged over the flow, meaning that the models neglect shear within the dense flow. The numerical models *RAMMS* (2008) [65] and *ELBA* (2005) (now ELBA+) [49, 66] are two examples of 2D models. Three-dimensional models also predict the velocity of the flow in the direction normal to the flow [60]. *SamosAT* (2007) [67] is one such 3D-avalanche model.

A simplified analysis of the forces acting on the snow masses in a flowing avalanche will be discussed in the following (as presented by Vegdirektoratet [9]): Consider a unit volume of avalanche masses

(snow) moving down a slope with inclination  $\alpha$  and flow height  $h$ , as illustrated in Figure 5.3. The masses will experience accelerating actions from the slope-parallel component of the gravitational forces  $P$ , and it will feel decelerating actions from friction  $F_F$ . According to Newton's second law of motion,  $\sum F = m \cdot a$ , the sum of the forces acting on the mass is equal to the mass times its acceleration. Equilibrium of the unit volume of snow in the slope-parallel direction is then given according to Equation 5.1:

$$P - F_F = m \cdot a \quad (5.1)$$

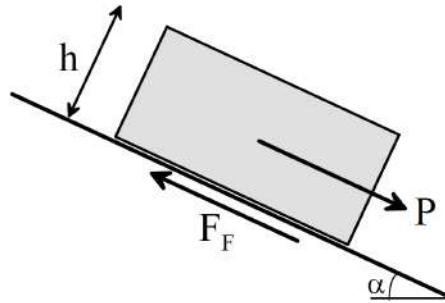
Here,  $m$  is the mass of the unit volume of snow, and  $a$  is the acceleration. The mass times acceleration for a unit volume with base area  $A = 1m^2$  and flow height  $h$  is:

$$m \cdot a = m \cdot \frac{dv}{dt} = \rho V \cdot \frac{dv}{dt} = \rho(h \cdot 1[m^2]) \cdot \frac{dv}{dt} = \rho \cdot h \cdot \frac{dv}{dt} \quad (5.2)$$

Density  $\rho$  is the flow density, and  $v$  is the flow velocity. The forces acting on the body are:

$$P - F_F = \rho \cdot g \cdot h \cdot \sin \alpha - (F_c + F_d) \quad (5.3)$$

Here  $F_c$  and  $F_d$  are friction terms independent and dependent on the velocity respectively. All numerical models today assume that the friction in an avalanche is the sum of one velocity-independent term and one velocity-dependent term [9]. The friction term that is *independent* of the velocity is commonly described by assuming a Mohr-Coloumb material model,  $F_c = c + \mu \cdot \rho g h \cdot \cos \alpha$ , where  $c$  is the cohesion of the masses, and  $\mu$  is the friction coefficient [9]. This represent a frictional shear force that is dependent on the normal stress. The velocity-independent term is important, as without it no avalanche would stop until the slope inclination was zero degrees. The frictional term that is *dependent* on velocity is essential as without it no avalanche would reach a terminal velocity (approximately constant maximum velocity). The term is modelled using hydrodynamic theories (flow in liquids),  $F_d = \kappa \left(\frac{v}{h}\right)^2$ , where  $\kappa$  represents the viscosity [9].



**Figure 5.3:** Unit volume of avalanche masses moving down a slope. Source: Aalberg [68].

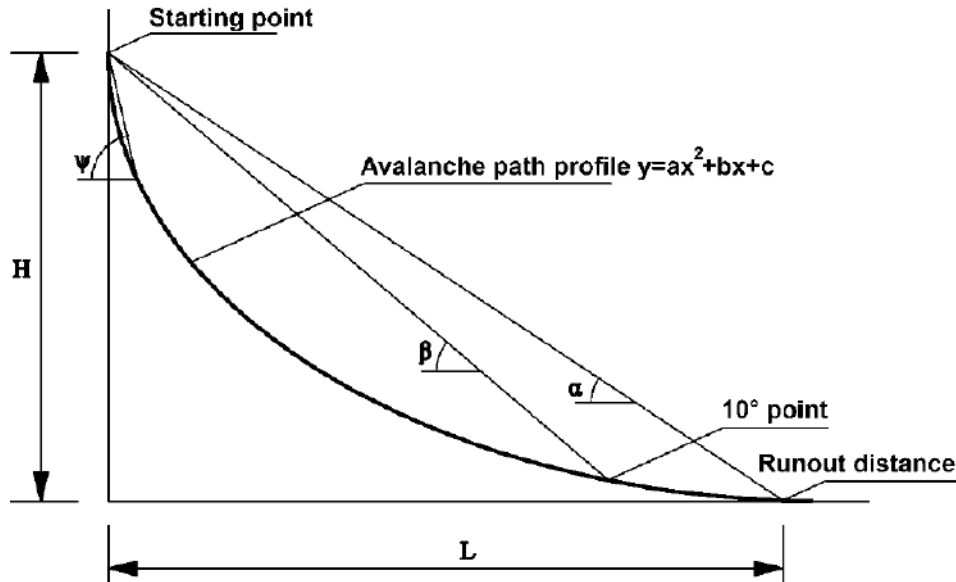
Some approximate maximum velocities of different types of avalanches are given in Table 5.1 [49]. Velocities have been added for slush flows even though they are considered a special type of wet-snow avalanche. Notice that slush flows can reach relatively high velocities while they at the same time have a high flow density. This make them capable of inflicting high impact pressures on obstacles in their path.

**Table 5.1:** Magnitude of avalanche velocities in the avalanche front. Source: Sauermoser et al. [49].

Avalanche type	Velocity m/s
Wet flow avalanche	10-20
Slush flow avalanche [32]	10-30
Dry flow avalanche	20-40
Powder avalanche	30-70

### 5.3 Calculating runout distance

The best policy to stay safe from avalanches is to avoid the avalanche catchment area, and especially to avoid placing residential houses or important infrastructure in this area. To achieve this, one has to know the point of farthest reach of the avalanche debris. This is defined as the *runout distance* of the avalanche (does not generally include the reach of the powder snow component). The runout distance is either described through the horizontal distance  $L$  from the point of release to the furthest reaching deposit, as shown in Figure 5.4, or by the *angle of maximum runout*  $\alpha$  [9].



**Figure 5.4:** Illustration of an avalanche catchment area in the longitudinal section, including the parameters of the alpha-beta model [62]. Source: Sauermoser et al. [49].

The determination of runout distances is best achieved through long-term observations of avalanche deposits, searching for damage to the vegetation, or by looking through historical records such as old newspapers or aerial photos [6, p. 136]. However, if this is not possible one can estimate the runout distance using (the previously mentioned) avalanche models.

A statistical-topographical avalanche model commonly used to calculate a first estimate of the runout distances is the *alpha-beta model* (1980) [62]. This model was developed by Lied and Bakkehoi at the NGI in Norway, and revised by the same authors in 1983 [69]. It was the first topographical model designed to calculate avalanche runout distance, and is based on a statistical study of 206 avalanches using multiple regression analysis. All these avalanches had a free outlet in the valley bottom, but there were large natural variations in the characteristics of the avalanche catchment area. The information about the maximum runout distance in each avalanche path was based on historical documents and interviews with the local population who have observed the paths for 100 – 300 years [62]. The maximum runout distance within the "corresponding" return period was assumed to have occurred, which means that the return period of an avalanche (with runout distance) calculated using the alpha-beta model is 100 – 300 years [9].

The model parameters were chosen by Lied and Bakkehoi [62] with the aim of keeping them as objective as possible, and ideally they wanted to choose parameters which can be measured directly in the field or from maps [62]. The chosen parameters are illustrated in Figure 5.4, and include the average gradient of the avalanche path  $\alpha$ , the average inclination of the avalanche track  $\beta$ , the inclination of the starting zone  $\psi$ , the second derivative  $y''$  of the parabolic slope function  $y = ax^2 + bx + c$  with the best fit to the terrain profile, and the height  $H$  from the starting point



to the vertex of the parabola [62]. The multiple regression analysis based on the 206 observed avalanches resulted in the expression for the total reach of the avalanche given by the  $\alpha$ -angle:

$$\alpha = 0.92\beta - 7.9 \cdot 10^{-4}H + 2.4 \cdot 10^{-2}Hy''\psi + +.04 \quad (5.4)$$

Equation 5.4 gave a correlation coefficient of  $R = 0.92$  and standard deviation of  $SD = 2.28^\circ$  [69].

A simplified version of this equation was also presented by Bakkehøi et al. [69] where the inclination of the avalanche track  $\beta$  is the only free variable:

$$\alpha = 0.96\beta - 1.4^\circ \quad (5.5)$$

Equation 5.5 gave a correlation coefficient of  $R = 0.92$  and standard deviation of  $SD = 2.3^\circ$ , which demonstrates a dominating dependence on angle  $\beta$  [69]. Vegdirektoratet [9] states that the design return period of important infrastructure should be 1000 years, while (as mentioned) the return period calculated with the alpha-beta model is 100 – 300 years. To obtain the needed safety margin corresponding to a return period of 1000 years, Vegdirektoratet [9] adds one standard deviation (reducing the  $\alpha$ -value by  $2.3^\circ$ ) according to Equation 5.6:

$$\alpha = 0.96\beta - 1.4^\circ - 2.3^\circ \quad (5.6)$$

Where a shorter return period is needed (as for highways), the added standard deviation is suggested reduced to  $0.25SD$  or  $0.5SD$  [9]. The alpha-beta model has also been calibrated for the Austrian alpine region [70] and the Catalan Pyrenees [71].

The runout distance (and avalanche speed) is commonly calculated using numerical, physical-dynamic models. As mentioned, an in-depth study will be left for further work, but a very general presentation of some well-known dynamic models follows: The physical-dynamic models are based on laws of hydraulics, and most of them refer to the *Voellmy-fluid constitutive law* which was developed by Voellmy [63] and assumes a combination of the Chezy friction term and the Colomb dry friction [49, p. 66]. The *Voellmy-Salm model* is a further development of Voellmy's model created by Salm [36] in 1966, where Salm considered avalanching snow to be a cohesionless material with internal friction [36]. This model was widely used until the development of the numerical model *AVAL-1D* [72], where a finite difference scheme is used to solve the governing equations of mass, energy, and momentum [60, p. 122]. A model that is still in use in the North and South America is a centre of mass model, called the *PCM model*, developed by Perla et al. [64] in 1980. This model describes the motion of the avalanche's centre of mass from the starting zone to the runout zone [60], and represents the avalanche as a granular continuum (1D) [49]. The 2D simulation model *ELBA+* (stands for *Energy line based Avalanche Model*) is used in hazard mapping of dense flow avalanches, and models the avalanching snow as a shallow flow in two dimensions on three-dimensional terrain surfaces [66, 73]. This means that no specific avalanche path must be defined [49], which also applies for the 3D simulation model *SamosAT* [67]. SamosAT has been available since 2008, and is used in both Austria and Iceland, as well as South Tyrol and Russia [49]. The 2D numerical simulation tool *RAMMS* is used in the dynamic modelling of dense flow snow avalanches, hillslope landslides and debris flows [65], and has been developed from the AVAL-1D model at the [WSL Institute for Snow and Avalanche Research](#) since 2005.

## 5.4 Calculating impact pressure

Structural avalanche mitigation methods constructed in the avalanche track or runout zone are meant to stop, deflect, or channelise the avalanching snow. Therefore they have to be designed to withstand great impact pressures, but to save cost and resources we want to calculate these pressures as accurately as possible. The different types of structural mitigation measures will be presented in Chapter 6, while some relevant avalanche actions on obstacles (i.e., impact pressures) will be discussed here. The impact pressures depend on the flow density, flow velocity, and the shape and orientation of the impacted object (obstacle). It is common to base the calculations of load actions on hydrodynamic calculation methods, as flowing avalanches to some extent are comparable to fluid flows [7, p. 186].

When an avalanche cannot flow freely around an object, such as when impacting a large wall standing perpendicular to the flow direction, the dynamic avalanche pressure  $p_f$  on the exposed area can be calculated according to Equation 5.7 [7, 9, 49, 60].

$$p_f = \rho_f \cdot v_f^2 \quad [\text{N/m}^2] \quad (5.7)$$

Here  $\rho_f$  is the flow density [ $\text{kg/m}^3$ ] and  $v_f$  [ $\text{m/s}$ ] is the depth-averaged velocity of the avalanche normal to the object surface. Equation 5.7 is used in the Austrian standard ONR 24805 [1], and assumes that the avalanche undergoes an inelastic collision [60].

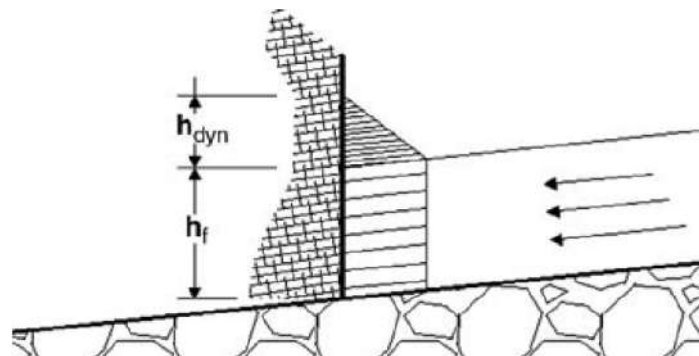
Barbolini et al. [59, p. 77] give a more detailed calculation procedure of avalanche impact pressures against walls and narrow obstacles. They recommend considering an initial peak pressure  $p_{peak}$ , calculated according to Equation 5.8, in addition to the stationary pressure in Equation 5.7.

$$p_{peak} = 3 \cdot \rho_f \cdot v_f^2 = 3 \cdot p_f \quad [\text{N/m}^2] \quad (5.8)$$

Figure 5.5 show how an avalanche impacting an obstacle will press on the obstacle over an additional height  $h_{dyn}$  as well as the flow height  $h_f$ . This height is called the *climbing height*, and is calculated according to Equation 5.9 when an avalanche impact a large object it cannot flow around [49]:

$$h_{dyn} = \frac{v_f^2}{2 \cdot g \cdot \lambda} \quad [\text{m}] \quad (5.9)$$

Here  $g$  [ $\text{m/s}^2$ ] is the gravitational acceleration, and  $\lambda$  [-] is an empirical *momentum loss factor* reflecting the loss of momentum when the avalanche impacts the obstacle [49]. The dynamic pressure against the obstacle reduces linearly with the climbing height (Figure 5.5).



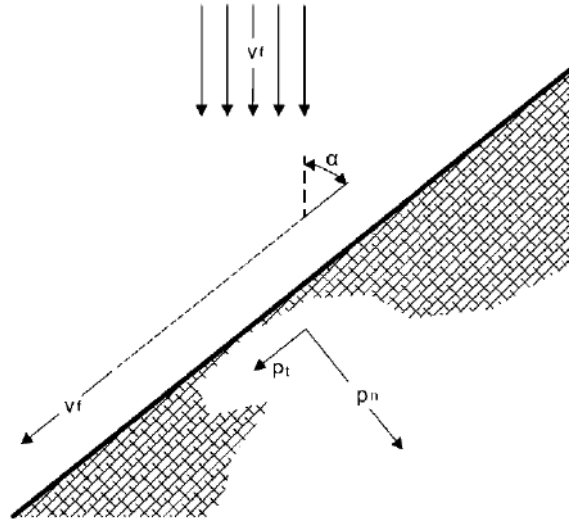
**Figure 5.5:** Illustration of the climbing height  $h_{dyn}$  of an avalanche impacting an obstacle that has not been surrounded by the avalanche flow. Source: Sauermoser et al. [49].

Avalanche protective dams or walls are often used to deflect the avalanche flow direction, and deflection also occurs on some snow sheds (though this is not favourable, see Section 6.3). The normal  $p_n$  and tangential  $p_t$  pressure against a structure deflecting an avalanche can be calculated according to Equation 5.10 and 5.11 respectively [49, p. 80], and are illustrated in Figure 5.6:

$$p_n = p_f \cdot v_f^2 \cdot (\sin\alpha)^2 \quad [\text{N/m}^2] \quad (5.10)$$

$$p_t = \mu \cdot p_n \quad [\text{N/m}^2] \quad (5.11)$$

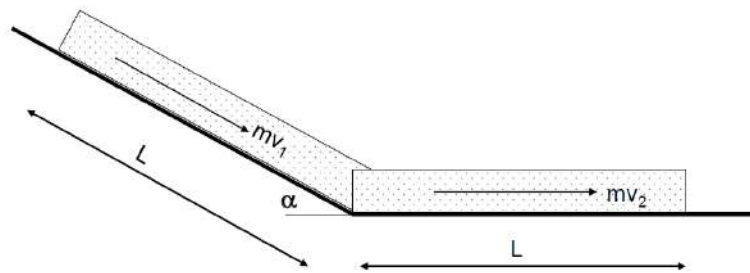
Here  $\alpha$  is the deflection angle between the obstacle and the avalanche flow direction, and  $\mu$  is the friction coefficient for the contact between the avalanching snow and the obstacle.



**Figure 5.6:** Normal  $p_n$  and tangential  $p_t$  pressure against a structure deflecting an avalanche with velocity  $v_f$  at a deflection angle  $\alpha$ . Source: Sauer Moser et al. [49, p. 80].

The Norwegian guideline Vegdirektoratet [9] gives similar calculation procedures for estimating dynamic pressures against constructions that deflect avalanches. These are based on conservation of impulse, see Figure 5.7, and assume a constant volume of avalanching snow before and after the deflection. The dynamic pressure  $k_a$  against an area, with length  $L$  and unit width  $b = 1\text{m}$ , when deflecting an avalanche with velocity  $v$ , flow height  $h$ , and density  $\rho$  is found according to Equation 5.12:

$$k_a = 2 \cdot \rho \cdot \frac{h}{L} \cdot v^2 \cdot \sin\left(\frac{\alpha}{2}\right) \quad [\text{N/m}^2] \quad (5.12)$$



**Figure 5.7:** Deflection of an avalanche with velocity  $v_1 = v_2 = v$  against an obstacle at a deflection angle  $\alpha$ . Source: Vegdirektoratet [9, p. 59].

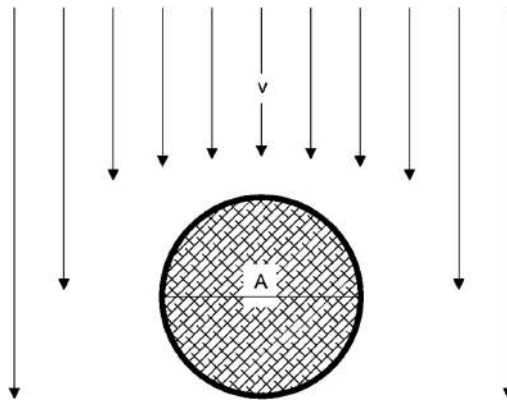
Narrow obstacles are defined by Barbolini et al. [59] as obstacles with a width on the same scale or smaller than the flow depth, and by Sauermoser et al. [49] as obstacles that are so small that the majority of the snow particles flow around it, see Figure 5.8.

The dynamic avalanche action  $p_f$  (drag) against narrow, stationary obstacles in an avalanche flow can be calculated according to Equation 5.13, where the constant  $C_d$  is a coefficient of resistance dependent on the shape of the obstacle and the snow type in the avalanche [7, 49, 59]:

$$p_f = \frac{1}{2} \cdot C_d \cdot \rho_f \cdot v_f^2 \quad [\text{N/m}^2] \quad (5.13)$$

The resulting force  $P_f$  on the narrow obstacle is found by multiplying the pressure  $p_f$  with the exposed area  $A$  perpendicular to the flow:

$$P_f = \frac{1}{2} \cdot C_d \cdot A \cdot \rho_f \cdot v_f^2 \quad [\text{N}] \quad (5.14)$$



**Figure 5.8:** Dynamic action on a narrow obstacle in avalanche flow. Source: Sauermoser et al. [49].

As we have seen from the formulas in this section, the dynamic impact pressure is dependent on the flow density  $\rho_f$  and the flow velocity squared  $v_f^2$ . This means that an increase in flow velocity has a bigger effect on the impact pressure than an increase in density, which leads to dry-flowing avalanches generally being more destructive [6, 22]. However, any combination of high speed and density have destructive potential. Thus, slush flows, with velocities up to  $30\text{m/s}$  and flow densities that may exceed  $700\text{kg/m}^3$  (and debris densities in excess of  $900\text{kg/m}^3$  [6]), may come close to the destructive power of big dry-flowing avalanches [6, 22].

# Chapter 6

## Avalanche mitigation measures

### 6.1 General

Mitigation is the process of making something less severe, dangerous, or damaging [74]. In relation to avalanches, mitigating measures reduce the hazard avalanches pose to human life, activity, and property [75]. The measures are often divided into two categories – structural and non-structural measures. There are three commonly used non-structural measures: The first measure is avalanche monitoring, forecasting and warning. The second measure is avoiding avalanche tracks and runout zones through temporary evacuation or land use restrictions, and the third is artificial triggering. These measures are presented in Section 6.2. Structural mitigation measures include the measures listed below, and will be presented in that order in Section 6.3.

- Snow supporting structures in the starting zone
- Deflecting and channelising structures
- Retarding and storing structures
- Direct protection of buildings, roads and valuable objects
- Snowdrift measures

In general, the structures giving the highest safety rating against landslides and avalanches are also the most expensive and comprehensive solutions [9]. The cheaper solutions are often specialised towards specific types of terrain or hazards.

D. McClung and Schaerer [6] propose a second way of categorising mitigation measures where they are categorised in terms of intervention (active or passive) and duration (temporary or permanent). This categorisation is summarised in Table 6.1 [6, p. 267], and is interesting because it clearly shows the available mitigation measures dependent on the desired philosophy, i.e. whether the objective is to prevent avalanches from starting (active) or mitigate the consequences of a potential hazard (passive). It is noted that all the structural measures are in the active-permanent category.

**Table 6.1:** *Avalanche protection methods in terms of intervention and duration [6].*

		Intervention	
		Active	Passive
Duration	Temporary	Avalanche control by explosives Road closures Precautionary evacuation	Avalanche forecasting / warning Seasonal occupation (summer houses) Seasonal road closures Warning signs
	Permanent	Supporting structures Snow fences Avalanche protection dams Retarding earth mounds Splitting wedges Reinforced construction Snow sheds (galleries) Forest management	Hazard mapping and land-use planning

Sauermoser et al. [44] gives an overview of avalanche defence structures classified by their function and location in the catchment area, with reference to Margreth [76]. This categorisation is presented in Table 6.2, and is useful when investigating which mitigation measures are available to achieve a specific protection effect and where in the avalanche catchment area the structure will be constructed.

**Table 6.2:** Overview of avalanche defence structures classified by their function and location in the catchment area. Note that avalanche path here means the same as avalanche track. Source: Sauermoser et al. [44].

Structural avalanche defense	Avalanche defense structures				Object protection
Category of defense measure	Snowdrift control structures	Snow supporting structures	Avalanche catching and retarding structures	Avalanche deflection structures, snow sheds and tunnels	Structural building protection
Function (protection effect)	Structures that control the snowdrift and snow accumulation in the starting zone.	Structures that stabilize and sustain the snowpack in the starting zone and prevent the release of avalanches.	Structures that stop or decelerate the motion of avalanches or dissipate the energy in order to reduce the run out distance.	Structures that deflect avalanches in motion from objects at risk or to by-pass them from traffic routes (roads, railway lines).	The building at risk is enforced in a way that it is able to withstand the impact (stress) of avalanches with little damage.
Type of defense structure	Snowdrift fence Wind baffle Wind roof (Jet roof)	Snow bridge/rake/net Combined snow bridge (steel/wood) Terrace	Avalanche catching or retarding wall (dam) Avalanche mound Avalanche breaker	Avalanche deflecting dam (wall) Gallery (shed) Tunnel	Avalanche splitting wedge Roof terrace Impact wall
Location in catchment area	Starting zone	Starting zone	Avalanche path Runout zone	Avalanche path Runout zone	Avalanche path Runout zone

## 6.2 Non-structural mitigation methods

### 6.2.1 Avalanche monitoring, forecasting and warning

Avalanche monitoring, forecasting and warning are passive defence measures with temporary protection effects [44, p. 9]. This is because no direct action is taken in the terrain and the measures are in effect for a specific duration of time.

Avalanche forecasting and warning consist of assessing the avalanche hazard in specific regions with the goal of creating daily updated status reports on the avalanche danger [44]. The daily reports can



be used in risk management by anyone planning to stay or work in avalanche prone terrain. Forecasting and warnings are based on snow and weather observations as well as weather forecasts, and require computer-based models and digital measuring technology. The European Avalanche Warning Services has created a tool called the EAWS Matrix to help avalanche forecasters determining the avalanche danger more objectively across Europe [77]. This Matrix is shown in Figure 6.1.

EAWS		Probability of avalanche release																			
		Generally only with high additional load				Primarily from high additional loads (perhaps low additional loads)				Already with low additional loads <b>possible</b>				With low additional loads <b>probable</b>				Spontaneous release of size 2 avalanches <b>possible</b>	Spontaneous release of size 3, in some cases size 4 avalanches <b>possible</b>	Spontaneous release of many size 3, in several cases size 4 avalanches <b>probable</b>	Spontaneous release of numerous size 4, often size 5 avalanches <b>probable</b>
Avalanche Size		1	2	3	4	1	2	3	4	1	2	3	4	1	2	3	4				
Distribution of hazardous sites	Single hazard sites (in the Avalanche Bulletin specifiable*)	1	1	1	1	1	1	2	3	1	1	2	3					1	2		
	Hazard sites on <b>some</b> slopes (in the Avalanche Bulletin specifiable*)	1	2	2	3	1	2	2	3	1	2	3	4	2	3	3	4	2	3	3	4
	Hazard sites on <b>many</b> slopes (in the Avalanche Bulletin specifiable*)	1	2	2	3	2	2	3	4	2	3	3	4	3	4	4	4	2	3	4	4
	Hazard sites on <b>many/most</b> slopes (in the Avalanche Bulletin not specifiable**)									3	4	4	4	3	4	4	4	3	4	4	5
	Hazard sites also in <b>moderately steep</b> terrain													4	4	5	5		4	5	5
		and / or																			

\* specifiable with respect to altitude, exposition and/or relief  
 \*\* The hazard sites are too numerous or too diffusely distributed to be specifiable with respect to altitude, exposition and/or relief

Figure 6.1: The EAWS matrix used as a tool by avalanche forecasters to determine the avalanche danger more objectively. Source: European Avalanche Warning Services [77].

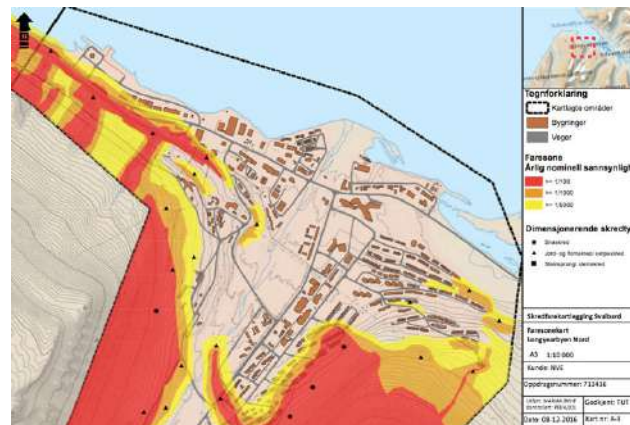
Stoffel et al. [78] give a thorough presentation of the different avalanche monitoring methods and technology available today. The monitoring mainly serves scientific purposes because the warning time is very short, and the goal is to observe and record the characteristics of the actual avalanche event and the conditions leading up to an event [78, p. 345]. The results are used to improve the technical avalanche defence. Avalanche monitoring methods as listed by Stoffel et al. [78] :

- Meteorological monitoring of climatic factors such as air temperature, precipitation, and wind speed and direction
- Monitoring snow depth and the spacial extent of the snow cover using terrestrial laser scanners (LIDAR) or integrated components of existing weather stations
- Monitoring snow temperature, typically using platinum resistance thermometers
- Monitoring the mechanical properties of the snowpack such as snow density, snow strength, shear strength, snow gliding, and snow creep
- Monitoring snow forces on avalanche defence structures to validate load and dimensioning assumptions and to improve or maintain the structures
- Monitoring avalanche motion, such as velocity and flow depth, and measuring dynamic impact forces from avalanches

### 6.2.2 Avoidance

Avoiding avalanche tracks and runout zones can be done through temporary evacuation or land use restrictions. Temporary evacuation is based on avalanche forecasting and warnings, and can involve evacuating residents from their homes or road closures. Land use restrictions involve prohibiting the construction of sensitive structures in avalanche prone areas (such as schools or residential buildings), or allowing only non-conflicting use of an area (such as agriculture that takes place during non-avalanche months).

A process used to regulate what types of land use are allowed in different areas is *avalanche zoning*. During avalanche zoning, avalanche-prone areas are identified on an *avalanche hazard map*, and then the type of land use allowed is regulated based on the level of acceptable risk [79]. An example of an avalanche hazard map for Longyearbyen, Svalbard is presented in Figure 6.2.



**Figure 6.2:** Snow avalanche hazard map of Longyearbyen from 2016, produced by Multiconsult. Source: Hannus [80].

In Norway, the level of acceptable risk is regulated through the Planning and Building Act (Norwegian: Plan- og bygningloven) [81], which is an important normative basis for avalanche zoning. In §28-1 it says that

"Land may only be developed, (...) when there is adequate safeguard against hazard or significant inconvenience as a result of natural or environmental conditions. (...) For land that is not sufficiently safe, the municipality shall prohibit the establishment or alteration of property or the erection of structures (...)." [81] §28-1

Byggteknisk forskrift (en. Regulations on technical requirements for construction works) [29] gives a more detailed description of the term "adequate safeguard against hazard" in its §7-3:

"The landslide or avalanche safety class of construction works in areas prone to landslides or avalanches shall be stipulated pursuant to the table below. Construction works and their related outside areas shall be sited, designed or protected against landslides or avalanches such that the largest nominal annual probability in the table is not exceeded." [29] §7-3

The table referred to by TEK17 is reproduced below as Table 6.3.

### 6.2.3 Artificial avalanche release

Artificial triggering is a widely used protection method of areas that can be evacuated and has little risk of property damage [79]. It is an active defence measure with temporary protection effects, where temporary refers to the likelihood of avalanches releasing in the secured zone being low for some



**Table 6.3:** Safety classes for siting construction works in areas prone to landslides or avalanches. Source: Byggt teknisk forskrift [29].

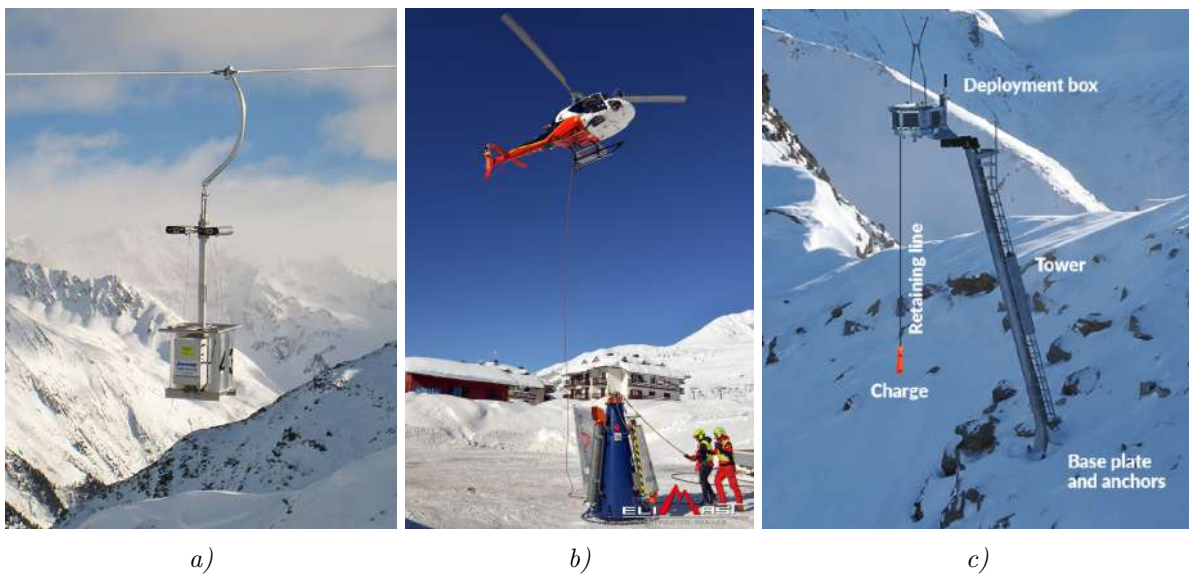
Landslide / avalanche safety class	Impact	Greatest nominal annual probability
S1	slight	1/100
S2	moderate	1/1000
S3	severe	1/5000

time after blasting [78, p. 325]. The goal of artificial avalanche release is to either trigger smaller avalanches with little damage potential to avoid larger spontaneous avalanches [78], or to remove the potentially dangerous snow cover in a controlled manner when the area below is evacuated.

There are several technological methods of artificial avalanche release. Some common methods are listed below [7, 9, 78]:

- Manual placement of explosive charges / hand charge
- Pre-placed explosive charges
- Avalanche blasting ropeways (explosive charges are transported from a ropeway)
- Helicopter blasting (placing explosive charges by dropping them from a helicopter)
- Avalanche mortars, artillery or specially constructed cannons (explosive projectiles)
- Gazex<sup>®</sup> fixed blasting system (propane-oxygen gas explosion from a pipe)
- Daisybell<sup>®</sup> Helicopter Avalanche Control System (hydrogen-oxygen gas explosion from a bell-shaped container hanging below a helicopter) [82]
- Wyssen Avalanche Tower<sup>®</sup> (tower containing 12 explosive charges that can be lowered on a string and detonated above the snow cover) [78, 83, 84]

In Norway, artificial avalanche release is mainly performed using 1) explosive charges that are pre-placed or dropped from an avalanche blasting ropeway, 2) gas-explosions deployed from a DaisyBell<sup>®</sup> hanging below a helicopter, 3) avalanche blasting ropeways, and 4) avalanche towers [9, 85]. These methods are presented in Figure 6.3. The NPRA administer four DaisyBells stationed in Leikanger, Tromsø, Arnøya, and Alta, and there are currently three avalanche blasting ropeways of an older type constructed in the early 90's at Haukelifjellet, Aurland, and Bremanger. A network of 14 Wyssen avalanche towers were installed in 2016 at Tyn, Årdal.



**Figure 6.3:** Three methods of artificial avalanche release: a) avalanche blasting ropeway of type Doppelmayr<sup>®</sup> [86], b) Daisybell<sup>®</sup> [82], c) Wyssen Avalanche Tower<sup>®</sup> [83].

## 6.3 Structural mitigation measures

### 6.3.1 Snow supporting structures in the starting zone

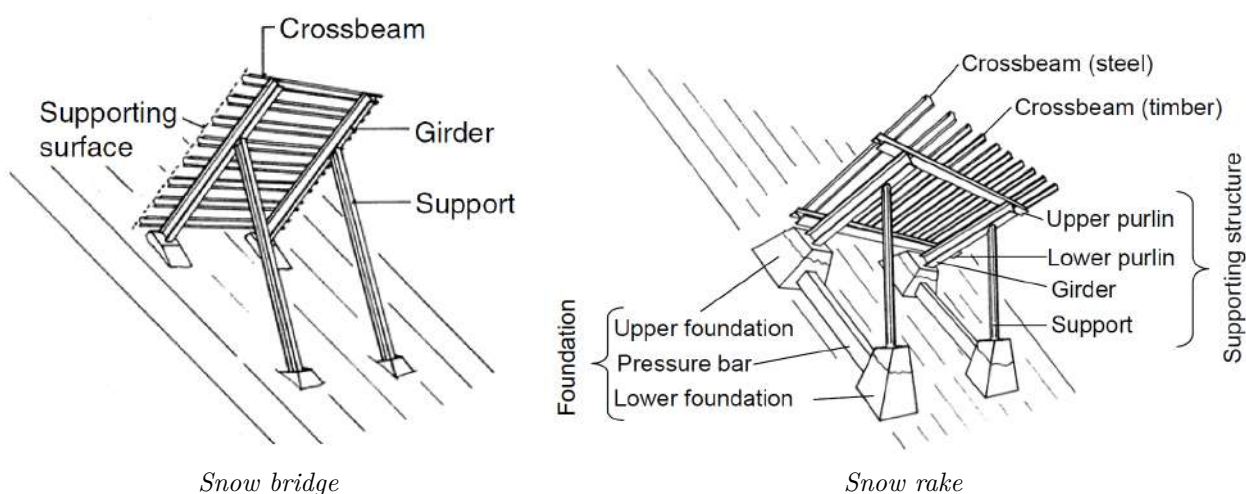
The purpose of snow supporting structures in avalanche starting zones is, according to the [Swiss Guideline](#), to "prevent avalanches from being triggered, or at least to prevent snow movements occurring that could lead to damage" [2, p. 21]. This is achieved by restricting the creep and glide in the snow layer, and thereby reducing the shear and tension stresses in the snowpack that could trigger an avalanche. The affected area in the snowpack is the previously mentioned *back-pressure zone* (see [Section 3.3.2](#)), and the structures are designed against the snow pressure from this area in cases of extreme snow depth. Support structures can also limit the size of avalanches through interrupting the continuity of the snowpack and thereby limiting the propagation of shear fractures in weak layers, and in addition stop small avalanches before they become large [87, p. 230].

Some of the most common snow supporting structures are snow bridges, snow rakes, and snow nets. In addition to these, there are structures such as massive support structures and the Ombrello snow supporting structure<sup>®</sup>. Massive support structures is an old construction type that has a limited effect because of the lower upslope structure height, while the Ombrello snow supporting structure is particularly common in Italy [88, pp. 132, 147]. The last two structure types will not be discussed further.

Reforestation and forest management can also help stabilising the snow in the starting zone. However, the tree trunks have to be strong enough to withstand the load actions from creep and glide, and the distance between the trees should not exceed 5 meters [87].

#### Snow bridges and snow rakes

Snow bridges and snow rakes have a rigid support surface consisting of crossbeams parallel to the ground (bridge) or at right angles to the ground (rake), see [Figure 6.4](#) [2, p. 15]. They have proven to be reliable avalanche defence, and are therefore widely used in Europe [87, p. 229]. Snow rakes made of steel have become a less common choice because they require more work than bridges when assembling intermediate structures, but wooden snow rakes are standard in Switzerland for structures with a shorter service life.



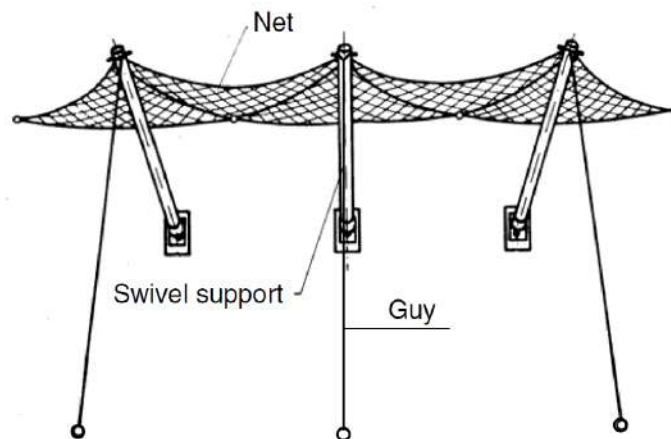
**Figure 6.4:** Drawing of the snow supporting structures, snow bridge and snow net. Source: Margreth [2, p. 15]

Steel and wood are the most common building materials for rigid support structures [7, pp. 165–167]. Steel is used when the service life is more than 80 years, while wood is used for smaller structures with a life expectancy less than 50 years [88, p. 131]. Structures have also been built with a supporting surface made of wood and girders, purlins and supports of steel. Generally, support structures made of steel cost three times as much as wooden structures [87, p. 230].

There are advantages and disadvantages with snow bridges and rakes (rigid structures) compared to snow nets (flexible structure). An advantage is that the rigid structures are easier to anchor on soil with low load carrying capacity. This is because they absorb more loading in compression while snow nets rely on strong ground tension anchors [87, 88]. Rigid structures also have less maintenance costs than snow nets, and are more adaptable to uneven terrain. However, snow nets are easier to transport, lighter and less conspicuous, less sensitive to creep movements in the ground, and are better at absorbing falling rocks [88, pp. 133–140].

### Snow nets

Snow nets have a flexible support surface made of rectangular or triangular, flexible steel cable nets (Figure 6.5) [2, p. 15]. As mentioned above, they are lighter and less conspicuous than rigid support structures, and can withstand greater rockfall energies. Brändle et al. [89] found that specially designed snow nets could achieve a rock fall capacity of up to  $500kJ$ , while snow bridges made of steel are not able to withstand rock fall energies of more than  $50kJ$ . The flexible cable connections on the snow nets are adjustable lengthwise, and therefore provide more flexibility when choosing anchoring points. The flexible nets absorb some of the snow creep resulting in a reduced snow pressure compared to rigid structures, but the anchoring forces are very large and the nets therefore require good foundation conditions [88, pp. 135–137].



**Figure 6.5:** Drawing of the snow supporting structure, snow net. Source: Margreth [2, p. 15]

### 6.3.2 Deflecting and channelising structures

Deflecting and channelising structures are walls, dams, or dikes that are built in the avalanche track or runout zone to contain an avalanche to a specific route or deflect the avalanche away from objects that need protection [6, 88]. They are most commonly constructed in the runout zone, and will then have the advantage of easier access than other structures built in the the avalanche track or -starting zone [87, p. 232]. However, a disadvantage is that they are only effective against an avalanches flowing component and have almost no effect against the powder component [87, 88]. This makes them less reliable than avalanche defence structures in the start zone [87]. Because the avalanche has been allowed tot gain full speed, the structures have to be designed to withstand high impact pressures. Barbolini et al. [59] gives a thorough description of avalanche deflection dams and their design.

### Deflecting dam (wall)

Deflecting dams are used to intercept avalanches and redirect their flow in a desired direction [6, 88], see Figure 6.6. They can be straight or curved, and their height and orientation are designed for a specific return period. However, to make sure the constructions are not destroyed from the pressure forces of deflecting an avalanche they are designed against forces from much bigger avalanches (with a greater return period than the one used for the design height) [87]. Deflecting dams are often a cost-effective solution, and have successfully diverted several medium-sized avalanches [59, p. 3].



**Figure 6.6:** Deflecting dam and retarding cones at Seljalandsmúli in Ísafjörður, northwestern Iceland. Source: [59, p. 117]. Photo: Tómas Jóhannesson.

### Channelising (guiding) dams

Channelising dams are similar to deflecting dams, but are used to limit the avalanches lateral expansion and to confine the flow in a narrow channel. They are built parallel to the avalanche-flow direction, and often in combination with avalanche galleries.

#### 6.3.3 Retarding- and storing structures

Retarding and storing structures are built in the avalanche track or runout zone. Their function is to either slow down the avalanche and reduce its energy and runout distance (retarding cones), or completely stop the avalanche before it reaches infrastructure (catching dams or walls).

### Catching dam (wall)

Catching dams are similar to deflecting dams, but are built transverse to the avalanches flow direction. They can be designed to stop the entire avalanche or to allow a partial overflow [88, p. 169].

The most important factors when designing catching dams are the effectual height, the gradient of the dam on the avalanche side, the placement in the avalanche track or runout zone, and the storage volume for the avalanche deposits in front of the dam [7, 88]. The effectual height is proportional to the avalanche speed squared ( $v^2$ ), which makes it important to place the catching dam as far down in the runout zone as possible [7, p. 177]. A steeper gradient facing the avalanche will reduce the avalanche energy, and so the gradient should be as steep as possible [7]. The volume of the



deposition zone have to be big enough to contain the expected avalanche volume (unless overflow is accounted for in the design). This storing capacity is often the defining factor of the catching dams size, as opposed to the pressure forces when an avalanche hits [88]. The designer also have to account for pre-filling of the deposition zone from previous avalanches, which can reduce the effective height and the storing capacity.

### Retarding cones

Retarding cones are used to reduce the avalanche speed and runout distance. They work by forcing the avalanche to push around and over the cones, which increases the flow friction and disrupts the flow direction [87, p. 242].

The cones can be built as mounds of local geomaterial, vertical silos, or as mechanically stabilised earth (see Figure 6.7). They are placed close together, in rows or staggered, and are most effective in slopes less than  $15^\circ$  [87, p. 242]. Retarding cones can be built alone or in combination with catching dams to reduce the necessary height of the dam. Both Lied and Kristensen [7, p. 185] and Schilcher et al. [88, p. 171] state that the height of the cones should be 2 – 3 times higher than the flow height, and that the gradient on the avalanche side should be approximately  $60^\circ$ .

Retarding cones have been proven experimentally to cause an avalanche velocity reduction of 20% to 30% using respectively one or two rows of cones [90]. They have best effect on flowing avalanches, while powder avalanches usually flow through [7, p. 185].



**Figure 6.7:** Photo of braking mounds in Neskaupstaður, Iceland, and the catching dam behind them. Each mound is 10 m high and the catching dam is 17 m high. Source: [90].

### 6.3.4 Direct protection of buildings, roads, and valuable objects

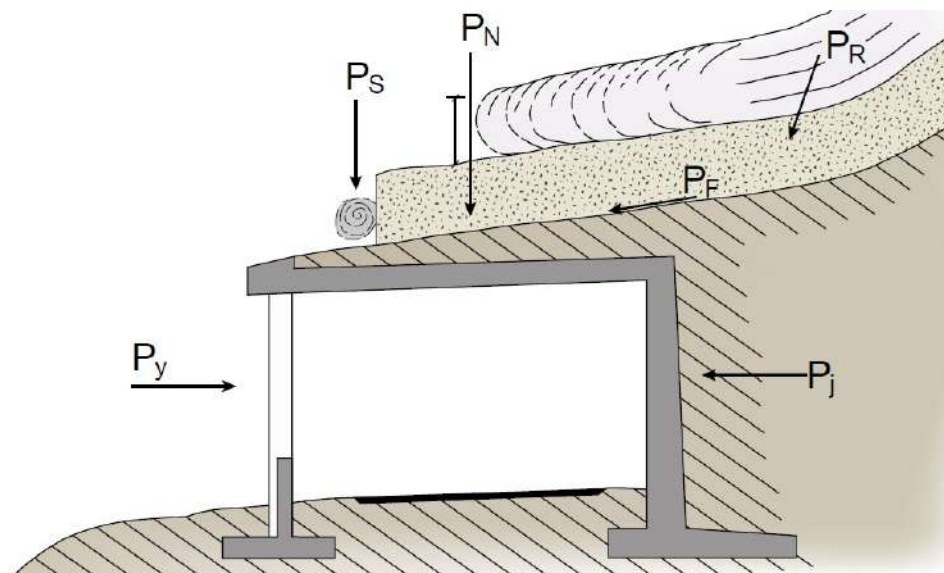
Buildings, roads, and other infrastructure can be protected directly through building design (reinforcement) (page 245), splitters [87, p. 240], ramps (page 245), snow sheds (also called avalanche sheds and galleries), tunnels and bridges.

#### Snow sheds and tunnels

A snow shed is mainly used to protect short sections of roads and railways by building a roof over which the avalanche can bypass, and it is one of the most reliable protection methods [7, p. 174]. They are especially effective when the starting zone is large but the avalanche track is narrow and well defined [88, p. 172]. However, snow sheds are also very expensive. Jamieson et al. [87, p. 243] gave an estimated price of \$50 000 to \$90 000 per linear meter of a two-lane snow shed in 2018.

Snow sheds are commonly constructed of reinforced concrete, and have to be designed against both static and dynamic loads, see Figure 6.8. Some of these loads are [32, p. 74]:

- Vertical (static) load on the roof from the snowpack and avalanche deposits ( $P_N$ )
- Horizontal friction forces between the avalanche and the snow shed roof ( $P_F$ )
- Deflection loads if the roof of the snow shed forms an angle with the velocity of the avalanche ( $P_R$ )
- Earth pressure consisting of pressure from the earth itself and increased pressure from the earth when loaded with a snowpack or avalanche deposits ( $P_J$ )
- Point-loads from rock fall or blocks in the avalanche ( $P_S$ )
- Static and dynamic load against the downstream wall caused by avalanche deposits or vacuum from an avalanche passing over the roof ( $P_Y$ )

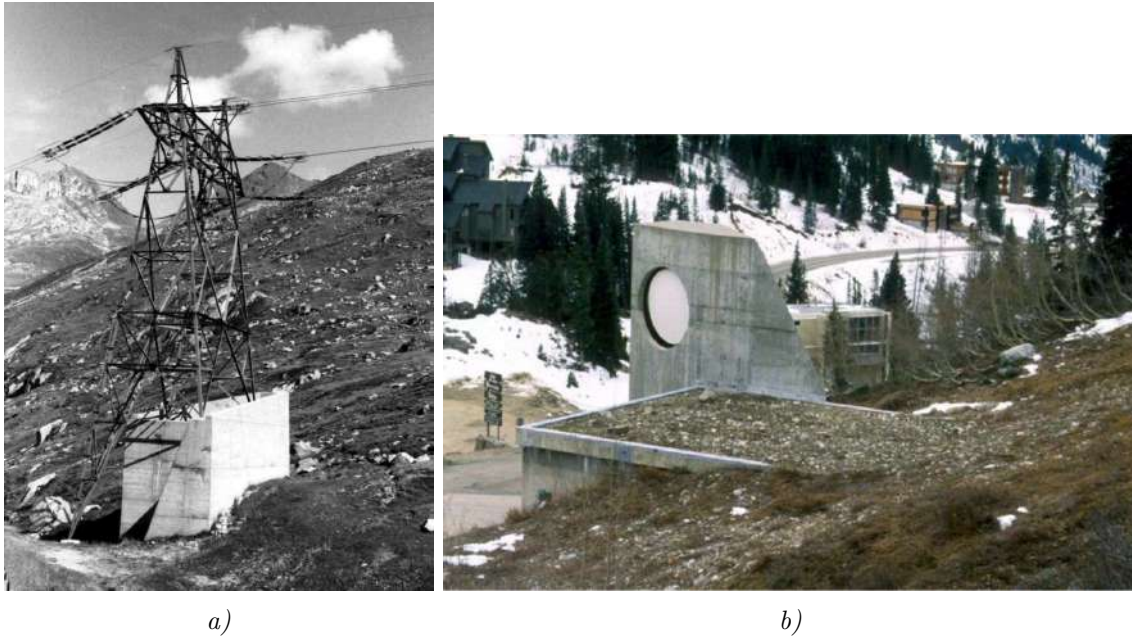


**Figure 6.8:** Loads against a snow shed according to Vegdirektoratet [32, p. 74].

If possible, the deflection of the avalanche should happen in the terrain before the snow shed to minimise the deflection loads on the roof. In addition, the upstream wall should have a ramp or be cut into the slope so the avalanche does not hit the upstream wall horizontally. To save cost, channelising dams can lead the avalanche to the snow shed so that a shorter snow shed is necessary.

### Building design, splitting wedge and ramps

If only a few buildings are to be protected, a direct protection option might be chosen. This can be a splitting wedge or ramp on the upper side of the building that leads a potential avalanche around or over the building, or the building itself can be reinforced to withstand the avalanche pressure (Figure 6.9). In the Alps, reinforced residences exist in High- and Moderate hazard zones [87, p. 245].



**Figure 6.9:** Direct protection measures. a) Concrete splitter around a transmission line structure. Photo: P. Schaerer. b) Concrete splitter around communication tower, and a ramp protecting the control building. Photo: B. Jamieson. Source: Jamieson et al. [87, p. 241].

#### 6.3.5 Snowdrift measures

Snowdrift measures are used to control the wind transport of snow, and especially to avoid snow accumulation in the avalanche starting zone. This is done either by vegetation and forest management, or by snowdrift control structures such as snowdrift fences (see Figure 6.11), wind baffles, and jet roofs. Schilcher et al. [88] illustrates the function and effect of the snowdrift control structures well with a table (see Table 6.4).

##### Snowdrift fences

The dominating mountain type in Norway have a flat mountain plateau with a marked transition to steep slopes below [7, p. 161]. Across these plateaus the wind can erode great amounts of snow and deposit it in the leeward terrain, allowing additional snow to build up in the avalanche starting zones (see Section 2.2.4).

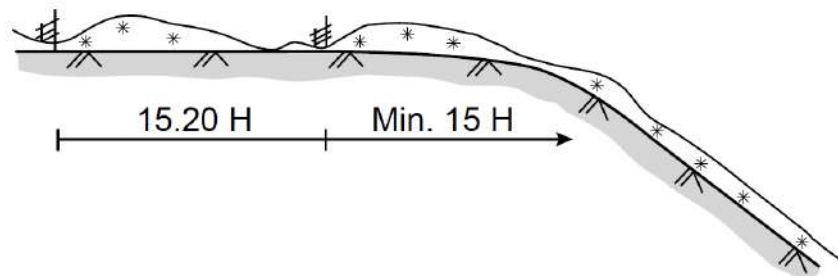
To avoid this, snowdrift fences are placed on the flat mountain plateaus above snow supporting structures to collect the snow on the flat area instead of the slope below. However, there are several requirements that need to be fulfilled for the snowdrift fences to be effective. First, the plateau need to be almost horizontal and at least 50 meters wide to have enough room for the fences and the collected snow [7, p. 162]. Second, it is critical that the slope avalanche starting zone lays in the leeward direction of the dominating wind direction, and that the structures are facing the wind [7, 88].



**Table 6.4:** Copy of Table 5.6 in Schilcher et al. [88, p. 156]. Classification of snowdrift control systems according to function and effect

Effect	Function	Construction type
Structures that prevent the transportation of drifting snow	Braking the wind speed, deposition of the drifting snow	Snowdrift fence with vertical beams
		Snowdrift fence with horizontal beams
Structures that further the transportation of drifting snow	The wind is deflected in such a manner that the drifting snow in particular avalanche starting zones is continuously brushed away, or the snowpack is prevented from carrying out its normal build-up because of turbulence effect	Wind baffle
		Wind roof

The fences can have either horizontal- or vertical beams, and are usually built in steel or wood. They are designed to withstand great wind-loads, and have a height of  $H = 3$  to 6 meters. The snow deposits behind each fence is commonly  $15 * H$ , and the structures should therefore be erected so that the first row is placed at a distance of 15 to  $20 * H$  away from the avalanche starting zone [7, 9, 88]. Jamieson et al. [87] gives a deposit length of 20 to  $30 * H$ .



**Figure 6.10:** Schematic of two rows of snowdrift fence given in Vegdirektoratet [9]. Here, the minimum distance to the starting zone is given as  $15H$  which is also the distance suggested by Lied and Kristensen [7], while Jamieson et al. [87] and D. McClung and Schaerer [6] recommends a distance of 20 to  $30H$ .

### Jet roofs and wind baffles

Cornice formation on ridgetops is a common avalanche danger caused by wind transport of snow (see Section 2.2.4). Two defence structures that are used to reduce the formation of cornices are jet roofs (also called wind roofs) and wind baffles (also called snow sails).

Jet roofs are used to accelerate the wind at the beginning of the lee, and thereby transport the snow further down the slope. This reduces cornice formation, but may cause wind slabs in the starting zone. In addition, jet roofs can be used in combination with snow supporting structures to prevent excessive snow accumulation around the top rows [88, p. 159]. According to Jamieson et al. [87, p. 226], jet roofs are typically 4 to 6 meters high on the windward side and 4 meters wide. Schilcher



**Figure 6.11:** Snowdrift fences with horizontal steel boarding in Longyearbyen, Svalbard. Photo: Haldis Døvre Kalland.

et al. [88] gives a height of 2 meters on the windward side and 1 meter on the leeward side while assuring that the inclination of the roof is slightly larger than the terrain inclination (creating a nozzle effect). An explanation for the deviation in structure height has not been found, though...

Wind baffles are structures that are placed in areas of potential cornice formation to influence the wind currents and thereby reduce the continuity of cornices and wind slabs near ridges [87, 88]. They can be rectangular, trapeze shaped, or cross-shaped, and with or without ground level gap. The effect of the wind baffles seems to vary between locations and for different designs. For example, at the Milepost 151 avalanche track in Wyoming 50 baffles were installed and found to be only marginally effective [87, p. 226], and cross-shaped wind baffles were installed on the top of Hafnarhryna, Iceland in 2013 that did not lead to a substantial change in the snow distribution in the following winter [91]. However, according to Schilcher et al. [88, p. 159] the cross-shaped wind baffles without ground level gap have been successful in Switzerland.

## 6.4 Mitigation measures against slush flows

Historically, slush flows have often been treated the same way as debris flows when planning mitigation measures. This experience has proven that mitigation measures against debris flows are to a large degree effective against slush flows [9, p. 29]. However, slush flows normally reach higher velocities and are less viscous than debris flows [32, p. 80]. This means that extra considerations have to be made when deciding on a solution.

The mitigation measures that are most commonly used against slush flows are trenching, deflecting- and channelising structures, catching dams, and moving necessary infrastructure such as roads up on bridges [32]. All these mitigation measures have been discussed in this chapter except for *trenching* and bridges.

Trenching is a mitigation measure used against slush flows where a bulldozer clear a path along the bottom of the valley of snow, and thereby open a drainage path for melt water (Figure 6.12). Trenching is an old mitigation measure against slush avalanches, and has been used in Vannledningsdalen, Svalbard since 1953 when a destructive slush flow released in the valley [92, 93]. The trenching is performed in spring after the wind drift of snow is minimal and the avalanche danger from valley sides are evaluated as safe for the operator. For these reasons, trenching does not mitigate against slush flows that happen midwinter. In Longyearbyen, higher temperatures, more rain and periods of mild weather in midwinter increase the risk of debris flows, avalanches and slush flows [5, p. 5]. Therefore, trenching is no longer considered to be an adequate solution [5, p. 16].



**Figure 6.12:** Picture of how the snowpack in Vannledningsdalen is prepared to minimise the slush flow risk using trenching. Source: Jónsson and Gauer [92].

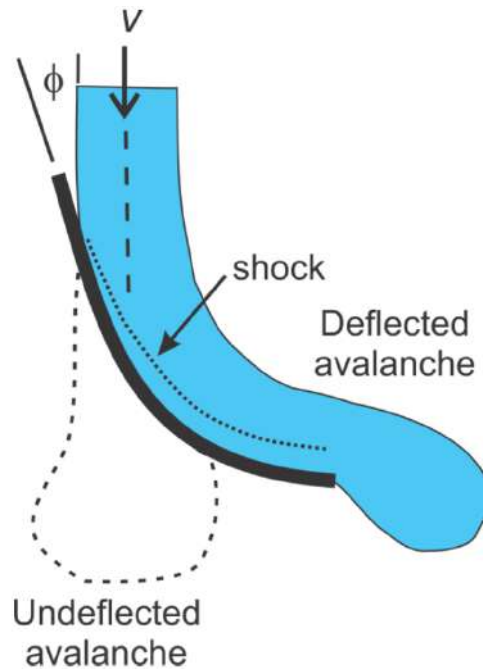
Bridges are used to move necessary infrastructure such as roads or railways out of the path of slush flows (Figure 6.13). This measure is effective because slush flows mainly follow distinct drainage roads [32, p. 82], so by using channelising dams or walls the slush flow can be directed under the bridge. When designing bridges as a mitigation measure, it is important that 1) the opening under the bridge is large enough to allow the full slush flow to pass, 2) the channelising walls should have small deflection angles (10 – 20°), and 3) the channel must have a constant slope gradient to avoid build-up of debris around the bridge [32, p. 83].



**Figure 6.13:** Bridge over slush flow drainage road with channelising walls on each side. Photo: Harald Norem. Source: Vegdirektoratet [32].

Because slush flows can reach higher velocities and are less viscous than debris flows, they can climb higher up on deflecting and catching dams [32, p. 80]. This might cause overflow of the dam if not properly dimensioned, as illustrated in Figure 6.14. According to Vegdirektoratet [32, p. 80], good

mitigating effect have been achieved using straight deflection dams with small deflection angles, while curved deflection dams have not been as effective in protecting roads against slush flows. Therefore, the effective height of a curved deflection dam has to be increased when designing for slush flows.



**Figure 6.14:** Illustration of how an avalanche or slush flow with speed  $v$  can partially climb over a curved deflection dam when encountering it at an angle  $\phi$ . Source: Jamieson et al. [87, p. 235].

A new concept for mitigating against slush flows is using flexible net barriers similar to debris flow barriers (as seen in Figure 6.15). This is a solution that has been proposed used in the ongoing project of mitigating against slush flows in Vannledningsdalen, Svalbard. No net barriers have previously been used in Norway as a mitigation measure against slush flows of this size [27, 94], and it is therefore a very interesting project that will be discussed in detail in Chapter 8.



**Figure 6.15:** Three multilevel debris flow barriers in Merdenson, Valais, Switzerland. Similar barriers are planned used as mitigation measures against slush flows in Longyearbyen, Svalbard. Source: Wendeler [95].





# Chapter 7

## A research trip studying avalanche-related structures near Longyearbyen, Svalbard

### 7.1 Highly relevant for Longyearbyen

Longyearbyen is one of the most northern settlements on Earth (78°N) and the largest settlement on Svalbard, Norway. It lays in Longyear valley (Norwegian: Longyeardalen) surrounded by steep mountain sides prone to avalanches, slush flows, debris flows, and rock fall. Longyearbyen is the location of [The University Centre in Svalbard \(UNIS\)](#), a higher education institution that provide university level education in Arctic studies.

There are several reasons why Longyearbyen is of interest for this thesis. The first reason is that there is an ongoing design and construction work of avalanche protective structures to protect the city against snow avalanches and slush flows. This work provides a great opportunity to learn through following the decisions made and computations done by experienced engineers. [Figure 7.1](#) gives an overview of the areas in Longyearbyen where mitigation measures have been constructed, are under construction or are planned.

The second reason is that because of Longyearbyen's geographical location, it is uncertain whether established computational parameters for calculating loads in mainland Norway or the Alps are representative in Longyearbyen's climate. Some of these factors are snow creep and glide, snow density, and wind transport and deposition of snow. The area is therefore of great interest for future research, and will likely be the location of field work for [this author](#) as a PhD candidate starting August 2022.

The third reason is that one of the mitigation works in Longyearbyen is the *Vannledningsdalen project*. Vannledningsdalen is a valley above Haugen ([Figure 7.1](#)) that is prone to slush flows, and these slush flows have previously caused great damage both material and to human life [80]. The Vannledningsdalen project aims to secure the population against future slush flows using flexible net barriers and channelising dams. This is especially interesting because no net barriers have previously been used in Norway as a mitigation measure against slush flows of this size [27, 94]. With the aim of learning the details in designing flexible net barriers against slush flows in arctic regions, [Chapter 8](#) provides a detailed study of the design process completed by [Skred AS](#), [HNIT verkfræðistofa](#) (consulting engineers) and [Geobrugg AG](#).

The fourth reason why Longyearbyen is of interest is that there is an already established collaboration between [NTNU](#) and [UNIS](#), which allows for easier knowledge exchange and teamwork. The collaboration includes an exchange of students, PhD candidates and professors, as well as an ongoing project measuring snow pressure that [this author](#) has taken part in (see [Section 7.3](#)). In addition, Longyearbyen is a relatively big settlement in the arctic, and with [UNIS](#) it has the necessary resources and infrastructure to conduct research in arctic climate.



**Figure 7.1:** Photo giving an overview of Longyearbyen centre including the areas of interest for mitigation measures. 1 - Lia above Spisshusene (residential houses) where snowdrift fences, support structures and a catching dam have been constructed. 2 - Sukkertoppen and Lia residential area where a catching dam and support structures are planned as mitigation measures against snow avalanches. 3 - Vannledningsdalen where flexible net barriers are planned as a mitigation measure against slush flows. 4 - Longyearelva where measures have been completed to avoid erosion and flooding. Source: Hoseth et al. [5].

## 7.2 Aim of the research trip

A research trip was conducted to Longyearbyen during March 2<sup>nd</sup> – 8<sup>th</sup> 2022. The group consisted of Arne Aalberg (supervisor), Haldis Døvre Kalland (this author), Bjørn Vetle Madsen Basma and Philip Olav Farstad Kunz (students at NTNU). Basma and Kunz are analysing data provided by the Snow Load Testing System (SLTS) (see Section 7.3) in their master thesis, and Aalberg is the supervisor for Basma, Kunz and Kalland. The group is pictured during field work in Figure 7.2.

The trip had four main aims. The first aim was to see the SLTS. Seeing the system on-site would provide a much better understanding of the equipment compared to looking at pictures, and this understanding is essential when analysing the data it provides. This aim was especially important since Basma and Kunz are writing about this data in their master thesis and Kalland will continue this work as a PhD candidate.

The two next aims are related to the extensive field work planned around the SLTS (Section 7.3). One aim was to obtain data that is needed when studying the resulting snow pressure against the SLTS. This data includes snow density and temperature profiles, snow height measurements up-slope of the SLTS, and checking that the automatic measurements of snow height are correct (Section 7.3). The other aim was to gain experience in arctic field work and using scientific equipment to measure snow density, temperature, and snow height profiles.

The last main aim was to look at the already constructed snow supporting structures and snow drift fences at Sukkertoppen (see respectively Section 7.5 and 7.4). They are of interest because of their location in an arctic climate, which provides a unique opportunity to study how arctic climate affect the snow pressures and snow accumulation around the structures.

In addition, a useful benefit of the trip was to meet other scientists working at UNIS. They are able to regularly visit the SLTS, as well as future project sites around Longyearbyen, and are therefore a highly valued partner.





**Figure 7.2:** Group photo of the participants of the research trip to Longyearbyen, March 2022. From the left: Arne Aalberg (supervisor), Haldis Døve Kalland (this author), Vetle Basma and Philip Kunz.

## 7.3 The Snow Load Testing System (SLTS)

### 7.3.1 About the Snow Load Testing System

The **SLTS** is an experimental system used to collect data of the snow pressures against a rigid support surface caused by creep and glide in the snowpack [96]. The system was designed by master student Jan Are Sunde Jacobsen in 2017 [34], and the testing is currently run by the Arctic Technology Department at UNIS.

An overview of the experimental setup of the **SLTS** is shown in Figure 7.3 as well as its location above Svalbard airport (coordinates  $N78.234444$   $E15.464722$ , 253m above sea level). The system consists of the following components [96]:

- Snow supporting surface: Smooth wall without aperture that is 3m wide and 1.5m high with a 16mm thick aluminium frame around (angle profiles for reinforcement)
- Force transducers: 4 load cells of HBM type S9M (S-shaped) with a load capacity of 20kN
- Temperature probes: 5 thermistor termometers of type Campbell Scientific model 107 Temperature Probe with 10m cables
- Air temperature and humidity probe: Humidity and Temperature Probe of type Vaisala HUMICAP HMP155A
- Snow depth measurements: Sonic distance sensor of type Campbell Scientific SR50A
- Logging unit: Data logger of type Campbell Scientific logger CR1000

The **SLTS** is designed to automatically record snow pressure against the plate, snow temperature in front of the plate, air temperature, and snow depth 130cm up-slope of the plate. The four force transducers in the **SLTS** can each measure up to 20kN and are set up to continuously log the snow load every minute. Automatic temperature measurements of the snow right in front of the plate are taken continuously every 10minutes by five temperatures probes. These probes are placed every 35 – 45cm along the centre line of the plate (bottom too top) through holes drilled in the plate (Figure 7.5b). The snow height is continuously measured every hour by a sonic distance sensor (Figure 7.8a).

In addition to the automatic measurements, manual measurements of snow density has to be performed regularly. Manual checks of snowpack temperature, air temperature, and snow height in front of the plate are also completed regularly to check that the automatic measurements are reasonable. These manual measurements were performed in March 2022 during field work, and is explained in more detail in the following sections. In addition, students at UNIS have completed the same snow density and temperature measurements over height from February through April 2022.



**Figure 7.3:** An overview of the original experimental setup of the *Snow Load Testing System* (a) and the location of the system between Longyearbyen airport and Platåberget (b). The setup currently being used has been slightly adapted compared from (a). Source: Arctic Technology Departmen, UNIS [96].

### 7.3.2 Snow density measurements

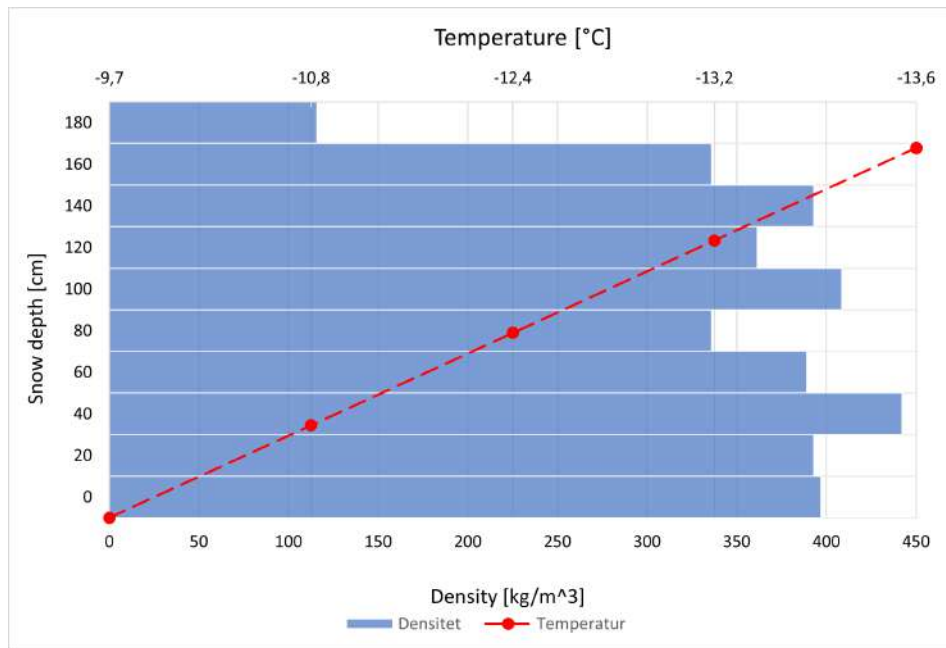
Snow density measurements over the snow height were performed on March 4<sup>th</sup> 2022 in a snow pit dug approximately 2m to the side of the SLTS support surface. At that location, the total snow height was approximately 180cm. A cylinder with known volume and weight was pressed into the snow at 20cm height intervals. Each time, the snow in the cylinder was extracted, weighted and the snow density  $\rho_{snow}$  calculated according to Equation 7.1.

$$\rho_{snow} = \frac{m_{snow}}{V_{cylinder}} = \frac{m_{snow}}{\pi \cdot r_{cylinder}^2 \cdot L_{cylinder}} \quad [\text{kg}/\text{m}^3] \quad (7.1)$$

Here  $m_{snow}$  is the measured snow mass,  $V_{cylinder}$  is the volume of the cylinder,  $r_{cylinder}$  is the radius and  $L_{cylinder}$  is the length of the cylinder.

The resulting snow densities are shown in Figure 7.4. It is observed that the snowpack has a fairly even density ranging between 330 and 450kg/m<sup>3</sup>. The exception is the top snow layer 180cm from the ground where the snow density was measured to be 116kg/m<sup>3</sup>. The low density of the topmost layer is reasonable since there had been a recent snow fall at the time of measurement, and a light, powder layer was observed as the top of the snowpack. The average snow density for the snowpack was calculated to 357.2kg/m<sup>3</sup>. A possible source of error in the density measurements is that the high density of the snowpack made it difficult to insert the cylinder. This might have caused an extra pressure on the snow in the cylinder resulting in a too high density.

The manual measurement of snow density has to be carried out regularly, as snow densities in the literature are often given by monthly average values [97]. For practical reasons UNIS students have completed the rest of the measurements. Snow density measurements have been performed on February 23<sup>rd</sup>, March 2<sup>nd</sup>, 8<sup>th</sup>, 22<sup>nd</sup> and 29<sup>th</sup>, April 5<sup>th</sup>, 20<sup>th</sup> and 28<sup>th</sup> 2022.



**Figure 7.4:** Density and temperature profile measured in a snow pit approximately 2m to the side of the SLTS. The snow depth is measured from the ground up, i.e. the snow depth of 180cm is at the snow surface.

### 7.3.3 Snowpack temperature measurements

Snow temperature measurements were taken in the same snow pit as the snow density measurements. The temperature was measured every 40cm using a digital pocket thermometer of type Milwaukee TH310 (Figure 7.5a). The resulting temperatures are presented in Figure 7.4, and show a linear increase from the snow surface to the ground. This corresponds well with the early spring situation when heating of the snowpack from solar radiation is low and the air is still cold.

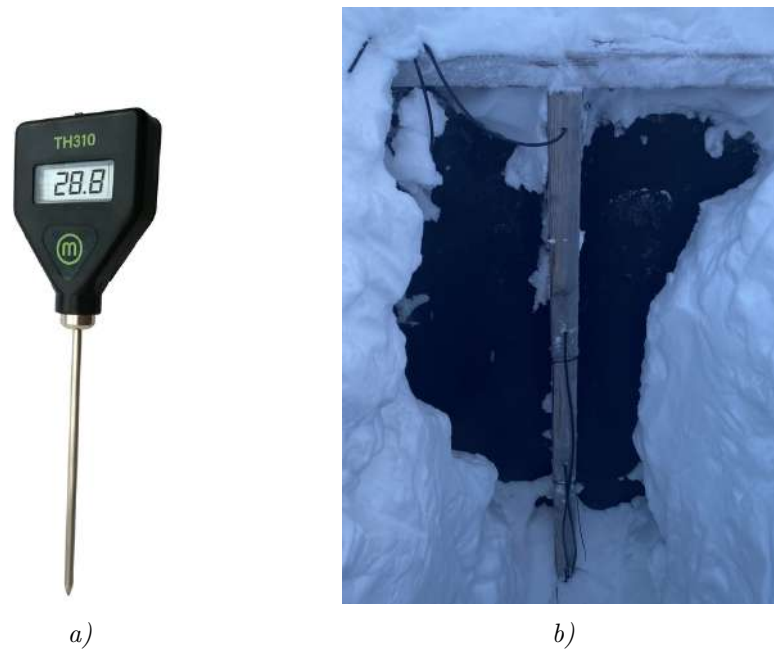
In addition to taking manual temperature measurements of the snowpack, a visual inspection of the automatic temperature probes was performed. As mentioned, these probes are placed through holes drilled in the plate along the plates centre line. The snow was partly cleared on the back side of the wall so that the placement of the automatic temperature probes were visible (Figure 7.5b).

### 7.3.4 Air temperature measurements

The air temperature next to the SLTS was measured to  $-9.6^{\circ}\text{C}$  at 5.30 PM on March 4<sup>th</sup> 2022, using a Milwaukee thermometer (Figure 7.5a). Historical data collected from the weather station at Svalbard Airport [98] show that the temperature at Svalbard Airport was  $-8.8^{\circ}\text{C}$  at the same time. This comparison is interesting because it provides a reference deviation between the two locations. The Airport is located close to the SLTS, but only 28 meters above sea level (compared to the SLTS at 253m) and closer to the sea, which is likely the reason for the small temperature deviation.

The SLTS automatically records measurements of air temperature, and it is of interest to control if these measurements are correct. This control has been performed by comparing the air temperature at the SLTS site with historical data collected from the weather station at Svalbard Airport. The results are presented in Figure 7.6 for the time period between January 2020 and June 2020, and shows good agreement in both patten and extreme values.

Data from Svalbard Airport is useful when interpreting the snow pressure results. For example, a clear increase in snow pressure was observed after March 18<sup>th</sup> 2022 (Figure 7.12). Studying the



**Figure 7.5:** Equipment used to measure temperature in the air and snowpack. a) Milwaukee TH310 Thermistor Pocket Thermometer with a stainless steel probe b) Picture of the back of the support surface where the centre part of the wall has been cleared of snow so the automatic temperature probes are visible. Photos: a) Milwaukee Instruments, b) Philip Kunz.

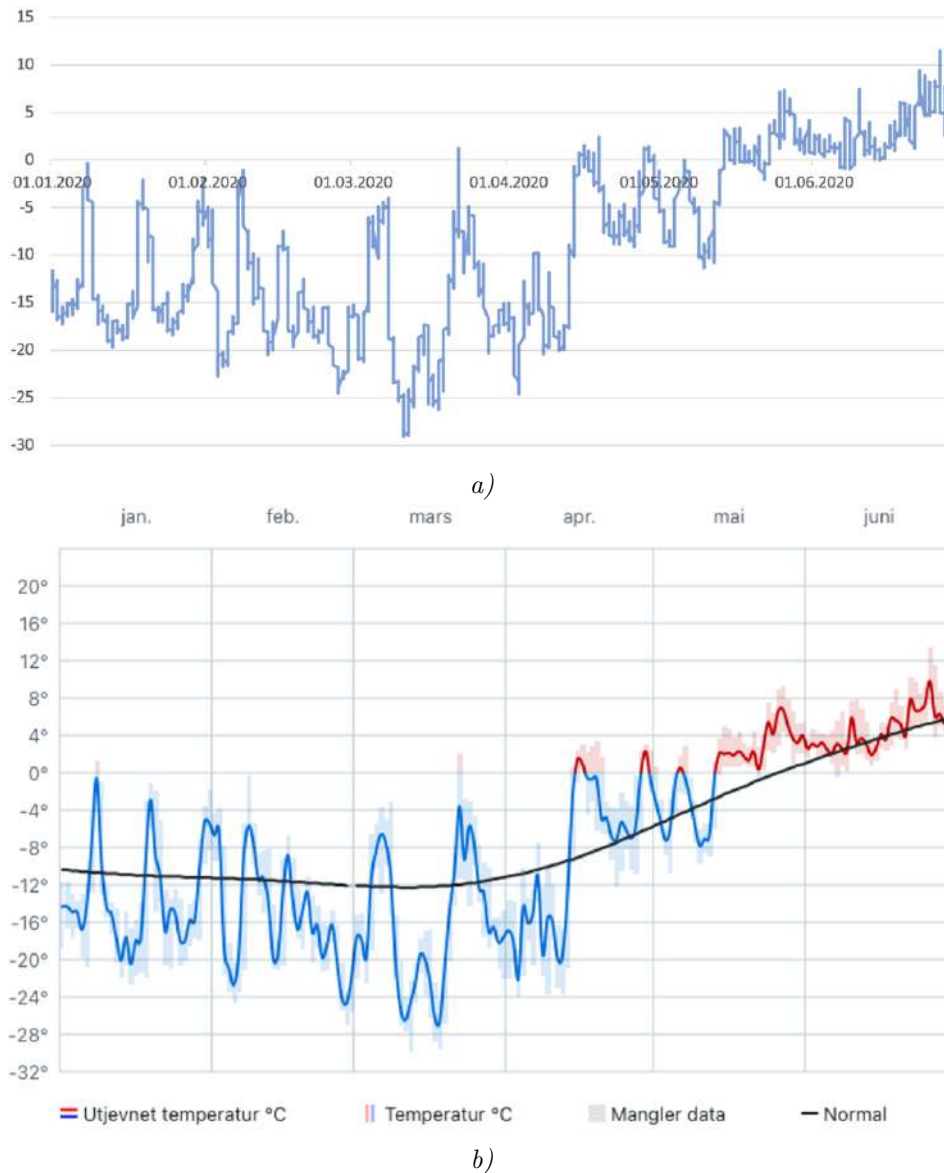
Airport weather data it can be seen that the weather was warmer (temperatures up to  $5.6^{\circ}\text{C}$ ) with precipitation from March 14<sup>th</sup> to 18<sup>th</sup> (Figure 7.7). This weather is associated with more creep and glide in the snow pack, and it is therefore reasonable that the snow pressure against the support surface increase.

### 7.3.5 Snow height measurements

The snow height  $H$ , as described in Section 3.3.4, is measured in the vertical direction and is independent of the slope inclination when the snow fall is vertical and uniform [2, p. 28]. This is an important input parameter when designing support structures, and it is therefore of interest to know what the snow height is above the SLTS. However, as seen in Figure 7.8b, the field work uncovered that the SLTS measures snow thickness  $D$  which is measured normal to the slope. This is not a problem since the snow depth is a function of the snow height according to  $D = H \cos \psi$ , but is important to account for when analysing the results.

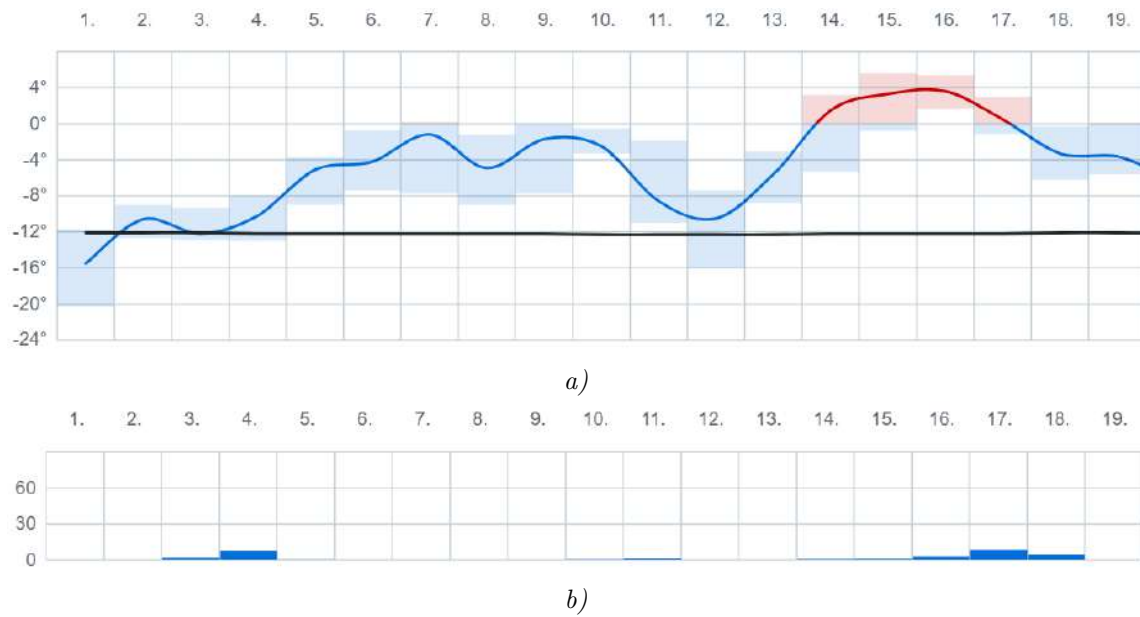
Automatic snow thickness measurements are continuously logged every hour by the Campbell Sonic distance sensor. The sensor measures the snow thickness in one location 130cm up-slope of the plate, and the resulting thickness are presented in Figure 7.12. A malfunction caused the equipment to stop measuring snow thickness during a 10 day period in March 2022.

In addition to the continuous measurements of snow thickness right in front of the snow supporting surface, it is of interest to know the snow height in a bigger area up-slope. This is because the snow pressure against snow supporting structures are dependent on the snow height in the previously mentioned "back-pressure zone" (Section 3.1). The snow height was therefore measured manually using avalanche probes on March 4<sup>th</sup> 2022. Three profiles were probed in a direction normal to the supporting surface: One from the centre of the plate and one from each short-end (1.5m to the left and right of the centre line looking up-slope). The first measurement was taken close to the plate, the second was taken 130cm up-slope (at the same distance from the plate as the automatic height measurements are taken), and the rest were taken at 2m intervals.

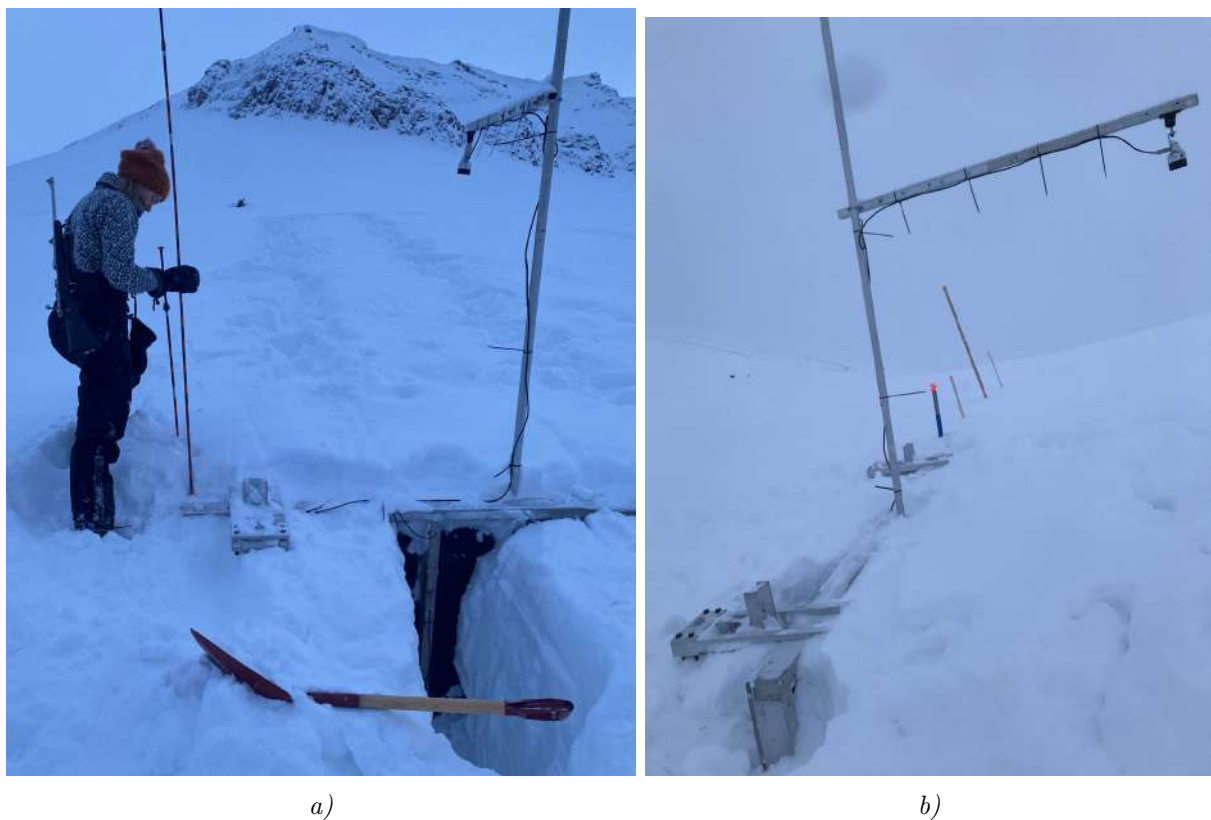


**Figure 7.6:** Comparison of air temperature measurements from January 2020 til June 2020 measured at a) the SLTS site and b) Svalbard Airport weather station [98]. On the graph from Svalbard airport, the shaded blue or red columns represent the daily temperature variation (minimum to maximum), the fully drawn line in blue or red represent the smoothed temperature, while the black line is the reference normal from the period 1991-2020. Figure created by Vette Basma and Philip Kunz.



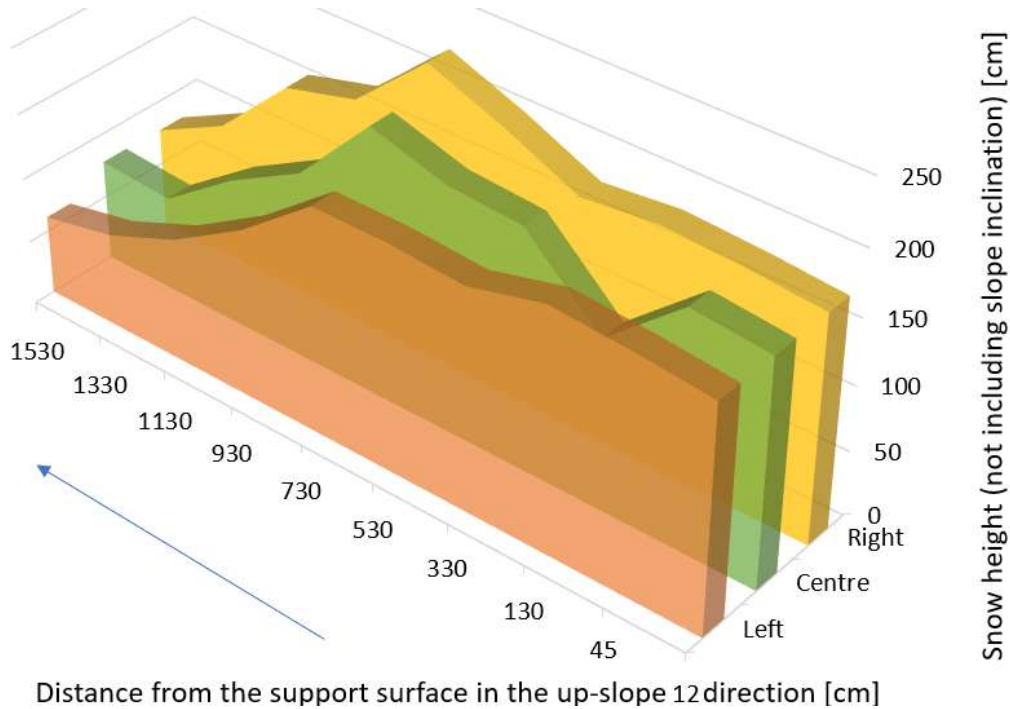


**Figure 7.7:** Weather data from Longyearbyen Airport during March 1<sup>st</sup> – 19<sup>th</sup> 2022 showing daily (a) air temperatures and (b) precipitation. Source: NRK and Meteorologisk institutt [98].



**Figure 7.8:** Field work March 4<sup>th</sup> 2022 by the SLTS. a) shows the support plate with the automatic snow height measurement equipment above, and Haldis Døvre Kalland manually measuring snow height using an avalanche probe. b) shows the back of the support surface where the centre part of the wall has been cleared of snow so the back of the automatic temperature probes are visible. Photo: a) Philip Kunz, b) Vetle Basma.

The resulting snow height profiles are shown in Figure 7.9. Note that the figure does not include the slope inclination. A clear dip is observed for the centre profile 130cm up-slope of the support surface. This is because the snow was disturbed when approximate measurements of the snow height were taken on March 3rd to check whether the automatic snow height measurements were reasonable. Beyond that, the snow height was found to be quite stable the first 10m before it reclined in the last 5m, though it was somewhat higher towards the right side of the plate compared to the left. The maximum measured snow height was 225cm.



**Figure 7.9:** Snow height profiles from the left side, centre and right side of the snow supporting surface

### 7.3.6 Slope inclination measurements

The slope inclination up-slope of the SLTS was estimated using a laser rangefinder of type Nikon Forestry Pro and two BCA avalanche probes of length 270cm (Figure 7.10). This was done because the inclination is an input factor when calculating snow pressure and is therefore important to consider when analysing the snow pressure data.

To measure the slope inclination, two avalanche probes of the same length were inserted vertically in the snow until they reached solid ground. The first probe was placed right next to the support surface of the SLTS, while the second probe was placed at distances 5m, 10m, and 15m up-slope. The laser was then placed on top of the first probe and pointed to a hand placed on top of the second probe. The slope inclination could then be read directly from the laser. Several control measurements were taken at each distance to minimise random error. This method gives an average slope inclination over the three intervals. A source of error is that the ground is rocky and the avalanche probes might have hit on top of a big rock or in a deeper hole. To minimise this error, the probes were inserted at several locations at approximately the same distance from the supporting surface.

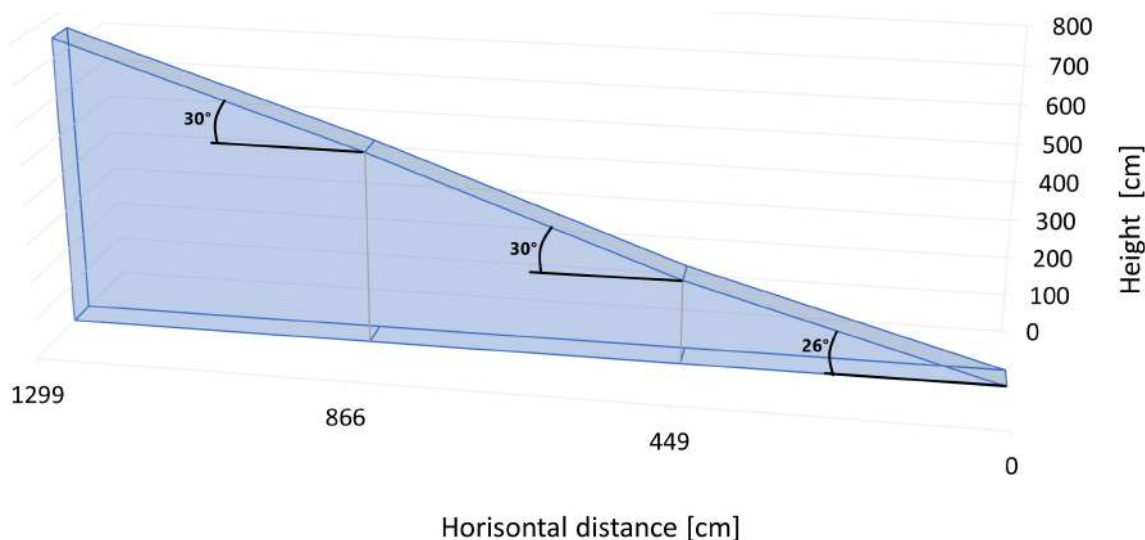
The resulting slope inclination is shown in Figure 7.11, and was found to be  $25^\circ - 26^\circ$  in the 5m closest to the support surface and  $29^\circ - 30^\circ$  higher up. The SLTS was supposed to be installed in a steeper part of the slope than it is in now, but the mechanical digger was unable to climb that far up the slope [34]. A slope inclination of  $28^\circ - 30^\circ$  is in the lower range of where formation of





**Figure 7.10:** Equipment used in measuring slope inclination: a) Laser rangefinder of type Nikon Forestry Pro (*nicon.no*), and b) BCA avalanche probe of length 270cm (*Fjellsport.no*).

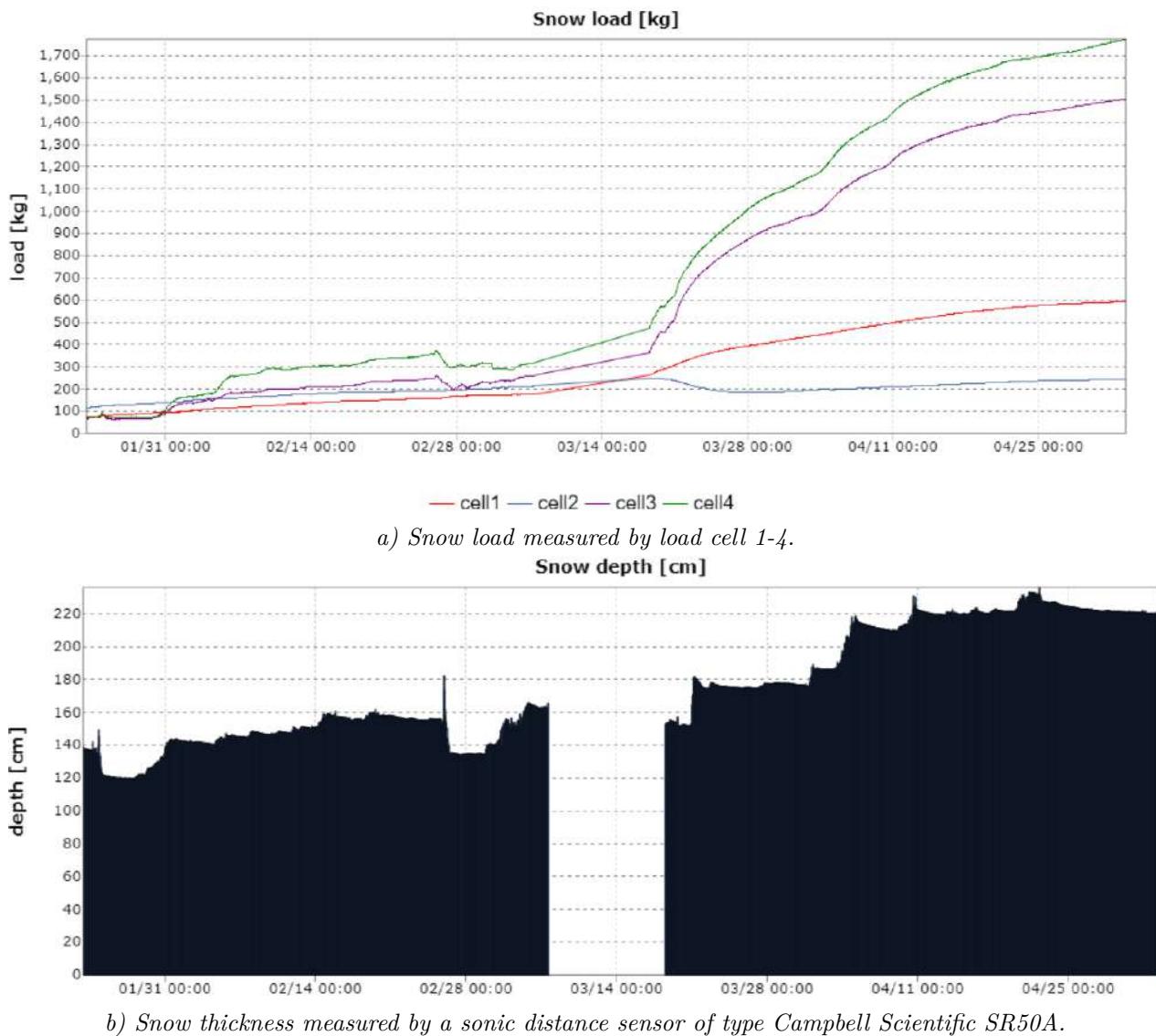
slab avalanches are possible [22, p. 40]. In addition, a big part of the area on Sukkertoppen where support structures are under construction (see Section 7.4) have a slope inclination of  $34^\circ - 38^\circ$  [99, vedlegg]. It has therefore been discussed if a snow pressure measurement system should be installed on a support structure on Sukkertoppen (where the slope inclination is steeper). This discussion is presented in Chapter 9, and the location on Sukkertoppen was inspected during this research trip (see Section 7.4).



**Figure 7.11:** Slope angles up-slope of the SLTS measured using a laser rangefinder of type Nikon Forestry Pro and two BCA avalanche probes.

### 7.3.7 Results from the Snow Load Testing System

The SLTS was installed in May 2017, and has been measuring snow pressure every winter season from 2017 to 2022. The results of the automatic snow pressure and snow thickness measurements taken between 2022-01-23 (10:00 AM) and 2022-05-03 (10:00 AM) are presented in Figure 7.12.



**Figure 7.12:** Snow load and snow thickness measured between 2022-01-23 (10:00 AM) and 2022-05-03 (10:00 AM) by the SLTS. It can be misleading that the SLTS records load with mass unit [kg]. The values are converted to load unit [kN] through  $1000\text{kg} = 10\text{kN}$ .

A closer study of the snow pressure data has not been performed in this thesis because the data is currently being analysed by Basma and Kunz in their thesis. However, a short presentation of Figure 7.12 follows. Load cell 1 and 2 are placed in the corners closest to the ground while load cell 3 and 4 are placed in the top corners (Figure 7.3). When the snow height is low, the pressures measured by load cell 1 and 2 are greater than those measured by load cell 3 and 4. However, when the snow height grows to approximately 130cm the load measured by the top load cells exceeds that measured by the bottom load cells. This happened close to January 31<sup>st</sup> 2022, as can be seen on Figure 7.12a. The reason for this change is assumed to be that the snow creep is largest close to the snow surface, and larger creep leads to higher pressures. As snow fills the area in front of the support surface, this higher pressure is measured by the top load cells.

The second interesting observation from Figure 7.12 is that a great increase in snow pressure is observed after March 18<sup>th</sup>. As mentioned earlier, this increase in snow pressure directly follows a period with warmer weather (temperatures up to 5.6°C) and rain. As this weather is associated with more creep and glide in the snow pack, the increased snow pressure loads are assumed to be the result of increased creep in the snowpack.

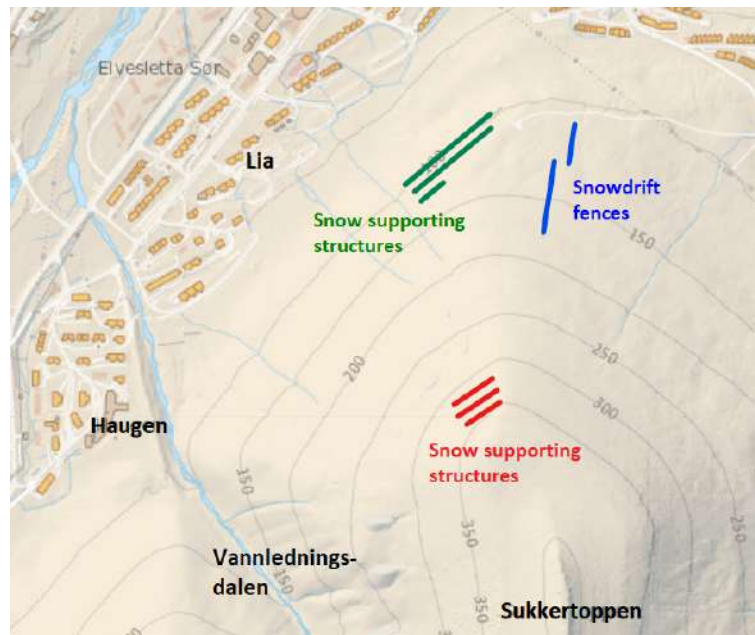
## 7.4 Snow supporting structures at Sukkertoppen

In the second part of the research trip, the snow supporting structures that has already been constructed on Sukkertoppen were inspected (location shown in [Figure 7.13](#) and structures shown in [Figure 7.14](#)). The aim was to: 1) see the structures at close range to better understand their magnitude and design, 2) see how wind transport of snow affect the snow cover around the structures and measure some representative snow heights, and 3) investigate the possibility of installing a snow pressure measurement system on one of the support structures.

Observations of the snow cover around the support structures showed that the snow distribution was greatly affected by wind transport. Most of the snow had been cleared away between the supporting surface and supports, while snow had accumulated in wind slabs between the structure lines ([Figure 7.14](#)). This is the same effect as observed around snowdrift fences. A question was therefore raised whether this could affect the structures ability in mitigating against avalanches, either because the maximum possible snow height is increased or because of a less effective back-pressure zone where greater tension stresses are allowed to build.

A literature study of these questions resulted in two main findings: 1) According to Margreth [2] snow supporting structures should be placed so that snow pressures from creep and glide are greater than the loads caused by avalanches releasing between the structure lines. 2) , Margreth [100] found that hard slabs released between structure lines were often stopped by the next line of structures, and that the catching capability of cohesive or wind-deposited snow was up to 100% for steel bridges with a distance between the crossbeams of about 25 cm. From this, it appears that the wind transport of snow does not negatively affect the structures ability in mitigating against avalanche because of a reduced back-pressure zone. However, future work should investigate whether the wind slabs alter the snow deposition so much that it is possible to reach a greater snow height than the structures are designed against. In regard to learning outcome, these questions were interesting an would likely not have been discussed without the visual inspection during field work.

To investigate where a possible new structure for measuring snow pressure could be constructed on Sukkertoppen, manual measurements of snow height were carried out in the area between the lines of snow supporting structures using an avalanche probe. The results showed a snow height of approximately 1.5 meter between the two upper structure lines, and therefore it was concluded that this could be a suitable location. Designing this new system is an interesting project that should be investigated further in future works.



**Figure 7.13:** Location of support structures on Sukkertoppen and above Lia, as well as location of snowdrift fences. The snow supporting structures discussed above are marked in red (highest up on Sukkertoppen).



a)



b)

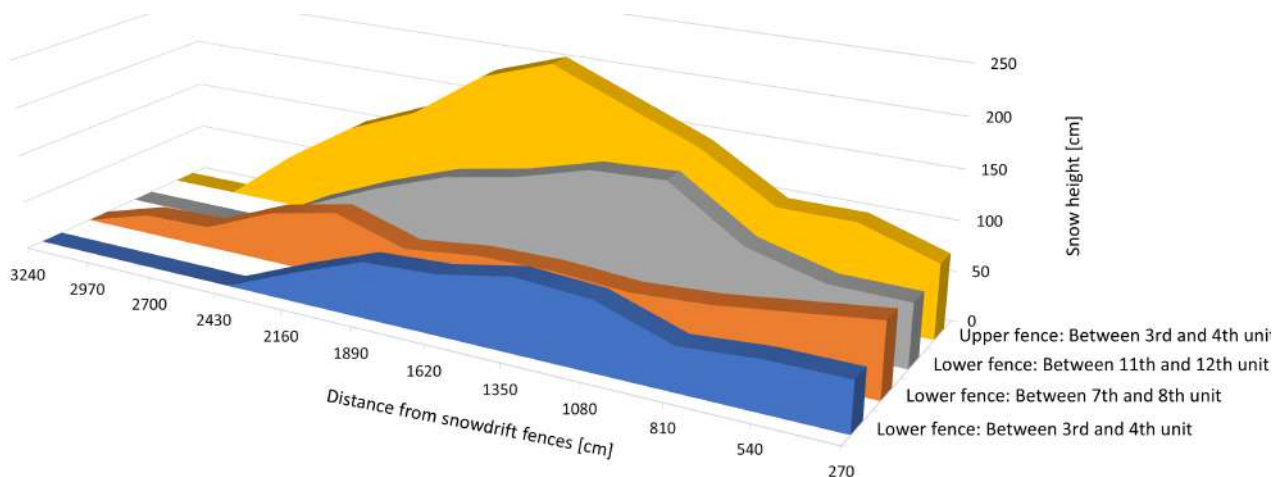
**Figure 7.14:** Support structures on Sukkertoppen photographed during field work on March 6<sup>th</sup> 2022 showing how the snow cover is affected by wind transport of snow. a) A wind slab between the two upper lines of support structures photographed from below, b) Most the snow has been blown away between the supporting surface and supports. Photos: Haldis Døvre Kalland.

## 7.5 Snowdrift fences - snow accumulation measurements

In the last part of the research trip, the snow accumulation around two rows of snowdrift fences was studied. The snowdrift fences are located on the area North of Sukkertoppen and East of Lia (Figure 7.13), and consist of 16 (lower fence) and 28 (upper fence) units. Each unit is approximately 4m high and 5m wide. The centre to centre distance between two neighbouring units was measured in field to 5m 15cm, and the basal opening of two units were measured in field to 0.85m.

Four snow height profiles were measured using avalanche probes in a direction normal to the fences on the West side. Three of the profiles were taken from the lower fence and one from the upper fence. To ensure the locations could be specified, each profile was started between two units counting from North to South.

The resulting snow height profiles are presented in Figure 7.15, and show that more snow had been deposited behind the upper fence than the lower fence. Three out of four profiles show an increase in snow height from the the snow fence until a peak between 8m and 16m, before the snow height reaches zero at 24 – 30m distance. The last profile show a more even decrease in snow height moving away from the fence, with only a small increase at approximately 22m distance.



**Figure 7.15:** Measured snow height profiles of wind slabs created by snowdrift fences above Lia, Longyearbyen.



# Chapter 8

## A study of the design of slush flow barriers in Vannledningsdalen

### 8.1 General

#### 8.1.1 Introduction to the Vannledningsdalen project

Vannledningsdalen ("Vannledning-valley") is a valley above Haugen in Longyearbyen that is prone to slush flows (Figure 8.1). These slush flows have previously caused the loss of 3 human lives and great material damage [80, 92], and therefore an ongoing project aims to safeguard the city against future slush flows using flexible net barriers. A big challenge with this solution is that no documentation exist that deals with how flexible net barriers can be used to mitigate against slush flows [93, 94]. Therefore, the pre-project and design phase has been very comprehensive in order to achieve a safe and cost efficient solution. The project with slush flow barriers in Vannledningsdalen is part of a bigger avalanche mitigation project in Longyearbyen, including snow supporting structures, snowdrift fences, and catching dams on and around Sukkertoppen (Figure 7.13).



**Figure 8.1:** *The Vannledningsdalen valley viewed from the top at Elvesletta. Source: Nordbrøden [27, p. 6].*

The current situation in Vannledningsdalen is that a deflecting dam protects parts of the settlement on Haugen, and a yearly "trenching" of the valley bottom is performed to reduce the risk of damage. Trenching is a mitigation measure used against slush flows where (for the Vannledningsdalen case) a bulldozer clears a path along the bottom of the valley of snow. Thereby it opens a drainage path for melt water (Figure 8.2). This measure was initiated after the big slush flow in 1953 and is still used yearly up till now. However, in the last years the weather conditions at Svalbard have changed. Higher temperatures, more rain and periods of mild weather in midwinter increase the risk of debris flows, avalanches and slush flows [5, p. 5]. Therefore, trenching is no longer considered to be a sufficient solution [5, p. 16] and flexible net barriers have been chosen as the replacement. Some alternative solutions that were considered were deflection dams, channelising dams and catching dams in the track and runout zone.

Longyearbyen Lokalstyre (en. Longyearbyen Community Council) (LL) is the local government for Longyearbyen and is responsible for the community development. They will be responsible for drift-

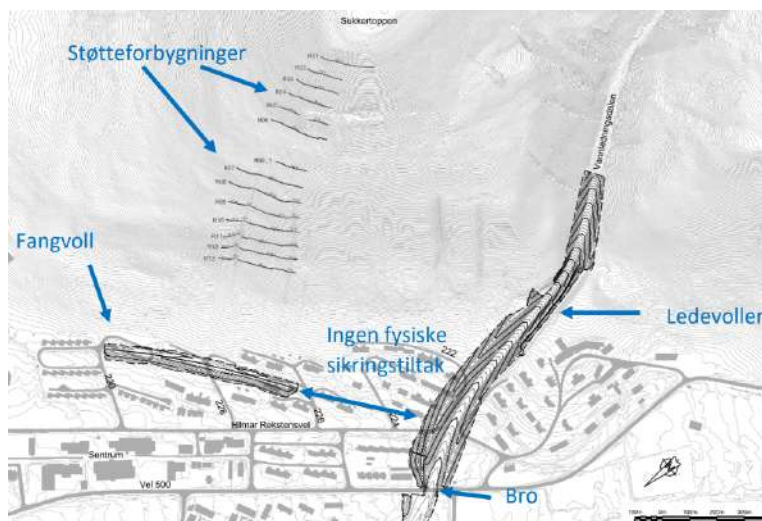




**Figure 8.2:** Picture of how the snowpack in Vannledningsdalen is prepared to minimise the slush flow risk using trenching. The same picture is presented in Section 6.4, but repeated here to improve readability. Source: Jónsson and Gauer [92].

ing the finished avalanche mitigation measures. However, it is Norges vassdrags- og energidirektorat (en. The Norwegian Water Resources and Energy Directorate) (NVE) that is responsible for the design and construction of the projects [101]. NVE collaborate with several consultants in finding the best solution in Vannledningsdalen, including NGI, Skred, HNTI, Rambøll, and Geobrugg.

The timeline of the mitigation project in Vannledningsdalen started in 2017 [101]. A changing climate and two avalanches, one in 2015 and one in 2017, initiated a process of safeguarding the population and infrastructure in Longyearbyen against future avalanches and slush flows. Preliminary studies were performed in 2017-2018 by NVE and LL, and in December 2018 a plan was accepted. This first plan consisted of channelising dams along the Vannledning-river. However, a new climate profile published in February 2019 delayed the project, and the realisation that the channelising dams would be very expensive and divide the settlement in two started the process of evaluating alternative options again. In June 2021 a new plan was accepted and represented the new concept of constructing flexible net barriers along the valley of Vannledningsdalen. The barriers will also protect against debris flows, but slush flows are considered to be the dimensioning load case. The construction process is planned to start in the summer of 2022 and be finished in the summer of 2023.



**Figure 8.3:** Original mitigation plan (2018) for Vannledningsdalen (and Sukkertoppen). English translation: "Støtteforbygninger"=snow supporting structures, "fangvoll"=catching dam, "ingen fysiske sikringstiltak"=no physical mitigation measures, "ledevoller"=channelising dams, "bro"=bridge. Source: Longyearbyen lokalstyre [101].

### 8.1.2 Aim, scope and relevant documents

In the following sections, the design and dimensioning of the flexible net barriers are studied in detail. The aim of this study is to learn the details in designing flexible net barriers against slush flows, to see which adjustments are needed when constructing avalanche protective structures in arctic regions, and to learn the process used by experienced engineers when undertaking such an innovative mitigation project that had many unanswered questions to begin with.

As previously mentioned, the Vannledningsdalen project is especially interesting to study because no net barriers have previously been used in Norway as a mitigation measure against slush flows of this size [27, 94]. According to Nordbrøden [27, p. 12], some rare mitigation solutions with dams have been built in Norway and barriers against slush flows might have been used. However, Nordbrøden [27] does not know how these mitigation measures were designed, and therefore assume that standard debris flow rheology was used without adopting it to the high speeds slush flows can reach. The lack of similar projects meant that several questions had to be answered in the pre-project about the fluid-structure interaction between slush flows and a flexible debris flow nets, and how this would differ from debris flows and avalanches.

Some other unanswered questions that had to be solved in the planning phase were: 1) how the snow would accumulate around the barriers because of wind transport of snow and if this would affect the retention volume of the barriers; 2) the dynamic modelling of slush avalanches used to determine runout distance and flow velocities; 3) the physical properties of the snow such as glide factors and snow density; 4) what return period the nets should be dimensioned to withstand as there are no Norwegian standards that give guidance for this [27, p. 19]. Understanding these challenges gives a good foundation for choosing research projects in [this authors](#) coming PhD studies. Vannledningsdalen was not visited during the research trip in March 2022 ([Chapter 7](#)) because the construction work had not yet started.

The focus of this study is the design and dimensioning of the net barriers, not the channelising dams in the track and runout zone. The study contains a description of the barrier components and placement, the load cases acting on the nets, and the analytical proofs of each components strength. More focus will be placed on the barriers superstructure compared to the anchoring because of [this author](#) background as a structural engineer. The goal is to reproduce and understand all concepts of the design, not to propose alternative or better solutions.

The documents that primarily were used when studying the details of the design and dimensioning of the net barriers are listed below. They were shared by Árni Jónsson ([HNIT](#)) in April 2022, and though they may have been updated since then it is these versions that have been used.

- Pre-project report: *Forprosjektering av nettløsning mot sørpeskred i Vannledningsdalen*, [HNIT](#) and [Skred AS](#), Kronholm et al. [94]
- OPM report: *Detailed design of slush-flow nets*, *OPM Report*, 18247-SK04-00, [HNIT](#), Jónsson [102]
- RISK report: *Mitigation against slush flows in Vannledningsdalen with debris flow barriers*, 18241-26-1, [Skred AS](#), Nordbrøden [27]
- RIB superstructure report 1: *Design report slush flow barriers, Vannledningsdalen Longyearbyen, Svalbard*, [Geobrudd AG](#), Feiger [103]
- RIB superstructure report 2: *Dimensioning slush flow barrier (Net 10) Vannledningsdalen Longyearbyen, Svalbard*, [Geobrudd AG](#), Feiger [104]
- RIB foundations: *Vannledningsdalen, Longyearbyen. Design of foundations for slush flow nets. RIB Report*, 18247-SK03-00, Steinarsson [105]

## 8.2 The barriers

The flexible net barriers to be used in Vannledningsdalen are debris flow barriers of the UX-barrier type with a ROCCO ring net system produced by Geobruigg AG [103, p. 10]. The two main functions of the barriers are to reduce the probability of a slush avalanche release by supporting the snowpack, and to slow down or stop a flowing slush avalanche [94, p. 24]. The ROCCO ring nets consist of high-strength steel rings woven together, and are used in the mitigation of debris flows and high-energy rock fall with impact energies up to  $8000kJ$  [106, p. 11]. An example of a UX-barrier with a ROCCO ring net is shown in Figure 8.4.



*Figure 8.4: UX-barrier with a ROCCO ring net. Source: Geobruigg AG [107].*

### 8.2.1 Barrier components

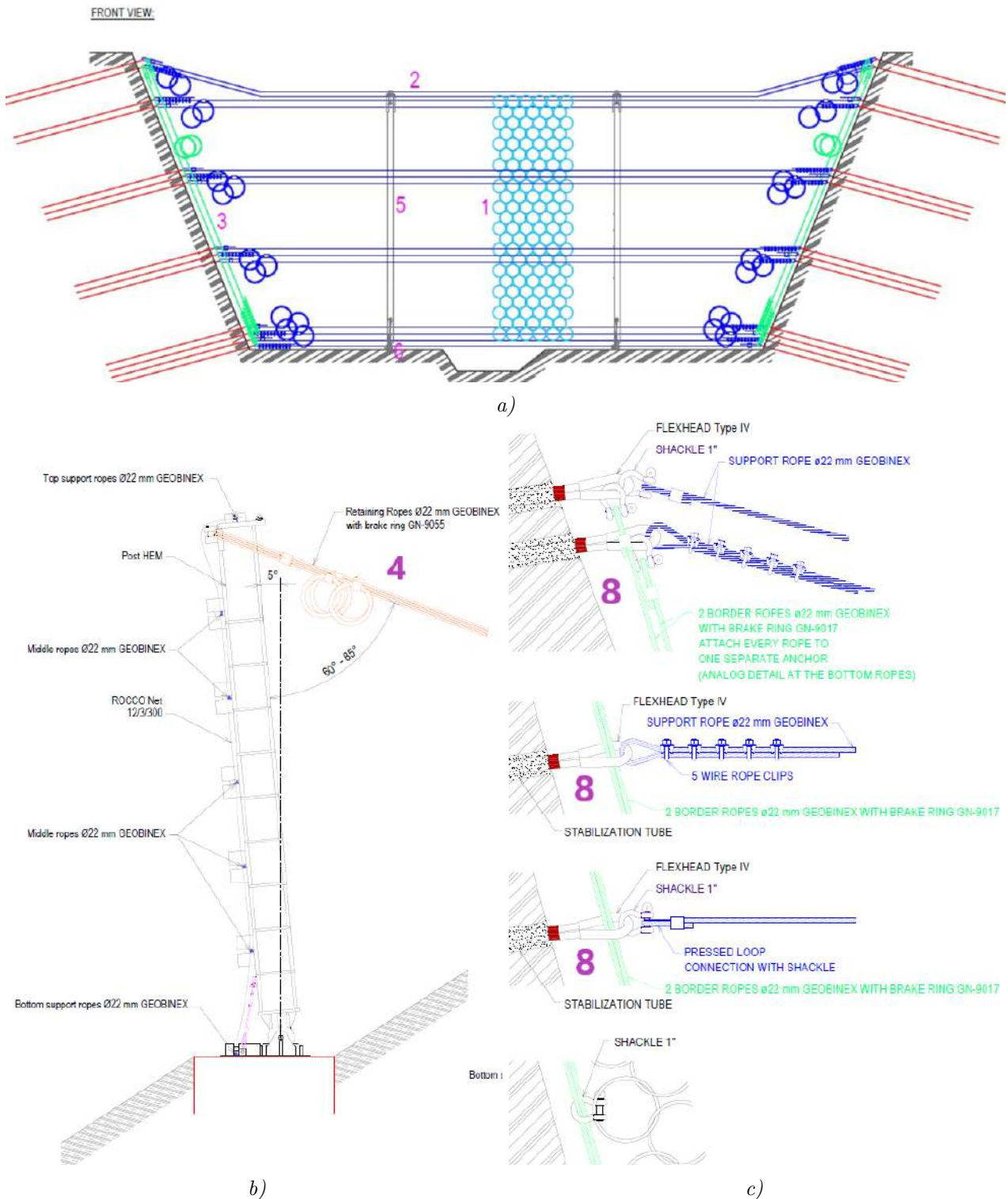
The 14 barriers (nets) that are planned in Vannledningsdalen are all debris flow barriers based on the same geometrical principles shown in Figure 8.5 [27, p. 14]. However, each net is adapted to the specific location in the valley and therefore the width of the barrier and the number and location of the posts will vary [27, p. 14]. A presentation of the geometrical principles will be given here, while the reader is referred to Feiger [103, pp. 24–29] for more details.

The main elements of the debris flow barriers are shown in Figure 8.5. For detailed system drawings of barrier number 10 the reader is referred to Appendix A. A ring net (1) is strung up to cover almost the whole section of the valley. The diameter of each ring is approximately  $300mm$  [102, p. 19], and each steel ring in the net strands 12 solid rings of  $3mm$  thickness. The barriers have a basal opening below the net to allow sediment transport in the stream. Horizontal support ropes with brake elements (2) hold up the net and absorb energy during impact. The ropes are connected to anchor nodes at the sides and guided (supported) by 2 – 3 support posts (5) (number depends on the valley width at the barrier's location). The support ropes are strung up at several heights, and each height has either 2 or 3 ropes (depending on the acting forces and net configuration) [102, p. 19]. Lateral ropes (3) attach the net to the valley sides. The ring net is connected to the ropes, and the ropes are attached to the anchors through FLEX Head connectors (8) [102, p. 19].

The support rope anchors are designed with long stiff bars to transfer the tension forces to ground. These bars would experience a creep load from the loose soil as a cantilever, so to minimise this bending moment on the bars a specially designed "house" will transfer the creep load from the loose material to permafrost or rock [102, p. 24]. An example of one such house is shown in Figure 8.6. A detailed description of the design principle for the concrete foundation blocks and the anchor points is given in Steinarsson [105].

As mentioned, the horizontal support ropes are supported by vertical posts (5). These posts are steel HEM-profiles between 3 and 7m high, and have an inclination of  $5^\circ$  downstream [102, p. 25]. The post ensure that the remaining barrier height after impact remains as large as possible, to achieve the





**Figure 8.5:** Basic geometry of the slush flow barrier system (nets). a) Front view showing the ring net (1), support ropes with brake elements (2), lateral ropes (3), support posts (5), and base-plate (6). b) Support post details and retaining rope with brake elements. c) Connection detail showing the FLEX Head connectors (8), the support ropes (2), and the lateral ropes (3). Source: Feiger [103, p. 20] and Geobrug system drawing net 10 (Appendix A).

largest possible retention volume [95, p. 37]. Each post is connected to a massive concrete foundation through a base-plate (6) which ensures a hinged connection. The posts are held in place by retaining ropes (4) at the top that go from the posts head to an H-beam anchoring solution upstream the net (Figure 8.6).

To ensure that the barrier has enough effect when catching the slush flow, a secondary net will be attached to the main net. The secondary net will have a mesh size of approximately  $50\text{mm} \pm 5\text{mm}$  and cover roughly 50% of the main net with stripes [102, p. 20]. The reason for covering only 50% of the main net is to minimise the snow accumulation around the nets. Both nets must be made of a high tensile strength material.



**Figure 8.6:** Drawing of what a) an anchoring "house" for the support ropes and b) an H-beam anchoring node for the retaining ropes could look like. From Jónsson [102, pp. 24, 25].

### 8.2.2 Barrier placement

The barrier placement has been decided by HNIL and Skred AS, and is fully described in Kronholm et al. [94, pp. 24–27] and Nordbrøden [27, p. 26]. Here, barrier placement means where along the valley bottom the barriers are placed. The planned barrier placement is shown in Figure 8.7 [102, p. 1].

As mentioned, the two main functions of the barriers are to reduce the probability of a slush avalanche release by supporting the snowpack, and to slow down a flowing slush avalanche [94, p. 24]. Therefore, these functions have been the most important factors to consider when placing the barriers. In addition, the placement of some barriers have been adjusted after field work to avoid gullies that may carry small avalanches or debris flows [27, p. 26].

Margreth [2] give guidelines for determining the distance between avalanche support structures to achieve the desired stabilising effect. However, these guidelines do not cover the supporting of snow with nets as a mitigating effect against slush avalanches, and no other guidelines have been found that cover this. Therefore, the stabilising effect of the barriers have not been a deciding factor for the barrier placement [94, p. 26].

When a slush avalanche hits a barrier, big drag forces will act from the the slush flow on the barrier. This slows down the avalanche, but is also a big load that has to be accounted for in the design of the barriers. Skred, HNIL and Geobrugg concluded that the barriers could withstand avalanche speeds above  $13\text{m/s}$ , but that less anchor points were necessary when speeds where kept below  $10\text{m/s}$  [94, p. 26].

To conclude, the most influencing factor for barrier placement has been to keep the maximum avalanche speeds close to  $10\text{m/s}$  and thereby saving costs through requiring less anchoring points.



**Figure 8.7:** Planned barrier placement in Vannledningsdalen. Source: Jónsson [102].

### 8.2.3 Retention volume of barriers

According to [27, p. 26], the barriers in Vannledningsdalen will function as multilevel barriers meaning that overflow of one barrier is accepted as long as the total retaining capacity of all the barriers is higher than the expected total flow volume. To check this the retention volume of each barrier has to be calculated, and Nordbrøden [27, p. 26] finds this volume according to Equation 8.1 with reference to Berger et al. [108]. An illustration of the retention volume of a debris flow net is shown in Figure 8.8 to illustrate the angles and lengths used in Equation 8.1 [108, p. 29].

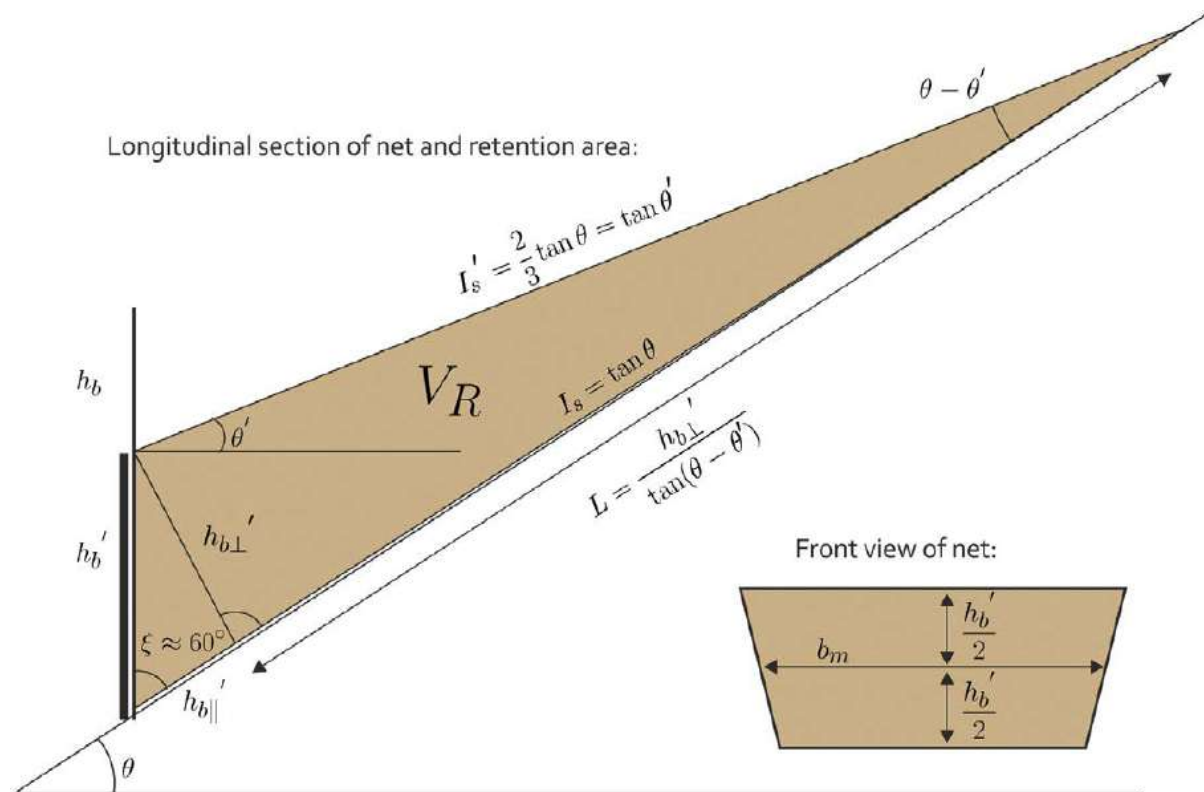
$$V_R = \frac{1}{2} \cdot (h'_b)^2 \cdot b_m \cdot \sin\xi \left( \frac{\sin\xi}{\tan(\theta - \theta')} + \cos\xi \right), \quad [\text{m}^3] \quad (8.1)$$

Here,  $h'_b$  is the residual height,  $b_m = (b_u + b_o)/2$  is the mean width of the barrier calculated from the top width  $b_o$  and bottom width  $b_u$  of the protection net,  $\xi$  is the angle between the stream bed and the barrier,  $\theta$  is the angle of the stream bed, and  $\theta'$  is the angle of the slush flow deposits.

The residual height  $h'_b$  is the remaining usable height in the barrier depending on the amount of snow already filling the net. Nordbrøden [27, p. 26] calculate the retention volume for both a maximum and minimum value of  $h'_b$ . The minimum residual height is calculated as the full barrier height subtracted the expected snow height on the ground, and where 0.5m are subtracted from the snow height due to erosion. This corresponds to a slush flow hitting the net when the net is partially filled with snow. The maximum residual height is the full barrier height, and corresponds to a slush flow hitting the net when there is no snow on the ground.

The angle of the slush flow deposits  $\theta'$  is uncertain as Nordbrøden [27, p. 27] is not aware of any sources discussing previous measurements or estimations. No such sources have been found by this author either. Therefore Nordbrøden [27] chose a value of  $\theta' = 10^\circ$  which was assumed to be conservative, and performed a sensitivity study to check the consequence of choosing a too big angle. The sensitivity study showed that for a deposition angle of  $\theta' = 5^\circ$ , nine out of thirteen barriers overtop in the minimum retention volume scenario and two out of thirteen overtop in the maximum retention volume scenario. However, even for small deposit angles the retention volume was observed to be significant for many of the barriers, and the total retaining volume was higher than the calculated slush flow volume. Therefore Nordbrøden [27] concluded that the retention volume of the barriers were satisfactory for this case.





**Figure 8.8:** Illustration of a longitudinal section of a debris flow net and retention area, and front view of the net, to illustrate angles and lengths used in calculating retention volume. Source: Berger et al. [108, p. 29].

A study has been performed by [this author](#) into how conservative a slush flow deposition angle of  $\theta' = 10^\circ$  is. Nordbrøden [27] compares slush flows with debris flows when estimating the deposition angle for slush flows. They argue that slush flows have a higher water content and less internal friction than debris flows. This is interpreted by [this author](#) as saying that slush flows should have a smaller deposition angle than debris flows.

However, according to Berger et al. [108, p. 29], the deposition angle  $\theta'$  of a debris flow can be estimated using Equation 8.2 (Figure 8.8 for illustrations of the angles).

$$\tan \theta' = 2/3 \cdot \tan \theta \quad (8.2)$$

Applying Equation 8.2 for barrier number 10, which in our case has the third greatest slope angle of  $\theta = 15^\circ$ , this gives a debris flow deposit angle  $\theta' = 10.1^\circ$ . And for a more common slope angle of  $\theta = 12^\circ$ , the debris flow deposit angle is  $\theta' = 8.1^\circ$ . This means Nordbrøden [27] argued that the slush flow deposition angle should be smaller than for debris flows, but estimated a bigger deposition angle for a slush flow than Berger et al. [108] would have estimated for a corresponding debris flow.

Therefore, [this author](#) asks whether there is a too significant uncertainty concerning the estimated slush flow deposition angle, i.e. if  $\theta' = 10^\circ$  is small enough to be a conservative estimation. Further investigations have not been performed by [this author](#) at this stage, but the deposition angle for slush flows is thought to be a very interesting subject for future work.

Two simplifications were used that both result in a more conservative estimation of the retention volume  $V_R$ . The first is that because of the V-shape of Vannledningsdalen, the cross section is smaller in the lower part of the valley where the snow is deposited than in the upper part [27, p. 26]. This gives a slightly smaller estimation of the minimum retention volume than what is actually the case. The second simplification is that the slush debris will loose volume both because of compaction and

because of drainage of water, and this factor has not been taken into account in the calculations. The retention capacity of the barriers can therefore be assumed to be higher [27, p. 27].

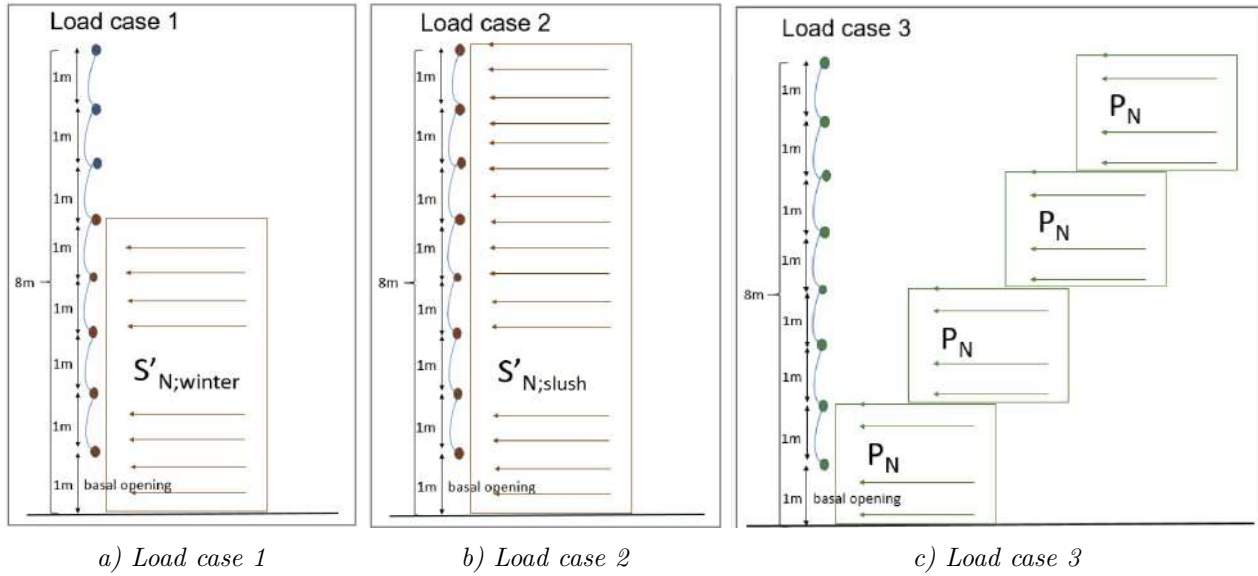
The values of relevant input parameters for calculating barrier retention volume are presented per barrier in Table 8.1 [27]. In addition, the calculated minimum and maximum retention capacity is compared to the calculated release volume above each barrier. Note that the release volume above each barrier is smaller than the minimum retention capacity of that barrier, for all barriers except barrier 9 and 11. The maximum retention capacity holds for all barriers.

**Table 8.1:** Values of relevant input parameters for calculating barrier retention volume in Vannledningsdalen presented per barrier. In addition, the minimum and maximum calculated retention volume is compared to the calculated release volume above each barrier. Source: textcite

Design value/ Barrier number	Barrier height	Mean barrier width $b_m$	Snow height on ground	Slope inclination at barrier $\theta$	Angle of deposits $\theta'$	Release volume above barrier	Min retention capacity $V_{R,min}$	Max retention capacity $V_{R,max}$
Unit	[m]	[m]	[m]	[°]	[°]	[m <sup>3</sup> ]	[m <sup>3</sup> ]	[m <sup>3</sup> ]
1	5.0	16	3.0	8.5	10	1 000	1 829	3 658
2	5.0	16	3.0	11	10	3 360	3 549	14 194
3	6.0	25	3.0	10	10	2 500	6 930	11 880
4	6.0	30	3.0	12	10	2 000	3 381	9 937
5	6.0	28	3.0	10	10	1 870	4 046	6 936
6	6.0	23	3.0	11	10	1 200	4 046	7 896
7	6.0	18	3.0	12	10	1 000	1 986	5 838
8	6.0	17	3.0	13	10	860	1 014	2 981
9	7.0	20	4.0	12	10	1 100	930	3 719
10	7.0	19	4.0	15	10	720	1 606	6 242
11	7.0	17	4.0	17	10	820	786	3 144
12	8.0	18	5.0	16	10	650	1 057	5 520
13	8.0	14	5.0	14	10	950	1 099	5 741
14	4.0	-	3.0	5	-	-	-	-
Total	-	-	-	-	-	18 030	32 819	87 869

### 8.3 Load cases and barrier design values

The flexible net barriers are dimensioned by Geobrugg to withstand load actions from resting snow and slush avalanches. The loads are divided into 3 load case scenarios, where each represent a process that can have an impact on the superstructure. In addition, several load cases are defined that correspond to the dimensioning loads for specific components of the barriers. This includes load case 4, which is used to verify the ring net, and two load cases used to verify the support ropes and support posts. Illustrations of Load case 1 – 3 are presented in Figure 8.9, and the remaining load cases are presented in Figure 8.10. The complete design calculations can be found in Nordbrøden [27], Feiger [103], Feiger [104], Kronholm et al. [94], and Jónsson [102], while an overview is given here that mainly follows Feiger [103] and Nordbrøden [27].



**Figure 8.9:** Illustrations of load cases 1-3, from Feiger [103].

### 8.3.1 Load case 1: Static load from the snowpack

Load case 1 is the static snow pressure against the barrier caused by creep and glide in the winter snowpack. The calculated pressure is based on the Swiss technical guidelines for defence structures in avalanche starting zones [2], and has been slightly adapted to the specific conditions in Vannledningsdalen. These adaptations include not using an altitude factor  $f_c$ , and (conservatively) not accounting for the reduced pressure against the support surface resulting from the flexibility of the nets (see Section 3.3.4). The resulting pressure is assumed to be conservative due to the low angle of Vannledningsdalen to which these guidelines were not developed for, and because arctic snow covers are expected to have less glide [27, p. 28].

The static snow pressure in line of slope  $S'_{N;winter}$  is given by Equation 8.3 and the resulting static snow pressure  $S'_{N;winterA}$  is given by Equation 8.4. They are both simplified as uniformly distributed across the snow height (Figure 8.9). The creep factor  $K_{winter}$  is determined using Equation 8.5, while the remaining parameters in Equation 8.3 are described in Table 8.2.

$$S'_{N;winter} = \rho_{snow} \cdot g \cdot K_{winter} \cdot N \cdot \frac{h_s^2}{2} \quad [\text{kN/m}] \quad (8.3)$$

$$S'_{N;winterA} = \frac{S'_{N;winter}}{h_s} \quad [\text{kN/m}^2] \quad (8.4)$$

$$K_{winter} = 0,83 \cdot \sin(2 \cdot \psi) \quad [-] \quad (8.5)$$

Nordbrøden [27, p. 38] present a thorough discussion of the considerations made when deciding on input values for the load calculations. The first factor discussed is the glide factor  $N$  which is set to  $N = 1.8$ . Nordbrøden [27] chose to follow the glide factor of the Swiss Guideline without adaptations to Nordic or Icelandic conditions, arguing that no measurements have been performed on Spitsbergen that rule out glide completely and that running water below the snow cover is to be expected when the chance of slush flows is high. Performing measurements of glide in the area around Longyearbyen, and especially at locations where snow supporting structures are constructed, is an interesting project for further work.

Two other factors Nordbrøden [27] discuss are the expected snow height  $h_s$  and the snow density  $\rho_{snow}$ . The snow height at each barrier location is based on both Lidar and manual point measure-

ments performed by UNIS and LL between 2013 and 2019. The resulting snow heights can be seen in Table 8.3. The snow density is assumed to be  $\rho_{snow} = 400 \text{ kg/m}^3$ , which is considerably higher than recommended in the Swiss Guideline for low altitudes. The reason for this is that snow densities have generally been found to be higher in marine climates in the northern hemisphere compared to the Alps (as discussed in Section 3.3.5). In addition, Nordbrøden [27] argue that they can determine the snow density with a higher accuracy than the glide factor, and it is therefore reasonable to make adaptations to this factor.

A discrepancy has been found between the calculations of the creep factor  $K$  in Nordbrøden [27] and Feiger [103]. The RISK-report Nordbrøden [27] describes the creep factor as  $K_{winter} = 1,05 \cdot \sin(2 \cdot \psi)$  while Feiger [103] uses  $K_{winter} = 0,83 \cdot \sin(2 \cdot \psi)$ . However, they both have the same input values and resulting forces. Therefore, calculations have been done comparing their input values and resulting  $S'_N$ -force, and these show that a value 0,83 has been used. This corresponds to the recommended factor in Table 6 in the Swiss Guideline for a snow density of  $\rho = 400 \text{ kg/m}^3$ . The factor 1,05 is the highest value given in the Swiss Guideline, and corresponds to a snow density of  $\rho = 600 \text{ kg/m}^3$ . This discrepancy shows that there is some uncertainty concerning how the snow pressure around Longyearbyen can be accurately described, and it would be interesting for future works to study.

### 8.3.2 Load case 2: Static pressure from slush flow debris

Load case 2 is the static pressure against the barrier caused by slush flow debris completely filling the net. As for load case 1, the calculated pressure is based on the Swiss technical guidelines for defence structures in avalanche starting zones [2], and is simplified as uniformly distributed across the height (Figure 8.9).

The static snow pressure in line of slope  $S'_{N;slush}$  is given by Equation 8.6 and the resulting static snow pressure  $S'_{N;slushA}$  is given by Equation 8.7. The creep factor  $K_{slush}$  in Equation 8.6 is determined using Equation 8.8, while the rest of the parameters are described in Table 8.2.

$$S'_{N;slush} = \rho_{slush} \cdot g \cdot K_{slush} \cdot N \cdot \frac{h_N^2}{2} \quad [\text{kN/m}] \quad (8.6)$$

$$S'_{N;slushA} = \frac{S'_{N;slush}}{h_N} \quad [\text{kN/m}^2] \quad (8.7)$$

$$K_{slush} = 0,92 \cdot \sin(2 \cdot \psi) \quad [-] \quad (8.8)$$

The glide factor  $N = 1.8$  is assumed to be the same for slush flow deposits as for the winter snowpack [27, p. 39]. This is because Nordbrøden [27] is not aware of a calculation methodology adapted for granular debris deposits, and therefore chose to follow the Swiss Guideline. The resulting snow pressure from the slush flow deposits is therefore considered conservative.

The density of the slush flow deposits  $\rho_{slush} = 500 \text{ kg/m}^3$  is based on the assumption that water will continuously drain through the net during impact. The possibility of a higher density during a short period of time is accounted for through the higher dynamic forces from a slush flow impact (see load case 3). The snow height used ( $h_N$ ) corresponds to the full height of the barrier.

The same discrepancy as in Load case 1 also applies for Load case 2, in which Nordbrøden [27] and Feiger [103] use different formulas to calculate the creep factor  $K$ .

**Table 8.2:** Parameter description for calculating static and dynamic pressures according to load case 1-4.

Description	Value	Comment
Static snow pressure in line of slope for winter snow [ $kN/m$ ]	$S'_{N;winter}$	Force per meter of support structure along the contour line
Static snow pressure in line of slope for slush flow debris [ $kN/m$ ]	$S'_{N;slush}$	Force per meter of support structure along the contour line
Dynamic slush flow pressure over flow height [ $kN/m$ ]	$P'_N$	Acts over flow height and can occur anywhere over the system height
Total load against net [ $kN$ ]	$Q_{tot}$	Used to determine the impact force $q$ in the rope equation in the ring net proof
Density of winter snow [ $kg/m^3$ ]	$\rho_{snow} = 400$	Density of snow pack
Density of slush flow debris [ $kg/m^3$ ]	$\rho_{slush} = 500$	Density of slush flow debris packed against a net
Density of dynamic slush flow [ $kg/m^3$ ]	$\rho_{flow} = 700$	Higher density to account for a high water content and possible entrainment of debris
Gravitational acceleration [ $m/s^2$ ]	$g = 10$	No value is explicitly given in the project reports, but the Swiss Guidelines give this value
Glide factor [-]	$N = 1,8$	The glide factor used follows the Swiss guidelines without adaptations to Nordic or Icelandic conditions. The ground is considered to be coarse scree, yielding a class 2 according to Table 5 in Margreth [2, p. 44], and a ENE-S-WNW exposure is set because of high amounts of melt water.
Snow height on ground [ $m$ ]	$h_s$	Measured in the vertical direction. Dependent on barrier placement
Height of net [ $m$ ]	$h_N$	Snow height corresponding to net height
Slush flow height [ $m$ ]	$h_{fl} = 2$	Set equal for all barriers based on RAMMS calculations
Terrain inclination at net [degrees]	$\psi$	Dependent on barrier placement
Drag coefficient [-]	$C_d = 1.0$	No previous estimations of drag coefficients for slush flows interacting with net structures are known. The value given applies for all mesh sizes, and is primarily based on recommendations for mud flows and granular flows, and discussions between Geobruigg and Skred.
Slush flow velocity [ $m/s$ ]	$v$	Based on RAMMS calculations, and dependent on barrier placement

### 8.3.3 Load case 3: Dynamic slush flow pressure over flow height

Load case 3 is the dynamic pressure against the barrier caused by a slush flow impact over flow height. The pressure only acts over the flow height, but can occur at any system height depending on the snowpack height in front of the barrier (Figure 8.9). The climbing height is neglected because its influence on the loads is assumed to be low. The dynamic pressure over the flow height,  $P'_N$ , is given by Equation 8.9, and the resulting dynamic impact pressure,  $P_N$ , is given by Equation 8.10. The parameter descriptions are given in Table 8.2.

$$P'_N = C_d \cdot \rho_{flow} \cdot v^2 \cdot h_{fl} \quad [\text{kN/m}] \quad (8.9)$$

$$P_N = \frac{P'_N}{h_{fl}} \quad [\text{kN/m}^2] \quad (8.10)$$

This is load case 3 as presented by Feiger [103], however, Nordbrøden [27] presents a load case 3 where the static snow pressure ( $S'_N$  from load case 1) is added to the dynamic pressure ( $P_N$ ). Only the first is presented here because it is the load case Feiger [104] uses to verify the barrier nets (through load case 4 below), and because Feiger [103]'s calculations are more conservative with the given load parameters and barrier geometries.

Nordbrøden [27, p. 38] discuss the considerations made when deciding on input values for the slush flow density  $\rho_{flow}$ , the flow velocity at each barrier location  $v$ , and the drag coefficient  $C_d$ . The slush flow density  $\rho_{flow} = 700 \text{ kg/m}^3$  is higher than the density of snow avalanches to account for a high water content and possible entrainment of debris. The slush flow velocity  $v$  was found through RAMMS calculations and depend on the barrier placement. To avoid too high velocities, the barrier placement has been adjusted for some nets (see Section 8.2). The drag coefficient  $C_d = 1.0$  applies for all mesh sizes. The value is primarily based on recommendations given by the WSL for mud flows ( $C_d = 0.7 - 1.0$ ) and granular flows ( $C_d = 2.0$ ), and on discussions between Geobruigg and Skred. The knowledge of slush flow to net interaction is limited, and no estimations of drag coefficients for slush flows interacting with nets structures are known. Estimating this drag coefficient through experiments in a snow chute could be an interesting project for future work.

The flow heights are based on RAMMS calculations in the pre-project [94, p. 27], and is set to  $h_{fl} = 2 \text{ m}$  at all barriers.

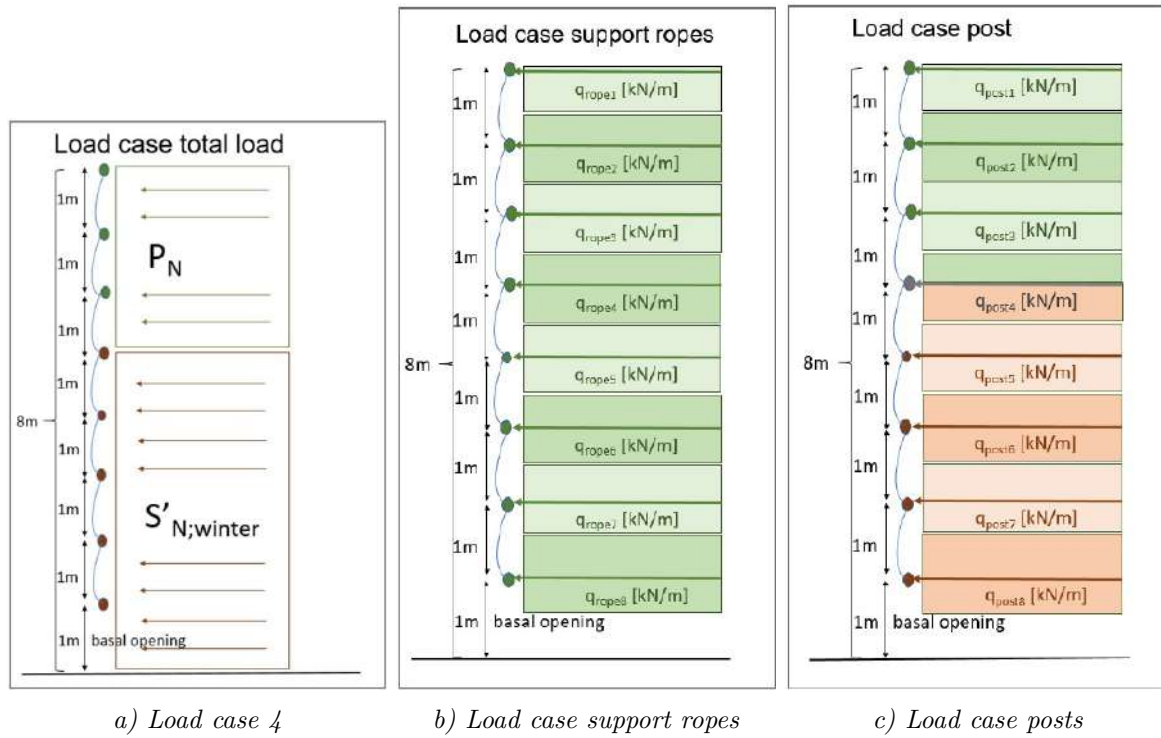
### 8.3.4 Load case 4: Total load from static and dynamic slush flow pressure

Load case 4 is the dimensioning load case for the ring net and corresponds to a dynamic slush flow impact on top of a static slush flow debris pressure. An illustration of the load case is shown in Figure 8.10a. The total load  $Q_{tot}$  is given by Equation 8.11.

$$Q_{tot} = (S'_{N;slush} \cdot h_s) + (P_N \cdot b_o \cdot (h_N - h_s)) \quad [\text{kN}] \quad (8.11)$$

Here  $b_o$  is the barrier width on top [ $m$ ], and the remaining parameter descriptions are given in Table 8.2.





**Figure 8.10:** Illustrations of load cases used to design a) the net, b) the support ropes, and c) the posts, from Feiger [103].

### 8.3.5 Load case: Support ropes

The dimensioning pressure for the support ropes is the dynamic impact of the slush avalanche  $P_N$ . This is because only one of load case 1-3 will act on a section of the net at once, and load case 3 is decisive. Each support rope have to withstand the force from this pressure acting over a height  $h_{rope} = 1m$ , where  $h_{rope}$  is the spacing between the rope layers (Figure 8.10b). The exception is the top support rope where the  $P_N$  only acts over a height  $h_{rope}/2$ . The resulting impacts,  $q_{rope1}$  and  $q_{rope2}$ , are given by Equation 8.12 (top rope) and Equation 8.13 (all ropes except the top rope).

$$q_{rope1} = \frac{P_N \cdot h_{rope}}{2} \quad [\text{kN/m}] \quad (8.12)$$

$$q_{rope2} = P_N \cdot h_{rope} \quad [\text{kN/m}] \quad (8.13)$$

Here  $h_{rope}$  is the spacing between the rope layers [m].

### 8.3.6 Load case: Support posts

The dimensioning load case for the support posts is a dynamic impact on the top 2.5 m of the barrier while a static slush flow debris load act on the rest of the barrier. This means that the support posts has to withstand the pressure from all support ropes, but each rope pressure depend on the support ropes placement in height (Figure 8.10c).

The top three rope layers act with a force against the posts according to the dynamic impact pressure in Equation 8.14 and 8.15. The force from the fourth rope layer consist half of the dynamic impact pressure and half of the static debris load according to Equation 8.16. The remaining rope layers act on the posts with a static debris load according to Equation 8.17.

$$q_{post1} = \frac{P_N \cdot h_{rope}}{2} \quad [\text{kN/m}] \quad (8.14)$$

$$q_{post2} = q_{post3} = P_N \cdot h_{rope} \quad [\text{kN/m}] \quad (8.15)$$

$$q_{post4} = \frac{S'_{N;slushA} \cdot h_{rope}}{2} + \frac{P_N \cdot h_{rope}}{2} \quad [\text{kN/m}] \quad (8.16)$$

$$q_{post5} = q_{post6} = q_{post7} = q_{post8} = S'_{N;slushA} \cdot h_{rope} \quad [\text{kN/m}] \quad (8.17)$$

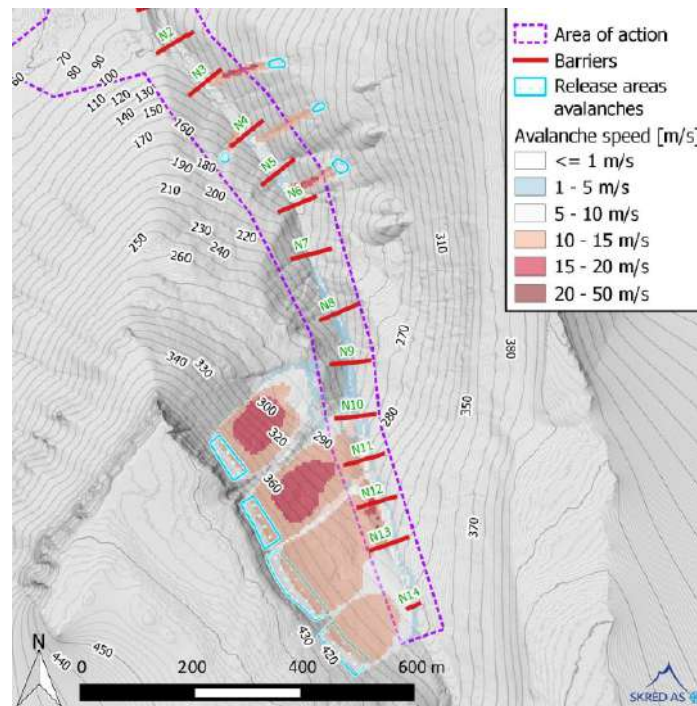
### 8.3.7 Load case: Snow avalanche

In addition to the loads from slush flows and static snow, some barriers are exposed to lateral avalanches due to the steep slope sides of Vannledningsdalen. Skred AS has done hazard mapping and avalanche calculations in RAMMS::Avalanche, and the results are illustrated in Figure 8.11. They concluded that barriers 3, 4, 6, and 10 – 14 are exposed to avalanche risk, and that the barrier dimensioning needs to check that they can withstand the avalanche forces from the side.

The load case for lateral avalanches consist of a dynamic snow avalanche pressure hitting the top part of the support posts. This is the worst case for the bending resistance, and assumes a high static snow cover in the valley. The dynamic impact acts over the avalanches flow height and the HEM profile width  $h$ , according to Equation 8.18.

$$P_{ava} = P'_N \cdot h \quad [\text{kN}] \quad (8.18)$$

Here  $P'_N$  is the dynamic impact over the snow avalanche flow height  $kN/m$ .



**Figure 8.11:** Release areas and avalanche tracks from the valley sides modelled in RAMMS::Avalanche by Skred AS using a fracture height of 100cm, return period 30years, and Tiny avalanche size. Source: Nordbrøden [27, p. 22].

### 8.3.8 Design values and barrier geometry

The design values for slush flows and static pressures for each barrier are shown in Table 8.3 along with resulting barrier geometries. Barrier 14 has only design values for the static snow load because it is not exposed to dynamic slush flow. The design parameters for the barriers exposed to lateral avalanche impact are shown in Table 8.4.

**Table 8.3:** The design values for slush flows and static pressure for each barrier, along with resulting barrier geometries. Source: Nordbrøden [27] and Feiger [103].

Barrier number/ Design value	Unit	1	2	3	4	5	6	7	8	9	10	11	12	13	14
Speed $v$	[m/s]	10	10	13	12	10	10	12	12	12	12	13	12	12	N/A
Drag coefficient $C_d$	[-]	1.0	1.0	1.0	1.0	1.0	1.0	1.0	1.0	1.0	1.0	1.0	1.0	1.0	
Glide factor $N$	[-]	1.8	1.8	1.8	1.8	1.8	1.8	1.8	1.8	1.8	1.8	1.8	1.8	1.8	
Slush flow height $h_{fl}$	[m]	2.0	2.0	2.0	2.0	2.0	2.0	2.0	2.0	2.0	2.0	2.0	2.0	2.0	
Climbing height	[m]	1.0	1.0	2.0	1.5	1.0	1.0	1.5	1.5	1.5	1.5	1.5	2.0	1.5	1.5
Density slush flow $\rho_{flow}$	[kg/m <sup>3</sup> ]	700	700	700	700	700	700	700	700	700	700	700	700	700	
Density slush debris $\rho_{slush}$	[kg/m <sup>3</sup> ]	500	500	500	500	500	500	500	500	500	500	500	500	500	
Density winter snow $\rho_{snow}$	[kg/m <sup>3</sup> ]	400	400	400	400	400	400	400	400	400	400	400	400	400	400
Snow height on ground $h_s$	[m]	3.0	3.0	3.0	3.0	3.0	3.0	3.0	3.0	4.0	4.0	4.0	5.0	5.0	3.0
Barrier height $h_N$	[m]	5.0	5.0	6.0	6.0	6.0	6.0	6.0	6.0	7.0	7.0	7.0	8.0	8.0	4.0
Basal opening net	[m]	1.0	1.0	1.0	1.0	1.0	1.0	1.0	1.0	1.0	1.0	1.0	1.0	1.0	1.0
Mean width of barrier $b_m$	[m]	15.5	20	25.5	28	26	19.5	18.5	14.5	16.5	17.5	15.5	18	16	34.5
Top width of barrier $b_o$	[m]	19	25	34	35	33	27	25	22	25	25	23	27	25	43
Bottom width of barrier $b_u$	[m]	12	15	17	21	19	12	12	7	8	10	8	9	7	26
Slope inclination barrier $\theta$	[°]	8.5	11	10	12	10	11	12	13	12	15	17	16	14	5
Post distance	[m]	9.0	9.0	7.5	8.0	7.5	8.0	8.0	5.0	6.0	7.0	6.0	6.0	5.0	10
HEM size	[m]	120	220	400	340	280	300	340	300	340	340	340	500	500	100

**Table 8.4:** The design values for the barriers exposed to lateral avalanche impact. Source: Nordbrøden [27].

Barrier number/ Design value	Unit	3	4	6	10	11	12	13	14
Avalanche speed $v$	[m/s]	10	10	10	10	12	14	12	8
Drag coefficient $C_d$	[-]	1.0	1.0	1.0	1.0	1.0	1.0	1.0	1.0
Avalanche flow height	[m]	0.5	0.5	0.5	0.3	0.5	0.7	0.7	0.5
Avalanche flow density	[kg/m <sup>3</sup> ]	300	300	300	300	300	300	300	300

## 8.4 Analytical proof of component strength

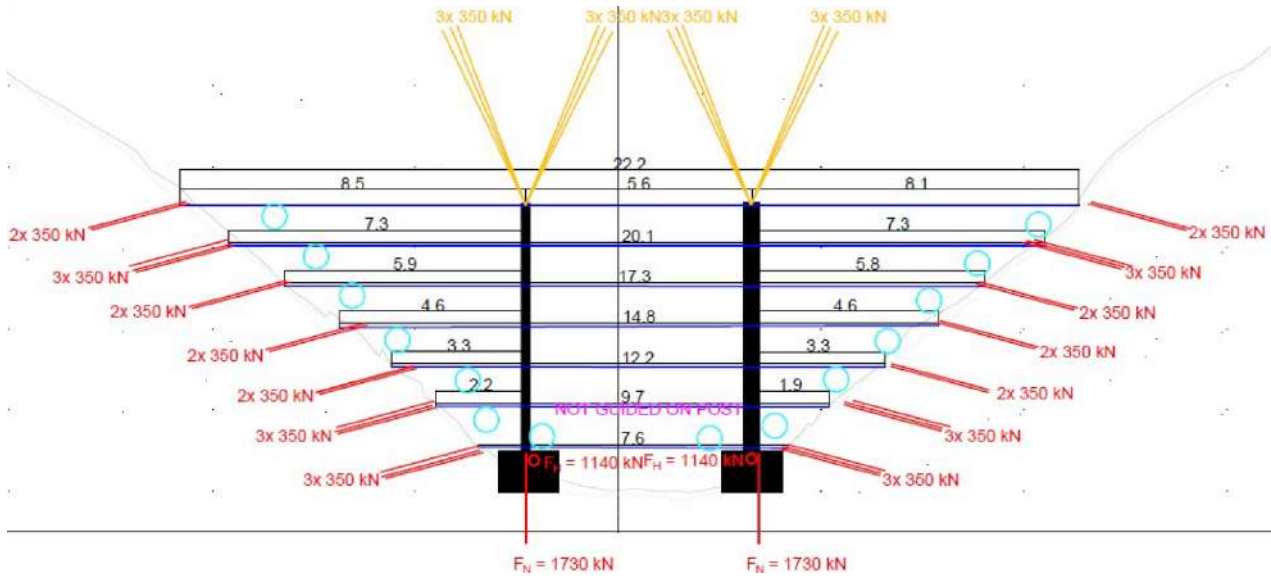
### 8.4.1 General

Analytical proofs of strength are given for each main component of the barriers superstructure. These proofs are calculated as for debris flow barriers, and greatly depend on the multiple field rope equation [109]. The calculations were carried out by Geobrugg and include proofs for the following main system components:

- ROCCO ring net
- Support ropes
- Brake element
- Lateral ropes
- Retaining ropes
- Support posts
- Post foundation

A partial safety factor for impact loads  $\gamma_G = 1.0$  is used for all components, while a material partial safety factor  $\gamma_M = 1.05$  is used for all components except the support posts. The material partial safety factor  $\gamma_{M1} = 1.10$  is used for the support posts. In verifying the ultimate limit state of the barriers, the design plastic resistance is used following Eurocode 3 (NS-EN 1993-1-1) [110] and the Swiss SIA technical standard (SIA 263) [28] [104].

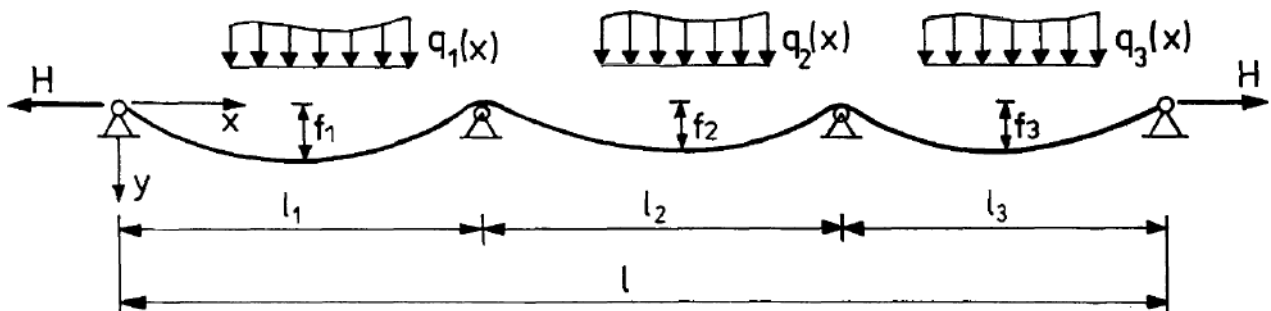
A system drawing of barrier 11 is shown in Figure 8.12 to give the reader an understanding of the scale of the forces and barrier components discussed. System drawings of barrier 10 are presented in Appendix A, while drawings of the other barriers can be found in Feiger [103].



**Figure 8.12:** Rough system drawing of barrier 11 with its main components and forces. Lengths are given in meters and forces are given in kN. Source: Feiger [103, p. 28].

### 8.4.2 Multiple field rope equation

To prove the strength of most components of the barrier, it is necessary to calculate the force that occurs in a rope which spans multiple supports and experience evenly distributed loads in each span. Geobrugg does this by using the multiple-field rope equation shown in Equation 8.19 [109]. Figure 8.13 shows an example of a multi-span rope where each field experience a distributed load.



**Figure 8.13:** Multi-span rope where each field experience a distributed load. For the barrier case, each load  $q_i(x)$  is assumed to be an evenly distributed load  $q_i$  [kN/m]. Length  $l_i$  [m] is the span of the rope in each field,  $l$  [m] is the total span of the rope, and  $f_i$  [m] is the rope sag in each field. The horizontal direction follows the  $x$ -axis, while the vertical direction follows the  $y$ -axis. Source: Palkowski [109].

The multiple field rope equation assume that the rope can slide on the inner supports without friction [109, sec. 2.4.1]. This simplifies the calculations because the horizontal component of the total rope force ( $H_A$ ) is then constant through all the fields. The horizontal direction follows the x-axis on Figure 8.13, while the vertical direction follows the y-axis. The horizontal component of the rope force is found by solving Equation 8.19 using Newton's Method.

The following calculations shows the procedure used to calculate the total rope force ( $F_{seil}$ ) starting with the multiple field rope equation:

$$H_A^3 + H_A^2 \cdot EA \cdot \left[1 - \frac{1}{s_0} \cdot l\right] = \frac{EA}{2 \cdot s_0} \cdot \left[ \int_0^{l_1} Q_1 dx + \int_0^{l_2} Q_2 dx + \int_0^{l_3} Q_3 dx \right] \quad (8.19)$$

Here  $H_A$  is the horizontal component of the rope force,  $E$  is the elastic modulus,  $A$  is the cross-sectional area of the wire ( $EA$  is the elongation stiffness),  $s_0$  is the initial rope length ( $q_i = 0$ ),  $Q_1, Q_2$ , and  $Q_3$  are the equal loads, and  $l_i$  is the span of the rope in each field (distance between supports). The equal load  $Q_n$  is determined according to

$$\int_0^{l_1} Q_1 = \frac{q_1^2 \cdot l_1^3}{12}. \quad [\text{kN}^2\text{m}] \quad (8.20)$$

where  $q_i$  [ $\text{kN}/\text{m}$ ] is a uniform load (the impact load). When the rope sag is small, i.e. when the horizontal component of the rope force is much larger than the cables self-weight, the initial rope length can be approximated as

$$s_0 = l \cdot \left[1 + \frac{8}{3} \cdot \left(\frac{f}{l}\right)^2\right] \quad [\text{m}] \quad (8.21)$$

where the initial rope sag  $f$  is given as

$$f = \frac{1}{30} \cdot l \quad [\text{m}] \quad (8.22)$$

and the total span of the rope is

$$l = l_1 + l_2 + l_3. \quad [\text{m}] \quad (8.23)$$

The vertical component of the rope force can be calculated as

$$R_A = \frac{q \cdot l}{2}, \quad [\text{kN}] \quad (8.24)$$

and after solving Equation 8.19 for  $H_A$ , the total rope force is calculated according to

$$F_{seil} = \sqrt{R_A^2 + H_A^2}. \quad [\text{kN}] \quad (8.25)$$

Equation 8.19 is solved for  $H_A$  using Newton's Method, where the first approximation  $H_1$  is

$$H_1 = \sqrt{\frac{Q_1 + Q_2 + Q_3}{2 \cdot (s_0 - l)}} \quad [\text{kN}] \quad (8.26)$$

and the second approximation  $H_2$  is

$$H_2 = \frac{(2 \cdot H_1^3) + (b \cdot H_1^2 + c)}{(3 \cdot H_1^2) + (2 \cdot b \cdot H_1)}. \quad [\text{kN}] \quad (8.27)$$

The constants  $b$  and  $c$  are defined according to Equation 8.28 and 8.29 to save time in the iterations.

$$b = EA \cdot \left(1 - \frac{l}{s_0}\right) \quad [\text{kN}] \quad (8.28)$$

$$c = \frac{EA \cdot (Q_1 + Q_2 + Q_3)}{(2 \cdot s_0)} \quad [\text{kN}^3] \quad (8.29)$$

Feiger [104] iterates 100 times to find the final horizontal component of the rope force  $H_{100}$ .

$$H_{100} = \left\| x_i \leftarrow \frac{(2 \cdot x_{i-1}^3) + (b \cdot H_{i-1}^2 + c)}{(3 \cdot x_{i-1}^2) + (2 \cdot b \cdot x_{i-1})} \right\| \quad (8.30)$$

*for*  $x_i \in 1 \dots 100$

The rope sag  $f_i$  for each field after loading is calculated according to Equation 8.31.

$$f_i = q_i \cdot \frac{l_i^2}{8 \cdot H_A} \quad [\text{m}] \quad (8.31)$$

As a final comment it is noted that a discussion was started with professor emeritus Kolbein Bell at NTNU to investigate whether the rope force  $F_{seil}$  could be estimated by idealising the cable as a beam with very low resistance to bending moments. This beam was analysed in Fap2D (Frame analysis program - 2D), which is a program developed at NTNU and used for static and dynamic analysis of 2D frame type structures [111]. The analysis was not finalised because of time restrictions, but it could be an interesting analysis in further work.

### 8.4.3 ROCCO ring net

In order to verify the strength of the ring net, the total impact force  $F_{Netz}$  have to be calculated. Utilising the multiple field rope equation,  $F_{Netz}$  correspond to the total rope force  $F_{seil}$  in Equation 8.25.

The total load on the ring net ( $Q_{tot}$ ) is found according to load case 4, and is used to determine the impact force  $q_i$  for the multiple field rope equation according to Equation 8.32.

$$q_i = \frac{Q_{tot}}{b_m} \quad (8.32)$$

where  $b_m = (b_o + b_u)/2$  is the average cross-section width of the net.

The other parameters used in the calculations are set to the following: The support distance is set to  $l_i = 1.0m$ , corresponding to the distance between each support rope. Since the net spans between several support ropes, the total span  $l$  has to correspond to the net height. For barrier 10, the total span is then  $l = 2l_1 + 2l_2 + 2l_3 = 6m$  [104]. For the ring net, the initial rope length  $s_0$  include both the rope sag and the possible elongation due to shape-deformations of the rings. This means that the elongation of the net rings have to be appended to the  $s_0$  given in Equation 8.21. The elongation of the ROCCO rings is set to  $l_{ring} = 0.05m$ .

After calculating the total rope force  $F_{Netz}$ , the proof of sufficient resistance in the ROCCO ring net is given when Equation 8.33-8.35 is fulfilled [103].

$$F_{Ed,Netz} \leq F_{Rd,Netz} \quad [\text{kN/m}] \quad (8.33)$$

$$F_{Ed,Netz} = \frac{F_{Netz} \cdot \gamma_Q}{H} \quad [\text{kN/m}] \quad (8.34)$$

$$F_{Rd,Netz} = \frac{F_{net,max}}{\gamma_M} \quad [\text{kN/m}] \quad (8.35)$$

Here  $F_{Ed,Netz}$  is the design impact load,  $F_{Rd,Netz}$  is the design resistance of the net,  $H$  is the height of the ring net [m] and  $F_{Netz}$  is the total force in the ring net [kN]. The resistance of the ROCCO ring net  $F_{net,max}$  is dependent on the number of rings per meter of net  $n_{ring}$  [ $m^{-1}$ ] and the resistance of each ring  $F_{ring}$  [kN].

$$F_{net,max} = n_{ring} \cdot F_{ring} \quad [\text{kN/m}] \quad (8.36)$$



#### 8.4.4 Support ropes

The force acting in each support rope layer  $F_{seil}$  is calculated using the multiple field rope equation. Since there are several rope layers and each layer has a different span and impact loading, Equation 8.19 to 8.25 has to be applied separately for each layer.

The uniform load  $q_i$  that acts on each rope layer is found according to load case support ropes (Equation 8.12-8.13). The support distances  $l_i$  are the distance between the support poles, and the distance from each pole to its closest anchor. Analogous to the ring net, the elongation of the brake elements have to be appended to the initial rope length  $s_0$  calculated in Equation 8.21. This elongation is set to  $l_{brake} = 1.0m$  per brake ring. An illustration of the brake rings are shown in Figure 8.14.

Proof of sufficient resistance in the support ropes is given when Equation 8.37-8.39 is fulfilled for all rope layers [103].

$$F_{Ed,Seil} \leq F_{Rd,Seil} \quad [\text{kN}] \quad (8.37)$$

$$F_{Ed,Seil} = F_{Seil} \cdot \gamma_Q \quad [\text{kN}] \quad (8.38)$$

$$F_{Rd,Seil} = \frac{n \cdot Seil_{xx}}{\gamma_M} \quad [\text{kN}] \quad (8.39)$$

Here  $F_{Ed,Seil}$  is the design impact load for the rope layer,  $F_{Rd,Seil}$  is the design resistance of the rope layer,  $F_{seil}$  is the total force acting in one rope layer,  $Seil_{xx}$  is the resistance of each rope, and  $n$  is the number of ropes needed at the rope layer. The number of ropes  $n$  is dependent on the design impact load  $F_{Ed,Seil}$  in respect to the limit load  $Seil_{xx}$ .

#### 8.4.5 Brake element

The brake elements are also verified for each rope layer, and their proof of sufficient resistance is given when Equation 8.40-8.42 is fulfilled [103]. An illustration and a picture of brake elements are shown in Figure 8.14.

$$F_{Ed,brake} \leq F_{Rd,brake} \quad [\text{kN}] \quad (8.40)$$

$$F_{Ed,brake} = F_{seil,br} \cdot \gamma_Q \quad [\text{kN}] \quad (8.41)$$

$$F_{Rd,brake} = \frac{F_{brake,xx}}{\gamma_M} \quad [\text{kN}] \quad (8.42)$$

Here  $F_{Ed,brake}$  is the design impact load on one rope,  $F_{Rd,brake}$  is the design resistance of one brake element,  $F_{seil,br}$  is the rope force per rope according to Equation 8.43, and  $F_{brake,xx}$  is the resistance load of one brake element.

$$F_{seil,br} = \frac{F_{Seil}}{n} \quad [\text{kN}] \quad (8.43)$$

$n$  is the number of support ropes at each rope layer.



**Figure 8.14:** Illustration and picture of brake elements. Source: Geobrugg AG.

#### 8.4.6 Lateral rope

The ring net is attached to the channel flanks with one or two lateral ropes on each side. The ropes are looped through the flexheads connecting the support ropes to the anchor bars (shown in Figure 8.6), and are fixed to the top and bottom flexhead. Therefore, the lateral ropes can be verified using the same procedure as for the support ropes [103]. The same rope is used as for the support ropes.

The uniform load  $q_i$  acting on the lateral ropes result from the forces in the ring net, and is set equal to the design impact load from the ring net proof (Equation 8.34).

$$q_i = F_{Ed,Netz} \quad [\text{kN/m}] \quad (8.44)$$

The support distance  $l_i$  correspond to the distance between the anchors, and the same brake element is used as for the support ropes. Proof of sufficient resistance in the lateral ropes is given when Equation 8.45-8.47 is fulfilled [104].

$$F_{Ed,lateral} \leq F_{Rd,lateral} \quad [\text{kN}] \quad (8.45)$$

$$F_{Ed,lateral} = F_{seil,lat} \cdot \gamma_Q \quad [\text{kN}] \quad (8.46)$$

$$F_{Rd,lateral} = \frac{n_{lateral} \cdot Seil_{xx}}{\gamma_M} \quad [\text{kN}] \quad (8.47)$$

Here  $F_{Ed,lateral}$  is the design impact load for the lateral ropes,  $F_{Rd,lateral}$  is the design resistance of the lateral ropes,  $F_{seil}$  is the total force acting in one lateral rope layer,  $Seil_{xx}$  is the resistance of each rope (same as for support ropes), and  $n$  is the number of lateral ropes needed at each side of the net. The number of ropes  $n$  is dependent on the design impact load  $F_{Ed,lateral}$  in respect to the resistance of a single rope  $Seil_{xx}$ .

#### 8.4.7 Retaining rope

The retaining ropes span between the top of the support posts and attach to the flexheads of anchor bars upstream of the barrier, as seen on Figure 8.15 [103]. The ropes keep a vertical retaining angle  $\beta = 60^\circ - 85^\circ$ , and an approximate horizontal retaining angle  $\alpha = 20^\circ$  while still being placed in the valley bottom [103].

Feiger [104] calculates the impact load on the retaining ropes  $F_{retainingRope}$  with two different approaches. The first approach is using the structural analysis software Rstab which directly gives the horizontal component of the impact load  $F_{retainingRope,H}$  from the support post proof discussed in the following section. The second approach is to assume that the horizontal component of the impact load  $F_{retainingRope,H}$  is equal to the dynamic impact load on one rope layer between the posts:

$$F_{retainingRope,H} = (P_N \cdot h_{rope}) \cdot b_{post} \quad [\text{kN}] \quad (8.48)$$

The impact load on the retaining ropes  $F_{retainingRope}$  is then calculated according to Equation 8.49.

$$F_{retainingRope} = \frac{F_{retainingRope,H}}{\sin(\beta)} \quad [\text{kN}] \quad (8.49)$$

where  $\beta$  is the vertical retaining angle seen on Figure 8.15. The approach resulting in the greatest impact load is used in the continued proof.

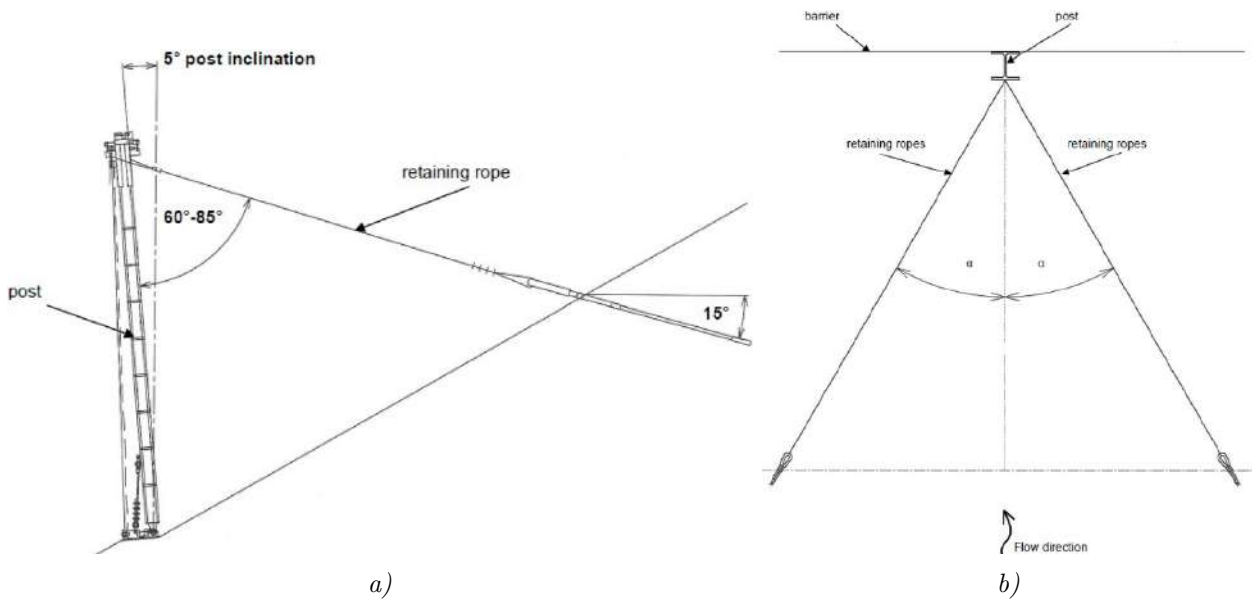
Proof of sufficient resistance in the retaining ropes is given when Equation 8.50-8.52 is fulfilled [104].

$$F_{Ed,retaining} \leq F_{Rd,retaining} \quad [\text{kN}] \quad (8.50)$$

$$F_{Ed,retaining} = F_{retainingRope} \cdot \gamma_Q \quad [\text{kN}] \quad (8.51)$$

$$F_{Rd,retaining} = \frac{n_{retaining} \cdot Seil_{xx}}{\gamma_M} \quad [\text{kN}] \quad (8.52)$$

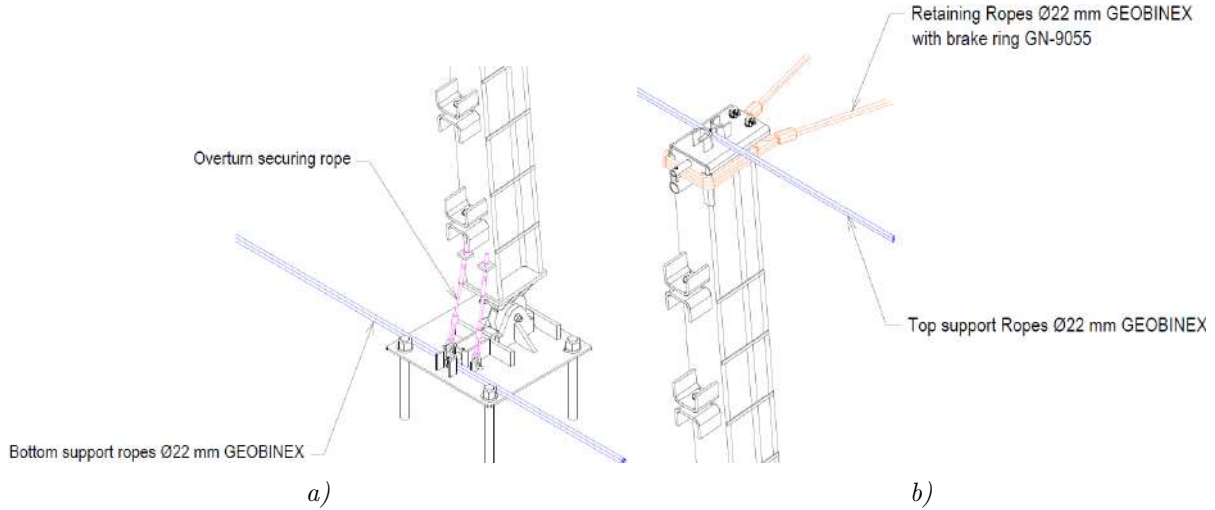
Here  $F_{Ed,retaining}$  is the design impact load for the retaining ropes,  $F_{Rd,retaining}$  is the design resistance of the retaining ropes,  $F_{retainingRope}$  is the total impact load acting on the retaining ropes, and  $n_{retaining}$  is the number of retaining ropes needed for one support post. The number of ropes  $n_{retaining}$  is dependent on the design impact load  $F_{Ed,retaining}$  in respect to the resistance of the ropes  $n_{retaining} \cdot Seil_{xx}$ . The same rope is used for the retaining ropes as for the support- and lateral ropes. Therefore,  $Seil_{xx}$  is the resistance of each rope.



**Figure 8.15:** Drawing of the support posts with retaining ropes and a) vertical retaining angle  $\beta$ , b) horizontal retaining angle  $\alpha$ . Source: Feiger [103].

### 8.4.8 Support posts

The analytical proofs of the support posts includes 1) calculating the rope force of each support rope layer using the multiple field rope equation, 2) calculating the impact load on the posts from each rope layer, 3) finding the design normal force, shear force and moment using the structural analysis software Rstab [112], and 4) a stability proof for uniform members in bending and axial compression according to Eurocode 3 [104]. The posts are also checked against the load case avalanche. Illustrations of the post foot and head can be seen in Figure 8.16, and more details are shown in Appendix A.



**Figure 8.16:** Detail of support post head and foot. Source: Geobrugg AG system drawing net 10 (Appendix A).

The total rope force  $F_{seil}$  is first found using the multiple field rope equation (Equation 8.19). The distributed loads ( $q_i$ ) are determined using the "support post"-load case, and the support distances  $l_i$  are the distances between the poles and anchors.

The posts experience a horizontal force  $F_H$ , a vertical force  $F_V$ , and a moment  $M$  from each support rope layer. After finding the total rope force  $F_{seil}$ , these impact loads are calculated according to Equation 8.53-8.55.

$$F_H = 2 \cdot F_{seil} \cdot \sin(\alpha) \quad [\text{kN}] \quad (8.53)$$

$$F_V = 2 \cdot F_{seil} \cdot \sin(20^\circ) \quad [\text{kN}] \quad (8.54)$$

$$M = \left( \frac{h}{2} + 30\text{mm} \right) \cdot F_H \quad [\text{kNm}] \quad (8.55)$$

where  $h$  is the width of the HEM beam, and  $\alpha$  is the rope elongation angle calculated as

$$\alpha = \arctan\left(\frac{f}{b}\right) \quad [\text{deg}] \quad (8.56)$$

Here  $f$  is the rope elongation. For the top rope, the vertical component of the retaining rope force  $F_{retainingRopeV}$  has to be added to  $F_V$ .

The calculated impact loads on the posts ( $F_H$ ,  $F_V$  and  $M$ ) are used as input in Rstab to calculate the design normal force  $N_{Ed}$ , design shear force  $V_{Ed}$  and design moment  $M_{Ed}$ .

The design normal force  $N_{Ed}$  and moment  $M_{Ed}$  are then used in the stability of proof for uniform members in bending and compression (Equation 8.57 and 8.58) according to Eurocode 3. This is done for barrier 2 – 13 .

$$\frac{N_{Ed}}{\frac{\chi_y \cdot N_{Rk}}{\gamma_{M1}}} + k_{yy} \cdot \frac{M_{y,Ed} + \Delta M_{y,Ed}}{\frac{\chi_{LT} \cdot M_{y,Rk}}{\gamma_{M1}}} + k_{yz} \cdot \frac{M_{z,Ed} + \Delta M_{z,Ed}}{\frac{M_{z,Rk}}{\gamma_{M1}}} \leq 1.0 \quad (8.57)$$

$$\frac{N_{Ed}}{\frac{\chi_z \cdot N_{Rk}}{\gamma_{M1}}} + k_{zy} \cdot \frac{M_{y,Ed} + \Delta M_{y,Ed}}{\frac{\chi_{LT} \cdot M_{y,Rk}}{\gamma_{M1}}} + k_{zz} \cdot \frac{M_{z,Ed} + \Delta M_{z,Ed}}{\frac{M_{z,Rk}}{\gamma_{M1}}} \leq 1.0 \quad (8.58)$$

Here  $N_{Ed}$  is the design compression force, and  $M_{y,Ed}$  and  $M_{z,Ed}$  are the maximum moments about the  $y - y$  and  $z - z$  axes respectively.  $M_{y,Rd}$  and  $M_{z,Rd}$  are the characteristic values of resistance to bending moments about the same axes.  $\Delta M_{y,Ed}$  and  $\Delta M_{z,Ed}$  are the moments due to the shift of the centroidal axis for class 4 sections,  $\chi_y$  and  $\chi_z$  are reduction factors due to flexural buckling,  $\chi_{LT}$  is a reduction factor due to lateral torsional buckling, and  $k_{yy}$ ,  $k_{yz}$ ,  $k_{zy}$ , and  $k_{zz}$  are interaction factors [103]. The material partial safety factor is set to  $\gamma_{M1} = 1.10$  for the posts. In both Norway and Switzerland, the material partial safety factor for steel buildings is defined as  $\gamma_{M1} = 1.05$ , and Eurocode 3 (NS-EN 1993-1-1) recommend and even lower value of  $\gamma_{M1} = 1.00$  [110, 113]. An explanation has not been found of why a higher value for the material partial safety factor has been chosen for the posts.

The support ropes at barrier 1 and 14 are either centred at the posts head or not supported by the post. Therefore, no moment occur and a full stability of proof for uniform members in bending and compression is not necessary. Instead, a stability proof of the buckling resistance for uniform members in compression was performed according to Equation 8.59.

$$\frac{N_{Ed}}{N_{b,z,Rk}} \leq 1.0 \quad (8.59)$$

where  $N_{b,z,Rk}$  is the buckling resistance about the  $z - z$  axis.

According to Eurocode 3, the effect of shear force on the moment resistance may be neglected if the shear force is less than half of the plastic shear resistance [110, p. 53]. This check is performed for the posts by applying Equation 8.60.

$$V_{Ed} \leq 0.5 \cdot V_{pl,Rd} \quad (8.60)$$

where the design value of the shear force  $V_{Ed}$  is found using Rstab and the  $V_{pl,Rd}$  is the design plastic shear resistance according to

$$V_{pl,Rd} = \frac{A_V \cdot (f_y / \sqrt{3})}{\gamma_{M1}} \quad (8.61)$$

$A_V$  is the shear area,  $f_y$  is the yield stress, and  $\gamma_{M1}$  is the material partial safety factor.

The strength of the posts against lateral avalanche impact is verified if the design moment due to the avalanche  $M_{Ed,ava}$  is smaller than the design moment resistance  $M_{Rd,ava}$  according to Equation 8.62.

$$M_{Ed,ava} \leq M_{Rd,ava} \quad [\text{kNm}] \quad (8.62)$$

Where

$$M_{Ed,ava} = P_{ava} \cdot H \cdot \gamma_Q \quad [\text{kNm}] \quad (8.63)$$

$$M_{Rd,ava} = \frac{M_{pl,z,Rd}}{\gamma_{M1}} \quad [\text{kNm}] \quad (8.64)$$

and  $H$  is the post height,  $\gamma_{M1} = 1.10$  is the material partial safety factor for the posts, and  $M_{pl,z,Rd}$  is the design resistance for bending about the  $z - z$  principal axis.

It is noted that Feiger [104] verifies the ultimate limit state of the posts by comparing the plastic bending- and shear resistance of the post with the elastically determined design loads. This is in correspondence with the Swiss Guideline where it is stated that "In verifying the ultimate limit state, the internal forces must be determined elastically".

### 8.4.9 Post foundation

The last barrier component that is checked is the post foundation. They are anchored to the ground with several anchors, and experience forces from the support post and lower support rope through a baseplate (Figure 8.17). The acting forces on the concrete foundation are compression force  $F_{N,foundation}$  and a shear force  $F_{H,foundation}$ . Geobruigg calculates the forces acting on the foundations, while the full post foundation is dimensioned by HNIT and will not be described in detail here.

The acting forces are calculated according to Equation 8.65 and 8.66.

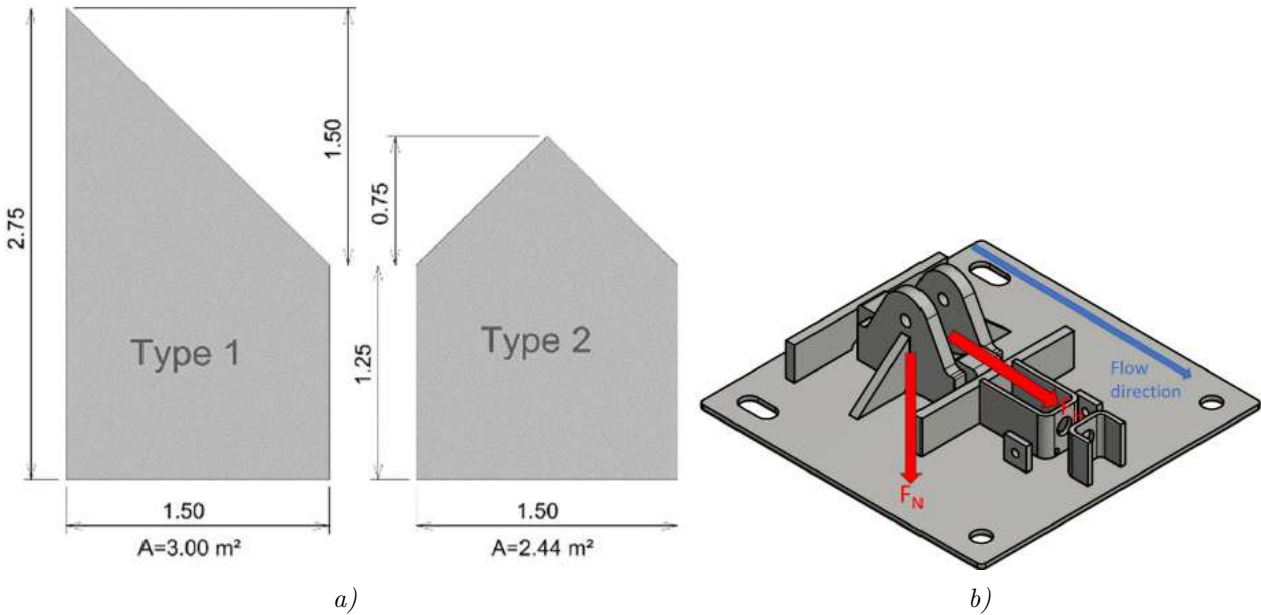
$$F_{N,foundation} = N_{Ed} \quad [\text{kN}] \quad (8.65)$$

$$F_{H,foundation} = V_{Ed} + F_H \quad [\text{kN}] \quad (8.66)$$

Here the design values for the compression force  $N_{Ed}$  and shear force  $V_{Ed}$  are found from the structural analysis program Rstab in the support post proof.  $F_H$  is the shear force component of the rope force in the bottom support rope, and is calculated according to Equation 8.67.

$$F_H = 2 \cdot F_{seil,bottom} \cdot \sin \left( \text{atan} \left( \frac{f_{2,7}}{b_{post}/2} \right) \right) \quad [\text{kN}] \quad (8.67)$$

where  $F_{seil,bottom}$  is the rope force in the bottom support rope,  $f_{2,7}$  is the rope sag of the bottom rope in the span between the support posts, and  $b_{post}$  is the post spacing.



**Figure 8.17:** Posts foundations and baseplate. a) Concrete foundation used for the posts at the side slopes (type 1) and the middle posts (type 2). b) Drawing of an example baseplate. Source: a) Jónsson [102], b) Feiger [103].





# Chapter 9

## Research gaps

### 9.1 General

An important objective of this thesis was to search for research gaps within the field of avalanche mitigation measures. The centre of focus has been on structural mitigation measures, and especially on the superstructure of snow supporting structures, slush flow barriers and snow drift measures. This focus was chosen because [this authors](#) is a structural engineer, and it is of interest to find research projects for the Department of Structural Engineering at [NTNU](#) and for [this authors](#) coming PhD work. Some research gaps have been mentioned earlier in the thesis but are repeated here for better readability.

The method used to find research gaps has been a comprehensive literature study of structural mitigation methods and discussions with experts on the area. The literature study included reading textbooks, guidelines in the design of protective structures, numerous reports from ongoing or finished mitigation projects, and research articles. Project reports were especially interesting because they addressed every aspect of the design and dimensioning and discussed their choices of values for design parameters. This made it clear what parameters were linked with most uncertainty and where the engineers could not find the needed information to make accurate dimensioning decisions. However, the most valuable information was gained from discussions with experts.

Three experts within the field of structural avalanche and debris flow mitigation measures have been asked what research projects they think would contribute most to their field of work. These experts were Kalle Kronholm with [Skred AS](#), Arni Jonsson with [HNIT verkfræðistofa \(consulting engineers\)](#), and Nadine Feiger with [Geobrugg AG](#). Their comments have given valuable insight into the challenges they face when designing and dimensioning avalanche mitigation structures, and the discussion of this chapter is to a large degree founded on outcome of conversations with them.

### 9.2 Flexible net barriers and slush flows

The most innovative project discussed in this thesis is probably the use of flexible net barriers as a mitigation measure against slush flows in Vannledningsdalen, Svalbard. According to Kronholm et al. [94, pp. 5, 11], there are no other examples of flexible net barriers being used as a mitigation method against slush flows in Norway, and no standard method exists for dimensioning mitigation measures against slush flows. Therefore, this project reveals several research gaps in its design reports. In addition, it is a project Kronholm, Jonsson and Nadine all have worked on, and where several issues have been debated. Jonsson also mentioned that [NGI](#) have expressed a wish for more research projects and experiments studying slush flows for a long time.

For better readability, the research gaps relating to flexible net barriers and slush flows have been arranged into five sections in the following. The first section discusses the fluid-structure interaction between flexible net barriers and slush flows, the second looks at slush flow dynamics, the third at the stabilising effect of the nets against slush flow release, the fourth at the barriers influence on snow drift, and the fifth comments on avalanche protection dams impacted by slush flows. After this, a separate section discusses snow supporting structures and snow pressures.

### 9.2.1 Fluid-structure interaction

The first research gaps pointed on by Kalle Kronholm were related to the fluid-structure interaction between flexible net barriers and slush flows. In a conversation on February 2<sup>nd</sup> 2022, Kronholm said that it is still uncertain exactly what happens when a slush flow impact a net, and mentioned the following points:

- How big is the impulse from the slush flow on the net?
- Does the first part of the slush flow pass the net so the impulse is reduced?
- How are the loads distributed on the net and into the foundations of the barrier?
- What will the maximum load (retaining forces) be on the anchors?
- How fast does the slush flow debris clog the net?
- How small must the net mesh size be to achieve the clogging-effect?
- What percentage of the slush flow volume will collect behind the net if it clogs?
- How high will the slush flow climb when impacting the barrier (climbing height)?
- How much is the slush flow slowed down when impacting or passing through the net (drag)?
- How much does the clogging or drag-effect influence the slush flow speed and runout distance?

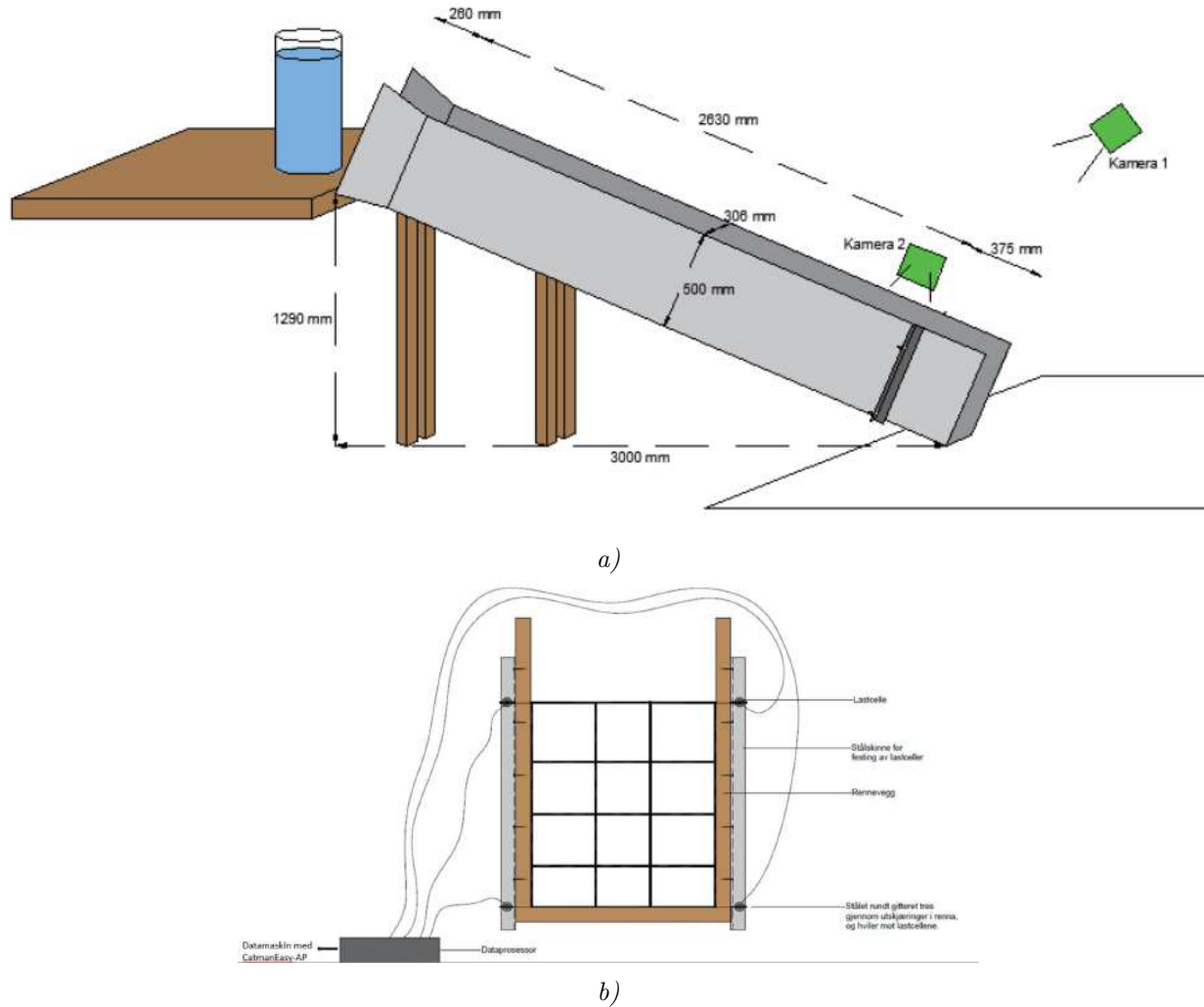
#### Experimental studies related to slush flows

In an attempt to answer some of these questions, part of the literature study was focused on finding experimental studies on slush flows and flexible net barriers. No experimental studies were found where slush flows impact *flexible* net barriers, but there have been experimental studies that are closely related to this problem.

A very relevant study when investigating slush flow impact on flexible net barriers is the master thesis of Thea Herberg that was conducted at the Department of Structural Engineering at NTNU [93]. Herberg conducted small scale laboratory tests of slush flows impacting *rigid* net barriers with two different mesh sizes. The experimental set-up of Herberg's tests is illustrated in Figure 9.1. These experiments were performed to address both the problem of calculating impact loads of slush flows on net barriers, and how the net barriers will affect the runout distance of slush flows. Herberg's results were used by Skred AS in the RISK-report for the mitigation project in Vannledningsdalen [27], which illustrates how important slush flow experiments are for the industry. For further work, Herberg recommended performing slush flow tests of larger scales, or even full scale tests.

Other experimental research that was found relevant to flexible net barrier and slush flow interaction include: 1) A chute experiment in Weissfluhjoch, Switzerland studying slush flow impact against a rigid column, seen in Figure 9.2 [57]; 2) A chute experiment in Dundhi, India investigating the dynamics of wet snow avalanches [114]; 3) Down-scaled and full size debris flows impacting flexible net barriers [95, 115–117]; 4) Full scale tests of rockfall net barriers loaded by avalanches and snow pressure [118].

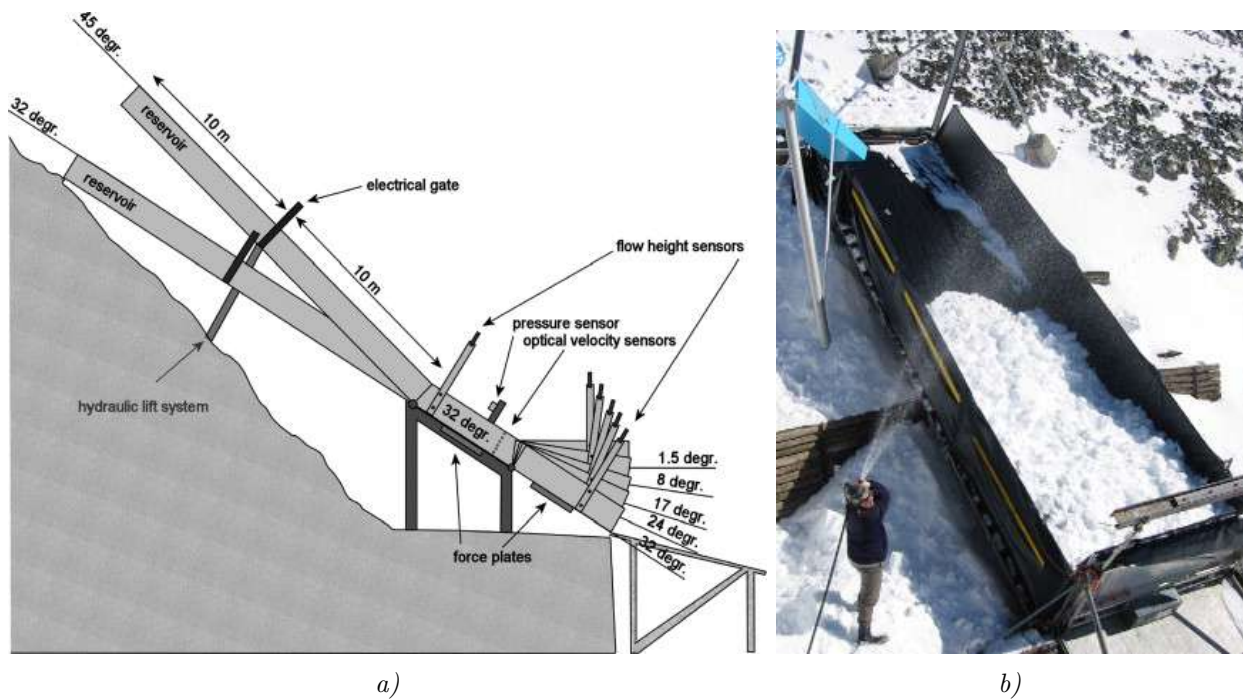
There are several reasons why these studies are interesting. The chute experiments in Weissfluhjoch and Dundhi [57, 114] are examples on how medium scale tests on slush flows can be conducted. Herberg's [93] laboratory setup is an example of an experiment requiring much less resources, but that is also of smaller scale. The debris flow experiments are relevant because slush flows and debris flows have many similar properties, and because methods for calculating impact loading from debris flows on net barriers are better established. Further work should asses whether these methods can be adjusted to slush flows. Last, the tests of rockfall net barriers against avalanche loads and snow pressure are relevant because they include calculations of the climbing height of snow avalanches on net barriers [118, p. 172]. This is used by Nordbrøden [27], who assume the climbing height of slush flows to be somewhere between that of dry snow avalanches and debris flows.



**Figure 9.1:** Illustration of experimental set-up of Herberg's laboratory tests of slush flows impacting rigid net barriers. a) Chute at  $23.3^\circ$  angle seen from the side. The barrier is drawn with a dark grey colour. b) Barrier set-up seen from higher up in the chute. Four load cells measure the load against the barrier. Source: Herberg [93].

Further work at the Department of Structural Engineering (NTNU) should consider possible chute and large scale experiments with slush flows. Performing small scale laboratory experiments would require less resources. However, since snow is a natural material these tests will likely experience scaling challenges [93]. Building a medium scale chute, similar to those of Jaedicke et al. [57] and Upadhyay et al. [114], might reduce some of the scaling problem. Further work should investigate whether such a chute could be constructed in the area close to Trondheim. One such location might be near Vassfjellet Ski Resort [119] because of its good access to snow and necessary infrastructure.

Full scale experiments will likely be challenging to conduct as the special conditions required for a slush flow to release are much more difficult to achieve at a test site than those of dry avalanches. However, collaboration with other scientists and organisations might make such a project possible. The NGI has initiated a working group of scientists and consultants working with slush flows called the Circum - Arctic Slushflow Network (CASN). The goal of the network is to share information and enable coordinated efforts and funding of costly and resource demanding full scale tests on slush flows [56]. This collaboration should be pursued, but scaled chute experiments are a more realistic project in the start-up phase.



**Figure 9.2:** Chute experiment in Weissfluhjoch, Switzerland studying slush flow impact against a rigid column. a) Illustration of the chute seen from the side. The inclination of the chute is adjustable. b) Picture during experiment preparations when a fire hose was used to add water to the snow (creating slush). Source: Jaedicke et al. [57].

### Fluid-structure interaction and the Vannledningsdalen project

Some of Kronholm's questions regarding fluid-structure interaction are discussed in the planning phase of the Vannledningsdalen project [27]. In this section, the research gaps related to the climbing height, the drag coefficient  $C_D$ , and the mesh size of the flexible net barriers will be addressed in relation to the Vannledningsdalen project.

The climbing height of slush flows is considered important both when calculating dynamic loading on a barrier generated by a slush flow, and when deciding the dimensioning height of structures [27, p. 41]. It is also considered when analysing overtopping of barriers. However, in the planning phase of the barriers in Vannledningsdalen, Nordbrøden [27] did not find any research studying the climbing height of slush flows on flexible net barriers, and found only one study observing the climbing height and overtopping of downscaled slush flows against *rigid* net barriers (the previously discusses laboratory tests performed by Herberg [93]). Therefore, Nordbrøden [27] assume the climbing height of slush flows to be somewhere between that of debris flows and that of dry avalanches. This assumption is clearly an approximation, and the climbing height of slush flows could be an interesting research area for further work.

The drag coefficient  $C_D$  is used when calculating the drag force  $F_D$  originating from a flow around an immersed slender obstacle (theory was presented in Section 5.4). Very few experiments have been performed that study the drag force on obstacles in slush flows, and no investigations have been found that consider the drag force of slush flows on flexible net barriers. However, Herberg [93] back calculated approximate values of the drag coefficient  $C_D$  for small scale slush flows impacting *rigid* net barriers. Studying the Vannledningsdalen RISK-report [27] it is seen that Nordbrøden [27] base the recommended drag coefficient,  $C_D = 1.0$ , on recommended values for mud flows, granular flows, and the values found by Herberg [93] for rigid net barriers. The lack of investigations studying this drag coefficient is therefore a significant research gap, and it is a very interesting research area for further work in a PhD study.

There are several factors that have to be considered when choosing the mesh size of the barrier's flexible net. The most important factor is that the mesh size have to be small enough to achieve a desired clogging-effect. *Clogging* means that the flow through the barrier stops because slush debris collects behind the barrier. This is a desired effect because the barriers are meant to retain as much of the slush flow as possible [27]. At the same time, a too small mesh size might cause bigger deposits of wind drifted snow around the barriers, and it will likely cause a higher drag coefficient  $C_D$  [27, 93] and higher wind loads. The solution proposed by Nordbrøden [27] for Vannledningsdalen is to use a mesh size of  $d = 300\text{mm}$  in the main barrier net, and to partly cover this net with a smaller meshed net. The goal is that the secondary net will increase the clogging effect, but that keeping a large mesh size on part of the net will hinder too much snow from accumulating. This solution is based on the considerations mentioned above, in addition to recommended mesh sizes for flexible debris flow barriers [120, p. 9] and the results of Herberg [93].

The discussion above illustrates that we do not know enough about how the mesh size influence the clogging effect of slush flows or the size of the drag coefficient. It also shows that we do not know how the mesh size influence the deposition of wind transported snow. The last factor (considering snow drift) is further discussed in Section 9.2.4.

### Numerical simulations of fluid-structure interaction

A last research gap mentioned in this section is the numerical simulation of the interaction between slush flows and flexible net barriers. Today, the [Rapid Mass Movement Simulation \(RAMMS\)](#) model with its debris flow module (i.e. RAMMS::Debris flow) is used in the hazard evaluation of slush flows to estimate the flow behaviour and runout distance. However, it does not simulate the interaction between slush flows and barriers correctly [93, p. 51], and therefore the full avalanche catchment area cannot be simulated after the installation of net barriers.

Creating reliable and accurate numerical models of slush flow interacting with the barriers would be beneficial for two reasons. The first is the mentioned ability to simulate the slush flow through the whole valley after the installation of net barriers. This could for example be done using RAMMS::Debris flow in combination with and a separate program simulating the fluid-structure interaction [93]. The second reason is that large scale experiments of slush flows will be time consuming and expensive. Simulating the fluid-structure interaction might reduce the need for physical experiments in the long run, and thereby save resources.

Herberg [93] made an initial attempt at simulating the slush flow interaction with rigid net barriers using a program called REEF3D. However, the results did not seem to give realistic simulations of the slush flow experiments she performed [93]. For debris flows impacting flexible barriers, numerical models have been developed that appear to agree with experimental results [121]. Since debris flows and slush flows have many similarities, further work should develop numerical models also for slush flows.

Computational mechanics and fluid-structure interaction is a central field of research at the Department of Structural Engineering at NTNU. It is therefore natural that further work will focus on this subject.

#### 9.2.2 Slush flow dynamics

During the literature study of structural mitigation measures it was noted that no sources use calculation procedures specifically designed for slush flow dynamics. Instead, they adapted numerical and analytical models designed for avalanches and debris flows. For example, Vegdirektoratet [32] estimates the runout distance of slush flows by adapting the energy-line method of debris flows, but they emphasise that this is a rough estimation. Also, Jónsson et al. [122] use the numerical



modelling tool [RAMMS](#): Debris flow when estimating slush flow velocity and runout distance in the Vannledningsdalen project, stating explicitly that a program dedicated to calculations on slush flows does not exist [122, p. 20].

Two other sources were found that explicitly mention the lack of dynamic modelling tools for slush flows. The first is Sauermoser et al. [49, p. 63], who state that there are still no appropriate calculation models for calculating avalanche pressures or runout distances for wet snow avalanches, and include slush flows as a special form of avalanche related to wet snow avalanches. The second source is Vegdirektoratet [32, p. 55], who state that there exist very few studies regarding slush flow speeds and runout distances, arguing that this is because slush flows are less frequent and only happen in limited areas. In addition, the lack of modelling tools for slush flows was discussed in the previously mentioned conversation with Kalle Kronholm.

Based on these findings it is safe to conclude that further work should focus on developing calculation procedures specifically designed for slush flow dynamics. This could be done in correlation with developing a tool for the fluid-structure interaction of slush flows and barriers, or it could be a separate study.

An additional research gap related to slush flow dynamics that was noted when studying the design of slush flow barriers in Vannledningsdalen is the previously mentioned angle of the slush flow deposits. This angle was found to be the biggest uncertainty when calculating the retention volume of the flexible net barriers, and analysing this deposit angle is thought to be an interesting subject for future work.

### 9.2.3 Stabilising effect of the net barriers against slush flow release

The use of snow nets as a support structures in avalanche starting zones is well established through the [Swiss Guideline](#) [2]. However, the guideline does not include the mitigating effect of nets (or any rigid structure) against the release of slush flows, and no other guidelines have been found that consider this effect.

The unknown parameter that needs investigating is how far away from the barriers the snowpack will still experience a supporting effect from the nets. This distance is important in order to decide the appropriate distance between the rows of slush supporting structures. The supporting effect is mentioned in the [RISK](#)-report of the Vannledningsdalen project, but no research is found (by Nordbrøden [27]) that provides a basis for estimating the maximum distance between the barriers [27, p. 26]. Further work could include experiments that investigate the supporting effect of slush from rigid or flexible barriers.

### 9.2.4 Snow accumulation around the barriers

As mentioned earlier, a research gap when considering the mesh size of the flexible barriers is to what extent the barriers influence the deposition of wind drifted snow. Bigger deposits of wind drifted snow could mean that the retention volume of the barriers is decreased and that the slush flow volume impacting the barriers is increased. Therefore it is important to know how the mesh size of the barrier influence the deposits. However, Nordbrøden [27] does not have any data indicating whether the barriers influencing the deposition is a problem or not.

Two different methods are suggested to investigate how the Vannledningsdalen barriers influence the snow deposits. The first method is to partly cover half of the barriers that are constructed the first summer with a chess board pattern consisting of a secondary finer mesh [27, p. 41]. The chosen barriers will likely be barrier number 7, 9, 11, and 13, and this is assumed ideal because most snow drift can be expected in the upper half of the valley. The effect of the barriers on snow drift

can then be observed the first winter and adjusted (if needed) the following summer. The second method suggested is to establish a separate research installation where snow drift around flexible barriers is studied. An equivalent research installation is already constructed for solar panels [123] in Adventdalen (Advent Valley, neighbouring valley to Vannledningsdalen). The barrier installation for snow drift could either be placed in conjunction with the solar panel installation, or in a valley with more similar wind conditions to those in Vannledningsdalen.

### 9.2.5 Avalanche protection dams hit by slush flows

Avalanche protection dams are structural mitigation measures that are also used in mitigation against slush flows. When dimensioning these structures, it is important to know the design loads from the slush flows, and how the slush flow will interact with the structure. However, this knowledge is not as well established for slush flows as for dry avalanches.

The fluid-structure interaction between avalanche dams and slush flows was mentioned in the conversation with Kronholm on February 2<sup>nd</sup> 2022. Kronholm highlighted the following points concerning avalanche protection dams in Longyearbyen:

- How high will the slush flow climb when impacting the dam (climbing height)?
- In what location and in what direction does a slush flow impact the dam?
- How are the shear forces in the dam act?
- Can the dam be protected against erosion using the same measures as for debris flows?
- Will slush flows erode rocks from the dam?
- Will the design load impact the dam when the dam material is frozen or thawed?

These questions have been left for further work, but prove with example that research gaps exist also when considering slush flow impact against other mitigation structures than flexible net barriers.

## 9.3 Snow supporting structures and snow pressure forces

### 9.3.1 Snow creep and glide

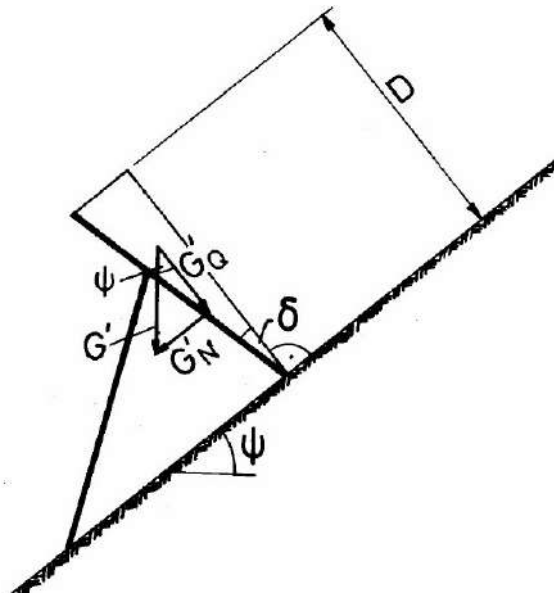
The design and dimensioning of snow supporting structures and calculating snow pressures have been discussed several times in this thesis. The [Swiss Guideline](#) is a well established guideline based on the continental climate of the Alps, and efforts have been made to adapt the [Swiss Guideline](#) to better reflect the maritime conditions of Iceland and mainland Norway [33, p. 25]. However, the snow pressure in arctic climate and permafrost areas is found to be a research gap within the field of snow pressure and supporting structures. This was confirmed in the conversations with all three experts; Kronholm, Jonsson and Feiger.

An example that supports this finding is the calculations performed in the planning phase of the Vannledningsdalen project. The pre-project reports thoroughly discuss how the snow pressure calculations of the [Swiss Guideline](#) can be adapted to the conditions around Longyearbyen, and especially whether adaptations should be made to the snow density or glide factor [27]. In addition, it was noted that Nordbrøden [27] and Feiger [103] use different creep factors when defining Load case 1 and 2 (snow pressure from winter snow and slush flow debris respectively). This has previously been discussed in [Section 8.3.1](#), but is repeated here for better readability. Feiger [103] use a creep factor given in the [Swiss Guideline](#) corresponding to the estimated snow density in Longyearbyen, while Nordbrøden [27] use a creep factor corresponding to the maximum snow density. The reason for this was explained by Nadine Feiger to be an ongoing evaluation of the snow density used in the calculations, so that the creep factors were based on different densities. This substantiate the idea that there is still some uncertainty concerning how the snow pressure around Longyearbyen can be accurately described.

In further works it could be interesting to conduct specific measurements of creep, glide and snow density at locations relevant for snow supporting structures, for example at Sukkertoppen or above Lia in Longyearbyen. An ongoing project (the Snow Load Testing System discussed in Section 7.3) already measure snow pressures in a slope above Longyearbyen Airport. However, these measurements are performed in a slope with inclinations of  $25^\circ - 30^\circ$ , and it would be interesting to measure the actual snow pressures around the already constructed supporting structures at Sukkertoppen where the slope inclination is steeper.

### 9.3.2 Downslope inclination of supporting surface

In the literature study of snow supporting structures it was noted that the Swiss Guideline recommend the angle between a rigid supporting surface and the normal to the slope to be  $\delta = 15^\circ$  in the downslope direction [2, p. 58]. This angle can be seen in Figure 9.3. However no literature was found that explained this grate inclination.



**Figure 9.3:** Illustration of the  $\delta = 15^\circ$  downslope inclination of the supporting surface of snow bridges. Source: Margreth [2, p. 47].

To find the explanation of the  $15^\circ$  grate inclination, an email was sent by a fellow student, Vetle Basma at NTNU, to Stefan Margreth at the WSL Institute for Snow and Avalanche Research. Margreth is the project leader and revising author of the Swiss Guideline [2] and therefore considered a very reliable source within the field of snow supporting structures. The explanation given by Margreth was that the foundation forces on the uphill side and the support length are somewhat smaller using a grate inclination of  $15^\circ$  than with a grate inclination of  $0^\circ$ . However, he emphasised that he does not know of any documentation describing the reasons for choosing exactly  $15^\circ$ , and recommended that Basma investigate the influence of different grate inclinations on the statics of the snow supporting system. This could be a very interesting project for future work.

### 9.3.3 Snow drift around support structures on Sukkertoppen

When snow supporting structures are constructed on a slope, they might affect the wind transport of snow. The exact result of the snow drift is often not known until after the structures have been observed during one or more winters. An example of one such project is the snow supporting structures that have recently been constructed at Sukkertoppen, Svalbard. These structures were inspected during the research trip to Longyearbyen in March 2022, and a detailed discussion of the snow drift around them was presented in [Section 7.4](#). The full discussion will not be duplicated, but to improve readability the observed research gap is repeated here.

During the field work at Sukkertoppen, observations of the snow cover around the support structures showed that the snow distribution was greatly affected by wind transport. Most of the snow had been cleared away between the supporting surface and supports, while snow had accumulated in wind slabs between the structure lines. A literature study concluded that this would likely not negatively affect the structures ability in mitigating against avalanche because of a reduced back-pressure zone, but that future work should investigate whether the wind slabs alter the snow deposition so much that it is possible to reach a greater snow height than the structures are designed against.

## 9.4 Discussion

The research gaps presented in this chapter are based on a literature study and a limited number of conversations with experts within the field of structural avalanche and debris flow mitigation measures. When [this author](#) have not been able to find literature documenting a design procedure or explaining a curiosity, the procedure or curiosity have been assumed to be a research gap. However, avalanche and debris flow mitigation is a very big research field with a lot of literature, and some relevant articles could have been overlooked. This represents a source of error. It is therefore important that future work thoroughly investigates their chosen research gap before initiating a project. The investigation can include talking to more experts, attending relevant conferences, and reading more textbooks and articles.

Another source of error is that a notable part of the literature referred to in this thesis is written by a limited number of experts. Also, some reports backing up an experts insight have been written by this experts associates. This is the case for some discussions of Kronholms questions, including the research gaps related to avalanche protection dams ([Section 9.2.5](#)) and the stabilising effect of the flexible net barriers ([Section 9.2.3](#)). To minimise these errors, objective sources have been sought after and the source of the literature kept in mind. However, the research field of slush flow mitigation measures is new, and it has been unavoidable to study many reports from the same authors.

As a final remark, it is noted that the field of avalanche mitigation measures is still a minor part of the research at [NTNU](#) in Trondheim. This means that it is not possible as a student to attend avalanche courses or technical avalanche mitigation courses, because they do not exist. The theory presented in this thesis is entirely based on a personal literature study and the previously mentioned conversations with three experts, and an obvious source of error is therefore that [this author](#) have not been aware of some important literature. Going forward, an aim at the Department of Structural Engineering ([NTNU](#)) is to increase the research related to structural mitigation measures against avalanches, slush flows, debris flows, and rockfall. This will likely decrease the chance of overlooking important research. In addition, this source of error can be minimised through attending relevant conferences, collaborating closely with experts and consultants, and through detailed investigations before starting big projects.



# Chapter 10

## Conclusion and further work

In this thesis, a literature review of snow, avalanches, and avalanche mitigation methods have been performed, the design of an ongoing slush flow mitigation project using flexible net barriers was studied, and a research trip was conducted studying avalanche related structures near Longyearbyen, Svalbard. The purpose was to map problem fields where future research projects can contribute most to the field of structural avalanche protection, and to learn about avalanches, avalanche protective structures, snow pressures, and load actions from avalanches.

The most important results and conclusions from the work with this thesis are presented in the following.

### Literature review

The literature review found that creep and glide in the snowpack is the main cause of snow pressures against structures built in steep slopes. A Swiss technical guideline [2] is predominantly used when designing snow supporting structures. There exist Norwegian and Icelandic adaptations to the Swiss guideline developed to better reflect their maritime climate, but knowledge on snow pressures in the arctic climate around Longyearbyen is limited. The numerical simulation tool RAMMS is used in the dynamic modelling of dense flow snow avalanches, slush flows and debris flows. Slab avalanches release when an additional load trigger a shear fracture in a weak layer at a depth in the snowpack, and they account for more than 90% of all avalanche fatalities. Slush flows are wet-snow avalanches with a liquid water content of minimum 15% that can occur at very gentle slope inclinations. Structural avalanche mitigation measures may comprise steel fences, flexible nets and wire systems, deflecting or catching dams, retarding cones, snow sheds or tunnels. In general, the structures giving the highest safety rating against avalanches are also the most expensive and comprehensive solutions. The cheaper solutions are often specialised towards specific types of terrain or hazards.

### Field work results

During the research trip to Longyearbyen, the average snowpack density in a snow pit was measured to  $\rho \approx 360 \text{ kg/m}^3$ , and snowpack temperature measurements showed a linear temperature increase from  $-13.6^\circ\text{C}$  at the snow surface to  $-9.7^\circ\text{C}$  at the ground. Manual snow height measurements were performed in the back-pressure zone of the Snow Load Testing System (SLTS) using avalanche probes, showing a relatively stable snow height over a 10m distance from the wall. The slope inclination of the back-pressure zone was measured to be between  $25^\circ$  and  $30^\circ$ . The SLTS measured greater snow pressure loads against the top part of the wall than against the bottom part when the wall was almost covered with snow. This corresponds well with snow creep being largest close to the snow surface. The system also measured a great load increase after a period of warm weather and rain in March 2022, which is in good correspondence with an increasing snow creep with increasing snowpack temperature. An inspection of the already constructed snow supporting structures at Sukkertoppen showed that the snow deposits were greatly affected by wind.



## Study of slush flow barriers in Vannledningsdalen

Debris flow net barriers with a ROCCO ring net system are used in Vannledningsdalen near Longyearbyen for the purpose of slowing down moving slush avalanches and reduce the probability of slush avalanche release by supporting the snowpack. The barriers consist of flexible ring nets and load bearing support ropes with brake elements that extend transversely to the streambed and are anchored to the valley sides. Support post ensure that the remaining barrier height after impact remains as large as possible, to achieve the largest possible retention volume. The barrier placement have been chosen to keep the maximum avalanche speeds close to 10m/s and thereby save costs through requiring less anchoring points. They function as multilevel barriers meaning that overflow of one barrier is accepted as long as the total retaining capacity is higher than the expected total flow volume. The static load actions on the barriers from snow and slush flow deposits are calculated according to the Swiss technical guideline (SLF) and depend on snow density, snow height, and creep and glide in the snowpack. The dynamic load actions are calculated according to Austrian normative documents for permanent technical avalanche protection (ONR), and depend on the square of the slush flow velocity, the flow density, the flow height, and a drag coefficient. In verifying the ultimate limit state of the barriers, the internal forces are found elastically and largely based on a multiple field rope equation. The design plastic resistance is used, and the proof of strength is in agreement with Eurocode 3 (NS-EN 1993-1-1) and the Swiss SIA technical standard (SIA 263).

## Research gaps and further work

Results from the literature review, and discussions with three experts within the field of structural avalanche and debris flow mitigation measures, showed that several research gaps exist regarding slush flows and flexible net barriers. It is suggested that further work conduct medium or large scale slush flow experiments investigating (1) the drag coefficient  $C_D$  and (2) climbing height of slush flows impacting barriers, (3) how mesh size influence the clogging-effect of slush flow debris behind net barriers, (4) the deposit angle of slush flows, (5) the stabilising effect of snow supporting structures against the release of slush flows, and (6) what happens when a slush flow impact avalanche protection dams. In addition, effort should be made to create reliable and accurate numerical models of slush flows interacting with barriers (i.e., fluid-structure interaction), and to develop calculation procedures specifically designed for slush flow dynamics. Further work could also investigate to what extent flexible net barriers influence the deposition of wind drifted snow, and how this is affected by net mesh size. The snow drift effects around rigid support structures built near Longyearbyen is of interest for further work, in addition to the snow pressures acting on these structures. Measurements of snow density, creep, and glide close to these structures should be performed in correlation with the snow pressure measurements, and tests can be performed to investigate the influence of different support surface inclinations on the statics of snow supporting systems.

# References

- [1] Trumer Schutzbauten GmbH. *Avalanche Standards*. NetClimber Web Design Inc. URL: <https://trumerschutzbauten.com/standards/avalanche-standards/> (visited on May 23, 2022).
- [2] S. Margreth. *Defense structures in avalanche starting zones*. Report. Swiss Federal Office for Environment FOEN, Bern; WSL Swiss Federal Institute for Snow and Avalanche Research SLF, Davos, 2007. URL: [https://www.slf.ch/fileadmin/user\\_upload/SLF/Permafrost/Bauen\\_im\\_Permafrost/Lawinenverbau\\_im\\_Anbruchgebiet\\_E.pdf](https://www.slf.ch/fileadmin/user_upload/SLF/Permafrost/Bauen_im_Permafrost/Lawinenverbau_im_Anbruchgebiet_E.pdf).
- [3] Norwegian Royal Ministry of Justice and Public Security. *Regjeringen gir mer penger til flom- og skredsikring*. regjeringen.no. 2021. URL: <https://www.regjeringen.no/no/aktuelt/regjeringen-gir-mer-penger-til-flom-og-skredsikring/id2884655/> (visited on May 3, 2022).
- [4] M. Eckerstorfer. *Snow avalanches in Central Svalbard*. The University Centre in Svalbard. 2013. URL: <https://www.unis.no/snow-avalanches-central-svalbard/> (visited on June 8, 2022).
- [5] K. A. Hoseth, I. Johnsen, and J. Gundersen. *Konseptstudie - Sikringstiltak Sukkertoppen og Vannledningsdalen*. Report 78-2018. ISBN: 978-82-410-1744-5. Norges vassdrags- og energidirektorat (NVE), Mar. 2018.
- [6] D. McClung and P. Schaerer. *The avalanche handbook*. 3rd ed. Seattle, Washington: Mountaineers Books, 2006. ISBN: 978-08-988-6809-8.
- [7] K. Lied and K. Kristensen. *Snøskred : håndbok om snøskred*. Nesbru, Oslo: Vett & viten I samarbeid med NGI, Norges geotekniske institutt, 2003. ISBN: 8241205686. URL: [https://bibsys-almaprimo.hosted.exlibrisgroup.com/permalink/f/13q4kuj/BIBSYS\\_ILS71512234630002201](https://bibsys-almaprimo.hosted.exlibrisgroup.com/permalink/f/13q4kuj/BIBSYS_ILS71512234630002201).
- [8] F. Rudolf-Miklau, S. Sauer Moser, and A. I. Mears. *The Technical Avalanche Protection Handbook*. Wilhelm Ernst & Sohn, Verlag für Architektur und technische Wissenschaften GmbH & Co. KG, 2015. ISBN: 9783433030349. DOI: 10.1002/9783433603840.
- [9] Vegdirektoratet. *Veger og snøskred (Roads and avalanches), Håndbok V138*. Report ISBN: 978-82-7207-675-6. Statens vegvesen, 2014. URL: <https://www.vegvesen.no/globalassets/fag/handboker/hb-v138.pdf>.
- [10] L. U. Arenson, W. Colgan, and H. P. Marshall. “Chapter 2 - Physical, Thermal, and Mechanical Properties of Snow, Ice, and Permafrost”. In: *Snow and Ice-Related Hazards, Risks, and Disasters*. Ed. by J. F. Shroder, W. Haeberli, and C. Whiteman. Hazards and Disasters Series. Boston: Academic Press, 2015, pp. 35–75. ISBN: 978-0-12-394849-6. DOI: <https://doi.org/10.1016/B978-0-12-394849-6.00002-0>.
- [11] USACE Hydrologic Engineering Center. *HEC-HMS Technical Reference Manual, Snowmelt Basic Concepts*. 2022. URL: <https://www.hec.usace.army.mil/confluence/hmsdocs/hmstrm/snow-accumulation-and-melt/snowmelt-basic-concepts> (visited on Apr. 30, 2022).
- [12] K. Libbrecht. “The physics of snow crystals”. In: *Reports on Progress in Physics* 68 (2005). DOI: 10.1088/0034-4885/68/4/R03.
- [13] International Ski and Snowboard Federation (FIS). *Snow Crystals*. 2010. URL: [https://wiki.fis-ski.com/index.php/Snow\\_crystals](https://wiki.fis-ski.com/index.php/Snow_crystals) (visited on Mar. 27, 2022).
- [14] C. Fierz, R. L. Armstrong, Y. Durand, P. Etchevers, E. Greene, D. M. McClung, K. Nishimura, P. K. Satyawali, and S. A. Sokratov. “The International classification for seasonal snow on the ground”. Unpublished Work. IHP-VII Technical Documents in Hydrology N° 83, IACS Contribution N° 1, UNESCO-IHP, Paris, 2009. URL: <https://unesdoc.unesco.org/ark:/48223/pf0000186462.locale=en>.

- [15] K. Müller and H. T. Larsen. *Snøomvandling*. Pamphlet. nve.no, 2020. URL: [https://publikasjoner.nve.no/faktaark/2020/faktaark2020\\_01.pdf](https://publikasjoner.nve.no/faktaark/2020/faktaark2020_01.pdf).
- [16] WSL Institute for Snow and Avalanche Research SLF. *Avalanche types*. n.d. URL: <https://www.slf.ch/en/avalanches/avalanche-science-and-prevention/avalanche-types.html> (visited on May 29, 2022).
- [17] R. Solberg, R. Frauenfelder, H. Koren, and K. Kronholm. “Could retrieval of snow layer formation by optical satellite remote sensing help avalanche forecasting? Presentation of first results”. In: *ISSW 09 - International Snow Science Workshop, Proceedings* (Jan. 2009).
- [18] avalanche.org. *Wind slab*. 2017-2022. URL: <https://avalanche.org/avalanche-encyclopedia/wind-slab/> (visited on Feb. 23, 2022).
- [19] Y. Tominaga. “Computational fluid dynamics simulation of snowdrift around buildings: Past achievements and future perspectives”. In: *Cold Regions Science and Technology* 150 (2018). Snow Engineering special issue – selected papers from 8th International conference on Snow engineering, Nantes, June 2016, pp. 2–14. DOI: <https://doi.org/10.1016/j.coldregions.2017.05.004>.
- [20] B. Jamieson. *Energy exchange (heat transfers) at the snow surface*. 2017. URL: <https://www.brucejamieson.ca/videos-snow-avalanche-science> (visited on Feb. 27, 2022).
- [21] Avalanche institute. *Metamorphism*. avalanche-center.org. 2021. URL: <https://www.avalanche-center.org/Education/glossary/metamorphism.php> (visited on Mar. 25, 2022).
- [22] P. Nairz, A. Mears, S. Sauer Moser, K. Gabl, M. Stoffel, and S. Margreth. “Avalanches: evolution and impact”. In: *The Technical Avalanche Protection Handbook*. John Wiley & Sons, Ltd, 2014. Chap. 2. ISBN: 9783433603840. DOI: <https://doi.org/10.1002/9783433603840.ch02>.
- [23] Norges Geotekniske Institutt. *Hva skjer med snøen når vi har kaldt, stabilt vintervær?* n.d. URL: <https://www.ngi.no/Tjenester/Fagekspertise/Snoeskred/snoskred.no2/Laer-om-snoeskred/Hva-skjer-med-snoen-naar-vi-har-kaldt-stabilt-vintervaer> (visited on June 5, 2022).
- [24] S. Margreth, J. Suda, M. Mölk, R. Hofmann, P. Gauer, W. Schilcher, C. Skolaut, A. Mears, and S. Sauer Moser. “Structural avalanche defense: design and construction”. In: *The Technical Avalanche Protection Handbook*. Ed. by F. Rudolf-Miklau, S. Sauer Moser, and A. I. Mears. John Wiley & Sons, Ltd, 2014. Chap. 6, pp. 177–254. ISBN: 9783433603840. DOI: <https://doi.org/10.1002/9783433603840.ch06>.
- [25] S. Margreth. *Effectiveness and maintenance of technical avalanche protection measures in Switzerland*. Conference Paper. Apr. 2019. URL: [https://www.vedur.is/gogn/snjoflod/varnarvirki/snow2019abstracts/Snow2019\\_MARGRETH\\_eabstract.pdf](https://www.vedur.is/gogn/snjoflod/varnarvirki/snow2019abstracts/Snow2019_MARGRETH_eabstract.pdf).
- [26] European Union. *EN Eurocode Parts*. European Commission. 1995-2022. URL: <https://eurocodes.jrc.ec.europa.eu/showpage.php?id=13> (visited on May 23, 2022).
- [27] H. S. Nordbrøden. *Mitigation against slush flows in Vannledningsdalen with debris flow barriers*. Report 18241-26-1. Internal document, Client: Norges vassdrags- og energidirektorat (NVE) (Norwegian Water- and Energy Directorate). Skred AS, Nov. 2021.
- [28] SIA. *sia-norm*. Schweizerischer Ingenieur- und Architektenverein. 2022. URL: <https://www.sia.ch/en/services/sia-norm/> (visited on May 23, 2022).
- [29] Byggteknisk forskrift. *Forskrift om tekniske krav til byggverk (en. Regulations on technical requirements for construction works)*. Legal. Direktoratet for byggkvalitet (en. The Ministry of Local Government and Modernisation), 2017. URL: <https://dibk.no/regelverk/byggteknisk-forskrift-tek17/> (visited on May 25, 2022).

- 
- [30] NVE. *Veileder for utredning av sikkerhet mot skred i bratt terreng (en. Guidelines for assessing safety against avalanches in steep terrain)*. Norges vassdrags- og energidirektorat (en. The Norwegian Water Resources and Energy Directorate). 2020. URL: <https://veileder-skredfareutredning-bratt-terreng.nve.no/> (visited on May 23, 2022).
- [31] Vegdirektoratet. *Veger og drivsnø (Roads and drifting snow), Håndbok V137*. Report ISBN: 978-82-7207-644-2. Statens vegvesen, 2014. URL: <https://www.vegvesen.no/globalassets/fag/handboker/hb-v137.pdf>.
- [32] Vegdirektoratet. *Flom- og sørpeskred (Flood- and slush flows), Håndbok V139*. Report ISBN: 978-82-7207-676-3. Statens vegvesen, 2014. URL: <https://www.vegvesen.no/globalassets/fag/handboker/hb-v139-121214.pdf>.
- [33] J. O. Larsen. *Skredsikring og fundamentering i permafrost. Case: Arktiske strøk - Longyearbyen, Svalbard (en. Avalanche protection and anchorage in permafrost. Case: Arctic regions - Longyearbyen, Svalbard)*. Drammen, Norway: Almaviva AS, 2016.
- [34] J. A. S. Jacobsen. “Måling av snøsig i et snødekke i den sentrale delen av Svalbard, Spitsbergen”. Thesis. 2017. URL: <https://nmbu.brage.unit.no/nmbu-xmlui/bitstream/handle/11250/2500302/Masteroppgave%20-%20Jan%20Jacobsen.pdf?sequence=1&isAllowed=y>.
- [35] R. Haefeli. “Schnee, Lawinen, Firn und Gletscher”. In: *Ingenieurgeologie: Ein Handbuch für Studium und Praxis*. Vienna: Springer Vienna, 1948, pp. 663–735. ISBN: 978-3-7091-5845-6. DOI: 10.1007/978-3-7091-5845-6\_13. URL: [https://doi.org/10.1007/978-3-7091-5845-6\\_13](https://doi.org/10.1007/978-3-7091-5845-6_13).
- [36] B. Salm. “A short and personal history of snow avalanche dynamics”. In: *Cold Regions Science and Technology* 39.2 (2004), pp. 83–92. ISSN: 0165-232X. DOI: <https://doi.org/10.1016/j.coldregions.2004.06.004>.
- [37] D. M. McClung. “A one-dimensional analytical model for snow creep pressure on rigid structures”. In: *Canadian Geotechnical Journal* 19.4 (1982), pp. 401–412. DOI: 10.1139/t82-045.
- [38] D. M. McClung, J. O. Larsen, and S. B. Hansen. “Comparison of snow pressure measurements and theoretical predictions”. In: *Canadian Geotechnical Journal* 21.2 (1984), pp. 250–258. DOI: 10.1139/t84-028.
- [39] T. Jóhannesson and S. Margreth. *Adaptation of the Swiss Guidelines for supporting structures for Icelandic Conditions*. Report VI-G99013-UR07. Veðurstofa Íslands, July 1999. URL: <https://www.vedur.is/gogn/snjoflod/varnarvirki/stodvstd-19990715.pdf>.
- [40] J. O. Larsen. *Design criteria for avalanche supporting structures exposed to snow creep forces in maritime climate*. Conference Paper. 2000. URL: <https://trid.trb.org/View/670312>.
- [41] Statens Vegvesen. *Tasks and responsibilities (under: About the Norwegian Public Roads Administration)*. URL: <https://www.vegvesen.no/en/about-us/about-the-organisation/about-the-norwegian-public-roads-administration/our-service-to-society-tasks-and-responsibilities/tasks-and-responsibilities/> (visited on Apr. 22, 2022).
- [42] D. McClung and J. Larsen. “Effects of Structure Boundary Conditions and Snow-Pack Properties on Snow-Creep Pressures”. In: *Annals of Glaciology* 13 (1989), pp. 175–179. DOI: 10.3189/S0260305500007849.
- [43] BUWAL/SLF. *Richtlinien für den Lawinenverbau im Anbruchgebiet Vertrieb*. Report. EDMZ, 3003 Bern, 2001.
- [44] S. Sauermoser, F. Rudolf-Miklau, and S. Margreth. “Introduction”. In: *The Technical Avalanche Protection Handbook*. John Wiley & Sons, Ltd, 2014. Chap. 1, pp. 1–16. ISBN: 9783433603840. DOI: <https://doi.org/10.1002/9783433603840.ch01>.
-

- [45] UNESCO. *Avalanche atlas : illustrated international avalanche classification*. Vol. 2. Natural hazards. Paris: International Commission on Snow and Ice of the International Association of Hydrological Sciences, IAHS, 1981. ISBN: 9230016969. URL: [https://bibsyst-almaprimo.hosted.exlibrisgroup.com/permalink/f/13q4kuj/BIBSYS\\_ILS71494493510002201](https://bibsyst-almaprimo.hosted.exlibrisgroup.com/permalink/f/13q4kuj/BIBSYS_ILS71494493510002201).
- [46] Avalanche.org. *Avalanche path*. 2017-2022. URL: <https://avalanche.org/avalanche-encyclopedia/#avalanche-path> (visited on June 1, 2022).
- [47] Avalanche institute. *Track*. avalanche-center.org. 2021. URL: <https://www.avalanche-center.org/Education/glossary/track.php> (visited on May 25, 2022).
- [48] Avalanche.org. *Loose snow avalanche*. 2017-2022. URL: <https://avalanche.org/avalanche-encyclopedia/loose-snow-avalanche/> (visited on June 1, 2022).
- [49] S. Sauermoser, M. Granig, K. Kleemayr, and S. Margreth. “Avalanche dynamics: models and impact”. In: *The Technical Avalanche Protection Handbook*. John Wiley & Sons, Ltd, 2014. Chap. 3, pp. 55–90. ISBN: 9783433603840. DOI: <https://doi.org/10.1002/9783433603840.ch03>.
- [50] J. Streater. *Off Piste Awareness Part 1 — Types of Avalanche*. 2016. URL: <https://maverixsnow.medium.com/off-piste-awareness-part-1-types-of-avalanche-eed17d12a713> (visited on June 1, 2022).
- [51] Safeback. *Slab Avalanches*. 2020. URL: <https://www.safeback.no/slab-avalanche> (visited on June 1, 2022).
- [52] B. Jamieson, S. Margreth, and A. Jones. “Application and Limitations of Dynamic Models For Snow Avalanche Hazard Mapping”. In: *Proceedings of the ISSW 2008. Wistler, Canada* (Jan. 2008).
- [53] C. Fierz, R. L. Armstrong, Y. Durand, P. Etchevers, E. Greene, D. M. McClung, K. Nishimura, P. K. Satyawali, and S. A. Sokratov. *The International classification for seasonal snow on the ground*. Generic. Incl. bibl. 2009. URL: [https://unesdoc.unesco.org/notice?id=p::usmarcdef\\_0000186462](https://unesdoc.unesco.org/notice?id=p::usmarcdef_0000186462).
- [54] Avalanche.org. *Avalanche*. 2017-2022. URL: <https://avalanche.org/avalanche-encyclopedia/#avalanche> (visited on June 1, 2022).
- [55] European Avalanche Warning Services. *Glossary*. 2021. URL: <https://www.avalanches.org/glossary/#slush> (visited on Feb. 15, 2022).
- [56] Norwegian Geotechnical Institute. *R&D program - Circum - Arctic Slushflow Network (CASN)*. 2017. URL: <https://www.ngi.no/eng/Projects/Circum-Arctic-Slushflow-Network-CASN/#About-the-project> (visited on May 25, 2022).
- [57] C. Jaedicke, M. A. Kern, P. Gauer, M. A. Baillifard, and K. Platzler. “Chute experiments on slushflow dynamics”. In: *Cold Regions Science and Technology* 51.2 (2008), pp. 156–167. ISSN: 0165-232X. DOI: <https://doi.org/10.1016/j.coldregions.2007.03.011>.
- [58] E. Hestnes and K. Kristensen. “The diversities of large slushflows illustrated by selected cases”. In: (2022).
- [59] M. Barbolini et al. *The design of avalanche protection dams Recent practical and theoretical developments*. Climate Change and Natural Hazard Research - Series 2. EUROPEAN COMMISSION, 2009, p. 212. ISBN: 978-92-79-08885-8. DOI: [10.2777/12871](https://doi.org/10.2777/12871).
- [60] B. Jamieson. *Planning Methods for Assessing and Mitigating Snow Avalanche Risk*. (contributions by Jamieson, B., Jones, A., Argue, C., Buhler, R., Campbell, C., Conlan, M., Gauthier, D., Gould, B., Johnson, G., Johnston, K., Jonsson, A., Sinickas, A., Statham, G., Stethem, C., Thumlert, S., Wilbur, C.) Canadian Avalanche Association, 2018. ISBN: 9781926497020. URL: <https://books.google.no/books?id=vLI0uwEACAAJ>.



- 
- [61] G. Håland, K. I. Orset, M. H. Frekhaug, and H. Norem. *Sammenligning av modelleringsverktøy for norske snøskred*. Report ISBN: 978-82-410-1159-7. 2015. URL: [https://publikasjoner.nve.no/rapport/2015/rapport2015\\_107.pdf](https://publikasjoner.nve.no/rapport/2015/rapport2015_107.pdf) (visited on Feb. 9, 2022).
- [62] K. Lied and S. Bakkehøi. “Empirical Calculations of Snow–Avalanche Run–out Distance Based on Topographic Parameters”. In: *Journal of Glaciology* 26.94 (1980), pp. 165–177. ISSN: 0022-1430. DOI: [10.3189/S0022143000010704](https://doi.org/10.3189/S0022143000010704).
- [63] A. Voellmy. “Über die Zerstörungskraft von Lawinen”. In: *Schweizerische Bauzeitung* 73 (1955). DOI: <http://doi.org/10.5169/seals-61891>.
- [64] R. Perla, T. T. Cheng, and D. M. McClung. “A Two–Parameter Model of Snow–Avalanche Motion”. In: *Journal of Glaciology* 26.94 (1980), pp. 197–207. DOI: [10.3189/S002214300001073X](https://doi.org/10.3189/S002214300001073X).
- [65] WSL Institute for Snow and Avalanche Research SLF. *RAMMS. Background Information*. 2010. URL: [https://ramms.slf.ch/ramms/index.php?option=com\\_content&view=article&id=57&Itemid=74](https://ramms.slf.ch/ramms/index.php?option=com_content&view=article&id=57&Itemid=74) (visited on May 14, 2022).
- [66] K. Kleemayr. “Modelling and simulation in snow science”. In: *Mathematics and Computers in Simulation* 66.2 (2004), pp. 129–153. ISSN: 0378-4754. DOI: <https://doi.org/10.1016/j.matcom.2003.11.009>.
- [67] P. Sampl and M. Granig. *Avalanche simulation with SAMOS-AT*. Conference Paper. 2009. URL: <https://www.scopus.com/inward/record.uri?eid=2-s2.0-82955178687&partnerID=40&md5=35d7b1d772f6550dc614e1dd57b667de>.
- [68] A. Aalberg. *Snow avalanche forces*. Compedium. The University Centre in Svalbard course AT-301, Aug. 2019.
- [69] S. Bakkehøi, U. Domaas, and K. Lied. “Calculation of Snow Avalanche Runout Distance”. In: *Annals of Glaciology* 4 (1983), pp. 24–29. ISSN: 0260-3055. DOI: [10.3189/S0260305500005188](https://doi.org/10.3189/S0260305500005188).
- [70] K. Lied, C. Weiler, S. Bakkehoi, and J. Hopf. *Calculation methods for avalanche run-out distance for the Austrian Alps*. English. 1995. URL: <https://pascal-francis.inist.fr/vibad/index.php?action=getRecordDetail&idt=6242799>.
- [71] P. Oller, C. Baeza, and G. Furdada. “Empirical alpha-beta runout modelling of snow avalanches in the Catalan Pyrenees”. In: *Journal of Glaciology* 67.266 (2021), pp. 1043–1054. DOI: [10.1017/jog.2021.50](https://doi.org/10.1017/jog.2021.50).
- [72] M. Christen, P. Bartelt, and U. Gruber. “AVAL-1D: An avalanche dynamics program for the practice”. In: *Proceedings Interpraevent 2002 in the Pacific Rim - Matsumoto 2* (2002), pp. 715–725. URL: [https://www.researchgate.net/publication/228934801\\_AVAL-1D\\_An\\_avalanche\\_dynamics\\_program\\_for\\_the\\_practice](https://www.researchgate.net/publication/228934801_AVAL-1D_An_avalanche_dynamics_program_for_the_practice).
- [73] P. Jörg, M. Granig, Y. Bühler, and H. Schreiber. “Comparison of measured and simulated snow avalanche velocities”. In: *12th Congress Interpraevent (2012)*. interpraevent.at. ISBN: 978-3-901164-19-4. URL: [http://www.interpraevent.at/palm-cms/upload\\_files/Publikationen/Tagungsbeitraege/2012\\_1\\_169.pdf](http://www.interpraevent.at/palm-cms/upload_files/Publikationen/Tagungsbeitraege/2012_1_169.pdf).
- [74] Merriam-Webster. *Mitigation*. URL: <https://www.merriam-webster.com/dictionary/mitigation> (visited on Feb. 10, 2022).
- [75] Colorado Geological Survey. *Mitigation and Land Use - Avalanches*. Dec. 2004. URL: <https://web.archive.org/web/20060917085424/http://geosurvey.state.co.us/Default.aspx?tabid=400> (visited on Feb. 10, 2022).
- [76] S. Margreth. “Technische Lawinenschutzmaßnahmen”. In: (2004). (in German).
- [77] European Avalanche Warning Services. *EAWS Matrix*. 2021. URL: <https://www.avalanches.org/standards/eaws-matrix/> (visited on May 25, 2022).
-



- [78] L. Stoffel, P. Nairz, K. Kleemayr, E. Procter, A. Kogelnig, R. Urschler, M. Larghi, and S. Sauermoser. “Artificial release and monitoring technology for avalanches”. In: *The Technical Avalanche Protection Handbook*. John Wiley & Sons, Ltd, 2014. Chap. 9, pp. 325–362. ISBN: 9783433603840. DOI: <https://doi.org/10.1002/9783433603840.ch09>.
- [79] A. I. Mears. *Avalanche mitigation*. 2014. URL: [https://mearsandwilbur.com/avalanche\\_mit.html](https://mearsandwilbur.com/avalanche_mit.html) (visited on Feb. 10, 2022).
- [80] M. Hannus. *Skredfarekartlegging i utvalgte områder på Svalbard*. Report 91-2016. Norges vassdrags- og energidirektorat (NVE), 2016. URL: [https://publikasjoner.nve.no/rapport/2016/rapport2016\\_91.pdf](https://publikasjoner.nve.no/rapport/2016/rapport2016_91.pdf).
- [81] The Planning and Building Act. *Lov om planlegging og byggesaksbehandling (en. Planning and the Processing of Building Applications)*. Legal. Kommunal- og distriktsdepartementet (en. Norwegian Ministry of Local Government and Regional Development), 2008. URL: <https://lovdata.no/lov/2008-06-27-71> (visited on May 25, 2022).
- [82] ELIMAST Helicopter Service. *Avalanche Control with Daisybell® System*. 2022. URL: <https://www.elimast.it/en/helicopter-services/avalanche-control.html> (visited on May 25, 2022).
- [83] Wyssen Avalanche Control. *Norways first operational avalanche control project at road FV53 Tyin - Årdal*. 2022. URL: <http://www.wyssenavalanche.com/en/portfolio/norways-first-operational-avalanche-control-project/> (visited on May 25, 2022).
- [84] B. Gould. *Remote Avalanche Control Systems: High Tech on the Mountain*. Report. 2014. URL: [https://static1.squarespace.com/static/51ace772e4b0a54238b8b419/t/539f53e0e4b014ec3a91482f/1402950624280/caj\\_vol106\\_pg22-25.pdf](https://static1.squarespace.com/static/51ace772e4b0a54238b8b419/t/539f53e0e4b014ec3a91482f/1402950624280/caj_vol106_pg22-25.pdf).
- [85] Vegdirektoratet, L. L. Kristensen, and e. al. et. *Forebyggende snøskredkontroll (Preventative avalanche release) - Erfaringsrapport fra RESPONS-prosjektet*. Report 623. Statens vegvesen, Jan. 2020. URL: <https://vegvesen.brage.unit.no/vegvesen-xmlui/bitstream/handle/11250/2673164/Rapport%20623%20Forebyggende%20sn%C3%B8skredkontroll.pdf?sequence=1&isAllowed=y>.
- [86] Doppelmayr Seilbahnen GmbH. *Based on mountain expertise - Developed for safety*. 2022. URL: <https://www.doppelmayr.com/products/avalanche-blasting-ropeway/> (visited on May 25, 2022).
- [87] B. Jamieson, A. Jones, and C. Wilbur. “Structural avalanche defenses”. In: *Planning Methods for Assessing and Mitigating Snow Avalanche Risk*. Ed. by B. Jamieson. Alberta, Canada: Canadian Avalanche Association, 2018. Chap. 13. ISBN: 9781926497020. URL: <https://www.avalancheassociation.ca/store/ViewProduct.aspx?id=12382344>.
- [88] W. Schilcher, S. Margreth, S. Sauermoser, C. Skolaut, M. Mölk, and F. Rudolf-Miklau. “Structural avalanche protection: defense systems and construction types”. In: *The Technical Avalanche Protection Handbook*. Ed. by F. Rudolf-Miklau, S. Sauermoser, and A. I. Mears. John Wiley & Sons, Ltd, 2014. Chap. 5, pp. 127–176. ISBN: 9783433603840. DOI: <https://doi.org/10.1002/9783433603840.ch05>.
- [89] R. Brändle, E. Gröner, and S. Margreth. “Avalanche Barriers in the Starting Zone Exposed to Rock Fall: Range of Capacity and 1:1 Rock Fall Tests With Flexible Snow Net”. In: *International Snow Science Workshop*. Ed. by F. Naaim-Bouvet, Y. Durand, and R. Lambert. 2013, pp. 836–839.
- [90] T. Jóhannesson and K. M. Hákonardóttir. *Remarks on the design of avalanche braking mounds based on experiments in 3, 6, 9 and 34 m long chutes*. Report 03024. Aug. 2003. URL: <https://www.semanticscholar.org/paper/Remarks-on-the-design-of-avalanche-braking-mounds-9-J%C3%B3hannesson-H%C3%A1konard%C3%B3ttir/4f8b1061ee9d0cb48085c8a38b9aa041a97597e0>.

- 
- [91] S. Margreth, T. Jóhannesson, and H. Stefánsson. “Avalanche mitigation measures for Siglufjörður – Realization of the largest project with snow supporting structures in Iceland”. In: Oct. 2014.
- [92] Á. Jónsson and P. Gauer. “Optimizing Mitigation Measures against Slush Flows by Means of Numerical Modelling-A Case Study Longyearbyen , Svalbard”. In: (2014), p. 6. URL: <https://www.semanticscholar.org/paper/Optimizing-Mitigation-Measures-against-Slush-Flows-Gauer/d1d44e2a3f325ba4d623402c6e23138a712c1df7>.
- [93] T. S. S. Herberg. “Fleksible nettkonstruksjoner som sikringstiltak mot sørpeskred i Vannledningsdalen”. Thesis. 2021. URL: <https://hdl.handle.net/11250/2824714>.
- [94] K. Kronholm, Á. Jónsson, and H. S. Nordbrøden. *Forprosjektering av nettløsning mot sørpeskred i Vannledningsdalen*. Report 18241-25-1. Client: Norges vassdrags- og energidirektorat (NVE) (Norwegian Water- and Energy Directorate). HNIT verkfræðistofa / Skred AS, Apr. 2021. URL: <https://www.lokalstyre.no/fagrappporter.488045.no.html>.
- [95] C. Wendeler. *Debris-Flow Protection Systems for Mountain Torrents. Basic Principles for Planning and Calculation of Flexible Barriers*. Report 2296-3456. 2016. URL: <https://www.wsl.ch/de/publikationen/debris-flow-protection-systems-for-mountain-torrents-basic-principles-for-planning-and-calculation-of-flexible-barriers.html>.
- [96] Arctic Technology Departmen, UNIS. *Snow Load Testing System (SLTS)*. 2022. URL: [http://158.39.149.181/Snow\\_wall/index.html#](http://158.39.149.181/Snow_wall/index.html#) (visited on Apr. 4, 2022).
- [97] J. T. Hewes, R. Decker, and M. Stevens. *Snow pressures on a rigid snow supporting structure at the milepost 151 avalanche, Jackson, Wyoming*. Conference Paper. 2016. URL: [https://arc.lib.montana.edu/snow-science/objects/ISSW16\\_P1.23.pdf](https://arc.lib.montana.edu/snow-science/objects/ISSW16_P1.23.pdf).
- [98] NRK and Meteorologisk institutt. *Historikk Svalbard Lufthavn*. 2007-2022. URL: <https://www.yr.no/nb/historikk/graf/9-14162/Norge/Svalbard/Svalbard%20lufthavn> (visited on May 6, 2022).
- [99] A. Jonsson, P. Gauer, C. Jaedicke, and Ø. Nerland. *Detaljprosjektering av sikringstiltak – Lia mellom veg 230 og 228: Prosjekteringsrapport for støtteforbygninger*. Report 20170299-05-R. 2017. URL: [https://www.lokalstyre.no/getfile.php/4395528.2046.7usp7ailqjasub/20170299-05-R\\_Prosjekteringsrapport+for+st%C3%B8tteforbygninger.pdf](https://www.lokalstyre.no/getfile.php/4395528.2046.7usp7ailqjasub/20170299-05-R_Prosjekteringsrapport+for+st%C3%B8tteforbygninger.pdf).
- [100] S. Margreth. “Experiences on the Use and the Effectiveness of Permanent Supporting Structures in Switzerland”. In: *The International Snow Science Workshop*. URL: <https://arc.lib.montana.edu/snow-science/item/1448>.
- [101] Longyearbyen lokalstyre. *Skredsikring*. 2020. URL: <https://www.lokalstyre.no/skredsikring.486358.no.html> (visited on May 10, 2022).
- [102] Á. Jónsson. *Detailed design of slush-flow nets, OPM Report*. Report 18247-SK04-00. Internal document, Client: Norges vassdrags- og energidirektorat (NVE) (Norwegian Water- and Energy Directorate). HNIT verkfræðistofa, Feb. 2022.
- [103] N. Feiger. *Design report slush flow barriers Vannledningsdalen Longyearbyen, Svalbard*. Report. Internal document, Client: HNIT verkfræðistofa. Geobrugg AG, Dec. 2021.
- [104] N. Feiger. *Dimensioning Slush flow barrier (Net 10), Vannledningsdalen Longyearbyen, Svalbard*. Report. Internal document, Client: HNIT verkfræðistofa. Geobrugg AG, Dec. 2021.
- [105] V. V. Steinarsson. *Design of foundations for slush flow nets, Vannledningsdalen Longyearbyen, RIB Report*. Report 18247-SK03-00. Internal document, Client: Norges vassdrags- og energidirektorat (NVE) (Norwegian Water- and Energy Directorate). HNIT verkfræðistofa, Jan. 2022.
-

- [106] G. Håland and A. Langelid. *Naturfareprosjektet. Delprosjekt 7. Skred og flomsikring*. Report 978-82-410-1108-5. Norges vassdrags og energidirektorat (NVE), 2015. URL: [http://publikasjoner.nve.no/rapport/2015/rapport2015\\_61.pdf](http://publikasjoner.nve.no/rapport/2015/rapport2015_61.pdf).
- [107] Geobruigg AG. *Nesselwängle bei Reutte*. 2010. URL: <https://www.geobruigg.com/en/Nesselwaengle-bei-Reutte-39557.html> (visited on June 4, 2022).
- [108] C. Berger, M. Denk, C. Graf, L. Stieglitz, and C. Wendeler. *Practical guide for debris flow and hillslope debris flow protection nets*. Report ISSN 2296-3456. 2021. URL: <https://www.wsl.ch/de/publikationen/default-d17f18e4e2.html>.
- [109] S. Palkowski. *Statik der Seilkonstruktionen, Theorie und Zahlenbeispiele (en: Statics of rope constructions, theory and numerical examples)*. 1st ed. Berlin: Springer-Verlag Berlin Heidelberg, 1990. ISBN: 978-3-540-51125-0. DOI: <https://doi.org/10.1007/978-3-642-52319-9>.
- [110] Standard Norge (SN) and European Committee for Standardisation (CEN). *Eurocode 3: Design of steel structures - Part 1-1: General rules and rules for buildings*. Standard. NS-EN 1993-1-1:2005+A1:2014+NA:2015. 2005. URL: <https://www.standard.no/no/Nettbutikk/produktkatalogen/Produktpresentasjon/?ProductID=755703>.
- [111] NTNU. *Fap2d*. Norges teknisk-naturvitenskapelige universitet (en. Norwegian University of Science and Technology). n.d. URL: <https://i.ntnu.no/wiki/-/wiki/English/Fap2d> (visited on May 17, 2022).
- [112] Dlubal Software GmbH. *RSTAB 9 - Structural Frame & Truss Analysis Software*. 2001-2022. URL: <https://www.dlubal.com/en/products/rstab-beam-structures/what-is-rstab> (visited on May 17, 2022).
- [113] R. Bärtschi and M. Spinnler. “Annex for Switzerland”. In: *Structural basics (Steel Design 1)*. www.szs.ch: Stahlbau Zentrum Schweiz, 2019. URL: [https://publicaties.bouwenmetstaal.nl/pdf\\_serve.lasso?p=pdf&n=1627-1.pdf](https://publicaties.bouwenmetstaal.nl/pdf_serve.lasso?p=pdf&n=1627-1.pdf).
- [114] A. Upadhyay, A. Kumar, and A. Chaudhary. “Velocity measurements of wet snow avalanche on the Dhundi snow chute”. In: *Annals of Glaciology* 51.54 (2010), pp. 139–145. ISSN: 0260-3055. DOI: [10.3189/172756410791386580](https://doi.org/10.3189/172756410791386580).
- [115] C. Wendeler and A. Volkwein. “Laboratory tests for the optimization of mesh size for flexible debris-flow barriers”. In: *Natural Hazards and Earth System Sciences* 15.12 (2015), pp. 2597–2604. DOI: [10.5194/nhess-15-2597-2015](https://doi.org/10.5194/nhess-15-2597-2015).
- [116] D.-Y. Tan, J.-H. Yin, W.-Q. Feng, J.-Q. Qin, and Z.-H. Zhu. “New simple method for measuring impact force on a flexible barrier from rockfall and debris flow based on large-scale flume tests”. In: *Engineering Geology* 279 (2020), p. 105881. ISSN: 0013-7952. DOI: <https://doi.org/10.1016/j.enggeo.2020.105881>.
- [117] J. S. DeNatale, R. M. Iverson, J. J. Major, R. G. LaHusen, G. L. Fliegel, and J. D. Duffy. *Experimental testing of flexible barriers for containment of debris flows*. Report. Open-file report 99-205. 1999. DOI: <https://doi.org/10.3133/ofr99205>.
- [118] S. Margreth and A. Roth. “Interaction of flexible rockfall barriers with avalanches and snow pressure”. In: *Cold Regions Science and Technology* 51.2 (2008), pp. 168–177. ISSN: 0165-232X. DOI: <https://doi.org/10.1016/j.coldregions.2007.03.008>.
- [119] Vassfjellet Vinterpark. *Velkommen til Vassfjellet Vinterpark*. 2018. URL: <https://vassfjelletvinterpark.no/vinterparken/> (visited on May 29, 2022).
- [120] A. Volkwein. *Flexible debris flow barriers - Design and application*. Report ISSN: 2296-3456. 2014. URL: [https://www.dora.lib4ri.ch/wsl/islandora/object/wsl%3A9080/datastream/PDF/Volkwein-2014-Flexible\\_debris\\_flow\\_barriers.\\_Design-%28published\\_version%29.pdf](https://www.dora.lib4ri.ch/wsl/islandora/object/wsl%3A9080/datastream/PDF/Volkwein-2014-Flexible_debris_flow_barriers._Design-%28published_version%29.pdf).

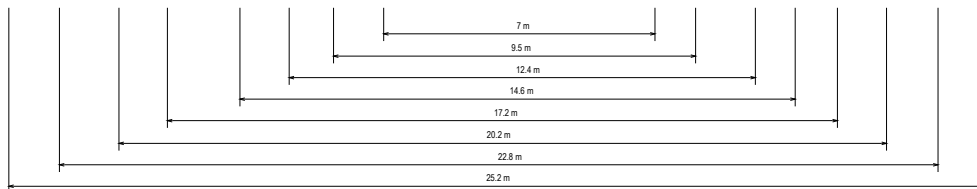
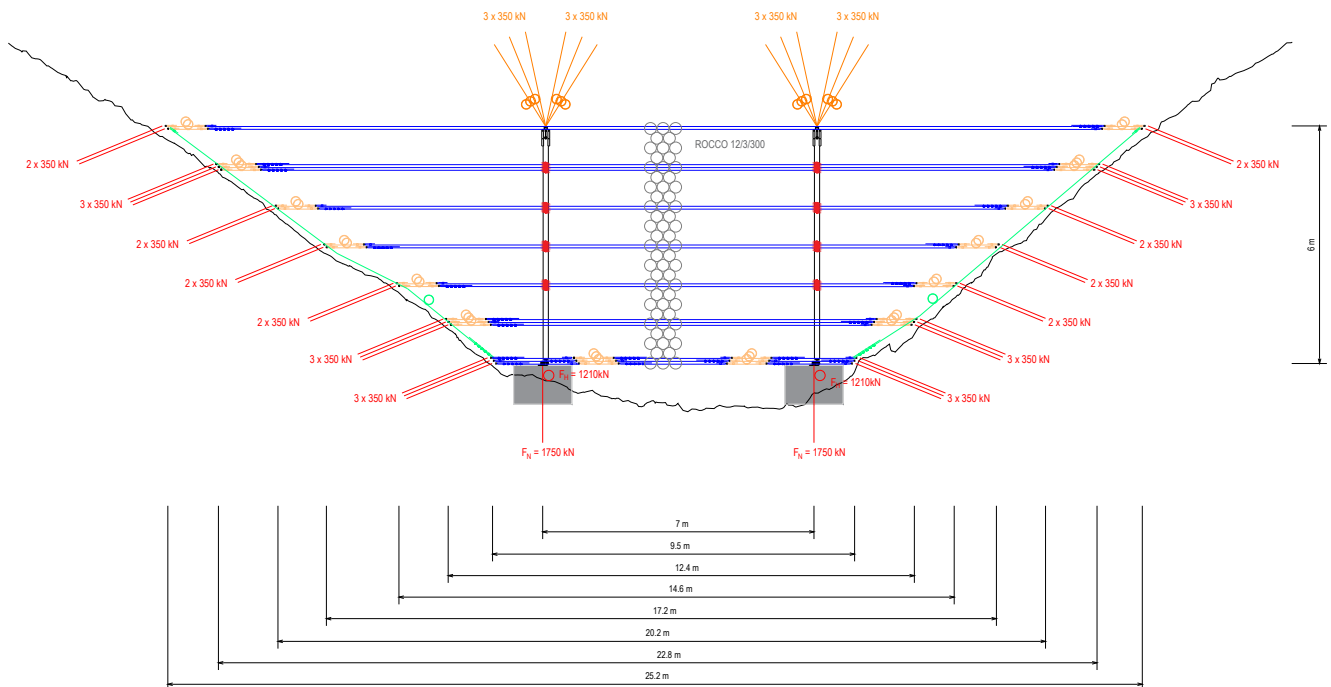
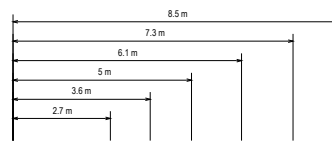
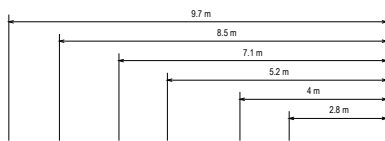
- [121] L. Zhao, J. W. He, Z. X. Yu, Y. P. Liu, Z. H. Zhou, and S. L. Chan. “Coupled numerical simulation of a flexible barrier impacted by debris flow with boulders in front”. In: *Landslides* 17.12 (2020), pp. 2723–2736. ISSN: 1612-5118. DOI: [10.1007/s10346-020-01463-x](https://doi.org/10.1007/s10346-020-01463-x).
- [122] Á. Jónsson, K. Kronholm, and L. E. Nielsen. *Forprosjektering av sikringstiltak – Fase B2*. Report 18241-03-4. Norges vassdrags- og energidirektorat (NVE), Dec. 2018.
- [123] I. Frimannslund, T. Thiis, A. Aalberg, and B. Thorud. “Polar solar power plants – Investigating the potential and the design challenges”. In: *Solar Energy* 224 (2021), pp. 35–42. ISSN: 0038-092X. DOI: <https://doi.org/10.1016/j.solener.2021.05.069>.



# Appendix

A System drawing of Flexible Net Barrier Nr. 10 - Geobruigg AS





**COMPONENTS:**

- SUPPORT ROPE ø22mm GEOBINEX
- BRAKE RING SLING WITH ONE BRAKE RING GN-9017
- RETAINING ROPE ø22mm GEOBINEX WITH BRAKE RING GN-9055
- BORDER ROPE ø22mm GEOBINEX WITH BRAKE RING GN-9017
- ROCCO RING NET 12/3/300
- FLEXHEAD Type IV
- Post: HEM 340

ChM-No:	Weight [kg]:		
Replacement for:			
Replaced by:			
Drawn by: VOS	Date:	17.02.2022	
Checked by: FEN	Date:	17.02.2022	
Released by: FEN	Date:	17.02.2022	

**Slush flow barrier Vld**

Net nr. 10  
HNIT C3 XST 39000 Stn1530



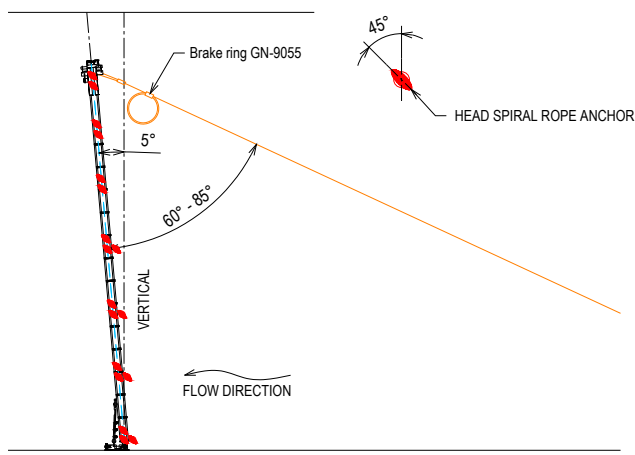
A4

**GD-9401e**

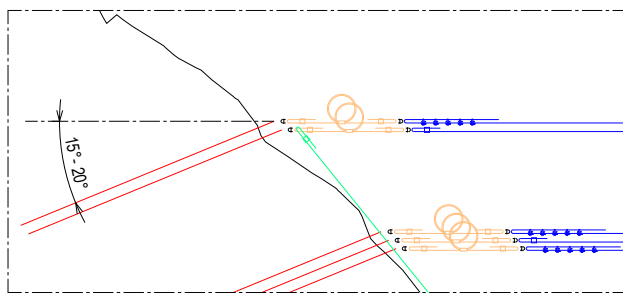
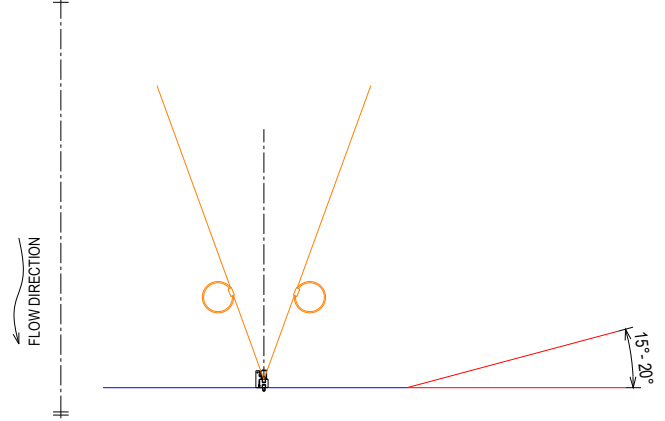
Page 10 / 17

This document is the property of GEOBRUGG AG and fully protected by copyright. It may not be distributed in whole or in part, in any way copied, translated or reproduced. This drawing will not be replaced when modified.

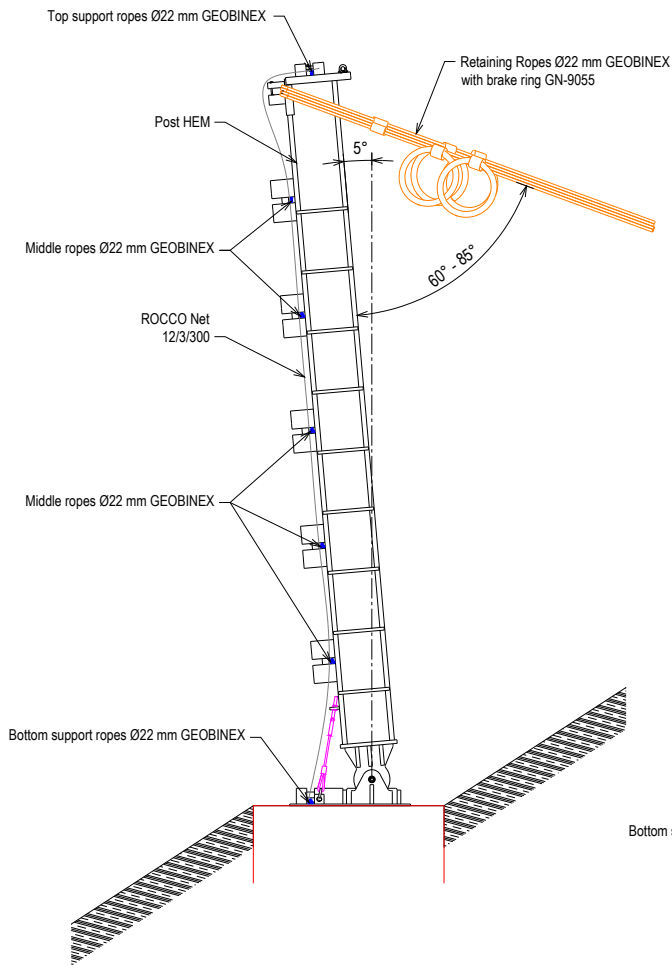
SIDE VIEW



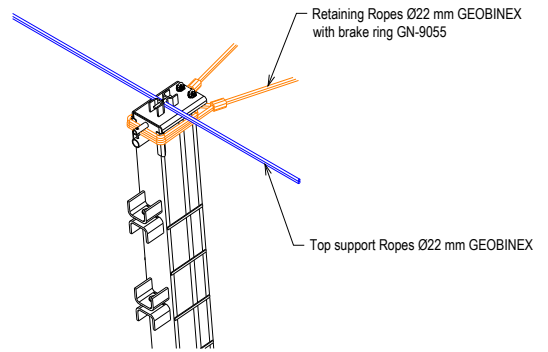
TOP VIEW



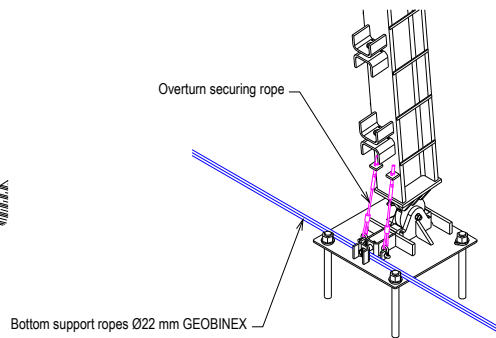
ChM-No:	Weight [kg]:		<b>Slush flow barrier V1d</b> Anchoring and system angle
Replacement for:			
Replaced by:			
Drawn by: VOS	Date:	17.02.2022	
Checked by: FEN	Date:	17.02.2022	
Released by: FEN	Date:	17.02.2022	
<b>GEOBRUGG</b> Safety is our nature			A4
			<b>GD-9401e</b>
This document is the property of GEOBRUGG AG and fully protected by copyright. It may not be distributed in whole or in part, in any way copied, translated or reproduced. This drawing will not be replaced when modified.			Page 15 / 17



**POST HEAD**

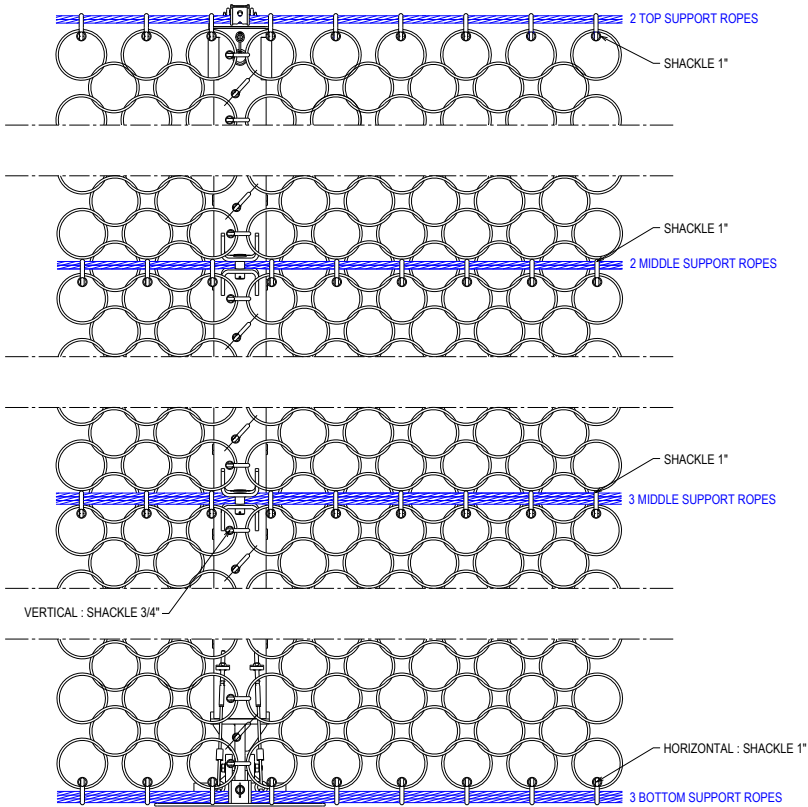


**POST FOOT**

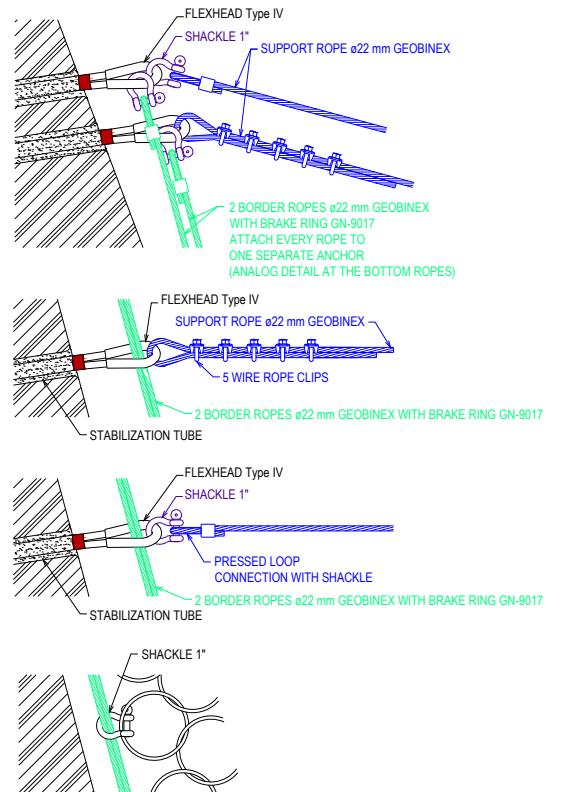


ChM-No:	Weight [kg]:		<b>Slush flow barrier Vld</b>
Replacement for:			
Replaced by:			
Drawn by: VOS	Date:	17.02.2022	
Checked by: FEN	Date:	17.02.2022	<b>Post Details</b>
Released by: FEN	Date:	17.02.2022	
 <b>Safety is our nature</b>			 <b>GD-9401e</b>
 <b>A4</b>			
<small>This document is the property of GEOBRUGG AG and fully protected by copyright. It may not be distributed in whole or in part, in any way copied, translated or reproduced. This drawing will not be replaced when modified.</small>			

NET DETAIL



CONNECTION DETAIL



ChM-No:	Weight [kg]:		
Replacement for:			
Replaced by:			
Drawn by: VOS	Date:	17.02.2022	
Checked by: FEN	Date:	17.02.2022	
Released by: FEN	Date:	17.02.2022	

**Slush flow barrier Vld**  
**Net and Connection Details**



A4

**GD-9401e**

Page 17 / 17

This document is the property of GEOBRUGG AG and fully protected by copyright. It may not be distributed in whole or in part, in any way copied, translated or reproduced. This drawing will not be replaced when modified.

